https://doi.org/10.35662/unine-thesis-3021

Rapid groundwater potential mapping in data-scarce regolithic landscapes: a contribution to hydrogeology in humanitarian contexts

PhD thesis submitted at the

Faculty of Sciences

Centre for Hydrogeology and Geothermics (CHYN)

University of Neuchâtel, Switzerland

for the degree of

Doctor of Sciences

presented by

Cyrille Damien SCHERRER

Accepted by the following evaluation committee

Prof. Ellen MILNES, director, University of Neuchâtel

Prof. Philip BRUNNER, co-director, University of Neuchâtel

Prof. Pedro MARTINEZ-SANTOS, Complutense University of Madrid

Dr. Ryan SCHWEITZER, Centers for Disease Control and Prevention

Defended on December 7, 2022

unine
Université de Neuchâtel
Faculté des sciences

Rue Emile-Argand 11
CH-2000 Neuchâtel
doctorat.sciences@unine.ch

IMPRIMATUR POUR THESE DE DOCTORAT

La Faculté des sciences de l'Université de Neuchâtel autorise l'impression de la présente thèse soutenue par

Monsieur Cyrille SCHERRER

Titre :

"Rapid groundwater potential mapping in data-scarce regolithic landscapes: a contribution to hydrogeology in humanitarian contexts"

sur le rapport des membres du jury composé comme suit:

- Prof. tit. Ellen Milnes, directrice de thèse, Université de Neuchâtel, Suisse
- Prof. Philip Brunner, Université de Neuchâtel, Suisse
- Prof. Pedro Martinez Santos, Universidad Complutense, Madrid, Espagne
- Dr Ryan Schweitzer, Centers for Disease Control and Prevention, Atlanta, USA

Neuchâtel, le 10 février 2023

Le Doyen, Prof. R. Bshary

‘‘Men will be taught that beneath and behind all the outward beauty of our lowlands, our uplands, and our highlands there lies an inner history which, when revealed, will give to that beauty a fuller significance and an added charm.’’

—Archibald Geikie

Acknowledgments

This thesis is the outcome of an applied research project conducted through a collaborative effort between the following three institutions: The Centre for Hydrogeology and Geothermics (CHYN) of the University of Neuchâtel, the Swiss Agency for Development and Cooperation (SDC), and the United Nations High Commissioner for Refugees (UNHCR). Consequently, I start by thanking these institutions. The CHYN has provided an excellent research environment, while SDC has generously provided substantial funding and technical support over the past four years. Additionally, UNHCR has been an invaluable partner, providing critical logistical support and security during field missions and granting us access to a vast database on water supply.

This thesis was directed by Ellen Milnes and co-supervised by Philip Brunner. Therefore, I would first like to express my deepest gratitude to Ellen Milnes. Her engagement and dedication have made all these years a rewarding experience. Second, I would like to thank Philip Brunner for his many valuable insights and analyses. Later, this thesis was examined by Pedro Martínez-Santos and Ryan Schweitzer. Many thanks to Pedro Martínez-Santos for his fruitful comments that greatly improved this document with his expertise on humanitarian aid in Africa. Ryan Schweitzer, in addition, also contributed significantly from the beginning of the project with his engineering perspective, so I am very grateful to him.

Subsequently, I would particularly like to thank the other two people who were deeply involved in this research. First, Pierre Perrochet (CHYN) who has always been available for answering mathematical and physical questions. Secondly, Marc-André Bünzli (SDC) deserves special recognition for his unwavering support and guidance throughout this project. Furthermore, I am grateful to him for sharing his fascinating worldview with me, which I hope is evident in this work.

Over the years of study and research, I have had the privilege of meeting many colourful people whom I wish to thank here. Starting with Valentin and Patrick with whom the adventure began with a memorable Bachelor at the University of Fribourg. Then, it continued with Álvaro during the intense years of the Master at the University of Neuchâtel. During these academic years, I found myself alongside Samir, a person I have always greatly admired. Through my doctoral years, I was fortunate to meet Saeed, who shared his everyday enthusiasm with me as much as possible. Finally, in these last years, I had the immense chance to share all my working time with Léa in a calm and always cheerful environment.

Afterwards, I would like to express my warmest feelings to my second family. First of all to Anne and Guy who have consistently demonstrated all their support to me. Then, to Claudine and Marc who

always knew how to make me smile. Next, to Clémentine, Lucie, Martin, Nicolas and Sébastien with whom I had the incredible luck to spend most of my little free time. I can never be grateful enough to all these people who have constantly given me so much motivation and energy.

Subsequently, I would like to give special thanks to some of my relatives. On my mother's side, to Marlies, Lucien, Kevin, and Justin. This wonderful and unique little family has always been there to cheer me up. On my father's side, I would like to thank Claude who, having had a similar journey, was very inspiring. Then, to Lucia who encouraged and supported me a lot in my studies and urged me to discover the world.

I especially thank my close family and most important individuals in my life, my parents Damien and Patrice and my brother Robin. My father has always believed in what I wanted to do and continues to encourage me until this day. My mother has always been kind and present for me. Finally, my brother, in addition to having always been considerate, has been a great source of inspiration in terms of daily commitment.

Lastly, I want to thank the love of my life, Manon. Without her, I would not have made it through. Eventually, I will spend less time trying to figure out the world with maps and more time exploring it in real life together with her.

I dedicate this thesis to Manon who shares the same passion as me with as much ardour. Ultimately, I dedicate it to my father, the most authentic and inspiring individual, but above all, the greatest scientist I know. Thank you for passing on to me the love of research and the desire to make this world a better place.

Abstract

The main objective of this thesis is to contribute to humanitarian efforts to provide responsive and reliable groundwater supply to displaced populations living in refugee camps or settlements across Sub-Saharan Africa. A large-scale transition is underway from rural towards peri-urban and urban settings, hence, from scattered hand pumps towards centralized motorized boreholes connected to distribution networks. However, with this shift in water supply strategy, the need to achieve yields an order of magnitude higher than those typically sought for hand pumps goes hand in hand with the need for changing the exploration strategy from 'drilling where the people are' to 'drilling where the water is'. However, comprehensive hydrogeological assessments can often not be carried out as time is limited and data are scarce. It is against this backdrop that this applied research has been carried out, aiming towards developing a practical tool which can rapidly inform stakeholders in planning the siting of boreholes and on sustainable groundwater exploitation.

The first section of this thesis is dedicated to the development of a rapid groundwater potential mapping methodology (RGWPM). It is based on the overlay of the two main groundwater relevant variables, i.e. the water availability (WA) reflecting hydrogeomorphological landscape units and the reservoir capacity (RC) being a proxy of the hydraulic properties, always retaining the lowest to define the groundwater potential (GWP). The RGWPM methodology was applied to the real case-study of Bidibidi refugee settlement (Northern Uganda) and used to implement eight new boreholes. The cross-validation revealed that its application significantly increased the average yield, justifying further applications in other settlements and camps.

The overlay process of the RGWPM methodology revealed that the WA variable is almost always inferior and dependent on the RC, leading to a proposed revision to the RGWPM, relying only on the WA mapping. The revised version was again evaluated using the Bidibidi case-study with similar results and was subsequently applied to fourteen different refugee camps situated in similar regolithic landscapes in Sub-Saharan Africa. A cross-validation of the borehole yield with the mapped RGWPM units was carried out for all sites, again revealing a high degree of predictability. Although the revised approach was very useful and practical in visualising the spatial probability for GWP, it did so far not include any information on sustainable exploitation, as for instance how many high-yielding boreholes one unit can accommodate.

The lack of information on sustainable exploitation of boreholes in the revised RGWPM methodology led to the second part of the thesis, which is dedicated to the exploration of the relationship between RGWPM units and water balance components, in particular groundwater

recharge. A hydrogeomorphological analysis was carried out on twenty reference catchments, selected in similar geological (regolithic) and climatic contexts in Sub-Saharan Africa, for which all water balance components were known (i.e. including data from gauging stations) and for which the revised RGWPM units were translated into hydrogeomorphological landscape (HGM) units. The hydrogeological frameworks of these environments all fall into the topography-driven water table settings, where HGM units can be associated with surface and groundwater dynamics. The hydrogeomorphological-water balance analysis resulted in an empirical formulation of groundwater recharge based on the mapped HGM units, precipitation, and evapotranspiration. Once there was an approach to estimate groundwater recharge in any catchment with similar geological characteristics it was possible to introduce the notion of sustainable exploitation into the revised methodology.

To do this on a real case-study, groundwater recharge was estimated using the empirical relationship for the Bidibidi settlement, for which the HGM units were directly obtained by analogy with the RGWPM units, while precipitation and evapotranspiration were obtained from remote sensing products. The Bidibidi RGWPM map was subsequently divided into sub-catchments, within which the cumulative extraction from motorised boreholes was compared to the sustainable groundwater potential, defined as a third of the sub-catchment groundwater recharge. This allowed mapping of the degree of sustainability of groundwater extraction within the sub-catchments. Some sub-catchments were identified to be in a state of over-exploitation, while others were identified where further groundwater development could be envisaged. In order to translate the sustainable groundwater potential into a map, the drainage sections corresponding to different sustainable cumulative sub-catchment extractions were added to the revised methodology.

In the last section of the thesis, the correlation between the HGM units and the water balance components, expressed in the empirical relationship, was addressed by articulating the conceptual framework by a simplified analytical approach, and applying the obtained solution to the twenty reference catchments. Comparing the analytical results with the empirical solution indeed suggested a meta-physically based relationship between the HGM units, the water balance components, and the hydraulic properties, thereby capturing some essential complex interactions between regolithic landscapes and climate. On the one hand, this supports the easier-to-implement empirical solution, and, on the other hand, it opened a wide range of new perspectives showing the path to expanding this type of hydrogeomorphological analysis to other geological landscapes, also under diverse and changing climatic conditions.

Keywords: Humanitarian aid, Groundwater water supply, Sub-Saharan Africa, Regolithic environments, Groundwater exploration, Groundwater potential mapping, Hydrogeomorphology

Résumé

L'objectif principal de cette thèse est de contribuer aux efforts humanitaires visant à fournir un approvisionnement en eau souterraine réactif, adapté et fiable aux populations déplacées vivant dans des camps de réfugiés à travers l'Afrique subsaharienne. De manière générale, une transition à grande échelle est en cours, de nombreuses zones rurales devenant périurbaines et urbaines, ce qui entraîne le passage d'un approvisionnement en eau basé sur des pompes à main, dispersées dans les villages, à des forages motorisés, centralisés et reliés à des réseaux de distribution. Avec ce changement de stratégie d'approvisionnement en eau, la nécessité d'atteindre des débits d'un ordre de grandeur supérieur à ceux généralement recherchés pour les pompes manuelles va de pair avec la nécessité de changer la stratégie d'exploration, de 'forer là où sont les gens' à 'forer là où est l'eau'. Dans le contexte humanitaire, il est souvent impossible de réaliser des études hydrogéologiques complètes, car le temps est limité et les données sont rares. C'est dans ce contexte que cette recherche appliquée a été menée, visant à développer un outil pratique qui puisse informer rapidement les parties prenantes dans la planification des emplacements de forage des meilleurs endroits où forer tout en visant une exploitation durable des eaux souterraines.

La première partie de cette thèse est consacrée au développement d'une méthodologie de cartographie qui permet de déterminer rapidement le potentiel en eau souterraine. Elle repose sur la superposition des deux variables principales pertinentes pour la quantification des eaux souterraines. Ces deux variables sont: la disponibilité en eau, qui est basée sur des unités de paysages hydrogéomorphologiques, et la capacité du réservoir, qui représente une approximation des propriétés hydrauliques. En retenant toujours la plus faible de ces propriétés, le potentiel en eau souterraine peut être défini en unités de potentiel. La méthodologie a été appliquée au cas du camp de réfugiés de Bidibidi (nord de l'Ouganda) et utilisée pour localiser huit nouveaux forages. La validation de la méthodologie a révélé que son application avait permis d'augmenter de manière significative le rendement moyen des forages de Bidibidi, justifiant alors son application à d'autres camps.

Le processus de superposition de la méthodologie a permis de constater que la variable de la disponibilité en eau est presque toujours inférieure, mais dépendante, à celle de la capacité du réservoir, ce qui a conduit à proposer une révision de la méthodologie basée uniquement sur la cartographie de la disponibilité en eau. Cette version révisée a été validée en utilisant à nouveau l'étude de cas de Bidibidi, et a donné des résultats similaires. Ensuite elle a donc été exportée à quatorze autres camps de réfugiés situés dans des paysages régolithiques similaires en Afrique subsaharienne. Une comparaison des débits de forage avec les unités du potentiel en eau

souterraine déterminés par la méthodologie a été effectuée pour tous les sites, révélant un haut degré de prédictibilité. Bien que l'approche révisée se soit avérée très utile et pratique pour visualiser la probabilité spatiale du potentiel en eau souterraine, elle ne comportait aucune information sur l'exploitation durable, notamment le nombre de forages à haut rendement qu'une unité pourrait contenir.

Le manque d'informations sur l'exploitation durable des forages dans la méthodologie révisée a conduit à la deuxième phase de cette thèse. Cette phase est consacrée à l'exploration de la relation entre les unités de potentiel des eaux souterraines et les composantes du bilan hydrique, en particulier la recharge des eaux souterraines. Une analyse hydrogéomorphologique a été réalisée sur vingt bassins versants de référence, sélectionnés dans des contextes géologiques (régolithiques) et climatiques similaires de l'Afrique subsaharienne, pour lesquels toutes les composantes du bilan hydrique ont été collectées (c'est-à-dire incluant les données des stations de jaugeage) et pour lesquels les unités de potentiel en eau souterraine ont été traduites en unités hydrogéomorphologiques. Les contextes hydrogéologiques de ces environnements s'inscrivent tous dans le cadre de nappes phréatiques contrôlées par la topographie, où des unités hydrogéomorphologiques peuvent être associées à la dynamique des eaux de surface et des eaux souterraines. L'analyse du bilan hydrique à travers l'hydrogéomorphologie a abouti à une formulation empirique de la recharge basée sur les unités hydrogéomorphologiques cartographiées, les précipitations et l'évapotranspiration. Une fois cette approche disponible pour estimer la recharge dans tout bassin versant ayant des caractéristiques géologiques similaires, il a été possible d'introduire le concept de durabilité dans la méthodologie révisée.

Afin de réaliser cela sur un cas réel, la recharge a été estimée en appliquant la relation empirique au cas de Bidibidi, pour lequel les unités hydrogéomorphologiques ont été obtenues directement par analogie avec les unités de potentiel en eau souterraine. Les précipitations et l'évapotranspiration ont été quant à elles obtenues à partir de produits de télédétection. La carte du potentiel des eaux souterraines de Bidibidi a ensuite été divisée en sous-bassins versants, dans lesquels l'extraction cumulée des forages motorisés a été comparée au potentiel durable en eau souterraine, défini comme un tiers de la recharge du sous-bassin versant. Cela a permis de cartographier le degré de durabilité de l'extraction des eaux souterraines dans les sous-bassins versants. Certains sous-bassins versants ont été identifiés comme étant dans un état de surexploitation, tandis que d'autres ont été identifiés comme étant dans un état où le développement des eaux souterraines pourrait être plus important. Pour refléter le potentiel durable des eaux souterraines de manière visuelle, des sections de drainage correspondant aux différentes extractions durables cumulées des sous-bassins versants ont été ajoutées à la carte obtenue avec la méthodologie révisée.

Dans la dernière partie de cette thèse, la corrélation entre les unités hydrogéomorphologiques et les composantes du bilan hydrique, exprimée dans la relation empirique, a été abordée en formulant le modèle conceptuel par une approche analytique simplifiée et en appliquant cette solution aux vingt bassins versants de référence. La comparaison des résultats analytiques avec la solution empirique a suggéré une relation métaphysique entre les unités hydrogéomorphologiques, les termes du bilan hydrique et les propriétés hydrauliques, capturant ainsi certaines interactions complexes essentielles entre les paysages régolithiques et le climat. D'une part, cela soutient la solution empirique plus facile à mettre en œuvre et, d'autre part, cela a ouvert un large éventail de nouvelles perspectives, montrant la manière d'étendre ce type d'analyses hydrogéomorphologiques à d'autres paysages géologiques se trouvant dans des conditions climatiques diverses et changeantes.

Mots-clés: Aide humanitaire, Approvisionnement en eau souterraine, Afrique subsaharienne, Environnements régolithiques, Exploration des eaux souterraines, Cartographie du potentiel en eaux souterraines, Hydrogéomorphologie

Abbreviations and mathematical symbols

RGWPM Rapid groundwater potential mapping

Map units

WA	Water availability (RGWPM mapping variable): very low; low; slope; medium; high
RC	Reservoir capacity (RGWPM mapping variable): very low; low; medium; high
GWP	Groundwater potential (RGWPM map result): very low; low; slope; medium; high

HGM Hydrogeomorphological landscape unit abbreviation

HGM units

Upland *(u)*	HGM unit (corresponding to very low & low WA map unit)	[L^2]
Slope *(s)*	HGM unit (corresponding to slope WA map unit)	[L^2]
Drainage *(d)*	HGM unit (corresponding to medium & high WA map unit)	[L^2]

Water balance components

P	Precipitation	[LT^{-1}]
ET	Evapotranspiration	[LT^{-1}]
P_{eff}	Effective precipitation	[LT^{-1}]
Q	Stream discharge	[LT^{-1}]
Q_0	Groundwater flow	[LT^{-1}]
Q_b	Base flow	[LT^{-1}]
Q_i	Groundwater recharge	[LT^{-1}]
R	Runoff	[LT^{-1}]

Mathematical symbols for HGM analysis

A	Upland (u)	[L^2]
B	Slope (s) & drainage (d)	[L^2]
c	Drainage perimeter	[L]
m	Slope of drainage system i.e. regional gw. gradient	[-]
α	Infiltration or runoff coefficient	[-]

Table of Contents

Chapter 1

Introduction

1.1. Background

This thesis is a contribution to humanitarian efforts to provide water to displaced populations living in refugee camps and settlements in Sub-Saharan Africa. Groundwater accessed through hand pumps is the most common approach to water supply in remote areas, but a transition is underway from numerous scattered hand pumps to centralised motorised boreholes with networks. However, with this shift in water supply comes the need identify boreholes with yields that are an order of magnitude higher than those acceptable for hand pumps. To do this requires a more meticulous approach to siting boreholes. Yet, in most emergency contexts, boreholes are sited based on the proximity to shelters with an aim to provide rapid assistance. However, this approach often fails due to general unfavourable hydrogeological conditions at these locations. This borehole siting strategy has been widely applied, since displaced people are most often hosted in remote and poorly surveyed rural areas, where a comprehensive hydrogeological assessment cannot be carried out due to limited time. Hence, there is a need for a robust, rapid, and reproducible borehole siting strategy based on physical processes of groundwater. The research presented in this document seeks to fill this gap.

1.2. Objectives

The main objective of the present applied research was to explore ways of filling the gap in data-scare areas by producing groundwater relevant information from landscape analysis and establishing relationships to groundwater recharge and translating this into easily accessible groundwater potential maps. The aim of these maps is to inform on optimal drilling locations, not only with respect to yield but also with respect to sustainable exploitation.

More specifically, the initial objective was to develop a methodology for quickly producing a map of the groundwater potential using a combination of data sets readily available everywhere, i.e. specific landscapes characteristics identified through classical hydrogeomorphological analysis and remote sensing data. Then, the subsequent objective became to introduce the notion of sustainable exploitation into the mapping methodology, requiring quantification of groundwater recharge.

The overall ambitious scientific objective of this work was to gain a more fundamental understanding of the relationship between landscape characteristics and the water balance

components and explore ways of quantifying or 'reading' groundwater recharge from the landscape. For that purpose, approaches from different fields of research have had to be combined.

The development of a rapid groundwater potential mapping methodology inserts itself into the vast field of groundwater potential mapping. The novelty in the mapping approach may be seen in the combination of classical approaches developed decades ago in the field of hydrogeomorphology 'revisited' with now readily available digital elevation models and combined with other remote sensing data sets.

1.3. Embedding rapid groundwater potential mapping in the relevant fields of research

The two main fields of research which have contributed to defining the approaches developed in this work are groundwater potential mapping and hydrogeomorphology. A brief overview of the state of the art in these fields and relevant concepts forming the basis of this work are presented in the following section.

1.3.1. Groundwater potential mapping

A recent review of groundwater potential mapping published by Díaz-Alcaide and Martínez-Santos (2019) concluded that there is no universal definition of groundwater potential, standardised method for developing maps, or commonly accepted set of units to measure the outcomes. Their review revealed that some groundwater potential maps provide an indication of the variations in groundwater storage across a given region, while other studies interpret the groundwater potential as a measure of how likely groundwater is to be found or where the highest yields may take place. The review concluded that the objective of most groundwater potential studies is to identify the optimal zone(s) for groundwater development, which is also the case for the RGWPM approach presented herein.

Díaz-Alcaide and Martínez-Santos (2019) further argued that 'potential' is related to a 'probability of something occurring' and defined it as a spatially distributed best estimate of the physical capacity of the terrain to yield enough groundwater for a given use based on a series of indirect indicators. Their analysis of 200 studies identified the following key parameters: lithology (geology), geomorphology, soil, land use, topography, lineaments, drainage and slope related variables, rainfall and groundwater recharge. RGWPM also directly or indirectly uses these key parameters.

Another characteristic of groundwater potential mapping is that variables are classified and zoned in a multi-criteria decision framework (Teixeira et al., 2015), followed by different map algebraic

approaches (Ettazarini, 2007; Elewa and Qaddah, 2011), leading to a classified likelihood of attaining a target value (e.g. sufficient yield for hand pump or motorized water supply).

The efficiency of recently discovered systems based on artificial intelligence or machine learning has attracted the attention of water resources experts. As a result, these techniques are commonly used to map and characterize groundwater potential (Diaz-Alcaide and Martinez-Santos, 2019). They have proven effective in combining and interpreting large amounts of data in various ways using powerful algorithms to instantly indicate the best location for a borehole (Martínez-Santos and Renard, 2019). Although these approaches rely on high computational capabilities, their effectiveness depends on the quality and amount of data used (e.g. Gómez-Escalonilla et al. 2021).

A major drawback of the groundwater potential mapping approaches evaluated by Diaz-Alcaide and Martinez-Santos (2019) is the lack of validation of the maps with field data. Díaz-Alcaide and Martínez-Santos (2019) concluded that remote sensing techniques in groundwater exploration have an enormous potential. However, for optimal results, groundwater mapping must be used as a tool to inform fieldwork rather than as a low-cost substitute for local-scale surveys (Abdalla, 2012; Mandal et al., 2016).

1.3.2. Hydrogeomorphological analysis and groundwater processes

The landscape results from the interaction of the lithosphere with the atmosphere, biosphere, and hydrosphere (e.g. Melton, 1957). If the processes leading to the landscape can at least partially be explained by the interaction with water, the reverse problem, i.e. explaining water processes by the landscape is also conceivable. This is indeed already well established and specifically described by hydrogeomorphology, the study of landforms resulting from the action of water (e.g. Scheidegger, 1973; Winter, 2001; Sidle and Onda, 2004). In regions where precipitation is sufficient to cause mechanical or chemical surface and subsurface erosion, the landscape is primarily shaped by the action of water. The extent of these erosional processes, and consequently the impact on the landscape, is largely controlled by the physical properties of the earth material. Ultimately, these properties control the amount of precipitation that is transformed into either surface or groundwater, shaping the landscape. This fundamental principle forms the basis of the rapid groundwater potential mapping (RGWPM) methodology developed in this work.

The hydrogeomorphological concept described by Winter (2001) forms a back-bone of this thesis, subdividing the landscape into units where either surface or subsurface water processes are most likely to occur. This simple concept is utilized in the mapping methodology and the subsequent hydrogeomorphological analyses, neglecting numerous complex processes. These analyses build on

some of these general landscape and water related processes, as well as more specific hydrogeomorphological notions presented for instance by Dunne et al. (1975) and Dunne (1990), describing the interdependency between water input/intensity and its transformation into surface runoff or infiltration as function of the hydraulic properties of the sub-surface. This dynamic interplay between hydraulic properties and rainfall (intensity) lead to the complex shapes of the landscape.

Most of the refugee camps and settlements across Sub-Saharan Africa, such as Bidibidi in Uganda, which is used in this work as a real case study, are located in the regolithic environments. These environments are primarily formed by groundwater-induced processes (e.g. Twidale, 1990). More importantly, these environments fall into the topography-driven water table settings (e.g. Haitjema and Mitchell-Bruke, 2005), in which some landscape features are related to groundwater dynamics (e.g. Coates, 1990).

1.4. Embedding the 'Rapid groundwater potential mapping' project in the humanitarian context

The lack of planned borehole siting is a widespread reality in most humanitarian emergencies, from a managerial, engineering, and hydrogeological perspective, resulting in a coincidental distribution of water infrastructures. This kind of circumstantial borehole distribution forms then the basis around which all remaining aspects of the water supply chain are accommodated. With a majority of humanitarian responses relying exclusively on groundwater supply with associated high capital investment and operational costs, targeting optimisation of boreholes has a domino effect on the entire water supply chain. It reduces expenditures and increases performance of the distribution systems with a long-term perspective, which in turn improves service delivery for beneficiaries. Hence, strategical borehole-siting targets the root of sustainable water resource management which is no longer 'nice to have', but is becoming compulsory, forming an integral part of Sustainable Development Goals (SDGs).

The Northern Ugandan refugee operation is a recent and representative example that sheds light on the importance of having an operational tool for optimised and strategic borehole siting. In this operation almost 1 million South Sudanese refugees are hosted in vast settlements. Water supply has been a critical issue, particularly since the peak influx in late 2016 and was running in emergency mode until 2018. This entailed massive expenditures for water trucking of 2.4 million $/month which amounted to $15.5 per m^3 and even then, it was challenging to meet basic humanitarian standards (15 l/person/day). There was an urgent need to meet these standards and to end the water trucking. Groundwater was the only alternative water source with which this goal could be achieved. As a

result, a drilling campaign funded by multiple partners was planned in 2018. In order to ensure the sustainability of the boreholes, the siting process had to be carefully planned.

A hydrogeological field mission in 2017 initiated the idea to plan the upcoming drilling campaign with rapidly established groundwater potential maps. The resulting trial received positive feedback from partners, authorities and especially the Ministry of Water of Uganda (MoW). This led to the project proposal that formed the basis of this PhD thesis, aimed at conceiving a systematic methodology for optimizing borehole sitting. The project was entitled 'Rapid groundwater potential mapping in refugee settings' and was jointly led by the Swiss Agency for Development and Cooperation (SDC), the United Nations High Commissioner for Refugees (UNHCR) and The Centre for Hydrogeology and Geothermics of University of Neuchâtel (CHYN) between 2018 and 2022.

1.5. Evolving rapid groundwater potential mapping (RGWPM) methodologies, variables, and units

The original RGWPM methodology, presented in Chapter 2, based on mapping, and overlay of the two variables i.e. the water availability (WA), defined by hydrogeomorphological landscape units (Winter, 2001) and the reservoir capacity (RC), based on a simplified geological mapping for characterizing the hydraulic properties. The groundwater potential was then derived by the overlay of the two variables, as schematically illustrated in Fig. 1.1. During the course of this work, it appeared that the independent mapping of the two variables could be reduced to only considering the WA variable, defined by hydrogeomorphological landscape units. Indeed, its morphological and hydrodynamic characteristics depend on the physical properties of the subsurface, thereby integrating the RC. This observation therefore led to a revised RGWPM methodology, schematically illustrated in the second block in Fig. 1.1.

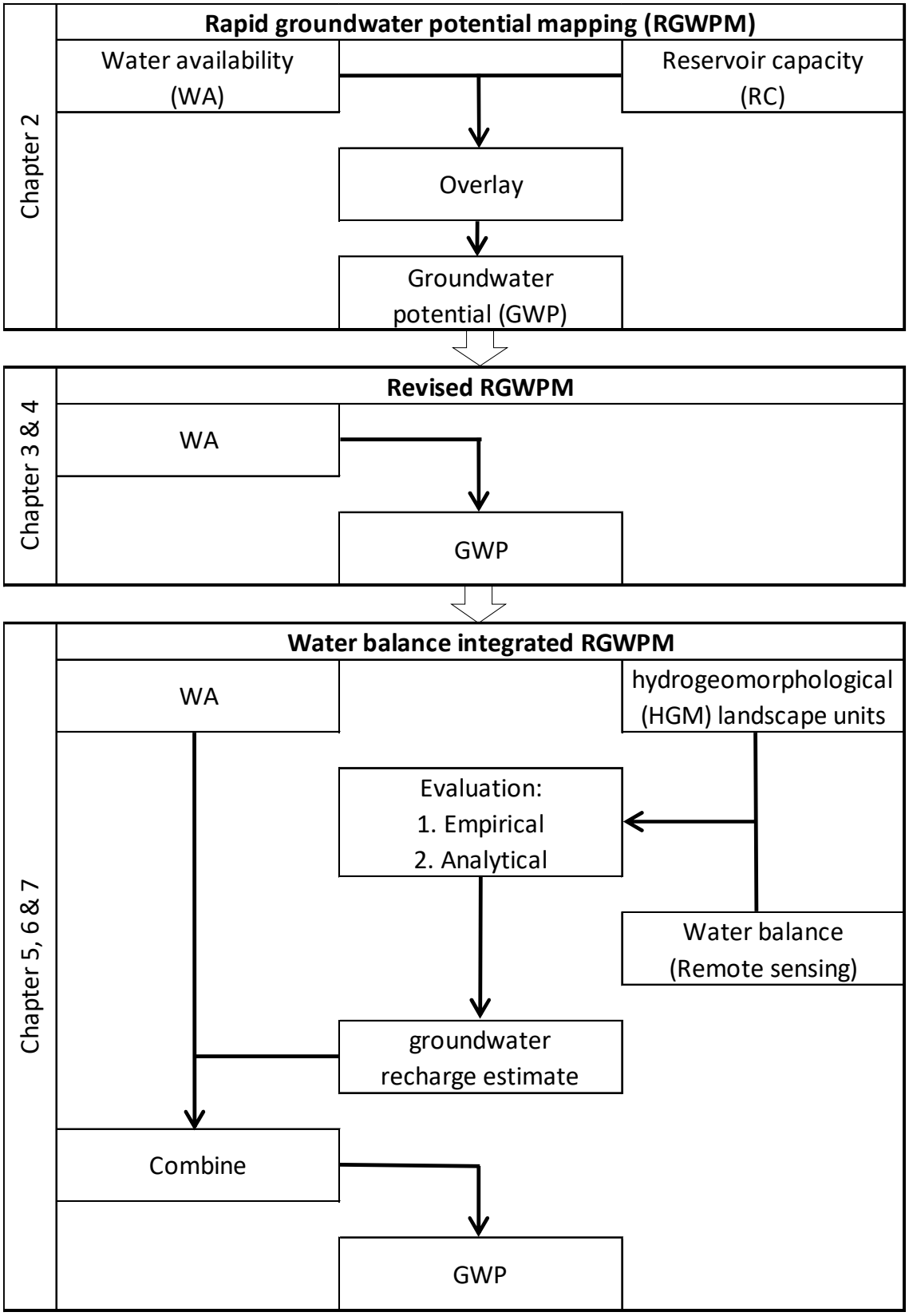

Fig. 1.1 *Workflow of the thesis and key points behind the three rapid groundwater potential mapping (RGWPM) methodologies.*

After applying the revised methodology to the wider humanitarian context in Africa it was concluded that it was applicable to most of Sub-Saharan Africa where regolithic environments are dominant. The overall hydrogeological framework of these environments falls into the topographically controlled water table settings (e.g. Lachassagne et al., 2021). Therefore, in these environments, certain landscape features and units can be associated with surface and groundwater dynamics.

The further development of the revised RGWPM methodology to include the possibility to assess sustainability of exploitation schemes formed the second part of the thesis and led to the third RGWPM approach, called the 'water balance integrated' RGWPM methodology, schematically illustrated in Fig. 1.1 in the third block.

The evolution of the RGWPM methodology, through revision of the original RGWPM method by omitting the RC variable, simplifying the method to only mapping the WA variable, to the water balance integrated RGWPM methodology required an evolution in the nomenclature, evolving from map units (WA) towards hydrogeomorphological (HGM) landscape units as illustrated in Fig. 1.2. This evolution, although perhaps confusing for the reader at times, was essential to decouple the initial WA variable, which is associated to yield-ranges, from purely naturalistic landscape characteristics. Hence, whenever reference is made to the WA variable, direct reference is made to the associated RGWPM legend, while when HGM landscape units are discussed, it is decoupled from the RGWPM legend but refers to the physical world.

Hydrogeomorphological (HGM) features and landscape units	Outcrops	Upland	Slope	Drainage	Lowland
Surface water and groundwater (gw) processes	Restricted diffuse recharge	Only diffuse recharge	Axial gw. flow, diffuse recharge and runoff	Axial gw. flow, concentrated recharge and runoff	Converging gw. flow and runoff
RGWPM Water availability (WA)	Very low GWP	Low GWP	Slope GWP	Medium GWP	High GWP
HGM landscape units for water balance analyses	Upland		Slope	Drainage	

Fig. 1.2 *Rationale illustrating the translation of hydrogeomorphological (HGM) features and units with associated surface water or groundwater processes, first into groundwater potential (GWP) zones to describe the water availability (WA) of the RGWPM methodologies and then into fundamental HGM landscape units for water balance analyses.*

Figure 1.2 presents the way the landscape is subdivided into 5 hydrogeomorphological features and units where either surface water or groundwater related processes are most likely to occur. Firstly, for the RGWPM methodologies (Fig. 1.1), these 5 and their associated processes are used to define the WA variable and are translated into groundwater potential (GWP) zones. Next, the

hydrogeomorphological features and units are simplified into 3 fundamental HGM landscape units for water balance analyses. These units are combined with remote sensing products as shown in Fig. 1.1 to derive an estimate of groundwater recharge.

1.6. Structure of the thesis

This thesis consists of seven chapters followed by a conclusion. The workflow is schematically illustrated in Fig. 1.1 where the chapters have been grouped into three blocks to present the evolution that took place during the project. The first block shown in Fig. 1.1 represents the mapping approach developed in Chapter 2, which introduces the original RGWPM methodology based on the overlay of water availability (WA) and reservoir capacity (RC) variables. In the second block, shown in Fig. 1.1, comprising Chapters 3 and 4, the revised RGWPM methodology based on the WA alone is developed and tested, however, lacking the link to the assessment of sustainable exploitation. Finally, the last block shown in Fig. 1.1, comprising Chapters 5 to 7, is dedicated to the estimation of groundwater recharge, based on the mapped hydrogeomorphological units of the revised RGWPM combined with remotely sensed water balance analysis, to assess sustainable borehole exploitation, resulting in the water balance integrated RGWPM methodology. Hereafter, the chapters are briefly presented one by one, highlighting the main topics developed in each one.

The RGWPM methodology is first presented in Chapter 2 and has been published (Scherrer et al. 2021). In this chapter, the requirements for borehole implementation in the humanitarian sector are first presented by describing the technical challenges that must be addressed. Then, a literature review of groundwater potential mapping approaches is conducted to support the need for an additional methodology although multiple products are already available (Diaz-Alcaide and Martinez-Santos, 2019). Subsequently, the methodology is developed step by step in order to be reproducible. Finally, it is tested and cross-validated using field data from the Bidibidi refugee settlement in Northern Uganda.

After a thorough analysis and evaluation of the RGWPM methodology, it became clear that the approach of independently mapping the two variables (WA and RC) could be simplified to consider only the WA to express the GWP (Fig. 1.1). Indeed, the attributes of one variable often depend on the characteristics of the other. As the WA variable is based on a hydrogeomorphological assessment, its morphological and hydrodynamic characteristics are logically a function of the physical properties of the subsurface, i.e. the RC. It was found that the advantage of focusing on WA is that it is the most obvious variable to map as it represents the landscape as seen. This is indirectly the case for the RC whose hydraulic properties may be reflected by specific landscape features but

whose dimensions are not visible. These considerations led to the revision of the methodology, presented in Chapter 3.

Subsequently, the revised RGWPM methodology was applied to fourteen sites with refugee camps/settlements in Sub-Saharan Africa. This is presented and analysed in Chapter 4 and enabled to determine that the revision was relevant. Having reduced the methodology to mapping only the WA variable or HGM landscape units may seem a dramatic simplification. However, by repeating this exercise for the many sites, it was found that the landscape unit sizes are partially correlated with hydraulic conductivity and effective precipitation, i.e. runoff and groundwater recharge. This resulted in the working hypothesis that the HGM landscape units could be used to quantify the actual groundwater potential. This potential depends on groundwater recharge, which is indeed a function of hydraulic conductivity and effective precipitation (e.g. Freeze, 1969).

Exploring the possibility of using the WA variable, i.e. HGM landscape units to quantifying groundwater recharge, required full control on the water balance. In order to establish a systematic analysis, a selection of 20 reference catchments was made, for which all water balance components are known, i.e. river discharge from gauging stations, precipitation, and evaporation from remote sensing products. All these catchments are located in the typical regolithic environments of Sub-Saharan Africa. Understanding how the HGM units dynamically evolve in reaction to the combined effect of water inputs/outputs and the bulk hydraulic properties is then the key to isolate the main missing link in the RGWPM methodology, i.e. the estimation of groundwater recharge and introducing the notion of sustainable exploitation. The goal being to overcome the data gap of missing hydraulic properties using known water inputs based on satellite products by combining them with the analysis of mapped HGM landscape units (corresponding to RGWPM units), in order to establish a relationship which leads to groundwater recharge estimate and sustainable levels for exploitation. Chapter 5 is exclusively devoted to describing the collection of water balance components in data-scarce environments and relating them to mapped RGWPM units, or HGM units. For each water balance component, a thorough literature review is conducted to justify the selected products, and, in some cases, a validity assessment is conducted.

In Chapter 6, the first evaluation of the data of the 20 reference catchments simply consisted of identifying possible relationships between HGM units and water balance components. This step allowed to express an empirical solution for estimating groundwater recharge at the catchment scale (Fig. 1.1). This solution is then applied to sub-catchments with motorized boreholes in Bidibidi to assess their sustainability. Finally, it is used to characterize the spatial distribution of groundwater recharge. This allowed for a better estimate of the sustainable groundwater potential and to add it

to the revised RGWPM methodology. The solution is easily applicable in data-scarce regions, relying only on readily available remote sensing products. However, remaining empirical, further analysis was required in order to grasp the physical meaning of the observed relationships between the landscape units and groundwater recharge.

The results obtained with the empirical solution pointed towards the general idea that the HGM concept can be used for the quantification of groundwater recharge. This led to further evaluations in the direction of this concept. The HGM landscape units and water balance components of the 20 reference catchments are again used in Chapter 7 to develop a simple analytical model expressing groundwater recharge (Fig. 1.1). This model is based on the groundwater flow equation and HGM concepts (e.g. Dunne, 1990). This second step supported the easier-to-implement empirical solution both at the catchment scale and sub-catchment scale. This allowed to conclude that combining regolithic landscape features, which are easy to map and an integral part of the RGWPM methodology, with readily available data from remote sensing products seems to be a novel manner to quantify groundwater recharge as well as runoff in data-scarce areas, where the alternatives are extremely limited or non-existent.

The main objective of this project was to explore ways of filling data gaps in Sub-Saharan Africa by introducing HGM concepts into a rapid groundwater potential mapping methodology. Ultimately, it was felt that by combining some of these concepts with the limited data available, it would be possible to provide a characterization of groundwater recharge. This raised a number of intriguing insights that are indeed encouraging and point in that direction. However, this study only scratches the surface of this idea and obviously requires further investigation. Some perspectives for future research in this field are presented in Chapter 8.

Chapter 2

Rapid groundwater potential mapping in humanitarian contexts: improving borehole implementation in basement environments

This chapter was published in Hydrogeology Journal (Scherrer, 2021) and was selected as 2021 Editors' Choice articles (Voss, 2021).

Authors: Cyrille Scherrer[1], Ryan Schweitzer[2], Marc-André Bünzli[3] and Ellen Milnes[1,2,3]

2.1. Abstract

Emergency responses in humanitarian contexts require rapid set-up of water supply. Boreholes are often drilled where the needs are highest and not where hydrogeological conditions are most favourable. The Rapid groundwater potential mapping (RGWPM) methodology was therefore developed as a practical tool to support borehole siting when time is critical, allowing strategic planning of geophysical campaigns. RGWPM is based on the combined analysis of satellite images, digital elevation models and geological maps, obtained through spatial overlay of the two main hydrogeological variables controlling groundwater potential: water availability (WA) and reservoir capacity (RC). The WA associates hydrogeomorphological features to groundwater dynamic processes, while the RC reflects estimates of the hydraulic conductivity. RGWPM maps are produced through an overlay of WA and RC with the overall groundwater potential (GWP) characterized as very low, low, medium, and high, with each zone associated to a specific water supply option. The first RGWPM map was elaborated during a drilling campaign in Northern Uganda. The average yield for the eight boreholes sited 'with' RGWPM was 35 m^3/h versus 3 m^3/h for the 92 preexisting boreholes that were sited 'without' RGWPM. Statistical comparison of the classified yields of all hundred boreholes with the RGWPM predicted-yield ranges revealed a good correlation for the low GWP unit, highlighting areas where well siting for motorised systems should be avoided. A rather poor correlation of 33% was found for the medium GWP unit, believed to be artificially induced by the numerous hand pumps (low yields) located in potentially higher yielding areas.

[1] The Centre for Hydrogeology and Geothermics of University of Neuchâtel, Rue Emile-Argand 11, 2000 Neuchâtel, Switzerland

[2] United Nations High Commissioner for Refugees, Rue de Montbrillant 94, 1201 Genève, Switzerland and Centers for Disease Control and Prevention, 1600 Clifton Rd, 30333 Atlanta GA, US

[3] Swiss Humanitarian Aid, Swiss Agency for Development and Cooperation, Effingerstrasse 27, 3003 Bern, Switzerland

2.2. Introduction: a growing need for motorised water supply systems

Globally, the number and duration of violent conflicts and forced displacements has increased significantly, from 42.7 million in 2007 to 79.5 million in 2019 (UNHCR, 2020) —*By the end of June 2022, the number of displaced persons was estimated at 103 million (UNHCR, 2022)*—, resulting in a rising number of people in refugee camps and settlements. Displaced persons are often hosted in areas with limited water supply infrastructure, where water scarcity and climate change are critical factors already affecting the host population (WWAP, 2019). To meet the increasing water demand in emergency contexts, it is key to quickly assess all possible water sources and plan sustainable water supply options in order to rapidly transition away from acute emergency phase water supply, often done with costly, unreliable and logistically challenging water trucking. In any humanitarian response, the choice of the water supply option in the early emergency phase is crucial, as it will impact the mid and long-term costs as well as issues related to water resource management.

When water demand dramatically increases due to high numbers of newly displaced people, hand pump water supply is often not the most cost-effective option. Hand pump water supply is not well suited for humanitarian situations with large displaced populations or where there is high population density—for example, over 16,000 hand pumps were drilled within only 10 km^2 in the recent Rohingya refugee crisis in Bangladesh between 2017 and 2018. Hand pumps have logistical and economic advantages, such as independence from external energy sources and relatively low capital, operation and maintenance costs. However, there are also considerable disadvantages to hand pumps—for example, their extraction rate is limited to 0.5 m^3/h, water treatment is difficult, and the time required for collection and transport disproportionally affects girls and women (Hutton et al., 2004). Water collection reinforces time poverty, disempowers women, reduces school attendance for girls, and exposes women and girls to sexual and gender-based violence and injuries associated with water carrying. With the general trend in humanitarian contexts moving towards sustainability-focused water resource management through motorized-solar driven pumping systems (e.g. Global Solar Water Initiative, UNHCR Clean Energy Challenge (UNHCR, 2021a), the target aquifer productivity has increased by an order of magnitude, from 0.5 m^3/h for hand pumps to over 5 m^3/h for motorised systems.

Target aquifer productivity is central for measuring ‘drilling success rates’, a widespread but poorly defined notion, mostly used to define if yields are sufficient to support hand pumps. It is often understood as binary, with a ‘dry borehole’ declared for yields below 0.5 m^3/h, while yields above this threshold are considered ‘successful’. If this same binary ‘drilling success rate’ definition were to be applied to motorized systems, which require yields exceeding 5 m^3/h, then all boreholes yielding

less than 5 m^3/h would have to be declared as 'dry boreholes', although they may be equipped with hand pumps; therefore, the 'drilling success' notion requires a more nuanced definition, which relates target aquifer productivity to yield ranges and to different water supply options. In essence, this means that the binary spatial 'drilling success rate' distributions ('dry' versus 'successful') for hand pumps and motorized systems, respectively are different. The spatial distribution of 'successful' motorized systems, targeting yields exceeding 5 m^3/h is of course contained within the spatial distribution of 'successful' hand pumps, since hand pumps will also function in areas yielding more than 5 m^3/h. On the contrary, motorized systems cannot be successfully implemented in areas yielding less than 5 m^3/h, while hand pumps can. As the siting process for motorised water supply boreholes requires identification of highly productive locations, it is crucial that such areas are rapidly identified on a scale that is relevant to water supply and distribution, typically within a radius of 10 km around the zones where water is needed and on a scale which allows planning of high-resolution geophysical campaigns.

The rapid groundwater potential mapping (RGWPM) methodology presented herein does not only seek to identify highly productive zones, but aims at complete mapping of areas of interest, identifying the likelihood of where and which water supply option is most adapted. The need for a tool for the rapid spatial assessment of 'yield range probabilities' associated to different water supply options emerged following a major refugee influx from South Sudan into Northern Uganda in 2017. During the acute emergency phase in 2017 water was supplied to approximately 400,000 people by as many as 630 trucks delivering 6,547 m^3/day, leading to extremely high costs and logistical challenges (UNHCR, 2017a). A drilling campaign in 2018, involving 52 boreholes for solarised water supply systems, was part of the long-term strategy for sustainable water supply. A pilot RGWPM was developed to guide the geophysical prospection for this drilling campaign and proved to be highly effective. The results of the RGWPM in Uganda were encouraging and suggested that the approach may be up-scaled and widely applicable within similar types of geological conditions found in Sub-Saharan Africa.

This paper (Chapter 2) reviews the literature on groundwater potential mapping approaches, putting the RGWPM methodology in context before focussing on the specific conceptual framework. Then, the Northern Ugandan case study is presented with the step-by-step description of the technical aspects of RGWPM. Finally, retrieved field data from Northern Uganda is used to quantify the impact of RGWPM, by comparing borehole yields of wells sited 'with' and 'without' RGWPM. The case study not only revealed substantial increase in cumulative yields for wells sited with RGWPM but also, and perhaps more importantly, high-lighted the usefulness of such maps in delimiting areas where no effort should go into well siting for motorised systems.

2.3. Embedding rapid groundwater potential mapping in the landscape of groundwater potential mapping

A recent review of groundwater potential mapping published by Díaz-Alcaide and Martínez-Santos (2019) concluded that there is no universal definition of groundwater potential and standardised method for developing maps, or commonly accepted set of units to measure the outcomes. Their review revealed that some groundwater potential maps provide an indication of the variations in groundwater storage across a given region, while other studies interpret the groundwater potential as a measure of how likely groundwater is to be found or where the highest yields may take place. The review concluded that the objective of most groundwater potential studies is to identify the optimal zone(s) for groundwater development, which is also the case for the RGWPM approach presented herein.

Díaz-Alcaide and Martínez-Santos (2019) further argued that 'potential' is related to a 'probability of something occurring' and defined it as a spatially distributed best estimate of the physical capacity of the terrain to yield enough groundwater for a given use based on a series of indirect indicators. Their analysis of 200 studies identified the following key parameters: lithology (geology), geomorphology, soil, land use, topography, lineaments, drainage and slope related variables, rainfall and groundwater recharge. RGWPM also directly or indirectly uses these key parameters.

Another characteristic of groundwater potential mapping is that variables are classified and zoned in a multi-criteria decision framework (Teixeira et al., 2015), followed by different map algebraic approaches (Ettazarini, 2007; Elewa and Qaddah, 2011), leading to a classified likelihood of attaining a target value (e.g. sufficient yield for hand pump or motorized water supply). Díaz-Alcaide and Martínez-Santos (2019) concluded that for optimal results, groundwater mapping must be used as a tool to inform fieldwork and that remote sensing techniques in groundwater exploration have an enormous potential.

The major drawback of the groundwater potential mapping approaches evaluated by Diaz-Alcaide and Martinez-Santos (2019) is the lack of validation of the maps with field data. Overall, groundwater potential maps should be used to optimise fieldwork, rather than as a low-cost substitute for local-scale surveys (Abdalla, 2012; Mandal et al., 2016). The RGWPM methodology presented hereafter is fully aligned with these conclusions, since the objective is to inform local geophysical field investigations for borehole siting. Considering the taxonomy of groundwater potential mapping approaches described by Diaz-Alcaide and Martinez-Santos (2019), RGWPM generated by the methodology presented herein are a priori high-resolution (20—100 km^2) and near-surface groundwater potential maps (depths reaching 100—150 m) with no or very little ground-

truth data. The additional and unique characteristic of RGWPM is the short amount of time required to produce the maps—just days or weeks.

2.4. Conceptual framework of RGWPM

The conceptual framework of RGWPM directly links to the overarching goals of groundwater potential maps described in the preceding, aiming at identifying different groundwater potential zones by map overlay of different groundwater relevant variables. In the RGWPM methodology, two spatial variables are defined: water availability (WA) and reservoir capacity (RC). The WA variable reflects the spatial distribution of groundwater recharge and discharge processes, while the RC variable is linked to hydraulic conductivity.

The overall objective of RGWPM is to identify which water supply options are most appropriate in a given area by mapping the two RGWPM variables and associating them to four yield classes which are correlated to water supply options: (1) the very low class for expected well yields smaller than 0.5 m^3/h, where no groundwater supply option (i.e. not even hand pumps) should be envisaged, (2) the low class for yield ranging between 0.5 and 5 m^3/h, typical for hand pump water supply (e.g. Chilton and Foster, 1995; Houston, 1992), followed by (3) the medium class, covering the range between 5 and 50 m^3/h, typical for small motorised systems and finally (4) the high class for yields exceeding >50 m^3/h, typical for large motorised systems. The choice of the yield ranges roughly corresponds to the ranges of typical submersible pump sizes required, which in turn govern the drilling diameter. Since drilling diameter has a major cost implication but will determine which maximum yield can be withdrawn, the water supply option has to be considered from the very start. Hence, the main objective of these yield ranges is to highlight the four orders of magnitude which are covered by the different water supply options, rather than pinpointing exact yield ranges. The main objective of RGWPM is to identify the most appropriate water supply option for a given location and NOT to precisely predict the yield of a specific well. The following section will explain the mapping process which relies on a qualitative assessment and spatial overlay of the variables, leading to probability distributions and not to precise predictions.

2.4.1. Water availability (WA)

In the RGWPM approach, the water availability (WA) is linked to groundwater flow and landscape features. The vast majority of landscapes result from physical and bio-chemical processes occurring in response to the interaction between the solid earth and the biosphere with surface water and groundwater. The discipline which addresses this interaction is hydrogeomorphology (e.g. Scheidegger, 1973; Sidle and Onda, 2004), which seeks to identify how different forms of water

transform different landscapes. Landscapes with their specific geomorphic features can be understood as a snapshot of the cumulative interaction between the solid earth and the main fractions into which rainfall is transformed: surface runoff and infiltration, with infiltration subdivided into evapotranspiration and groundwater recharge. Hence, specific landscape features reveal both surface and groundwater dynamic processes. Scientists interested in the understanding of surface-water systems have long recognized that drainage basins are a fundamental hydrologic feature, controlled to a large extent by their geologic framework and climatic setting (Horton 1945; Leopold et al., 1964; Chorley et al., 1984). Groundwater flow is also governed by the geologic framework, climatic setting (Tóth, 1963; Freeze and Witherspoon, 1967) and interaction with surface waters, with aquifer systems considered as fundamental hydrogeologic units (Meinzer, 1923; Heath, 1984).

Surface runoff leaves a fingerprint in the landscape by physical erosion, sediment transport and deposition, while infiltration contributes to landscape features through (bio-)chemical erosion such as weathering. For a given rainfall intensity, the proportion contributing to either physical or chemical erosion processes is related to the hydraulic properties of the earth material. A lower permeability of the substratum combined with a higher rainfall will lead to a higher physical erosion as compared to chemical weathering and vice versa.

The conceptual framework for WA involves analysing the landscape for specific hydrogeomorphological features related to such physical and chemical interaction between water and the solid earth in order to extract relevant indicators of groundwater dynamic processes (i.e. groundwater recharge and discharge). For the purpose of the WA conceptualisation, Winter's (2001) definition of three fundamental hydrologic landscape units, as shown on the left in Fig. 2.1, is very useful. This classification subdivides landscapes into three building blocks, i.e. upland, slope and lowland, each of which is related to the geologic framework and the climatic setting. These landscape building blocks are mirrored on the right in Fig. 2.1 into the RGWPM conceptualisation of the hydrologic system consisting of surface runoff, groundwater flow and interaction with atmospheric and surface water.

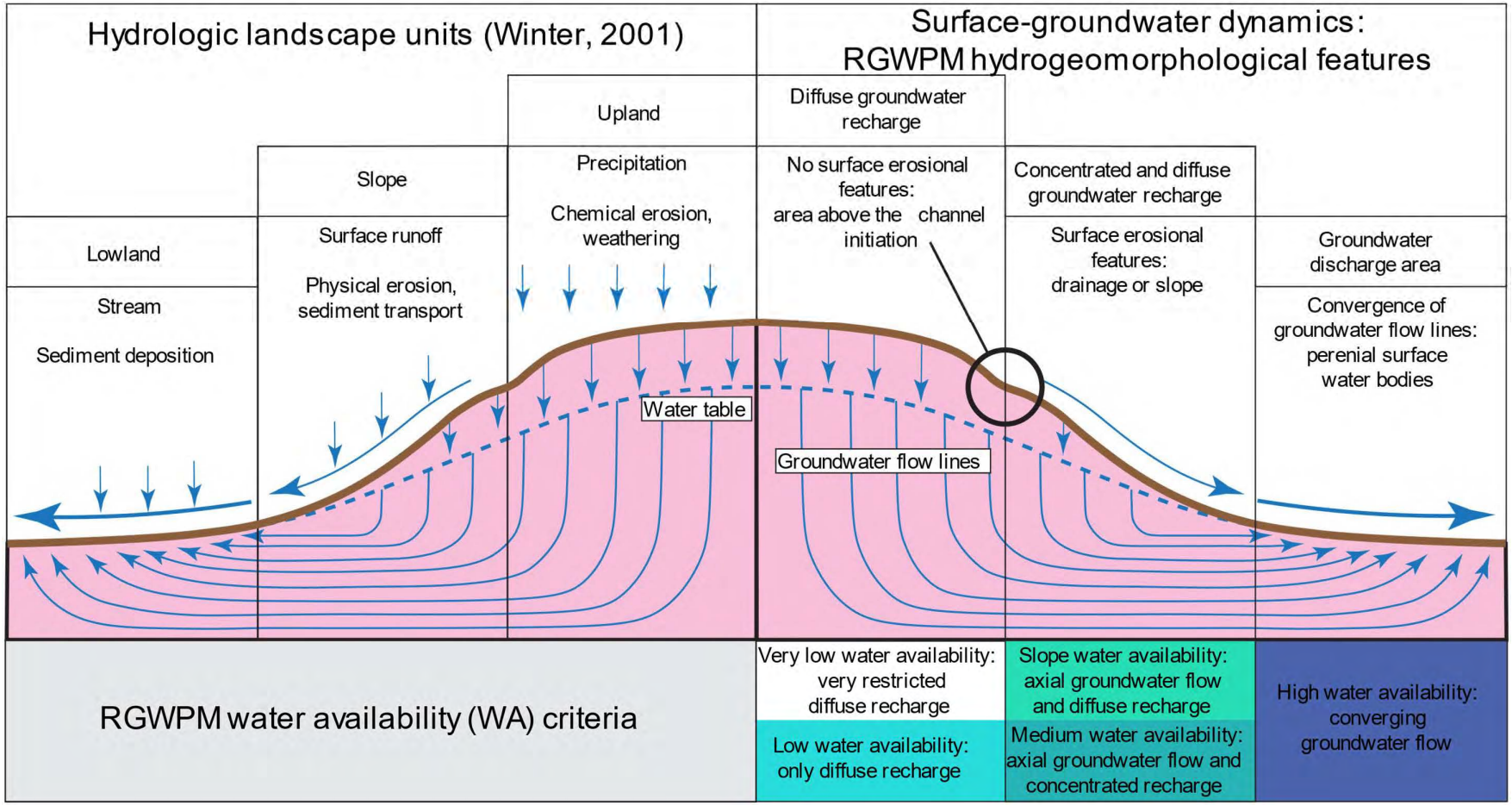

Fig. 2.1 *The left side of the figure shows a conceptual illustration of the landscape subdivision defined in Winter's (2001) fundamental hydrological units, with the upland being separated from the lowland by the valley or slope-side. The right side shows analogue units defined in the RGWPM methodology with the associated hydrogeomorphological features and groundwater relevant processes. Bottom: definition of water availability (WA) criteria in the RGWPM space.*

The upland unit as defined by Winter (2001) has no geomorphological features indicative of physical erosion and is defined by the area situated above channel initiation points. This area is characterised by diffuse groundwater recharge and divergence of groundwater flow in the RGWPM approach (Fig. 2.1), resulting in the absence of axial groundwater flow. In the RGWPM terminology, which presents groundwater availability within a landscape on a relative scale, this unit is associated with a low WA, as shown on the bottom in Fig. 2.1. In terms of water supply class, this area can at best support hand pump water supply. No groundwater supply option (very low WA class) can be expected in areas within the upland unit, where bedrock is exposed or where regolithic (weathered surface layer) thickness is thin, being areas highly unfavourable for diffuse groundwater recharge.

Within the Winter (2001) slope unit (Fig. 2.1), runoff is conveyed within the drainage systems developed through physical erosion, with sediment transport taking place. The slope unit is associated with concentrated groundwater recharge along the drainage systems and diffuse recharge on the lateral slopes combined with axial groundwater flow from the upland unit (right side Fig. 2.1). The main groundwater relevant geomorphological features characterising the slope unit are ephemeral streams, typical of groundwater being disconnected from surface-water bodies. In the RGWPM terminology for WA, this landscape unit is subdivided into medium and slope WA (bottom Fig. 2.1). The medium WA, associated with the potential for small motorised systems, is defined by the existence of both concentrated recharge along the drainage network and axial groundwater flow from the upland unit. The slope WA class within the slope unit, however, is only associated with diffuse recharge. Hence, the slope WA class, although associated with low WA, and thus with the hand pump water supply option, distinguishes itself from the low WA class of the upland unit by the presence of axial groundwater flow coming from the upland, rendering these areas more favourable with regard to groundwater availability than the upland.

Winter's (2001) lowland unit distinctive geomorphological characteristics include perennial surface-water bodies and sediment deposition. In terms of WA in the RGWPM space, perennial surface-water bodies occur where aquifers are connected to surface-water bodies, which in terms of regional groundwater flow only takes place in discharge areas where groundwater flow converges, as illustrated in Fig. 2.1. These areas are associated with the high WA class, as shown on the bottom in Fig. 2.1, designating areas, where, from a groundwater availability perspective, large motorised systems can potentially occur, depending on the hydraulic properties of the subsurface, i.e. reservoir capacity.

2.4.2. Reservoir capacity (RC)

The second RGWPM variable is the reservoir capacity (RC), which is a relative measure of hydraulic conductivity, reflecting how easily groundwater is estimated to circulate in the subsurface. Estimating hydraulic properties on a regional scale is a difficult task. The authors fully acknowledge that the approach described hereafter is simplistic; however, as previously mentioned, the objective of RGWPM does not seek to map or predict yields of specific wells, but rather estimate probabilities. For this reason, the variable name has been adapted to reservoir capacity (RC), in order to avoid any direct linkage to hydraulic conductivity. In the RGWPM approach, RC classification is done by assigning hydraulic conductivities extracted from literature (e.g. Freeze and Cherry, 1979) to lithologies and to tectonic features such as faults and fracture zones. The lithologies are identified from existing geological maps, while the tectonic features are identified using high resolution satellite images such as Bing or by combining bands from LandSat images (e.g. Sikakwe, 2020).

Just as for the WA, RC is divided into four classes (very low, low, medium and high), which are associated with yield classes and the most likely water supply options. To obtain estimated well yields, the estimated hydraulic conductivity of a lithology is introduced into the analytical solution of Dupuit for confined aquifers (Dupuit, 1857), making the assumptions that aquifer thickness is 60 m, with a drawdown of 20 m, the borehole radius is 4" (10 cm) and the average radius of influence is 15 m. These assumptions correspond to widely observed average values encountered in boreholes drilled in fractured aquifers in the Sub-Sahara. This approach produces four hydraulic conductivity ranges corresponding to the four RC classes: (1) estimated hydraulic conductivities K smaller than 10^{-7} m/s assigned to the very low RC class, (2) with K ranging between 10^{-7} and 10^{-6} m/s assigned to the low class, followed by (3) the medium class for estimates of K ranging between 10^{-6} and 10^{-5} m/s and (4) with the high class for all estimates of K exceeding 10^{-5} m/s. Table 2.1 shows these classes and the associated water supply options.

Table 2.1 *Reservoir capacity classification for estimated hydraulic conductivity ranges and estimated yield ranges, as well as associated water supply options.*

Reservoir capacity (RC)	Hydraulic conductivity K (m/s)	Estimated yield range Q (m^3/h)	Associated water supply option
High	$>10^{-5}$	>50	Large motorised systems
Medium	10^{-6}–10^{-5}	5–50	Small motorised systems
Low	10^{-7}–10^{-6}	0.5–5	Hand pumps
Very low	$<10^{-7}$	<0.5	Groundwater use may not be appropriate

Literature suggests that hydraulic conductivity in fault zones may increase as much as 2–3 orders of magnitude from the bulk rock hydraulic conductivity, depending on fracture density and connectivity (e.g. Evans et al., 1997; Bense et al., 2013). To address this challenge in the RGWPM approach, the hydraulic conductivity estimation made for fault zones is increased by one order of magnitude as compared to the surrounding host rock. This implies a shift into the next higher RC class, according to Table 2.1.

2.4.3. RGWPM: spatial overlay of WA and RC

The spatial overlay of WA and the RC determines the groundwater potential (GWP) of the RGWPM, with the lower class of the two variables dictating the GWP. Figure 2.2 shows the RGWPM matrix with the RC classes on the vertical axis and the WA classes on the horizontal axis. The mapping criteria of the two variables, as described in the previous section are summarised in the matrix and five groundwater potentials (GWP) are distinguished: very low, low, slope, medium and high which in turn are associated to the different water supply options, also mentioned in the diagonal of the matrix in Fig. 2.2. The slope GWP, although very similar to the low, due to diffuse groundwater recharge only, is distinguished as a separate unit, due to the higher WA derived from axial groundwater flow, as discussed in section 'Water availability' (Section 2.4.2).

		Water availability (WA) i.e gw. recharge or discharge				
		Very low : restricted diffuse recharge	Low: only diffuse recharge	Slope: axial gw. flow and diffuse recharge	Medium: axial gw. flow and concentrated recharge	High: converging gw. flow
Reservoir capacity (RC) i.e hydraulic conductivity, K (m/s)	Very low: K ≈< 10^{-7}	Very low GWP: Surf. water option <0.5m^3/h	Very low GWP	Very low GWP	Very low GWP	Very low GWP
	Low: K ≈ 10^{-7}- 10^{-6}	Very low GWP	Low GWP: Hand pump ≈ 0.5 - <5m^3/h	Low GWP	Low GWP	Low GWP
	Medium: K ≈ 10^{-6}- 10^{-5}	Very low GWP	Low GWP	Slope GWP: Hand pump ≈ 0.5 - <5m^3/h	Medium GWP: Small moto. ≈ 5 - <50m^3/h	Medium GWP
	High: K ≈> 10^{-5}	Very low GWP	Low GWP	Slope GWP	Medium GWP	High GWP: Large moto. ≈ >50m^3/h

Fig. 2.2 *RGWPM matrix showing the mapping criteria for the overlay of the two variables, water availability (WA) and reservoir capacity (RC), with the associated groundwater potential (GWP) and associated dominant water supply options.*

The matrix reveals that the lower of the two variables will determine the potential, e.g. low WA combined with high RC will lead to a low groundwater potential and similarly for any combination of

the two variables. Hence, the probability of high groundwater potential is restricted to zones with both high WA and high RC, explaining why these areas are the least frequently encountered.

With the mapping criteria for WA being easier to implement than for RC, it is useful to start with this variable. This allows reducing the mapped area of the RC by excluding the very low WA area, because whatever the RC in this area is, the associated GWP will be limited by the very low WA variable. Similarly, the mapping area for RC can be further reduced by excluding the low and slope WA areas for RC mapping, unless hydraulic conductivity estimates are lower than 10^{-7} m/s, i.e. very low.

2.4.4. Limitations and validity of conceptual framework

The RGWPM conceptual framework, as described previously, is only valid in topography-driven groundwater settings, in which landscape features can be related to groundwater dynamics. Haitjema and Mitchell-Bruke (2005) identified the conditions for topography-driven groundwater flow systems on a regional scale and therefore neglecting the process of interflow, based on analytical Forchheimer-Dupuit assessments (Dupuit, 1863; Forchheimer, 1986), in which several dimensionless ratios were used. The ratio between groundwater recharge (R) and hydraulic conductivity (K) relates to the geological and climatic framework. Haitjema and Mitchell-Bruke (2005) concluded that topography-controlled water tables are most likely to occur in low-permeability earth materials such as in the Precambrian basement shield covering vast areas of the Sub-Saharan belt. This vast basement complex is characterised by a typical regolithic weathering profile (e.g. Taylor and Howard, 2000) leading to continuous topography-driven small groundwater bodies within the saprolite forming the interface between the weathering front and the fresh bedrock, overlying deeper fracture zones. Very often, the weathering front and interface with the fresh bedrock is situated at depths of 20—40 m below the topographic surface (Wright, 1992).

A second limitation of RGWPM is related to its near-surface character. In areas where geological conditions within the first 150 m below the surface are highly heterogeneous, the projection of surface lithological information from geological maps cannot be done and therefore estimates for the RC variable may not be meaningful.

Nearly two thirds of all humanitarian camps and settlements located in Sub-Saharan Africa are in the geologic basement complex, for which the conceptual framework is valid. Therefore, there is considerable potential for applying the RGWPM methodology within humanitarian contexts. In the next section, the application of the RGWPM methodology in Northern Uganda is described, first

setting the scene of the general context of the case study area, before discussing step-by-step the details of the construction of the map layers.

2.5. RGWPM of the Bidibidi refugee settlements (Northern Ugandan)

The Bidibidi refugee settlements are located in Northern Uganda in the district of Yumbe, close to South Sudan and the Democratic Republic of Congo (Fig. 2.3). These settlements hosted over 280,000 refugees in 2017, mostly from South Sudan, making it one of the largest refugee settlements in the world (UNHCR, 2017b). The settlements are situated in a semiarid environment, or, more specifically, in a Tropical Savannah climate (Beck et al., 2018). Northern Uganda has a wet season from March to November and a dry season from December to February. The precipitation in this region is between 1,200 and 1,400 mm/year, while evapotranspiration is around 900—1,000 mm/year (e.g. Kyatengerwa et al., 2020). Like most of Sub-Saharan Africa, the Bidibidi settlements in Northern Uganda are located on the basement, i.e. the Precambrian shield (e.g. Wyns et al., 2015), consisting of igneous or metamorphic rocks, with a regolithic weathered carapace (e.g. Taylor and Howard, 2000). The geological map (bottom right of Fig. 2.3) shows that the Bidibidi settlements are located on the Mirian gneiss complex which are flaggy gneisses affected by the Mirian tectonics in West Nile (DGSM 2004). The western branch of the East African rift terminates at the height of the settlements of Bidibidi (Purcell 2018) and induced large regional faults, shown as red lines in the tectonic sketch in Fig. 2.3 (Thiéblemont et al., 2016). The RGWPM developed for the Bidibidi settlement area, as shown in Fig. 2.3, is located on the left margin of the rift (Horst) along regional NE—SW normal fault systems, which can be followed over tens of kilometres. These normal faults induced a graben along the east where the Nile flows to South Sudan, filled with sediments. Fresh bedrock crops out only rarely in the Bidibidi area, since most of the bedrock is covered by typical regolith resulting from chemical weathering.

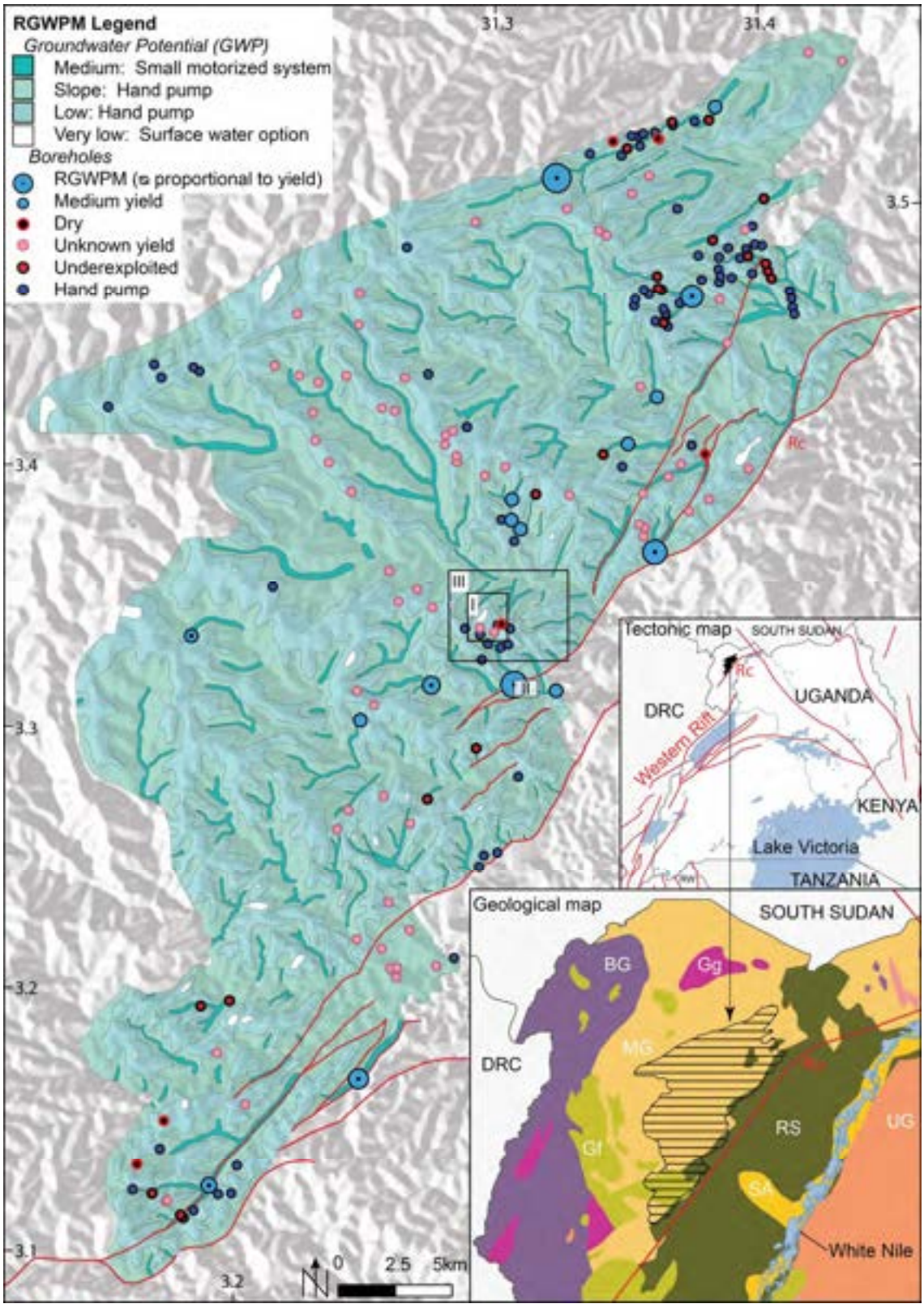

Fig. 2.3 *Caption on next page.*

Fig. 2.3 *RGWPM for Northern Uganda, in the district of Yumbe (Bidibidi refugee settlement). Four GWP zones are shown: medium (dark green), slope (green), low (light green) and very low (white). The red lines (Rc) are faults. Light blue circles with black dots: boreholes sited with RGWPM (diameter proportional to yield); light blue circles: boreholes located within medium RGWPM zones; red dots with black border: boreholes in medium GWP zone, either underexploited (yield <5* m^3/h*) or with unknown yield; black circles with red border: dry boreholes (<0.5* m^3/h*); dark blue circles: hand pumps with yield information; pink circles: boreholes with unknown yield. Zones I, II and III are three close-ups referred to in following figures. Bottom right: tectonic sketch (1:10 M) with regional faults along western branch of the East African rift (Thiéblemont et al., 2016); geology map (1:2 M) with major geological formations (DGSM 2004): BG banded gneisses, Gf granulite facies, Gg granitoid and highly granitized, MG Mirian gneisses, RS rift valley sediments, SA sediments, alluvium, black soils; UG undifferentiated gneisses; in north granulite facies, the fault is one of the regional faults of the rift. DRC Democratic Republic of Congo; RW Rwanda.*

In the early stages of a humanitarian crisis, humanitarian actors may opt to drill boreholes close to people in need of water and in the places most easily accessible to drilling rigs, without siting boreholes based on hydrogeological criteria. Since the beginning of the South Sudanese refugee influx to Uganda in 2016, hundreds of the boreholes that were drilled failed to achieve sufficient yields to warrant the installation of motorized pumps, since only a few humanitarian actors used hydrogeological investigations to site boreholes. After numerous 'dry boreholes' had been drilled, the need for strategic well siting became evident. In 2018 UNHCR carried out a major drilling campaign in refugee settlements. It was during this drilling campaign that RGWPM was first field tested (Fig. 2.3). Geophysical campaigns were planned using this RGWPM and 52 wells were drilled, with 8 of them in Bidibidi (blue circles with black dots in Fig. 2.3), in an area where already 176 wells had been drilled by numerous different humanitarian actors in 2016–2017, without RGWPM.

Figure 2.3 shows the map resulting from the RGWPM procedure for the district of Yumbe (Northern Uganda). The detailed methodology which led to this map will be discussed step-by-step in the next section. The map reveals four groundwater potential (GWP) zones: very low shown in white, low in light green, the slope GWP in green and the medium groundwater potential area in dark green. In the whole area, no high groundwater potential exists. In Fig. 2.3, the small circles represent boreholes, which existed prior to the RGWPM drilling campaign, while boreholes sited with the RGWPM are shown as blue circles with black dots with variable sizes, proportional to the yields. Three close-ups are shown in Fig. 2.3 (I, II and III) which will be referred to in the next section to illustrate specific mapping procedures.

The RGWPM map in Fig. 2.3 reveals that most wells drilled without the use of RGWPM (i.e. the small circles) are situated either in the low or slope GWP zones. The light blue larger circles with black dots show the positions of the eight wells sited using the RGWPM, which all fall within the medium GWP zone. The small light blue circles reflect wells within the medium GWP zone which were drilled prior

to the development of RGWPMs and which are motorised with yields exceeding 5 m^3/h, all of which coincide with medium GWP zones, as shown in the RGWPM. The dark blue small circles reflect hand pumps with yields of 0.5–5 m^3/h and can be seen to be mostly located in the low or slope area, while the black small circles filled with red reveal hand pumps which are located within the medium GWP area, but exploited at lower yields (<5m^3/h). These hand pumps are potentially higher yielding indicating a potential for motorisation (therefore shown as 'underexploited' in the legend). The pink circles reflect hand pumps for which no yield data exist, most of which are also located within the low and slope GWP area.

The vast data set related to the wells shown in Fig. 2.3 will be further discussed in section 'Case study Bidibidi: quantifying impact and predictability of RGWPM' (Section 2.7), which focusses on quantifying the impact and predictability of RGWPM. Statistics of cumulative yields of the wells sited 'with' and 'without' RGWPM are then discussed, on the one hand, and, on the other hand, correlations are established between the classified yield data of all wells as related to the associated GWP zones to assess a posteriori the predictability of the RGWPM. In the following, the technical aspects of the RGWPM methodology which led to the RGWPM shown in Fig. 2.3 are discussed in detail and illustrated using the Bidibidi case.

2.6. Constructing the map layers and RGWPM

In this section, the technical aspects of constructing the RGWPM are discussed. First, the WA mapping procedures are presented, followed by the RC mapping procedures, and finally the overlay of WA and RC. The mapping of the different layers of the WA and the RC was done with the QGIS 3 software, while only the interpolation described in section 'low WA' (Section 2.6.1.1) was done with SAGA GIS 2. Any mapping software allowing basic raster and vector operations are suitable for producing a RGWPM. In short, the main GIS manipulations are limited to a few subtractions of raster layers, combined with some manual corrections of morphological features using high-resolution satellite images. The satellite images used for mapping the starting points such as the Bing are brought in QGIS as XYZ tiles and the geological maps as WMS layers.

Table 2.2 summarises all the mapping steps, from 1 to 11 which lead to the RGWPM. This table shows that the mapping methodology does not follow the units from one end to the other, but rather follows the logics of mapping units starting from the easiest to map unit towards the more difficult ones.

Table 2.2 *The schematic step-by-step process, from 1 to 11, leading to RGWPM, revealing for each overlay unit which data sets were used. Figure references are given which are further discussed in the text. DEM digital elevation model; WA water availability; RC reservoir capacity.*

Map variable	Figure references 2.4–2.7	Map units				
		Very low	Low	Slope	Medium	High
Water availability (WA)	2.4	–	Step 1	–	–	–
	2.4	Step 2	–	–	–	–
	2.5	–	–	–	–	Step 3
	2.6	–	–	–	Step 4	–
	2.6	–	–	Step 5	–	–
	Required data sets	DEM, LandSat, Satellite image	DEM, Sat. image	–	DEM, Sat. image	LandSat, Sat. image
	Step 6: Water availability overlay WA: combination of steps 1–5					
Reservoir capacity (RC)	–	Step 7		–	–	–
	2.7	–	–	–	Step 8	–
	–	–	–	–	–	Step 9
	Required data sets	Geological map, LandSat, Satellite image		–	Geol. map Sat. image	Geol. map Sat. image
	Step 10: Reservoir capacity overlay RC: combination of steps 7–9					
Step 11: RGWPM: Overlay of WA and RC						

2.6.1. Mapping the water availability (WA)

The mapping procedure for the WA layer does not follow sequentially from low to high. Rather it starts with the construction of the low WA zone, within which the very low WA zone is then distinguished, as shown in Fig. 2.4. Then, in the second stage, the high WA is mapped. The remaining area reflects the slope unit, within which the medium WA is mapped. The remaining, unmapped areas then automatically fall into the slope WA.

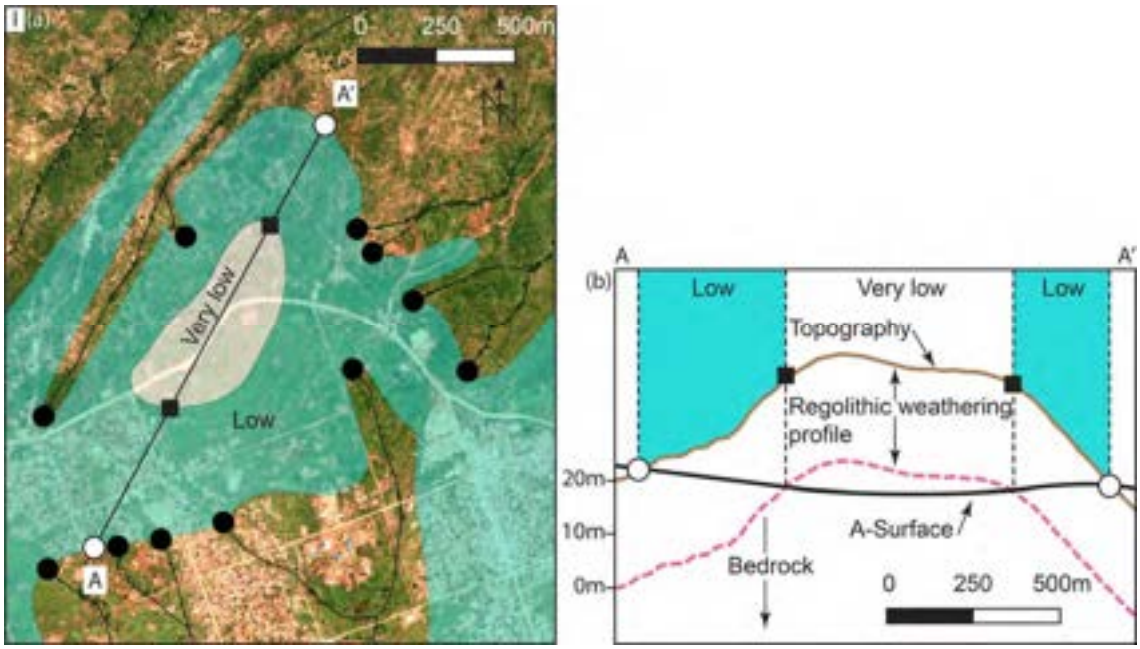

Fig. 2.4 a *Close up I of Fig. 2.3 with starting points or channel initiation points (black dots) and drainage network (thin back lines). The light green and white areas present respectively low and the very low water availability (WA).* ***b*** *Cross-section AA' showing the constructed 'A-surface' (bold black line) intersecting the topography (brown line). The hypothetical bedrock is shown as dashed pink line, 20 m below topography: intersection with A-surface delimits the very low GWP area. White circles and black squares illustrate the intersection of the A-surface with topography profile AA' delimiting the low and very-low WA, respectively.*

2.6.1.1. Low water availability

The zone of low WA corresponds to the diffuse recharge zone, which is defined by the absence of any surface-water erosional features. It is obtained by mapping all starting points (i.e. channel initiation points), as indicated by black circles in Fig. 2.4. The mapping process of the starting points is a combination of computed drainage systems using the DEM (SRTM 1 arc-second) and then manually editing and correcting the points using high-resolution satellite images. The result of this process is a distribution of points (x,y,z) defined by their coordinates and elevations extracted from the DEM. A simple natural neighbour interpolation was used to generate a surface containing all starting points, called 'A-surface', shown as a bold black line in the vertical cross-section in Fig. 2.4. The purely diffuse recharge area (low WA) is obtained by intersecting the constructed A-surface with the digital elevation model. The area which lies above the intersection of the two surfaces designates the area where no surface erosional features exist and thus qualifies as low WA zone, as shown in Fig. 2.4 as a map view (blue), as well as in the cross-section AA'.

2.6.1.2. Very low water availability

The very low WA zone is always contained within the low WA zone, i.e. within the area of the purely diffuse recharge zone and delimits areas where diffuse recharge is substantially restricted. There are two criteria that are used to map this zone: (1) outcropping bedrock or, (2) unsaturated regolithic weathering profile. Outcropping bedrock indicates that physical erosional processes dominate the weathering processes, suggesting lateral sediment transport rather than vertical infiltration. Using satellite imagery to identify exposed bedrock is one way of identifying the very low WA within the low WA. Additional remote sensing products, such as NDVI or LandSat can be used in combination, particularly in areas where intertwined vegetation and slight soil cover blur outcrops.

In most regoliths encountered across the Sub-Saharan region, groundwater accumulation is very often encountered at the interface between the weathered profile and the unaltered bedrock (Chilton and Foster, 1995). Groundwater flow along this interface can substantially contribute to groundwater resources in the low WA area but also contributes to recharge of groundwater in deeper fractured zones. Hence, in areas where the base of the weathering profile is topographically higher than the surface erosional features of the channel initiation points, i.e. above the A-surface, it is argued that the formation of a continuous groundwater body is greatly reduced. This argument has led to simply deducting from the digital elevation model 20 m, assumed this as an average depth of the regolith weathering profile where such groundwater bodies can occur (Taylor and Howard, 2000; Chilton and Foster, 1995; stippled line in cross section AA' of Fig. 2.4). Intersecting this fresh bedrock hypothetical topography with the A-surface results in the very low WA zone, being the area above the A-surface (white area Fig. 2.4).

2.6.1.3. High water availability

The high WA corresponds to discharge areas of groundwater where water is always available. Groundwater discharge areas are either connected to surface-water bodies, such as to lakes and streams, or they form springs or wetlands. Hence, the mapping process for this zone consists of mapping perennial surface-water features. The mapping process should be done using dry seasonal satellite images—as an example, Fig. 2.5 shows one of the few areas where a perennial stream could be mapped in the Bidibidi (dark blue area). The dry season in 2018 in Uganda extended from January to March, as shown in the bottom left graph illustrating the daily precipitation as obtained from Google Earth Engine (CHIRPS). A Google Earth image from 01/02/2018 (Fig. 2.5a) taken in the middle of the dry season shows where the stream becomes perennial, i.e. starts to exfiltrate. In order to cross-validate the positioning of the high WA with the Google Earth image, a composite NDVI image, also obtained with Google Earth Engine (LC08) between January and March 2018 (Fig. 2.5b), shows

healthy vegetation (high NDVI values) along this stream, indicating the presence of near groundwater or perennial surface water.

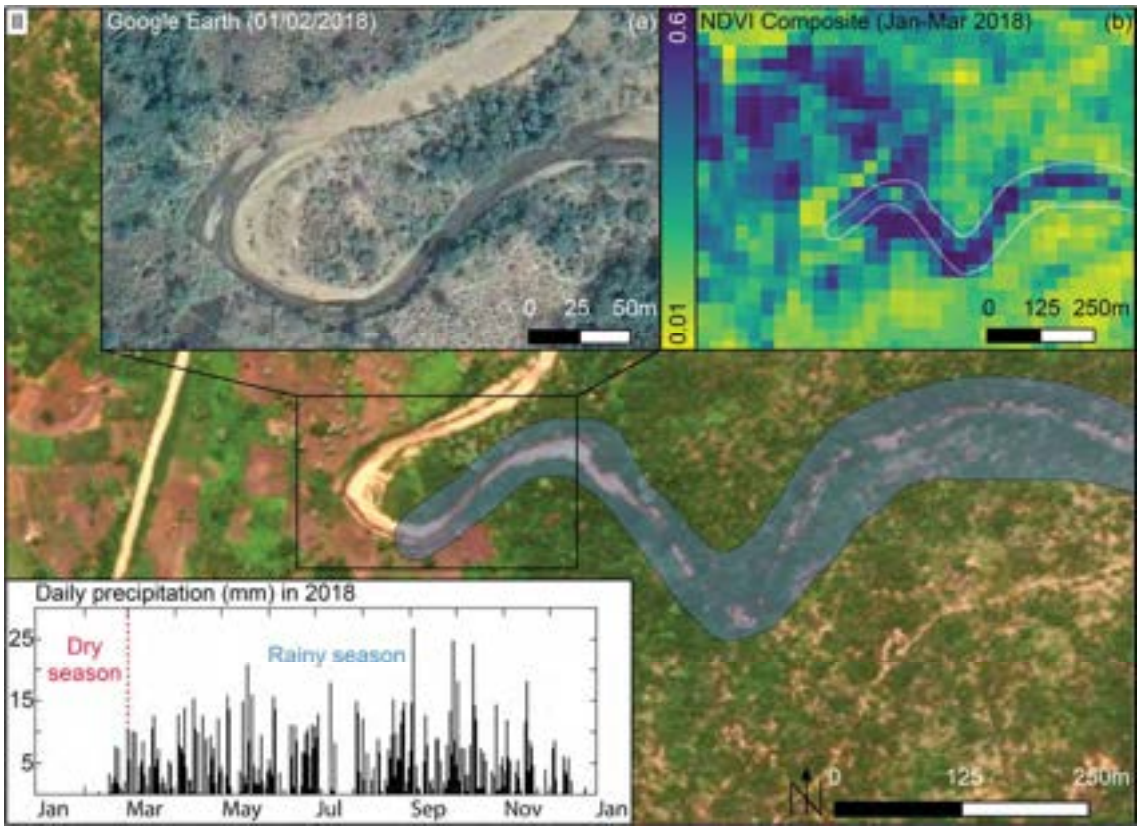

Fig. 2.5 *Close up II of Fig. 2.3 with the High WA zone (blue). This zone is defined by a perennial stream mapped using the Google Earth image of 01/02/2018.* ***a*** *The beginning of the perennial stream is where the colour of the streambed becomes darker;* ***b*** *cross-validation with NDVI composite (January—March 2018) where high (blueish) values indicate healthy vegetation due to the proximity of groundwater or perennial surface water. The 2018 daily precipitation in millimetres (bottom left) illustrates the dry season from January to March 2018.*

2.6.1.4. Medium water availability

According to the conceptual framework (Fig. 2.1), the medium WA is situated in the slope unit, along the drainage network, where concentrated recharge can take place. A method is proposed to distinguish the low WA from the medium WA, since these are adjacent in the conceptual model, meeting at the channel initiation points. If the medium WA goes all the way to the starting points, the starting point itself would belong to both the low and the medium WA zone at the same time, which is misleading. As concentrated recharge cannot really take place at the channel initiation point, where runoff only just begins, it is conceptually reasonable to start the medium WA zone at the first order junction, as illustrated in Fig. 2.6 by large light blue dots. A buffer of 100 m is drawn

around the drainage network to delimit the medium WA, coherent with the target resolution of the maps for geophysical campaigns.

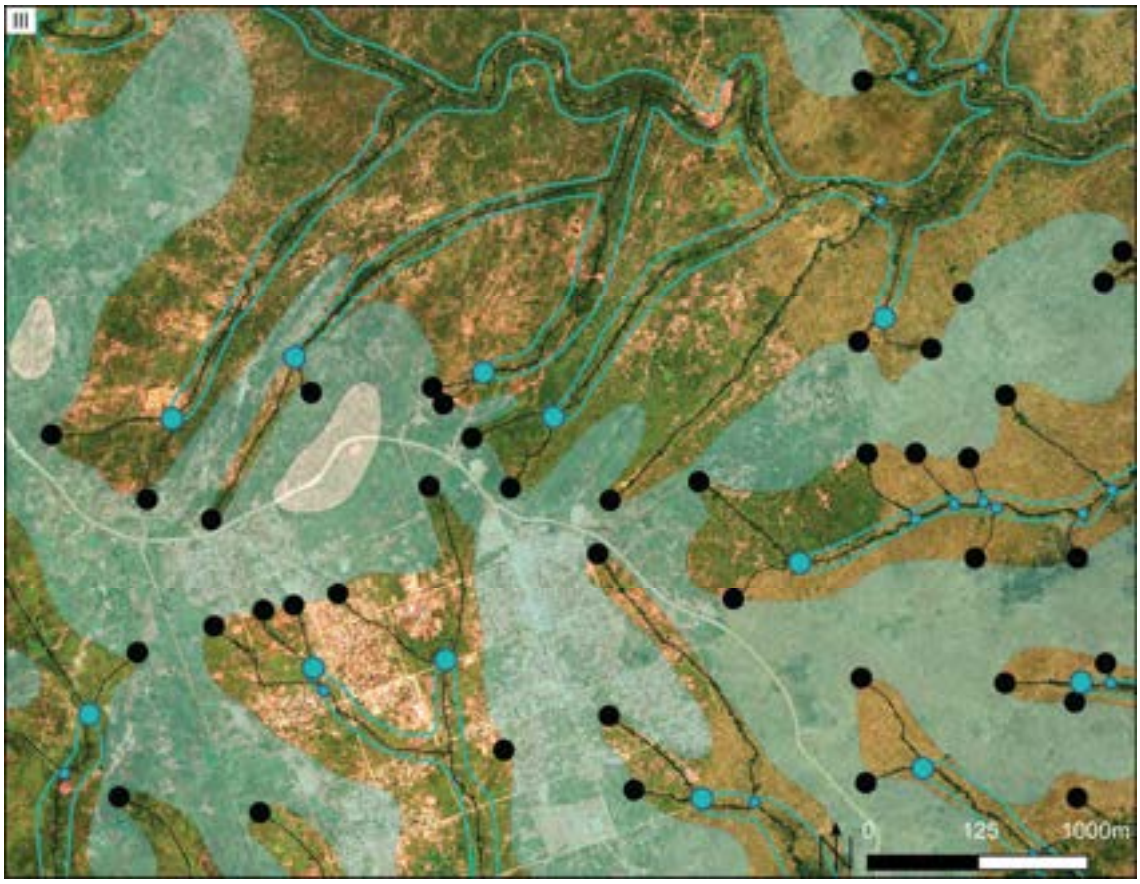

Fig. 2.6 *Close up III of Fig. 2.3 showing the mapping procedure of the medium WA. The black dots mark the starting points used to construct the low WA zones. Light blue dots indicate first order junctions of drainage channels with the basin network. Large blue dots indicate upstream second order junctions defining the beginning of the medium WA. Buffer of hundred meters around the channels is then added to define the medium WA (green lines).*

2.6.1.5. Slope water availability

As can be seen in Fig. 2.6, the only zone which remains unmapped at this stage is the slope WA area, as discussed and shown in Figs. 2.1 and 2.2. Hence, this zone is in an intermediate position between the low and the medium WA, characterised by purely diffuse recharge like in the low WA, but also with axial groundwater flow, as in the medium WA. This intermediate position has led to this separate WA class. Since it is the only unmapped area at the end of the WA mapping procedure, slope WA is simply assigned to the entire unmapped area.

2.6.2. Mapping the reservoir capacity (RC)

In this section, the mapping procedure leading to the RC layer is presented. The RC attempts to assign one of the four hydraulic conductivity classes defined in Table 2.1 to all lithologies and tectonic features in an area of interest. The errors committed in assigning hydraulic conductivities are somewhat alleviated by the fact that the estimations are made on orders of magnitude rather than on absolute hydraulic conductivities. In the RGWPM matrix shown in Fig. 2.2, the sign ≈ used for the hydraulic conductivity classes suggests that the absolute range end-member values require some hydrogeological expert judgement, and, whenever possible, on data from existing boreholes.

2.6.2.1. Low reservoir capacity

In vast areas across the African Precambrian shield covered with regolith it has been demonstrated that the saprolite has a typical hydraulic conductivity around 10^{-6} m/s (e.g. Dewandel et al., 2006). Hydraulic tests conducted in saprolite in Uganda reveal a median hydraulic conductivity of 4.6×10^{-6} m/s (Taylor and Howard, 2000) and for less specific weathered granite a range between 3.3×10^{-6} and 5.2×10^{-5} m/s has been documented (Domenico and Schwartz, 1990). Within the RGWPM this hydraulic conductivity range would ascribe the regolith to the medium RC class according to the hydraulic conductivity ranges of Table 2.1 (10^{-6}—10^{-5} m/s). However, the groundwater bodies contained within saprolite will hardly ever yield more than a few m^3/h, colloquially known as 'hand pump' country. Therefore, the RC would probably be overestimated by the use of textbook hydraulic conductivities and therefore, if hydraulic conductivities are expected to be close to the lower end of the range, it is advisable to assign it to the lower RC class. However, hydraulic conductivities should not be underestimated by setting it below a low RC either, as the majority of hand pumps across Africa prove the opposite, since they are drilled in nonfractured regolith. In both cases, this balancing act between medium and low RC is largely alleviated by first mapping the WA overlay and excluding the low and very low WA areas from the RC mapping domain.

2.6.2.2. Medium reservoir capacity

In a regolithic environment, the mappable fracture zones are assigned to the next higher RC class as compared to the host rock. In regolithic areas such as in Bidibidi, these faults and fracture zones are therefore assigned to the medium RC class, since the surrounded host rock was assigned to the low RC class. It must be kept in mind that fractured igneous and metamorphic rocks according to Freeze and Cherry (1979) are unlikely to have a higher hydraulic conductivity than approximately 10^{-4} m/s, which means that high RC in fracture zones can in some rare cases be expected. Assigning a fracture zone to the high RC class, requires, however, some sound hydrogeological rationale. In the majority

of cases, where fault zones appear as geomorphological features it seems reasonable, therefore, to assign them to the medium RC class.

In the Bidibidi case study, fault and fracture zones were mapped by identifying rectilinear lineaments using satellite images. These features range between a few hundred meters for fractures to several kilometres for the fault zones, as shown in Fig. 2.3 (red lines). The vegetation is an additional useful indicator for mapping these features, because evergreen plants such as large trees preferentially grow along them. This type of vegetation usually draws a line of darker shade of green than the surrounding smaller plants such as grass. In Fig. 2.7, the red lines show the fracture zones mapped within the medium WA (light blue). Lineaments are also encountered within low or slope WA zones, but do not have to be mapped, since the GWP will be dictated by the lower WA during the overlay process.

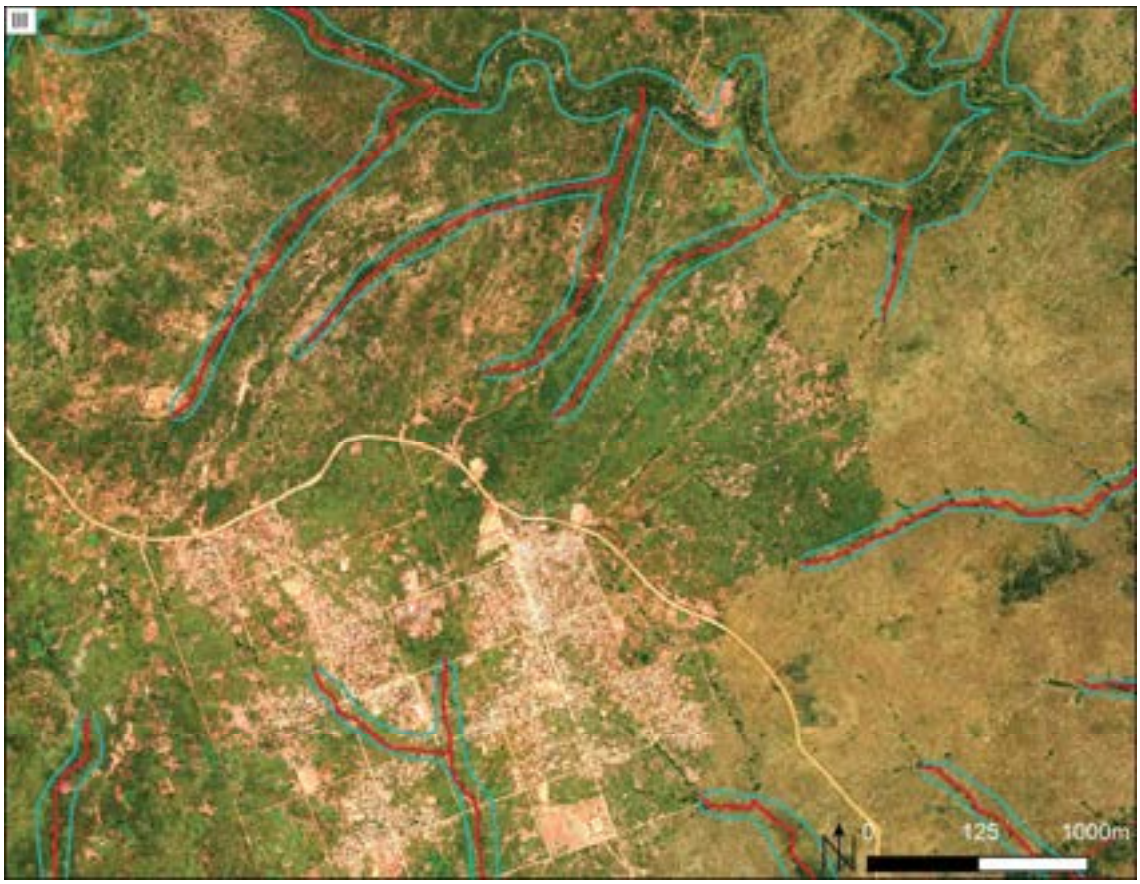

Fig. 2.7 *Close up III of Fig. 2.3 showing the lineaments related to fractures (red lines) associated with medium RC mapped within the medium WA areas (green lines).*

2.6.2.3. High reservoir capacity

The earth material which can most safely be assigned to the high RC class with hydraulic conductivity easily exceeding 10^{-5} m/s are alluvial deposits such as sand and gravels, for instance along Wadis. This type of material was not encountered anywhere in Bidibidi.

2.6.3. RGWPM: overlay of the water availability and the reservoir capacity

The WA and RC being mapped, the last step of the RGWPM methodology consists in overlaying the two variables and determining the GWP according to the matrix (Fig. 2.2) with the lower of the two classes defining the GWP. The variable WA has been mapped regardless of RC but not vice-versa. In this case study, the largest area of the RGWPM is covered by low and slope WA, which will define the GWP. Many fracture zones (medium RC) fall within the large low and slope WA zone, but did therefore not need to be mapped at all, since a medium RC will not change the resulting GWP, set by the low WA. For that reason, the fracture and fault zones were only mapped within the medium WA. In that sense, the term overlay is conceptual rather than practical, since the overlay process evolves while the mapping proceeds, which resulted in the RGWPM shown in Fig. 2.3.

2.7. Case study Bidibidi: quantifying impact and predictability of RGWPM

This section explores the impact and predictability of the RGWPM used in the Bidibidi refugee settlements to site eight boreholes (Fig. 2.3). Two different analyses are presented—the first compares the yield as well as drilled depth of the boreholes sited 'with' the RGWPM with the boreholes drilled without RGWPM (hereafter called 'existing boreholes'); the second analysis uses the data from the existing boreholes to compare the actual well yields with the RGWPM predicted yield classes. These data are independent and were not used to establish the RGWPM. This comparison allows cross-validation of the RGWPM approach by assessing the match between the RGWPM predicted yield classes and the reality.

Throughout this section, it has to be kept in mind that the quality of the borehole data retrieved from numerous humanitarian agencies is highly heterogeneous. With yield data forming the most important data set for the following analysis, interpretation seeks to account for the different 'data quality' and origins. In the best case, yield data are based on pump test interpretation and in the worst case they are simply a driller's estimate during borehole development, or simply the highest pump test yield. This was typically found to be the case for numerous pump tests carried out for hand pumps, which simply document the maximum test yield of 0.8 m^3/h as borehole yield. This kind of yield data may be misleading, because it does not necessarily reflect the actual borehole yield, but simply confirms that the highest test yield can be sustained.

2.7.1. Comparative statistics of borehole sites with and without RGWPM

The data for the comparative analysis of the eight boreholes sited with the RGWPM in Bidibidi and the 176 existing wells sited without RGWPM are shown in Fig. 2.8. Figure 2.8 is subdivided into three 'data families' shown horizontally: those with yield data, those with drilling depth data and those with both yield and drilling depth data. Data from boreholes drilled without RGWPM and those drilled with RGWPM are presented for each of these groups.

			BH sited without RGWPM (existing)	BH sited with RGWPM	All BH
Number of boreholes (BH) in RGWPM Bidibidi (Figure 2.3), with and without yield & depth data			176	8	184
BH with yield data	Number of boreholes	No. BH	92	8	100
	Cumulated	m^3/h	272	283	555
	Relative	%	49	51	100
	Average	$m^3/h/BH$	**3**	**35**	6
BH with depth data	Number of boreholes	No. BH	76	8	84
	Cumulated	m	6115	964	7079
	Relative	%	86	14	100
	Average	m/BH	**80**	**121**	84
BH with yield and depth data	Number of boreholes	No. BH	69	8	77
	Cumulated yield	m^3/h	242	283	525
	Average yield	$m^3/h/BH$	4	35	7
	Cumulated depth	m	5516	964	6480
	Average depth	m/BH	80	121	84
	Specific BH depth-yield	$m_{BH}/[m^3/h]$	**27**	**3**	15

Fig. 2.8 *Table showing the key data used for the statistical comparison of existing boreholes sited without RGWPM (first column) and for boreholes sited with RGWPM (second column) and all boreholes (last column), with subdivision of data into boreholes containing yield data and boreholes with depth data. Boreholes with both yield and depth data are shown in the dark grey table section.*

The first line in the table of Fig. 2.8 shows the total number of boreholes used for the analysis. Below, there are three separate boxes highlighted in different white-grey shadings. The white data box shows the sub-data set which includes all boreholes for which yield data are available. A total of 92 existing boreholes were used, meaning that no yield data are available for 84 boreholes, which are shown as pink circles in the RGWPM in Fig. 2.3, all of which are hand pumps. The second line in the table shows the cumulative yield, revealing 272 m^3/h for the existing wells versus 283 m^3/h for the RGWPM sited boreholes. Hence, 8% of the boreholes (8 RGWPM boreholes) extract 51% of the total yield, while 92% of the boreholes (92 existing boreholes) extract 49%. This leads to an average borehole yield of 3 m^3/h for the existing boreholes versus 35 m^3/h for the RGWPM sited boreholes.

On the other hand, considering the cumulative yield of the existing boreholes of 272 m^3/h, 135 m^3/h, i.e. 50%, are extracted from 8 motorised systems (all located within the medium GWP zone, shown as blue circles in Fig. 2.3), most probably sited based on expert advice. Adding the yields of the 16 motorised boreholes, representing 10% of all boreholes, the existing 8 boreholes (135 m^3/h) and the 8 RGWPM sited boreholes (283 m^3/h), yields 418 m^3/h, corresponding to 75% of the total yield.

This very simplistic statistical comparison definitely suggests that RGWPM siting has had a major impact on the borehole yields on the one hand and, on the other hand, that the medium GWP zone is far more high-yielding than the rest, increasing the average borehole yield by approximately one order of magnitude.

This result may be distorted by the fact that 84 existing boreholes without yield data have not been included in this assessment. If an average yield of 2 m^3/h is assumed for all these boreholes, corresponding to the average yield of boreholes with yield data located within the low GWP zone, then the cumulative yield of the existing 176 wells would be 440 m^3/h, versus 283 m^3/h of the 8 RGWPM sited wells. In that case, the RGWPM boreholes would still be extracting 39% of the cumulative yield with only 4% of the boreholes.

Belonging to the second data family are those boreholes with data on depth or drilled length. These are presented in the section shown as a light grey box in Fig. 2.8. For this analysis, 76 existing boreholes were identified containing this information. The cumulative borehole depth of the existing wells is 6,115 m, reflecting 86% of the total drilled length in Bidibidi, while the eight RGWPM sited boreholes have a cumulative depth of 964 m, corresponding to 14% of the total drilled length. The average borehole depth of the existing wells is 80 m/BH, while for the RGWPM sited boreholes it is 121 m/BH. Hence, borehole depth may also be relevant and is of course completely independent of the RGWPM approach, which does not suggest any drilling depth.

Belonging to the third data family are those boreholes with both yield and drilling depth, and are shown in the dark grey box in Fig. 2.8. The 69 existing boreholes with both data sets had a cumulative yield of 242 m^3/h, versus a cumulative yield of 283 m^3/h for the RGWPM sited boreholes, leading to average yields of 4 and 35 m^3/h and average borehole depths of 80 and 121 m, respectively. From these data, the specific borehole depth-yield was calculated, reflecting how many meters were drilled to for each m^3 of water, which is a very visual way of quantifying productivity of wells. For the existing boreholes, an average of 27 mBH/[m^3/h] is obtained, versus only 3 mBH/[m^3/h] for the RGWPM sited boreholes, again pointing towards a far higher productivity per meter drilled of the RGWPM sited boreholes. This is an operationally interesting result, pointing

both towards positive impact of RGWPM for siting and also towards positive impact of increased borehole depth (80 m for existing BH and 121 m for RGWPM sited BH).

Although the data quality is highly heterogeneous and the statistical comparison was made with only eight RGWPM sited boreholes, the results suggest that using a physically based, although simplistic approach such as the RGWPM, has had a significant positive impact on the yield in the Bidibidi case study.

2.7.2. Assessing actual borehole yields with RGWPM predicted 'yield classes'

In this section, the data set of the existing boreholes, sited without the RGWPM containing yield data, is used to assess how the RGWPM map, shown in Fig. 2.3, performs in predicting the yield range. For that purpose, it is important to leave aside the boreholes sited with RGWPM, in order to have an independent data set. The process involves extracting the 'GWP' zone associated to each existing borehole from the RGWPM and classifying the yields of all wells into the RGWPM yield classes. This leads to a matrix, shown in the table of Fig. 2.9a, in which the GWP zones of the RGWPM are shown in columns and the classified yields in lines, indicating the number of boreholes falling into each yield class. The matrix shows that 20 of the existing boreholes fall into the low GWP zone, 48 into the slope GWP zone and 24 into the medium GWP zone. In Fig. 2.9b, the individual yields of the eight RGWPM sited boreholes, all located within the medium GWP zone, are shown in a separate graph, revealing that six boreholes fall into the medium yield class (5—50 m^3/h) and three boreholes fall into the high yield class (>50 m^3/h). The average yield of 35 m^3/h is indicated with a red stippled line. In Fig. 2.9c, the data from the existing boreholes shown in the matrix in Fig. 2.9a are represented as percentages of boreholes assigned to different yield classes within each GWP zone.

(a)

				GWP zones		
			Existing BH	"Low"	"Slope"	"Medium"
BH with yield data	Number of boreholes	No. BH	92	20	48	24
	Cumulated	m^3/h	272	40	75	157
	Average	$m^3/h/BH$	3	2	2	7
Number of existing boreholes in RGWPM yield classes	"Very low" : < 0.5 m^3/h	BH/class	5	3	2	0
	"Low" : 0.5 - 5 m^3/h	BH/class	74	15	43	16
	"Medium" : 5 - 50 m^3/h	BH/class	13	2	3	8

(b)

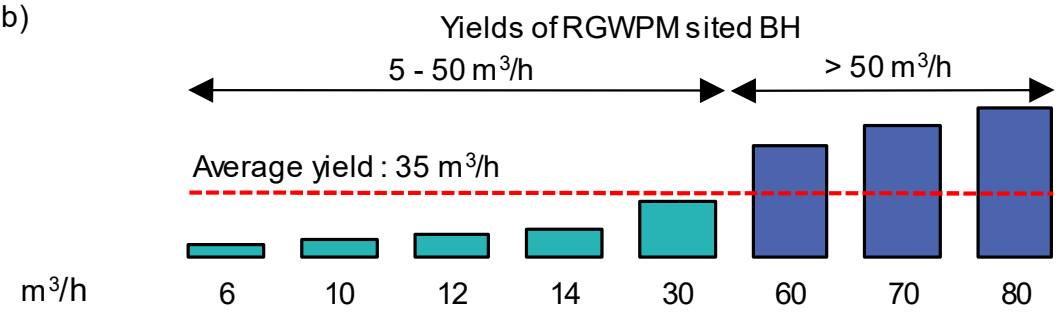

(c)

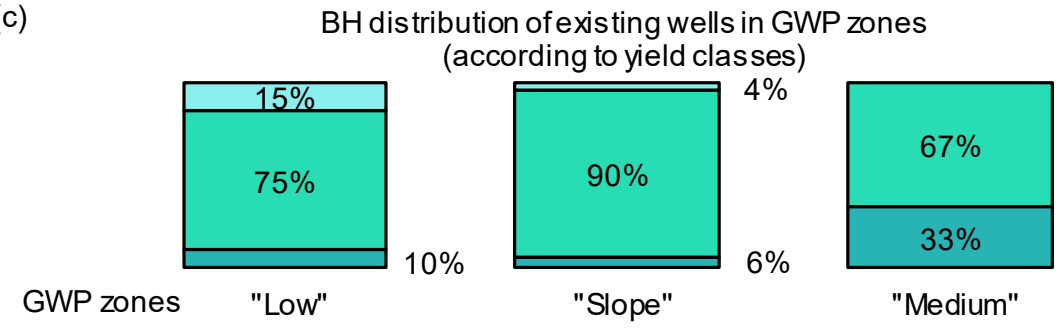

Fig. 2.9 a *Table showing the data from existing boreholes (sited without RGWPM) and subdivided into the different GWP zones (columns), low, slope and medium obtained from the RGWPM, classifying all yields according to the three RGWPM yield classes, very low (<0.5 m^3/h), low (0.5–5 m^3/h) and medium (>5 m^3/h); **b** graph showing yield data for the eight boreholes sited with RGWPM, with six within the medium yield class (5–50 m^3/h) and three boreholes within the high yield class (>50 m^3/h), with indicated average yield of 35 m^3/h; c graphs showing the relative distribution of existing boreholes within each GWP zone with the colours referred to (**a**).*

2.7.2.1. Low and slope GWP zone

In the RGWPM approach, these two GWP zones are associated with the low yield class, i.e. to yield ranging from 0.5 to 5 m^3/h. The difference between the two GWP zones, as discussed earlier, is mainly the fact that the slope GWP zone is not only related to diffuse recharge but is better positioned with respect to axial groundwater flow from the upland unit, suggesting more stable groundwater conditions with smaller seasonal variations, but not higher yields.

Figure 2.9c reveals that 15% of the 20 boreholes drilled in the low GWP zone have very low yields, <0.5 m^3/h, while 75% of the boreholes have yields falling into the low yield class, which is the class associated with the GWP zone. Only 10% of the boreholes (2 BHs) have medium yields, exceeding 5 m^3/h. This suggests a rather good predictability of the RGWPM for the low zone, with only 25% of outliers on each side.

Similar to the low GWP zone distribution, the slope GWP zone borehole yield distribution shown in Fig. 2.9c reveals that 90% of the boreholes (43 BHs) located within the slope unit, have low yields ranging between 0.5 and 5 m^3/h, with only 4% (2 BHs) having lower yields and 6% yields exceeding 5 m^3/h (3 BHs). Here again, the predictability of the RGWPM is very good.

Overall, for the low and slope GWP zones together, both zones associated with the yield range of 0.5—5 m^3/h, 85% of the existing borehole yields actually do so, while 7.5% have higher and 7.5% lower yields. Hence, the yields of these 68 boreholes could have been predicted with 85% certainty if the RGWPM had already existed at the time of drilling. A highly relevant aspect of the high predictability of the RGWPM for low yield classes is that low yield class areas can rapidly be defined, thus rapidly excluding uninteresting zones for water development.

2.7.2.2. The medium GWP zone

The medium GWP zone in the RGWPM approach is associated to yields in the range of 5—50 m^3/h, for small-to-medium motorised systems. Figure 2.9c reveals that only 33% of the 24 boreholes located in this zone having documented yields exceeding 5 m^3/h, all of which are motorised. In all, 67% of the medium zone boreholes (16 BHs, all hand pumps) have yields in the low yield class range, of 0.5—5 m^3/h. One reason for this mismatch could possibly be 'poor' predictability of the RGWPM for the medium GWP zone; however, having performed 100% for the boreholes sited with the RGWPM within the medium zone points towards another explanation. The high percentage of boreholes in the medium GWP zone having a low yield class may therefore simply be related to the fact that they were drilled to be hand pumps (all of them are), leading to low documented yields. All these boreholes are shown in Fig. 2.3 as black circles filled with red and are described as

'underexploited', since they have a medium RGWPM predicted yield class, suggesting they could be motorised (>5 m^3/h). This observation was an unexpected result of this cross-validation process, suggesting an alternative use of RGWPM to identify existing wells which could potentially be upgraded to motorised pumping or even solar pumping systems. This is highly relevant, since conversion to solar pumping is an operational priority for UNHCR and its partners. Using the RGWPM to prioritise wells to be retrofitted, concentrating on hand pumps located within the medium GWP zone, may be a significant added value of these maps.

Although the RGWPM approach has only been cross-validated in the Bidibidi case study, the results suggest that significant improvements can be made by using RGWPM and targeted geophysics. Particularly in humanitarian contexts, where the alternative is mostly 'no strategy' other than drilling rapidly and close to people. The RGWPM is believed to be a highly useful approach, which certainly has a potential to be replicated in other areas in the Sub-Saharan belt with similar geological conditions.

The Bidibidi case-study and RGWPM cross-validation process has revealed that not only is the predictability of the expected 'yield classes' quite good, allowing strategic planning of small-scale geophysical investigations, but this also highlighted that the low and slope GWP areas should be avoided for prospection, if solarised/motorised systems are targeted. A surprising but operationally significant result of this case study was also to identify numerous hand pumps situated within the medium GWP zone, suggesting that such boreholes should be prioritised if retrofitting of hand pumps to solar-powered motorized systems is envisaged.

Looking at the results presented in the preceding section, revealing significant differences in yields between boreholes sited with and without RGWPM, one is tempted to ponder on what the borehole map would have looked like in Bidibidi, if a RGWPM would have been available upon onset of the drilling campaigns during the early emergency phase.

In the humanitarian context, staff turnover is high which can result in low institutional memory and data loss. To mitigate this issue, UNHCR and its partners have developed an online database (UNHCR, 2021b). Loss of data may be one reason for the failure to get high-yielding boreholes prior to the use of RGWPM, but another reason may also be related to the lack of a common borehole siting strategy. Whatever the reason may be, the boreholes' yields are eventually translated into water production figures for refugees, which in turn are reported as indicators (minimum standard of 20 L per person per day). Hence, if wells are not adequately sited and exploited, as suggested by the aforementioned simple analysis, the derived indicators will call for additional funds to fill any gaps in the water demand. In that respect, the results obtained from the boreholes sited with the

RGWPM are highly encouraging. Moreover, the boreholes sited with the RGWPM can also support the trend in the humanitarian context towards solarisation/motorization, suggesting that it is possible to move away from the classic hand pump water supply scheme.

2.8. Conclusions

The main objective of this work was to support humanitarian efforts to site boreholes more efficiently using a methodology called Rapid Groundwater Potential Mapping (RGWPM). RGWPM is in line with the humanitarian needs during emergencies, being rapid, providing humanitarian agencies with a practical tool within days or weeks. It is also in alignment with the increasing trend towards solarisation of boreholes, which commonly requires higher yields than what hand pumps need. The mapping done in a few days delimits the groundwater potential zones and informs water supply options. The RGWPM methodology cannot be fully automated and requires an experienced hydrogeologist to be implemented. The results can be shared with site planers to allow them to factor in borehole siting with overall site plans taking into account demographical and socio-economic factors.

The groundwater potential zones of RGWPM were obtained from the spatial overlay of the WA and RC, with the lower of the two variables determining the GWP. The WA is better defined and more quickly mapped, thus limiting the area where the RC is evaluated to areas with a medium WA or high WA. The WA mapping criteria are based on a simplistic but physically grounded transposition of the conceptual framework of Winter (2001) hydrological landscape units into hydrogeological processes by the identification of geomorphological features. The RC overlay expresses the geological features as hydraulic conductivities.

The Ugandan case study results showed that although there is a degree of uncertainty related to the mapped variables, the mapped units and the groundwater potential zones based on physical processes increase success rates as opposed to alternative borehole siting strategies used by humanitarian agencies (e.g. siting based on demographic criteria). The cross-validation on the Northern Ugandan refugee settlement of Bidibidi highlights that the eight boreholes sited with RGWPM extract more than 92 existing boreholes, with average yields of 35 m^3/h as compared to 3 m^3/h for boreholes sited without RGWPM. The semiquantification of RGWPM reveals that the medium groundwater potential zones correlate with motorised systems and the low and slope zones with hand pumps.

Rapid Groundwater Potential Mapping has so far only been applied to the fractured aquifer systems In Bidibidi, in a humid to semiarid region, where the landscape dominantly results from erosional

processes linked to water. There are a number of limitations to RGWPM, with the highest uncertainty related to the mapping process of the reservoir capacity. Another limitation is that complex geological settings such as multilayered systems, cannot be addressed with this methodology. Finally, these maps do not consider existing boreholes; hence, implementing numerous boreholes within the same medium or high groundwater potential zone will always have to be associated with considerations on the sustainability of the exploitation.

The authors fully acknowledge that considering groundwater recharge and hydraulic conductivities through hydrogeomorphological classification, as done in this work, is an extremely simplified approach. Nevertheless, during acute emergencies when crucial decisions are being made which have considerable financial and operation implications, RGWPM has the potential to foster more successful geophysical and subsequent drilling campaigns. Also, it is believed that RGWPM has the future potential for establishing a common framework or approach for groundwater exploration in humanitarian situations. Since only one RGWPM map needs to be established for one area, it could even be used as a coordination tool, allowing different humanitarian actors in water supply to join efforts using a common (physically based) approach.

Chapter 3

Revised RGWPM methodology: merging the WA and RC

3.1. Introduction: rationale for revising and simplifying the RGWPM methodology

The RGWPM methodology, described in Section 2.4, is based on mapping the water availability (WA) and reservoir capacity (RC) variables independently and then overlaying them for comparison before retaining the lower of the two as the groundwater potential (GWP). The objective of this chapter is to show that the two variables as defined in the RGWPM methodology are directly correlated and that the WA can be understood as a function of the RC. Due to this relationship, it is possible to simplify the RGWPM methodology to mapping only one variable, and since the WA has a direct link to the observable landscape it becomes the preferred variable to map. The reduction of the RGWPM methodology to only mapping the WA results in a revised RGWPM methodology, with a slight tendency to overestimate the medium GWP zones. This overestimation is compensated by the immense advantage of simplifying the mapping process, rendering it even more rapid and more reproducible. In this chapter, the revised RGWPM methodology is applied to the Bidibidi case study, and the results reveal that there is no major impact on the cross-validation.

The foundation of the WA is based on the hydrogeomorphological concept (Winter, 2001), according to which the landscape can be divided into different units where certain surface and groundwater processes predominantly occur. Whereas the RC is mapped using information from geological maps and analyses involving remote sensing. In contrast to the RC mapping, the WA is deduced from the analysis of landscape characteristics which are patently visible in readily available satellite imagery (Section 2.6). The WA is mapped using the visible features resulting from surface erosional processes which shape landscapes, predominantly through the agent ‘water’. These same erosional processes dictate the hydraulic properties (RC) of the regolith. It is the connection of both the WA and RC to those erosional processes that permits the RGWPM methodology to be simplified. This correlation can be seen in the RGWPM of Bidibidi (Fig. 2.3), in which the WA and RC in all areas apart from the drainage system are identical.

Preferential physical erosion can either arise along changes in lithology or along tectonic features (faults and fractures) or in conjunction of both. Regolithic landscapes, as encountered in Bidibidi (Section 2.5), are characterised by a thick weathered layer, typical feature of chemical erosion, often acting at its base as a continuous groundwater conducting body, overlying a far less conductive bedrock (Lachassagne et al., 2021). Weakness zones are most likely caused by tectonically induced

heterogeneities in the underlying bedrock, i.e. faults and fractures, leading to preferential surface erosion along such features, shaping the drainage system (Schumm et al., 2000). Such tectonically induced 'weakness' zones are mapped and captured by the medium RC in the RGWPM methodology (Section 2.6.2) but are only captured when clearly identified and non-equivocal. This is done mainly by using high-resolution satellite imagery. This expert-based mapping procedure resulted in a high degree of disruptions in the medium GWP zones in the RGWPM of Bidibidi (Fig. 2.3), which is believed to be at least partially a bias, induced by the mapping methodology itself. A disruption of the medium GWP zone can either result from an unidentified fault or fracture zones or be related to fracture being unconnected. Hence, in the likely event that faults are not correctly identified, the medium GWP zone is artificially reduced, thereby also reducing the area where geophysical investigations could be planned for motorised systems.

With the above drawback in mind, a revised RGWPM methodology is proposed in this chapter, assimilating the entire drainage system to the medium GWP. This alleviates the difficulty of correctly identifying fault and fracture zones, while drastically simplifying the mapping procedure, but it leads to an overestimation of the medium GWP, suggesting potential fault and fracture zones within the entire drainage system. It can be argued that overestimating the medium GWP zone is rather conservative, by enlarging the spectrum for motorised system exploration, while drastically simplifying the mapping procedure.

This chapter is structured as follows: First, the rational of revising the RGWPM methodology is discussed with its implications on the RGWPM matrix (Fig. 2.2). Then, the Bidibidi case study of Section 2.7 is again used to cross-validate the revised methodology.

3.2. Revised RGWPM matrix

The underlying principle of the RGWPM methodology was described in detail in Section 2.4. It based on translating and mapping the WA, indicator of groundwater recharge and discharge processes, and the RC, understood as a proxy of the hydraulic properties, before overlaying both. The overlay yields the GWP, which is defined by the lower of the two variables. This procedure is again briefly summarized in Fig. 3.1 along with the revised RGWPM approach, which aims at only mapping the WA variable. The original mapping procedure follows three steps where the first is to map the spatial distribution of the water availability indicated by WA and then the spatial distribution of the reservoir capacity RC. Finally, the two mapped variables are overlain for comparison. At each location where the RC potential is lower than that of WA, the WA dictates the groundwater potential GWP and vice versa. However, with respect to the revised methodology, to obtain the GWP, it is now possible to skip the RC, mapping step to obtain the GWP. This is because the main assumption

that the properties of the RC are implicitly reflected in the WA, leading to RC almost always being equal or higher than the WA.

Steps	Variables	RGWPM (Chapter 2)	Revised RGWPM (Chapter 3)
1	Water avalability (WA): Spatial distributions of groundwater processes	WA	WA
2	Reservoir capacity (RC): Hydraulic conductivities of geological features	RC	RC properties reflected in WA
3	Groundwater potential (GWP)	GWP = WA if RC > WA or GWP = RC if RC < WA	GWP = WA

Fig. 3.1 *Workflow of RGWPM (Section 2.4) and the revised RGWPM methodology. The water availability variable WA represents the spatial distribution of groundwater process, and the reservoir capacity RC refers to the spatial distribution of hydraulic properties inferred from geologic features. In the case of the RGWPM methodology, the overlay of WA and RC leads to the spatial distribution of the groundwater potential GWP while for the revised version it is immediately derived from WA.*

The observation that the RC properties are reflected in the WA was reached by reconsidering all WA and RC combinations understood as the overlay process (Section 2.4) summarized above (Fig. 3.1) and assigning the GWP. The different WA and RC combinations are given in the RGWPM matrix in Fig. 2.2. Analysing each combination, it was realized that some combinations are more/less probable than others. By excluding the least probable combinations, the matrix can be simplified, resulting in a more straightforward mapping approach based on WA only. Therefore, the revised matrix is presented first before providing the rationale for its development in the next section and, finally, its implications on the mapping procedures.

The new RGWPM matrix shown in Fig. 3.2 is constructed similarly to the previous one (Fig. 2.2), where the WA variable and its classes are shown in the columns and the RC variable in the rows. The main difference between the two matrices is that the colour code of the cells giving the GWP is no longer the result of the overlay with the lowest variable dictating the GWP but is instead only that of the WA classes. The colours of the cells refer to the legend bellow the matrix indicating what type of water supply should be considered for each case. The hatched cells show WA and RC combinations that do not occur (conflicting). The dotted cells illustrate the rarely observed WA and RC combinations. If the combination is frequently encountered, the respective hydrogeomorphological unit or feature of the WA and the geological feature of the RC is given, e.g. lowland & fault. But if the combination is a typical feature itself, its common name is given, e.g. the combination of high WA,

i.e. perennial surface water in the lowland, and high RC, i.e. unconsolidated deposits, which essentially represents a perennial stream with alluvial deposits. For all the commonly encountered combinations, the potential of the two variables is compared, e.g. WA < RC.

Revised RGWPM Matrix		Water availability (WA) i.e groundwater recharge or discharge				
		Very low : restricted diffuse recharge	Low: only diffuse recharge	Slope: axial gw. flow and diffuse recharge	Medium: axial gw. flow and concentrated recharge	High: converging gw. flow
Reservoir capacity (RC) i.e hydraulic conductivity, K (m/s)	Very low: K ≈< 10^{-7}	Outcrop or very thin rego. **WA = RC**	...	...	...	...
	Low: K ≈ 10^{-7}- 10^{-6}	///	Upland & rego. **WA = RC**	Slope & rego. **WA = RC**	Drainage & rego. **WA > RC**	...
	Medium: K ≈ 10^{-6}- 10^{-5}	///	Upland & fault **WA < RC**	Slope & fault **WA < RC**	Drainge & fault **WA = RC**	...
	High: K ≈> 10^{-5}	///	...	...	Wadi or ephemeral stream **WA < RC**	Perennial stream **WA = RC**

...	Less probable WA and RC combination
///	Conflicting WA and RC combination

RGWPM legend				
Very low GWP: Surf. water option <0.5m^3/h	Low GWP: Hand pump ≈ 0.5 - 5m^3/h	Slope GWP: Hand pump ≈ 0.5 - 5m^3/h	Medium GWP: Small moto. ≈ 5 - 50m^3/h	High GWP: Large moto. ≈ >50m^3/h

Fig. 3.2 *Revised RGWPM matrix of Fig. 2.2 where the groundwater potential (GWP) referring to the colour of the cells no longer results from the variable overlay but corresponds to the WA classes. The colours refer to the legend bellow the matrix showing the type of water supply that can be considered for each case, in analogy with the RGWPM methodology presented in Section 2.4. The dotted cells represent WA and RC combination unlikely to be found and the hatched, the ones that do not exist. If the combination is encountered the respective hydrogeomorphological unit and geological feature for WA and RC are indicated (e.g. Upland & fault). In addition, in each cell, the potential of the two variable is compared and there is only one combination for which WA > RC, shown in red.*

The revised matrix shown in Fig. 3.2 resulted from examining of the most and least probable combinations of the WA and RC variables. The reason why certain combinations are less probable is that some features of one or the other variable defining the potential of the classes do not or only rarely occur together in nature. The features of the WA are the hydrogeomorphological landscape units (upland, slope, and lowland) described by Winter (2001) as shown in Fig. 2.1 as well as the outcrops and the drainage system (Section 2.6). They are related to different groundwater recharge and discharge processes which are directly translated into very low (outcrops), low (upland and

slope unit), medium (drainage system unit) and high (lowland/perennial surface water) potential classes in the matrix. For the reservoir capacity RC in regolithic environments, the features associated with the four ranges of hydraulic conductivity are outcrop, regolith, faults, and unconsolidated deposits which are also translated into very low, low, medium, and high potential classes respectively. The detailed description of the WA and RC features and how they are translated into a potential class is given in Section 2.6.

In Fig. 3.2 the combinations between the cells in the top row of the matrix, i.e. the low WA, slope WA, medium WA, and high WA classes, with the very low RC class, are reconsidered here first. The very low RC class essentially represents outcrops that are commonly found on hilltops. As one descends from the upland (low WA) into the slope (slope WA), the outcrops usually disappear since the regolith thickens downwards. For a medium WA and a very low RC to coexist is very uncommon in regolithic landscapes as it means that a drainage system is working its way through hard rock. Finally, a high WA and a very low RC is also uncommon as it essentially represents discharge from an impermeable rock.

Secondly, at the bottom of the matrix (Fig. 3.2), two combinations can also be neglected, namely the slope WA and low WA classes with the high RC class. This would mean that there is a significant amount of unconsolidated deposits (high RC) on top of the upland or slope. The probability of encountering these two cases decreases from right to left because the amount of unconsolidated deposits logically increase as one moves towards the lower part of the landscape. This is due to the erosive processes that drive the deposits downwards. In any case, according to the original methodology, the WA in these areas is always lower and therefore determines the GWP.

Thirdly, the two other cells that can be neglected in the new RGWPM matrix (Fig. 3.2) are the ones on the right, i.e. high WA with low or medium RC. These two cells, compared to the others discussed above, are probable WA and RC combinations because they can be commonly found in nature. Indeed, a high WA, i.e. perennial surface water, and a low RC, i.e. regolith, is a combination that could result in a feature such as a spring. A spring can appear almost anywhere in a landscape if certain specific hydrogeologic conditions are met, i.e. the groundwater table intersects the topographic surface (e.g. Fetter, 1980). The other combination, i.e. high WA, and medium RC is actually surface water that flows all year-round on a fault. The problem with these two combinations is that they are for the former rare and furthermore barely visible on satellite images. Indeed, a typical spring is a very small feature which, moreover, can be well hidden if there is vegetation. On the other hand, for a typical fault of a few tens of meters wide, it is difficult to see effectively if there is water crossing it.

Lastly, the combinations in the left column of the matrix (Fig. 3.2) are reconsidered, which are highlighted as conflicting WA and RC combinations. These are the very low WA with low to high RC. In the RGWPM methodology, very low WA, and RC both refer to outcropping rocks. Except that in the methodology's approach (Section 2.4), very low WA is only searched for and mapped in the uplands. This means that the combination between very low WA and low RC is simply contradictory because if outcrops have been identified in the WA mapping step, there is necessarily no regolith (low RC). In the case of very low WA and medium RC (fault), this does not make much sense either because even though some outcrops in the uplands may be fractured, they ultimately remain only outcrops. Finally, a very low WA and high RC is not possible as outcrops and unconsolidated deposits are two different features. Although the above rational seeks to explain the probability of occurring combinations, the resulting GWP for any of the combinations in the RGWPM methodology (before revision) would in any case lead to a very low GWP, with the lower of the two variables being retained.

Having eliminated the least probable, rare, and conflicting WA and RC combinations in the RGWPM matrix of Fig. 3.2, one can now turn to the most likely ones. For these combinations, the WA and RC features that dictate the potential of the classes are now given in each cell. First, combinations of low WA and slope WA with low and medium RC are considered; these are essentially the result of the absence or presence of a marked fault in the upland, slope. Second, for medium WA with low or medium RC the question is whether a drainage makes its way only through the regolith or through a fault. Finally, for cells named wadi or ephemeral stream and perennial stream, the main interest is whether or not there is a year-round stream flowing through unconsolidated deposits.

Ultimately, out of the 20 WA and RC combinations of the original RGWPM matrix (Fig. 2.2), only 9 (Fig. 3.2) are probable to occur. Considering these 9 combinations in the matrix of Fig. 3.2, it can be noticed that, with one exception, the potential of WA is always lower or equal to RC. This is indicated and highlighted in green in each cell by WA = RC or WA < RC.

The only exception where WA > RC (highlighted in red in Fig. 3.2), are areas located within the drainage system with no clearly identified fault or fracture zone (medium RC). In this case, if only WA is mapped, it actually means that one could assign a higher groundwater potential, i.e. a medium WA where it is actually low RC because of the regolith. Experience shows that it is not always easy to identify faults in a drainage system based on remote sensing. This means that the opposite problem can appear, meaning that one could miss out on mapping a fault and thus underestimate the potential that could be medium (WA = RC). To avoid such underestimation, it seems wise to only consider WA in drainage systems as well, which is certainly better defined and easier to map. Since

RGWPM are not precise well implementation tools but used to plan geophysical investigations, is another reason to avoid such GWP underestimations.

With the WA > RC exception adopted it leads to the conclusion that it is indeed no longer necessary to map the RC. In the RGWPM logic, after the overlay, the variable with the lowest potential class dictates the ultimate GWP (Section 2.4 and Fig. 3.1). This means that since the WA variable is mostly lower or equal, it alone imposes the GWP. Therefore, in the revised RGWPM matrix (Fig. 3.2), the GWP illustrated by the colours of the cells referring to the legend bellow the matrix is now drawn in each column only from the WA classes.

In nature, there are always exceptions and what is discussed above can of course be questioned. When reference is made to the most probable combination, it rather means the most frequently observed in regolithic landscapes. The two variables are often related, and the existence of one often logically depends on the other. For example, in order to form a highly productive aquifer, a thick unconsolidated layer (high RC) is required, and the sediments forming the unconsolidated deposits will naturally accumulate in the lowlands (high WA). Another example is the drainage system (medium WA) which preferentially digs its way along weakness zones (e.g. Howard, 1967) such as faults and fractures (medium RC), so here again one has a logical combination between a similar degree of RC and WA potential.

In the following, the revised RGWPM methodology, i.e. reducing the mapping methodology to WA only is applied to the Bidibidi case-study, in order to assess the impact on the cross-validation which was presented in Section 2.7.

3.3. Revised RGWPM of Bidibidi and cross-validation

Based on the above discussion, it was concluded that for the revised RGWPW methodology, it is sufficient to map the WA to obtain the GWP. In order to illustrate this revised approach, it is applied to the Bidibidi settlement as in the case study of Section 2.7. In short, the WA map from the previous RGWPM (Fig. 2.3) is used, but the overlay process with the RC is simply not applied. This resulting revised RGWPM is presented in Fig. 3.3. The revised RGWPM, along with the original Bidibidi RGWPM maps and additional information such as boreholes database etc. are available in digital format in Appendix A.

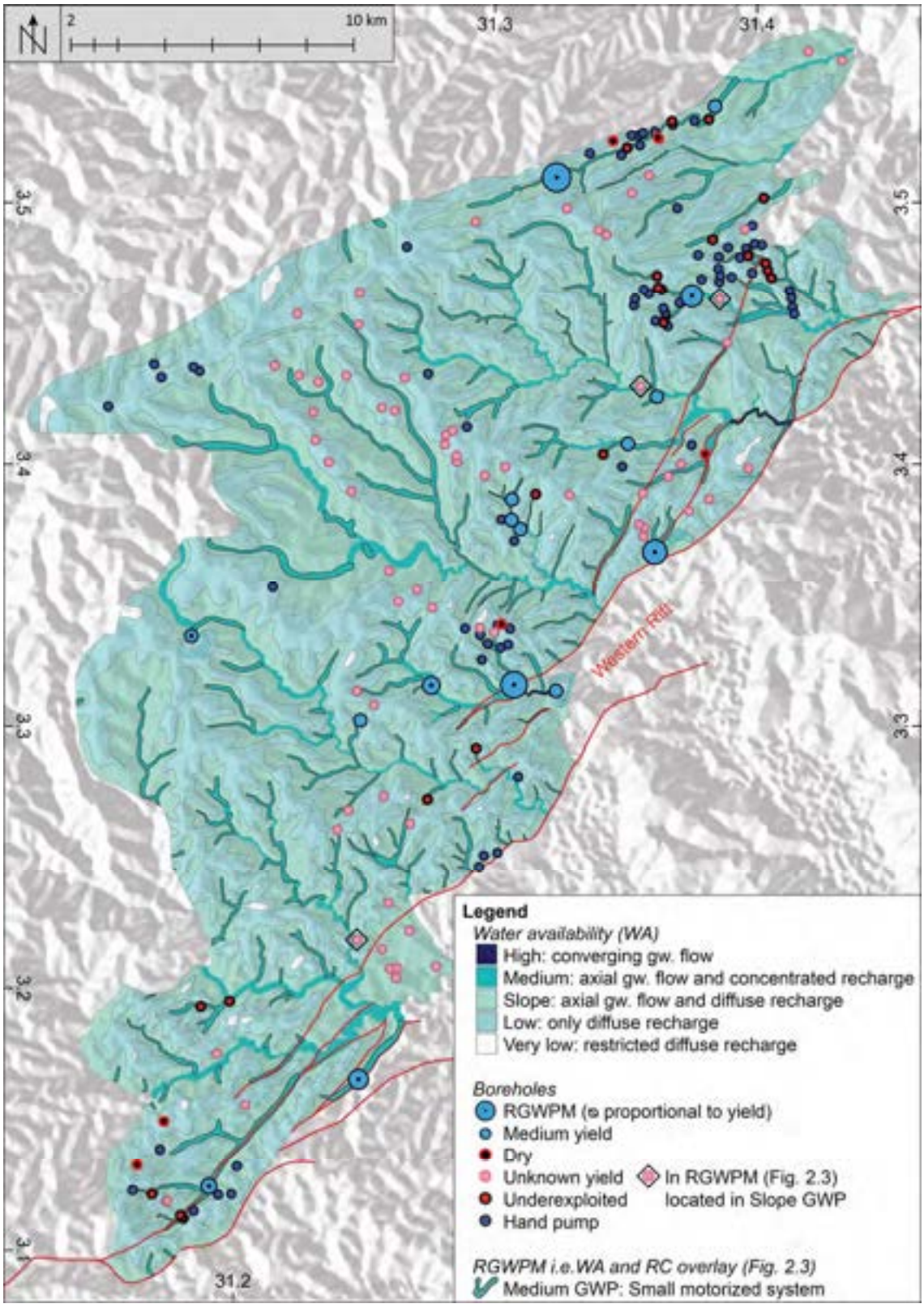

Fig. 3.3 *Caption on next page.*

Fig. 3.3 *Revised RGWPM of Bidibidi refugee settlement. Five WA zones are shown: high (blue), medium (dark green), slope (green), low (light green) and very low (white). The medium GWP from the previous RGWPM (Fig. 2.3) is presented again here for comparison with the medium WA. The red lines are faults. Light blue circles with black dots: boreholes sited with RGWPM (diameter proportional to yield); light blue circles: boreholes located within medium RGWPM zones; red dots with black border: boreholes in medium GWP zone, either underexploited (yield <5 m^3/h) or with unknown yield; black circles with red border: dry boreholes (<0.5 m^3/h); dark blue circles: hand pumps with yield information; pink circles: boreholes with unknown yield. For additional information such as the location and geological setting one is referred to Fig. 2.3.*

The revised RGWPM, i.e. a WA map is shown in Fig. 3.3 where the colours indicate the five different WA that are now the GWP zones, i.e. high (blue), medium (dark green), slope (green), low (light green) and very low (white). The boreholes encountered in Bidibidi have also been added to the map with the same colour coding as used in Fig. 2.3 and are described again in the legend and caption of Fig. 3.3. These boreholes were used in Section 2.7 for the quantification and predictability of the RGWPM methodology. Finally, the medium GWP of the previous RGWPM resulting from the overlay of the WA and RC is also indicated by the dark green zone with a bold highlighting.

The RGWPM of Fig. 2.3 obtained from the overlay of WA and RC indicating GWP zones is briefly compared here with the WA map of Fig. 3.3. For the low and slope zones, the revised approach and the RGWPM methodology produce exactly the same result. In fact, where there is a low or slope WA, if there are no outcrops (very low RC), the WA either reduces RC or remains the same depending on whether or not there is a fault (low or medium RC). In contrast, the medium WA extension is now significantly larger than the medium GWP of Fig. 2.3. This is due to the fact that one no longer distinguishes whether there is a mappable fault or not (low or medium RC) in the drainage (medium WA); thus this medium WA is no longer interrupted but ends up following the entire drainage system. As for the high GWP it remains the same and appears only very locally. Year-round surface water appears only on a short distance in the vicinity of the settlements of Bidibidi.

Regarding the cross-validation of the revised approach with the RGWPM methodology (Section 2.4), if in the end, only the extent of the medium GWP zone changes, it is enough to focus on this zone to validate this approach. For that purpose, the borehole database i.e. UNHCR database plus newly implemented boreholes (Appendix A) used in the validation of Section 2.7 can be used again here. It turns out that only 3 hand pumps now fall into a medium WA where there was low GWP in the original RGWPM (Fig. 2.3). These 3 boreholes are highlighted by squares in Fig. 3.3. The 3 boreholes have no yield data, so one cannot discuss whether there are major changes. If only 3 hand pumps are concerned, it is likely that all other boreholes in the medium WA/GWP zone were drilled on the basis of some hydrogeological and geophysical expertise as discussed in Section 2.7. This could have been effective in evaluating the locations presenting the best RC. Ultimately, this result tends to show that this revised approach produces similar results to the RGWPM methodology, but far more

'rapidly' and still with the objective that the maps are used to plan geophysical investigations and not for immediate drilling or groundwater development.

3.4. Conclusions

The revised version of the RGWPM methodology presented in this chapter results from the removal of the least likely combinations of WA and RC described via the revised GWP matrix (Fig. 3.2). It was concluded that it is only necessary to map the WA to obtain the revised RGWPM. Indeed, according to more likely combinations, the potential of WA is with one exception always less than or equal to the potential of the RC, so that in the end it prevails since the weaker of the two variables is retained in the methodology. The reason for a more or less likely combination comes from the close interdependence of the two variables from a hydrogeomorphological and geological point of view.

The particularity of the WA is that it is very easy and quick to cover large areas with the upland (Low WA) and slope (Slope WA) approach (Section 2.6). Eventually, no matter the potential of the RC in a low or slope WA zone, it will be equal or reduced to low GWP. Therefore, the revised RGWPM approach is consistent with this previous process. It is similar for the high GWP that usually occurs when both RC and WA are high (Fig. 3.2). Ultimately, compared to the RGWPM (Fig. 2.3), only the extent of the medium WA/GWP zone changes. This is because it is no longer examined in the drainage whether or not it overlaps with a noticeable fault so that the medium WA/GWP zone simply ends up following the entire drainage system. Therefore, the question that arises is what would actually happen if new boreholes were drilled in the medium WA without any RC evaluation. In this case, it has been argued that geophysics play a crucial role in deciphering the presence or absence of a fault or large amounts of unconsolidated deposits. It can be concluded that while one can easily identify most of the areas where the GWP is low only with the WA, one should perhaps not try to further reduce the medium WA zones. In fact, it is not easy to determine whether or not there is a productive fault on satellite images. This may lead to missing some promising location for the implementation of boreholes.

The revised RGWPM methodology was again applied to Bidibidi (Fig. 3.3) and re-assessed with the same borehole database (Section 2.7). Based on a brief validation, it was concluded that the revised methodology works as good as the original, since only three boreholes, i.e. hand pumps that were previously in a low GWP, are now in a medium GWP. Nevertheless, it must be concluded that in order to thoughtfully assess this revised approach, it needs to be evaluated once on a larger scale than Bidibidi. Thus, it was applied to fourteen sites in similar regolithic landscapes which is discussed in the next chapter.

Chapter 4

Applying the revised RGWPM methodology to Sub-Saharan humanitarian contexts in regolithic landscapes

4.1. Introduction

The RGWPM methodology presented in Chapter 2 was initially developed and validated in Northern Uganda, in the Bidibidi settlements (Section 2.7). A revised approach was developed in the previous chapter in which the groundwater potential (GWP) was only derived from the water availability (WA) and no longer based on the combination of WA with the reservoir capacity (RC) as in the original methodology. This revised methodology was applied using the Bidibidi data (Section 3.3). In this chapter, the revised RGWPM methodology is applied to fourteen settlements in Sub-Saharan Africa. Some maps were made on the basis of requirements communicated by UNHCR and partner organizations, while other sites were selected based on the availability of data in the UNHCR borehole database. These data are necessary to assess the general applicability and to test the assumptions underlying the new approach.

In order to evaluate the revised methodology (Section 3.2), it is needed to assess whether the GWP zones yield similarly coherent results in the different locations. This is done using data from existing boreholes, in analogy to the Bidibidi case-study (Section 2.7). However, this is a binary result, i.e. evaluating how well the mapped GWP zones yield what the methodology predicts. Therefore, in this chapter, an additional dimension is added to this evaluation which is the characterization of the climatic and hydrogeological settings of each site in order to discuss the degree of applicability of the methodology because the actual groundwater potential derives from them. The climatic setting is discussed hereafter by means of precipitation, evapotranspiration, and effective precipitation. Effective precipitation, which is the difference between precipitation and the evapotranspiration, translates into runoff and groundwater recharge and is therefore closely related to the groundwater potential. If effective precipitation is put into perspective with the hydrogeological context, i.e. with the proxy of hydraulic conductivity, it is possible to qualitatively assess the degree of recharge. (e.g. Freeze, 1969). Furthermore, the characterization of the distinct hydrogeological contexts with different hydraulic properties, i.e. varying RC potential ranges, allows for an independent evaluation of the performance of the revised approach based on WA mapping alone (Section 3.2).

A key limitation of the RGWPM methodology, as discussed in Section 2.8, is that although it may predict a range of well yields, it does not give an indication of how many boreholes could be

implemented within a given GWP zone. Therefore RGWPM maps could be misleading if there were a large number of boreholes in a limited area (i.e. GWP zone). In order to know the state of the groundwater resource, it is necessary to have a clear idea of the groundwater recharge. Currently, there is no easy and reliable way to estimate groundwater recharge in data-scarce areas without measuring instruments (e.g. Fayer et al., 1996). Most refugee camps and settlements are in fact located in poorly studied and data-scare hydrogeological terrains. Thus, a preliminary reflection on a different approach to assess groundwater recharge is presented. This approach is based on the relative sizes of WA zones, i.e. hydrogeomorphological landscape units. According to the hydrogeomorphological concept (Winter, 2001), the landscape units reflect zones where different groundwater or surface water processes occur and indicate for example that on uplands (low GWP) only diffuse groundwater recharge takes place (Section 2.4). Assuming that the same amount of effective precipitation is applied on two landscapes with different hydraulic properties, it can therefore be expected to translate into different fractions of runoff and groundwater recharge, which in turn would translate into different ratios of the mapped hydrogeomorphological units, i.e. the mapped GWP zones. If a possible relationship between the mapped GWP zones and groundwater recharge fraction could be established, this might then be the key to introduce the notion of water balance and sustainability into the RGWPM methodology, only using already existing mapped units and satellite derived information for effective precipitation. Using this as working hypothesis, the possible relationship of the mapped landscape units (i.e. GWP zones) combined with estimated groundwater recharge derived from remote sensing products are explored in the last section of this chapter, setting the scene for the subsequent in-depth study of this topic in the next chapters.

4.2. Settings of the RGWPMs

This section provides background on the 14 sites (camps or settlements) for which RGWPMs were elaborated. The sites are listed in Table 4.1 in alphabetical order, along with the country in which they are located. Table 4.1 also shows the number of refugees living in each camp and settlement. These figures, obtained from UNHCR fact sheets and/or ReliefWeb, are not updated annually and should be considered with caution. Table 4.1 also shows the number of operational boreholes in each camp, as well as the cumulative yield obtained from the UNHCR WASH GIS database. All RGWPMs elaborated for these sites are presented in Appendix B and given in digital format but were also uploaded online to the UNHCR WASH GIS database to be available for future drilling (https://wash.unhcr.org/wash-gis-portal/).

Table 4.1 *List of camps and settlements with the country for which revised RGWPMs were elaborated. The number of refugees living in each camp or settlement is also indicated, as well as the number of boreholes and their cumulative yield.*

Camp or settlement with RGWPM		Country	Nb of refugees*	Nb of boreholes	Cumulated yield [m^3/h]
1	Adjumani	Uganda	243292	54	136
2	Bidibidi	Uganda	243292	100	555
3	Boyabu	DRC	15524	18	58
4	Dzaleka	Malawi	44000	6	18
5	El Radoon	South Soudan	22314	8	36
6	Farchana	Chad	31104	9	69
7	Goudebou	Burkina-Faso	10536	3	25
8	Goz Beida	Chad	7000	**	
9	Kakuma	Kenya	173742	17	415
10	Kyangwali	Uganda	136741	100	253
11, 12	Modale + Yakoma	DRC	6455	**	
13	Tigray (3 camps)	Ethiopia	28424	11	108
14	Timangolo	Cameroon	7202	11	13
* ⚠ UNHCR or ReliefWeb estimates for different years					
** New camps and boreholes to be implemented					

Hereafter, the general geographical situation of the sites where RGWPMs were elaborated is presented first, followed by the specific climatic and hydrogeological setting of each site. In Fig. 4.1, the small map (Fig. 4.1a) shows the African continent, highlighting in grey the nine countries where the RGWPMs are located and indicated by black circles with white contours. All refugee camps or settlements in Africa are indicated with red dots. Figure 4.1b, presents the specific locations of the sites. The base map in Fig. 4.1b illustrates the broad environmental framework of Africa where the four colours, red, orange, yellow, green, and blue, indicate hyper-arid, arid, semi-arid, dry-sub-humid, and humid regions, respectively (UNEP, 1997). This framework is simply used here to illustrate that all sites and most of the camps or settlements are located in Sub-Saharan Africa. Around 15° north latitude, arid and semi-arid regions mark the limit with the Sahel (e.g. Beck et al., 2018).

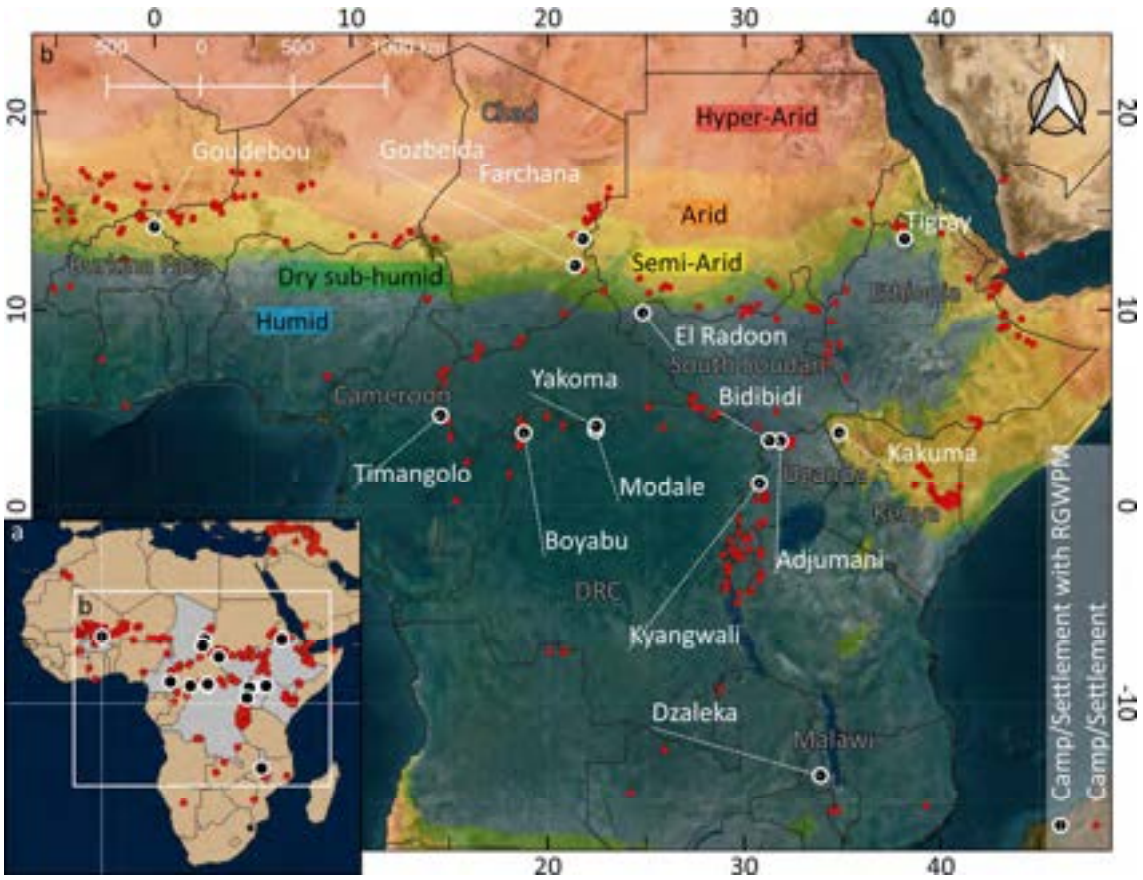

Fig. 4.1 *Location of the 14 sites (camps or settlements) where RGWPMs were elaborated.* ***a*** *Map of Africa showing in grey the 9 countries where the sites indicated by black circles with white contours are located.* ***b*** *Map showing the exact location of the sites with the names of the camps or settlements. In both maps the locations of all camps or settlements of Africa are shown with red dots. In* ***b*** *the colours of the base map refer to the general environmental framework where: red indicates hyper-arid, orange arid, yellow semi-arid, green sub-humid, and blue humid.*

4.2.1. Climatic framework

The climatic setting of the sites (Table 4.1) where the RGWPMs were realised is discussed hereafter by means of precipitation, evapotranspiration, and effective precipitation. Precipitation data were obtained with Google Earth Engine (GEE) and the Climate Hazards Centre InfraRed Precipitation with Station data (CHIRPS). Evapotranspiration data have also been obtained from GEE with the Moderate Resolution Imaging Spectroradiometer (MOD16A2 Version 6). For both, the annual mean values were generated based on a 10-year period, from 2010 to 2020. The technical nature and accuracy of these data are addressed in detail in Appendix C.3. In the graph in Fig. 4.2, the precipitation (P), evapotranspiration (ET) and the effective precipitation (P_{eff}) are represented and the average values given for each site. Evapotranspiration is given as negative values to illustrate the

fraction that is lost and yielding the effective precipitation ($P - ET$), shown as black line. The sites have been ranked according to increasing effective precipitation.

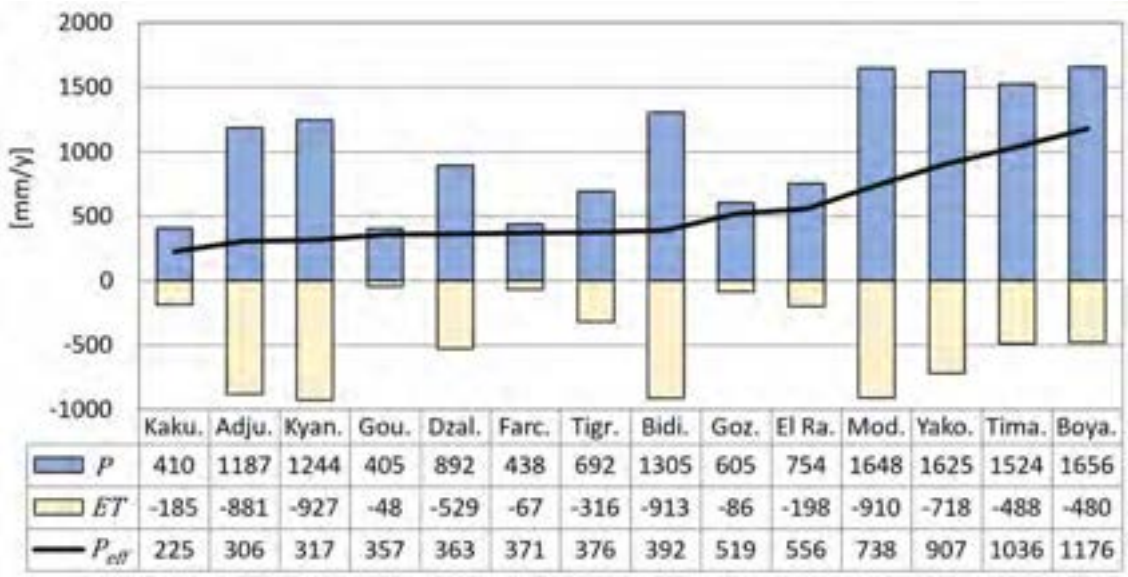

	Kaku.	Adju.	Kyan.	Gou.	Dzal.	Farc.	Tigr.	Bidi.	Goz.	El Ra.	Mod.	Yako.	Tima.	Boya.
P	410	1187	1244	405	892	438	692	1305	605	754	1648	1625	1524	1656
ET	-185	-881	-927	-48	-529	-67	-316	-913	-86	-198	-910	-718	-488	-480
P_{eff}	225	306	317	357	363	371	376	392	519	556	738	907	1036	1176

Fig. 4.2 *Graph and table presenting the annual average precipitation (P), evapotranspiration (ET), and effective precipitation (P_{eff}) for the time period 2010–2020 for the fourteen sites (camps or settlements, Fig. 4.1) for which RGWPMs were elaborated.*

In the table in Fig. 4.2, precipitation (P) ranges from a minimum of 405 mm/year at Goudebou to 1656 mm/year at Boyabu. For the evapotranspiration (ET), the minimum is again found at Goudebou, where it is 48 mm/year, and the maximum is at Modale, where it reaches 910 mm/year. Thus, the ranges are large, for precipitation it is 1251 mm/year and for evapotranspiration it is 862 mm/year. In between the extremes, the precipitation and evapotranspiration values are well distributed amongst the 14 sites. Effective precipitation ($P - ET$), shown as a black line has been ranked from the lowest to the highest value. It varies between 225 mm/year in Kakuma to 1176 mm/year in Boyabu, hence a factor of 5 between the extremes. The effective precipitation can be seen as the net water balance, either transformed into runoff or into groundwater recharge. The latter is required to determine the sustainable groundwater potential. If there is such a difference in effective precipitation from one place to another, variation in the sustainable groundwater potential can also be assumed to be significant. However, in order to approach this subject, one must first have a grip on the hydrogeological context, which will be done in the following section, before focussing on a thorough assessment of groundwater recharge, the topic of the coming chapters.

4.2.2. Lithologcial and hydrogeological framework

The fourteen selected sites are located in Sub-Saharan Africa, where regolithic environments dominate (e.g. Twidale, 1990). The unique aspect of regolith is that the hydrodynamic properties have been thoroughly studied (e.g. Lachassagne et al., 2021). Indeed, the main aquifer transmitting most of the groundwater is located between the base of the regolith and the unweathered rock Thus, in Section 2.4 since the methodology was designed in these environments, it was simply proposed that it is valid for regolithic landscapes typical in Sub-Saharan Africa, characterised by topography-driven groundwater flow. Although the characteristics of the regolith are similar, i.e. forming a more or less thick weathered carapace, the underlying unweathered rock can be of very different nature. This is indeed the case for the different sites where the revised RGWPM methodology has been applied and therefore presents an ideal situation to assess its broader application throughout Sub-Saharan Africa.

The hydrogeological setting of the RGWPM maps is presented in Fig. 4.3, where, for each site (Table 4.1), the simplified dominant lithologies from which one has deduced a hydraulic conductivity based on literature values are listed (Freeze and Cherry, 1979). The lithological information was derived from various geological maps. Supplementary information such as the source, author etc. is found in Appendix B. According to a lithological synthesis, a first category was identified consisting of plutonic and metamorphic rocks with for which an average hydraulic conductivity of $10^{-7} - 10^{-6}$ m/s was assigned. In this first category, for sites (Modale, Timangolo and Yakoma) that do not show outcrops (very low WA), it was assumed that there must be a significant regolithic layer. The second category includes a mixture of volcanic to volcano-sedimentary and metamorphic rocks. A hydraulic conductivity range of $10^{-6} - 10^{-5}$ m/s was attributed typical for fractured basalts. Finally, the third category includes sites with unconsolidated lithologies so that the hydraulic conductivity range is the highest, ranging between $10^{-5} - 10^{-4}$ m/s.

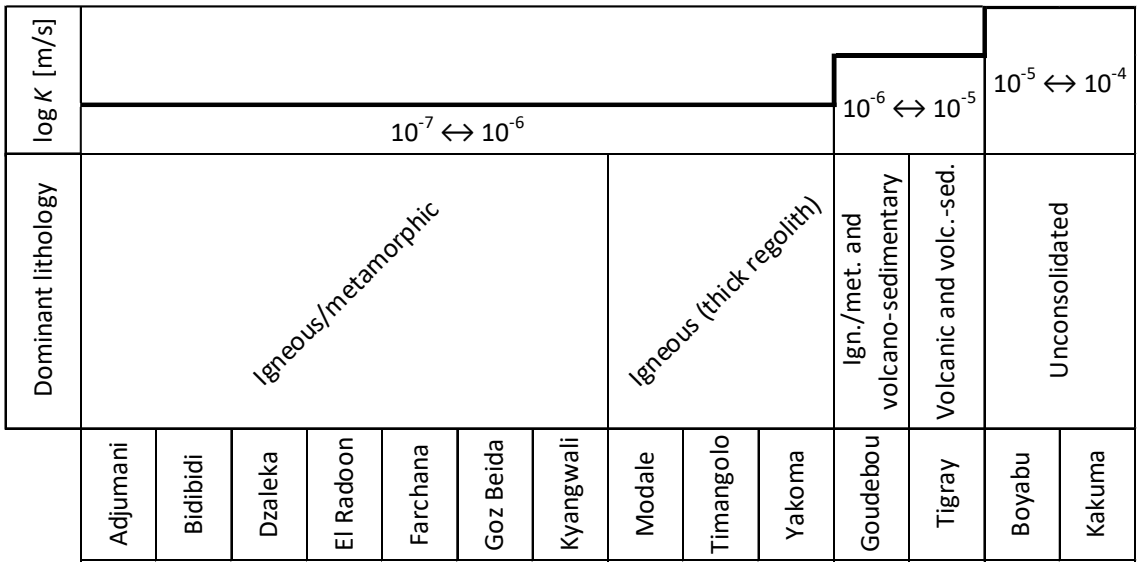

Fig. 4.3 *Dominant lithology and associated hydraulic conductivity (K) range (Freeze and Cherry, 1979) encountered at the fourteen sites (camps or settlements, Fig. 4.1) for which RGWPMs were elaborated.*

According to Fig. 4.3, of the 14 sites, 10 are located in similar lithologies, i.e. in the first category of igneous and metamorphic rocks, which in turn have similar hydraulic properties. However, considering the other sites, the hydraulic conductivity varies between 10^{-6} and 10^{-4} m/s. This implies that it differs by three orders of magnitude. In the original RGWPM methodology, described in Section 2.4, the geological framework is used to characterize the bulk hydraulic conductivity (e.g. Freeze and Cherry, 1979) of the RC. This bulk hydraulic conductivity then determines the one of the more permeable features, such as faults or the alluvial deposits in wadis, which are assigned to a higher order of magnitude of hydraulic conductivity. In the revised RGWPM approach presented in Section 3.2, it is stated that it is no longer necessary to consider or map the RC because the WA alone reflects the properties of either and is thus sufficient to characterize the GWP. The boreholes at each site provide an ideal data base to test this assumption and study the actual implication of such an important range of hydraulic conductivity in combination with the significant variation in effective precipitation.

4.3. Validation of the revised RGWPM methodology

The predictability of the revised RGWPM methodology (Section 3.3) is quantified hereafter with the entire analysis shown in Table 4.2. In this table, the first group of columns (Borehole (bh) database), indicates for each site (Table 4.1) the available borehole data, which are the number of boreholes, the number of low and medium yielding boreholes (i.e. below or above 5 m^3/h), the cumulated and average yield. After giving this information individually for each site, the total of the different categories is shown in the last row. The three groups of columns labelled low, slope and medium

GWP zone, are structured in the same way as the real borehole data base and present the individual GWP zone of each location in which the boreholes are located. In this table, only the number of boreholes located within the mapped low and medium GWP zones is shown since none of the boreholes has a high yield (exceeding 50 m^3/h). In addition, only the low, slope and medium GWP zones are shown as none of the boreholes at the 14 sites were found to be in a very low or high GWP zone. The bottom row of the table, indicated as 'predictability' indicates the accuracy of the revised RGWPM methodology in predicting the actual borehole yield, i.e. the percentage of low and medium yielding boreholes that are actually located in a low or slope (both low GWP) and medium GWP, averaged for all locations. The locations of the boreholes are shown in the maps attached in Appendix B and additional data for the individual boreholes are provided in digital format.

Table 4.2 *Quantification of the revised RGWPM methodology. The first group of columns (Borehole (bh) database) indicates for each site the number of boreholes within the different yield classes, above or below 5 m^3/h, as well as the cumulated and average yield. The three other groups of columns, i.e. low, slope and medium GWP count how many boreholes located within the respective GWP zones have yield ranges below 5 m^3/h (nb low), or above (nb medium). The bold numbers reflect the average yield of boreholes located within the predicted yield class. The bottom row (predictability) indicates the accuracy of the revised RGWPM methodology, i.e. the percentage of low and medium yielding boreholes that actually fall into the low or slope (both low GWP) and medium GWP zones, averaged over all sites.*

Borehole (bh) database						Low GWP zone < 5 m^3/h					Slope GWP zone < 5 m^3/h					Medium GWP zone > 5 m^3/h				
Camp/settl.	Number (nb)	Nb low < 5 m^3/h	Nb medium > 5 m^3/h	Cum. Yield m^3/h	Ave. Yield $m^3/h/bh$	Number	Nb low	Nb medium	Cum. Yield	Ave. Yield	Number	Nb low	Nb medium	Cum. Yield	Ave. Yield	Number	Nb low	Nb medium	Cum. Yield	Ave. Yield
Goudebou	3		3	25	8											3		3	25	**8**
Dzaleka	6	6		18	3	4	4		9	**2**	2	2		8	**4**					
El Radoon	8	6	2	36	4	6	6		25	**4**						2		2	11	**6**
Farchana	9	3	6	69	8						2	2		1	**1**	7	1	6	67	**10**
Tigray	11	1	10	108	10						3	1	2	15	**5**	8		8	93	**12**
Timangolo	11	11		13	1	11	11		13	**1**										
Kakuma	17		17	415	24											17		17	415	**24**
Boyabu	18	18		58	3	18	18		58	**3**										
Adjumani	54	49	5	136	3	37	34	3	91	**2**	10	8	2	30	**3**	7	7		15	**2**
Kyangwali	100	93	7	253	3	57	55	2	77	**1**	30	30		37	**1**	13	8	5	139	**11**
Total	237	187	50	1130	5	133	128	5	273	**2**	47	43	4	92	**2**	57	16	41	765	**13**
Predictability (i.e. nb low or medium yielding bh in respective GWP zone)						**96%**					**91%**					**72%**				

In Table 4.2, according to the first group of columns presenting the dataset, the boreholes are unevenly present at each site and their number vary between 3 to 100 (Goz Beida, Kyangwali). However, considering the whole dataset, a total of 237 boreholes can be counted for this analysis. The vast majority of boreholes, 187, are in the low yield class (< 5 m^3/h), accounting for almost 78% of the boreholes but only 32% of the yield while only 50 boreholes, 22% of the total number of boreholes fall into the medium yield class, extracting 68% of the cumulated yield. The average yield of each site varies considerably, ranging from 1 to 24 m^3/h. The average yield of all boreholes falling into either the low or slope GWP zones are 2 m^3/h, while it is 13 m^3/h for the boreholes falling into the medium GWP zone.

According to Table 4.2, in the groups of columns of low, slope and medium GWP zones at each location, the average yields of boreholes fall fairly well within the predicted yield classes. In fact, for the low and slope GWP zone the average yield is between 1 and 5 m^3/h which is in the range (0.5 and 5 m^3/h) of what the revised RGWPM methodology predicts. Regarding the average yield of the medium GWP zones, with the exception of Adjumani, all have a yield that can indeed be associated with medium GWP (5 and 50 m^3/h) as it varies between 6 and 24 m^3/h.

In Table 4.2, the boreholes that fall in the low GWP zones return an average yield of 2 m^3/h which is actually in the middle of a low potential yield class. In this zone, out of the 133 boreholes, only 5 (Adjumani and Kyangwali) have a yield exceeding the predicted low yield range, which means that the potential of this zone has been predicted with an accuracy of 96%. The average yield of the slope zone is also 2 m^3/h and thus it is also within the range of a low potential yield class. For this zone, out of the 47 boreholes, 4 (again Adjumani and Tigray) have a yield exceeding the predicted low yield range, leading to an overall predictability of this zone of 91%. The boreholes in the medium GWP zone present an average yield of 13 m^3/h, falling well into the predicted range of a medium yield class. However, out of the 57 boreholes, 16 are hand pumps, 8 in Adjumani, 7 in Kyangwali and 1 in Farchana have a lower yield than predicted by the revised RGWPM methodology, i.e. medium yield class. These 16 boreholes lead to a large error in the overall predictability so that it was only possible to predict the potential of this zone at 72%.

The above analysis indicates that overall, the revised RGWPM methodology performs well and gives similar results as Bidibidi in Uganda (Section 3.3). In fact, the low and the slope GWP has been predicted with an accuracy of 96% and 91% respectively, but the potential of the medium GWP zone can only be correctly captured at 72%. However, all the low yielding boreholes in these medium GWP zones are hand pumps. As already discussed in Section 2.7, hand pumps located within the medium GWP zone may easily bias the cross-validations, since the assigned yield in the data base

may not actually reflect the safe yield of the well but simply the exploitation rate, limited by the hand pump itself.

If the low and slope GWP zones have been predicted so accurately, it can be explained by the fact that the largest part of the camps and settlements are located in these zones. Camps and settlements are placed uphill, for obvious construction and engineering reasons, where the GWP is indeed mostly low. Therefore, if the usual strategy of drilling as close to people as possible is applied to these places, it will obviously lead to low yielding boreholes.

The low and slope GWP zone make up most of the landscape (e.g. Fig. 3.3). The remaining part, which is the medium GWP i.e. the drainage network is much thinner. This disproportion between the low, slope and the medium GWP raises the question of the resolution of the mapping which may explain the lower correlation (72%) found for the medium GWP. This lower correlation is here, as in the Bidibidi case study, mainly attributed to the fact that the majority of the boreholes used in these analyses are hand pumps and therefore should not have a higher than low yield. Alternatively, this error can indeed be explained by the mapping approach itself. It is likely that when mapping the drainage network for the medium GWP, the boundary is drawn a few tens of meters away from the actual extension of the drainage. In addition, the spatial resolution of the data, whether from DEMs or satellite images, is also subject to bias with respect to reality. This could therefore lead to some hand pumps on the slope being artificially included in the medium GWP and thus disturb the validation.

This resolution problem, which is mainly due to manual mapping, also justifies foregoing more complex statistical analysis than that presented here and summarized in Table 4.2. It would be biased from the outset because the revised RGWPM methodology is indeed an expert-based approach. This means that the best way to evaluate this methodology in an unbiased manner would be to have a large number of people replicate these 14 maps and compare their results. However, it must be remembered that the original idea of RGWPM was to incorporate some basic hydrogeological principles without the pretention of providing the most accurate groundwater potential mapping tool, but which would certainly give better results than simply drilling next to people, which is broadly demonstrated by this simple statistical evaluation.

After this evaluation, the revised RGWPM methodology appears to be applicable to a broad range of environments between 15° north and south latitude, commonly referred to as Sub-Saharan Africa where most of the camps and settlement are located (Fig. 4.1). At these latitudes, the general climate ranges from semi-arid to humid with effective precipitation varying by a factor of 5 (Fig. 4.1 and 4.2). The dominant lithologies are plutonic and metamorphic. The hydraulic properties of these

similar lithologies do not necessarily vary significantly but can increase considerably if unconsolidated material is present. It was concluded that the hydraulic conductivity may vary by 3 orders of magnitude (Fig. 4.3). Despite these significant climatic and hydrogeological differences, the range of GWP assigned to the low, slope and medium zones yields meaningful results at each location.

Moreover it is very reassuring to have significant variability in hydraulic conductivity or RC but that the GWP obtained with the revised RGWPM approach (Section 3.2) is still in line with the one defined in the initial methodology. In some ways, this is consistent with the fact that it is primarily the regolith that transmits groundwater and not so much the underlying rock. In fact, fractured bedrock may have locally high hydraulic conductivities, but on a regional scale they become very low (e.g. Lachassagne et al., 2021). This is because these fractures are not necessarily connected, so water that percolates from the regolith into these fractures may be trapped there (e.g. Alazard et al., 2016). In conclusion, applying the revised RGWPM methodology (which maps only the WA) to fourteen sites with different climatic settings has shown that the method can be applied to regolithic landscapes in different climatic settings, since the surface features of those landscapes reflect the interplay of surface and groundwater processes and render them visible.

4.4. Implications for sustainability due to GWP zones based on yield ranges

The trend in humanitarian contexts is toward solarized/motorized boreholes, and to justify the increased capital expenditure requires a yield of higher order of magnitude than for hand pumps (Section 2.2). To this end, the above discussion and the Bidibidi case study (Section 3.3) emphasized that the siting should be considered somewhere in a medium GWP zone, yielding more than 5 m^3/h. It may be the case that there are no medium GWP zone within the camp or settlement boundaries, however, mapping should extend at least 10 km around the camp, which is the upper limit of an economically viable solar water supply system (Section 2.2). For the fourteen sites presented earlier, a medium and sometimes even high GWP zones were encountered within a 10 km radius of the sites (Appendix A). Given that most refugee camps are located in the Sub-Saharan region and that it is possible to find some medium GWP that is likely to yield enough for motorization, this revised RGWPM methodology is indeed appropriate for this part of Africa.

At this point, one is able to indicate by means of yield classes where one is most likely to succeed in implementing either type of water supply (hand pump or motorized system). However, this range is wide, as for the medium GWP, it is estimated that it can range from 5 to 50 m^3/h. Moreover, having a better understanding of what we will call the sustainable GWP at an earlier stage is necessary, particularly in areas where boreholes have already been drilled and are extracting water. Indeed, a

certain medium GWP zone may no longer yield enough for additional motorized systems if it is already overexploited. The lack of this information in the current methodology is considered as a major drawback. To understand the sustainable GWP it is necessary to understand recharge on the catchment and sub-catchment scale.

Groundwater recharge can either be directly measured or indirectly estimated (e.g. Scanlon et al., 2006). In reviews by e.g. Gee et al. (1988), Amrit et al. (2016) or Xu et al. (2019), these approaches are evaluated when applied to arid to humid regions of Sub-Saharan Africa, such as those where many refugee settlements and camps are located (Fig. 4.1). The authors point out that all these approaches need to be conducted over a long period of time to obtain an accurate understanding of recharge. Due to the time constraints of the humanitarian contexts, this type of long-term assessment is not reconcilable with the RGWPM methodology. Therefore, a far more appropriate method is the water balance approach (Scanlon et al., 2006). The information needed for a catchment water balance approach to estimate groundwater recharge is: precipitation, evapotranspiration, and runoff. While fairly good precipitation and evapotranspiration products are available today from remote sensing products, obtaining runoff in ungauged basins is extremely difficult (Blöschl, 2006).

Before digging into a systematic approach of catchment water balancing in regolithic landscapes with known water balance components in the next chapter, a first attempt is made in the next section to empirically analyse the relationship between the water balance components obtained from remote sensing products (Fig. 4.2) and the mapped RGWPM units. The mapped RGWPM units reflect hydrogeomorphological entities, which are directly linked to the interplay of physical and chemical erosion by means of water, which in turn depend on the hydraulic properties of the area.

4.5. Empirical relationship between mapped RGWPM units and water balance

The purpose of this section is to present some preliminary thoughts on how mapped RGWPM could possibly be related to the catchment water balance and to the hydraulic properties. At present, as mentioned above, there is no simple approach to estimate groundwater recharge in data-scarce areas. Nevertheless, there are global datasets available that estimate the precipitation, evapotranspiration (e.g. Google Earth Engine) and a number of basic lithological data as presented in this chapter. These data allow a first assessment of the hydrogeological framework. Furthermore, according to the hydrogeomorphological landscape units (Section 2.4) defined by Winter (2001) on which RGWPM is based to characterise the WA zones, it is possible to understand where the different groundwater processes are most likely to occur.

The unit where, by definition, only one groundwater process occurs is in the upland unit (i.e. low WA zone in the revised RGWPM). In this unit, only diffuse groundwater recharge occurs. In the lower units of the slope and lowland there is both diffuse and/or concentrated groundwater recharge, but also axial groundwater flow, exfiltration, and runoff. Hence, the further downstream, the higher the complexity. Thus, intuitively, for a unit water input (effective precipitation), a higher groundwater recharge fraction can be assumed in an area with higher hydraulic conductivity, which would probably be reflected in a higher fraction of upland area (low WA). At this stage, this intuition can only be assessed by cross-referencing the size of the upland with the available data, i.e. the effective precipitation and estimated hydraulic properties of the lithologies. In Fig. 4.4, the catchment fraction covered in the RGWPM by the low WA unit (upland HGM unit) is shown versus the effective precipitation (Fig. 4.2) along with the lithological information (Fig. 4.3) for each site.

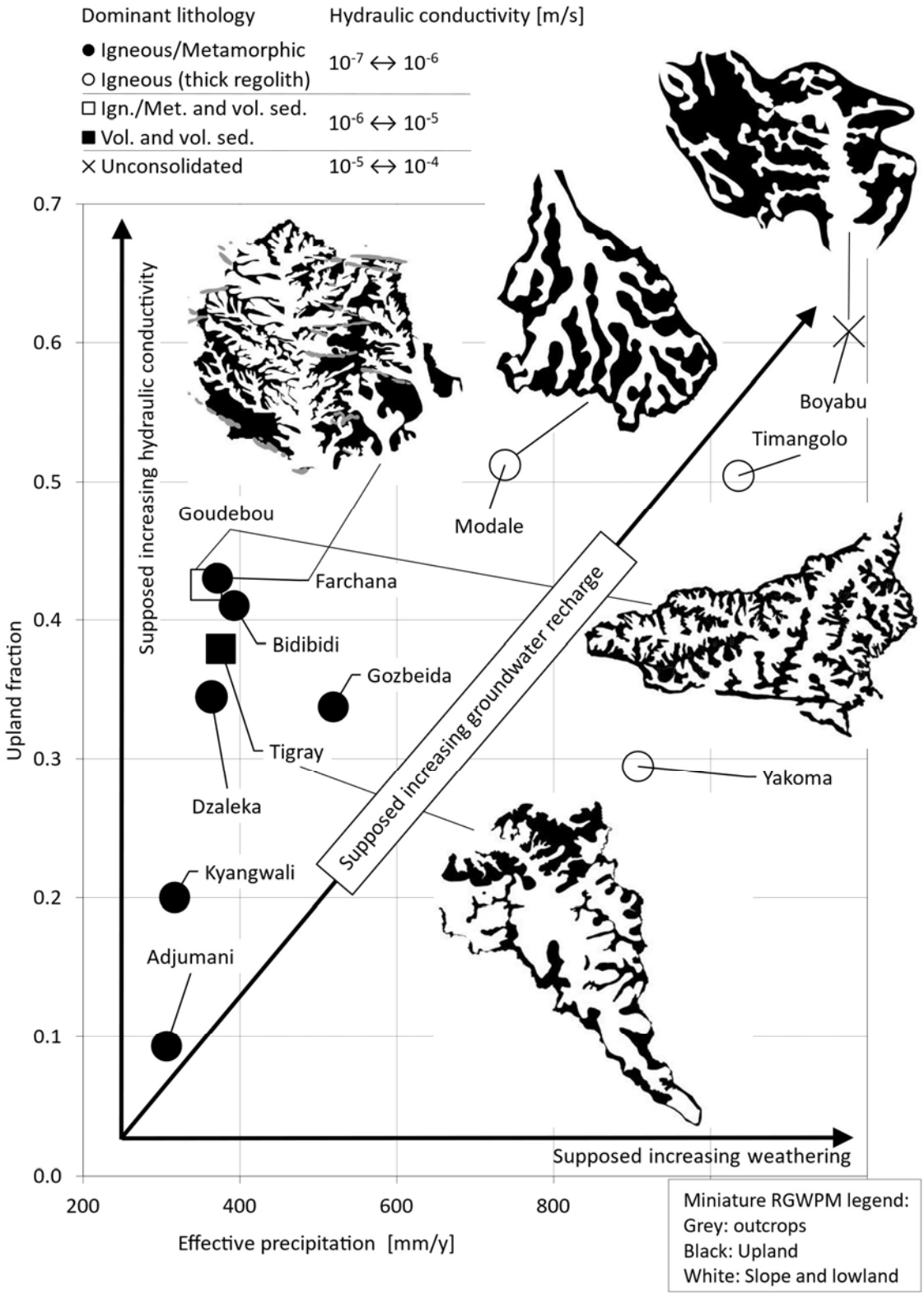

Fig. 4.4 *Caption on next page.*

Fig. 4.4 *Graph showing for each site the fraction of upland hydrogeomorphological unit (i.e. low water availability) in relation to the effective precipitation* ($P - ET$) *from Fig. 4.2. The symbols refer to the lithological information in Fig. 4.3 and are again referred to in this figure in the upper left corner. For some sites, a miniature RGWPM (Black surfaces) showing only the upland (low WA) unit is presented.*

In the graph of Fig. 4.4, a qualitative correlation can be derived between effective precipitation and the upland hydrogeomorphological unit fraction (i.e. low WA fraction). If groundwater recharge is assumed to be a function of upland size, even if that size in Fig. 4.4 appears to be a function of effective precipitation, groundwater recharge in turn is not necessarily a function of that precipitation but certainly of the subsurface properties (Freeze, 1969). Effective precipitation is one of the major factors affecting the landscape. In the regolithic environments, chemical weathering is the primary driving force in shaping the upland because there is only diffuse groundwater recharge (Section 2.4). This suggests that the greater the intensity, the higher the dissolution rates, resulting in greater planarization (Twidale, 1990) and thus a larger upland area (lower arrow). In addition, the dissolution rates are also dictated by the recharge capacity in turn dictated by the hydraulic properties (Freeze, 1969). It indeed seems that the size of the upland increases from the lower to the more permeable lithologies (vertical arrow). In fact, the smallest fraction of low WA zone can be associated to plutonic or metamorphic lithologies and the largest to the unconsolidated sediments and in between are found those with a mixture with volcanic material and the ones with an important regolithic layer (Fig. 4.3). Lithologies with a significant regolithic layer have been associated with lower hydraulic conductivities than the volcanic ones because the underlying rocks are granitic (Section 4.2). However, depending on the degree of alteration, these granitic lithologies could have hydraulic characteristics close to those of the volcanic and even the unconsolidated ones which is indeed better reflected in this assessment than with the typical hydraulic conductivity ranges in Fig. 4.3.

In Fig. 4.4, the shape of the upland (miniature RGWPM) is relevant to this idea that the larger it becomes, the more permeable it is and thus the more easily weathered. Indeed, the shape of these associated with low permeability lithologies are less rounded than the more permeable ones. In conclusion, it seems that the fractions of the low WA zones may have a physical basis that could reflect some subsurface processes that dictate groundwater recharge (diagonal arrow). Further studies and especially additional data are needed to investigate this issue in greater detail, which is addressed in the next chapters.

4.6. Conclusions

The revised RGWPM methodology presented in Chapter 3 was applied to 14 camps and settlements (Table 4.1) across Sub-Sahara Africa (Fig. 4.1). The general framework within which RGWPM has been conducted, has been characterized via the climatic (Fig. 4.2) and hydrogeological setting (Fig. 4.3). This is useful to understand the range of applicability. From one site to another, effective precipitation and hydraulic conductivity can vary considerably, on the order of 5 (225—1176 mm/year) and 1000 (10^{-7} and 10^{-4} m/s), respectively. On the whole, the methodology has been shown to be applicable to wider Sub-Saharan humanitarian settings (Fig. 4.1) and not only to Bidibidi in Uganda (Section 3.3), where the RGWPM methodology was developed. In fact, according to the average yield obtained from all the recovered boreholes found in the RGWPMs, the low, slope, and medium GWP zones yield what the methodology predicts (Table 4.2). In the low and slope GWP zone 96 % and 91 % of the boreholes respectively yield what the methodology predicts while in the medium GWP zone only 72 % yield what is predicted. If the largest errors are found for the medium GWP zone, it can be attributed to the fact that all the boreholes with lower yields are fitted with hand pumps and therefore technically not intended to give a higher than low yield, i.e. between 0.5 and 5 m^3/h (e.g. Chilton and Foster, 1995; Houston, 1992). These few boreholes aside, the same predictability is found as for the other two GWP zones (Slope and low).

All the sites are located in Sub-Saharan Africa characterized by the regolithic environments. However, the underlying lithology varies considerably from one site to another (Fig. 4.3). Hence, excluding RC mapping in the revised RGWPM methodology does not appear to have an effect on the resulting GWP zones. In regolithic environments, most groundwater is transmitted through the weathered layer (e.g. Lachassagne et al., 2021) and little into the fractured bedrock (e.g. Alazard et al., 2016). The revised approach (Section 3.3) relies only on the mapping of the WA, which is in fact only a mapping of the geomorphological features of the regolith. This mapping therefore implicitly includes the hydraulic properties (RC) of this regolith, which is the main aquifer in such settings.

Nonetheless, while one is able to comment on the best location for a borehole, the issue of sustainability has not yet been evaluated. Indeed, it has been concluded that if several boreholes are already drilled in the same area, the methodology will certainly fail at characterizing the sustainable GWP. In order to assess the issue of sustainability, the concept of water balance in order to estimate groundwater recharge on the catchment scale must be incorporated into the methodology. In general, where the camps are located, data are scarce or non-existent, so it is not possible to estimate this recharge simply. As a first step, the hydrogeomorphological landscape units (Winter, 2001) have been very helpful in describing where either main process, i.e. recharge, discharge and

runoff is most likely to occur and set the basis for the identification of the WA (Section 2.6). The unit where one is certain that only diffuse recharge occurs is on the upland, i.e. low WA. The obvious thought that comes to mind is that the larger it is, the higher the recharge should be and the higher the hydraulic conductivities are. At the end of this chapter, a first attempt was proposed to evaluate this idea. It is shown that there seems to be a correlation with the fraction of low WA to effective precipitation and hydraulic properties (Fig. 4.4). At this stage, it is not possible to comment on the fraction of effective precipitation that explicitly becomes recharge, so the correlation with the size of the low WA is not direct, but it is likely that its intensity is responsible for the degree of weathering. This degree is dictated by the hydraulic properties that govern recharge intensities and thus chemical dissolution rates (e.g. Twidale, 1990). Hence, the magnitude of effective precipitation and hydraulic properties are indeed most certainly related to the size of the low WA. The identification of this initial correlation is encouraging and sets the basis to further explore the relationship between the mapped RGWPM units and water balance components in the next chapters.

Chapter 5

Water balance components and hydrogeomorphological (HGM) landscape units compilation in data-scarce regolithic catchments: perspective for quantifying groundwater recharge

5.1. Introduction

The revised RGWPM methodology presented in Section 3.2 is well suited to characterize groundwater potential (GWP) zones across the regolithic environments of Sub-Saharan Africa. The GWP zones are linked to different types of water supply (e.g. hand pumps or small to large motorised systems). However, there is no information on the sustainability of implemented water schemes and the catchment scale water balance. The only way to have a better understanding of the sustainable GWP is to have the ability to introduce estimates on the catchment and sub-catchment scale of groundwater recharge.

In Sub-Saharan Africa where most camps and settlements are located (Fig. 4.1), it is difficult to obtain a meaningful estimate of groundwater recharge because data are scarce. Without any measuring instruments, recharge can be obtained by solving the water balance (e.g. Scanlon et al., 2006). Precipitation and evapotranspiration are readily available through remote sensing. From the difference between the two, one fraction becomes runoff and the other recharge. To solve the water balance for recharge, runoff must be known, which, similarly to recharge, is currently challenging to estimate easily at a required location (e.g. Blöschl, 2006).

The RGWPM methodology relies on the hydrogeomorphological concept (Winter, 2001) described in Section 2.4. This concept is convenient because it allows to identify the landscape units where one or the other processes, i.e. recharge, runoff, or discharge are most likely to occur. At the end of the previous chapter in Fig.4.4, a preliminary consideration was presented regarding whether these units in addition to indicating where either surface or groundwater processes occur could also be used for the actual quantification of the processes. If only diffuse groundwater recharge occurs on the upland, the larger its surface is the higher the recharge would be. It was shown that there is indeed a relationship between its size and the hydraulic conductivity of the dominant lithologies at each site, which in turn effectively dictates the degree of recharge (Freeze, 1969). With limited water balance components, i.e. without recharge or runoff data, a preliminary assessment of the units where only one process is occurring is necessary. In order to further develop this idea and to analyse

the relationships with the other landscape units, i.e. the slope and the drainage system where recharge and runoff might occur simultaneously, data regarding all water balance components are required.

The revised RGWPM methodology has been developed and its range of validity demonstrated in Sub-Saharan Africa (Section 4.3). The general lithologic context of this part of the world is characterized by typical regolithic environments (e.g. Twidale, 1990). In these environments, the water tables are topographically controlled, meaning that the hydrogeological basin is similar to the hydrological catchment (e.g. Lachassagne et al., 2021). Therefore, the groundwater leaves the catchment at the same location as the surface water. Hence, the water balance expressing such systems turns into a very simple formulation where the sum of all evapotranspired water, runoff and groundwater recharge is the precipitation falling on the catchment. Since RGWPM are not meant to be high-precision tools but rather operationally practical guidance documents, it seems adapted to establish water balances using data from precipitation and evapotranspiration from remote sensing products. However, to be able to systematically analysis the relationship between water balance components and mapped RGWPM units, it is necessary to have the whole set of water balance components.

To obtain the required data, the approach was to select a number of catchments meeting certain criteria in order to quantify the water balance components and map the landscape units. Approximately thousand gauged catchments were considered, and an analysis identified 20. For these 20 catchments, all water balance components were compiled and the hydrogeomorphological landscape units mapped. The units are the outcrops (very low WA), upland (low WA), slope (slope WA), drainage system (medium WA) and the lowland (high WA) units (Section 2.4). For the following analysis, these five units are no longer expressed in terms of GWP zones but in their respective hydrogeomorphological terminology is adopted as summarized in Fig. 1.2 and illustrated in Fig. 2.1. This is done for clarity when discussing their relationship to the water balance components later. In addition, they are grouped together for simplicity and logic as described in Fig. 1.2. First, as presented in the Bidibidi RGWPM (Fig. 2.3), outcrops are very sporadic, and become insignificant at the catchment scale compared to the upland that encompasses them. Thus they are neglected. Second, the drainage unit and the lowland are considered as a single entity because in regolithic environments, the lowland is part of the drainage system, constituting the perennial streams and rivers. It also proved complicated to successfully identify the exact location where groundwater actually exfiltrates within the 20 catchments. Also, even though the lowland can be correctly identified, it only appears locally on a short length compared to the drainage system, allowing it to be overlooked (Section 3.2). Ultimately, the three mapped hydrogeomorphological landscape units

are the upland (low WA), slope (slope WA), and drainage system (medium and high WA), referred to in the following analysis as HGM units.

This phase of data collection having required a significant amount of time in the project, it seems relevant to devote a specific chapter to it. It is also helpful in order to clearly distinguish the next chapters which are based upon this data set. Above all, such a data assessment in the regolithic environments having never been carried out at this scale to our knowledge, it is an additional reason to detail all the steps. Indeed, this chapter is thought to serve also as a basis for further work on this subject. However, in order to remain streamlined, this chapter only briefly presents the main information which is subsequently used for all analyses. The details are to be found in a separate chapter in Appendix C.

Appendix C has a review of the literature on the regolithic environments and includes a discussion of the lithologic, hydrogeologic, and hydrogeomorphological characteristics. Although the main information was presented in Section 2.4, this additional material is important in order to be referred to in the subsequent chapters regarding some groundwater-related processes occurring in these environments. In addition, some parameters such as the hydraulic properties of the regolith are used to estimate the axial groundwater flow. The axial groundwater flow component was used to attempt validation and justification of direct use of MODIS evapotranspiration data by solving the water balance for it, with the components having the highest confidence, i.e. precipitation and streamflow. Indeed, this remotely sensed evapotranspiration appears to have reliability problems according to several literature reviews summarized in Appendix C.3.2. However, the analysis presented in Appendix C.3.2.2 revealed that the error in the water balance when using uncorrected MODIS data is fairly reasonable for the following analysis and that the errors raised by some authors are rather due to the way they evaluate this product (Appendix C.3.2.1).

In Appendix C.3 it is described in detail how the water balance components are obtained and why their source or the techniques to measure them is better than another. For precipitation and evapotranspiration, remote sensing data has been used. Although a large number of products for calculating these two components have recently been made available through convenient portals such as Google Earth Engine, the selection of the optimal product that returns the most accurate values needed to be assessed and validated. Also to be found in Appendix C.3 is the literature review of the methods for analysing discharge records to obtain runoff. The most frequently used methods are presented and discussed in detail before describing the mathematical derivation of the one chosen for this study.

This chapter first presents the criteria for selecting the catchments defined by the locations of the gauging stations, for which discharge data were used, from the Global Runoff Data Centre (GRDC) platform. These criteria, such as avoiding sites with anthropogenic impact on groundwater, must be met in order to work with a simple, conventional water balance approach. In addition, the catchments must be located in typical regolithic environments. To carry out this identification step, a detailed description of the lithology was necessary and was therefore carried out for each catchment. Next, the water balance and its components are briefly presented. Then, the hydrogeomorphological units and the water balance components used in the following analyses are summarized. Finally, the water balance and its components are embedded in the hydrogeomorphological concept (Winter, 2001). This allows to introduce supplementary notions that revolve around this concept and serve as a basis for the next two chapters which are dedicated to link the mapped RGWPM units to groundwater recharge estimation and to defining a way to represent the sustainable groundwater potential in the RGWPM map.

5.2. Reference catchments for HGM and water balance analyses

For this study catchments have been selected in order to carry out a systematic analysis of hydrogeomorphological units (HGM) and the associated water balances. The discharge of these catchments is monitored by gauging stations. The discharge records are collected by the Global Runoff Data Centre (GRDC). The GRDC compiled data for 1,708 catchments in Africa, including about 1,000 in Sub-Saharan Africa, of which 20 were selected because they met the selection criteria discussed in the next paragraph. These 20 are all located in the typical regolithic environments of Sub-Saharan Africa. For theses catchments, the hydrogeomorphological units were mapped and the water balance components, in addition to discharge, i.e. precipitation and evapotranspiration, have been retrieved. This section first presents the general criteria that these catchments had to meet in order to be used in this study. Then, their environment and geological contexts are described.

The first, and probably the most important criterion that the catchment must meet is that it does not include vast alluvial plains which distorts the catchment-scale drainage system fraction which includes such alluvial plains being the lowland or high WA. This also adds a different aquifer system (i.e. unconsolidated and alluvial) to that of the regolith to be studied here. The second criterion is that the catchment must not contain surface water retention infrastructures, such as hydropower plants or small irrigation dams in order to be sure that the discharge measurements data reflect the natural environment and are free from storage/buffer effects (e.g. Scanlon et al., 2006). The third criterion is that the catchment is free from industry (e.g. mining), agriculture, or large cities all of which result is considerable groundwater extraction and so disequilibrate the natural water balance

(e.g. Scanlon et al., 2006). These activities and areas are easily identifiable using satellite imagery. In summary, catchments devoid of vast alluvial plains, water storage infrastructure, irrigated infrastructure, or industry were selected. In addition, large towns in the catchment were avoided and only catchments with small, scattered villages were considered.

The locations of the 20 selected catchments is shown in Fig. 5.1. This figure displays two maps (Fig. 5.1a and Fig.5.1b). In both, the catchments are labelled with capital letters in reference to Table 5.1. Figure 5.1a shows the regional location of the catchments. The base map is the aridity index, and the colour refers to the legend on the left. It also shows the extent of deep weathering (Tardy, 1992), i.e. regolithic environments. Figure 5.1b shows the general geological and structural setting of Africa (Provisional Structural Scheme of Africa, Furon 1958) to discuss the catchments environment in more detail. The legend to this map is presented in Fig. 5.2. The extent of certain catchments is visible at this scale but some are too small to be seen, so their location is indicated by white dots. In both maps, the locations of the 14 RGWPM discussed in Chapter 4 are also added and are represented by black dots numbered according to Table 4.1.

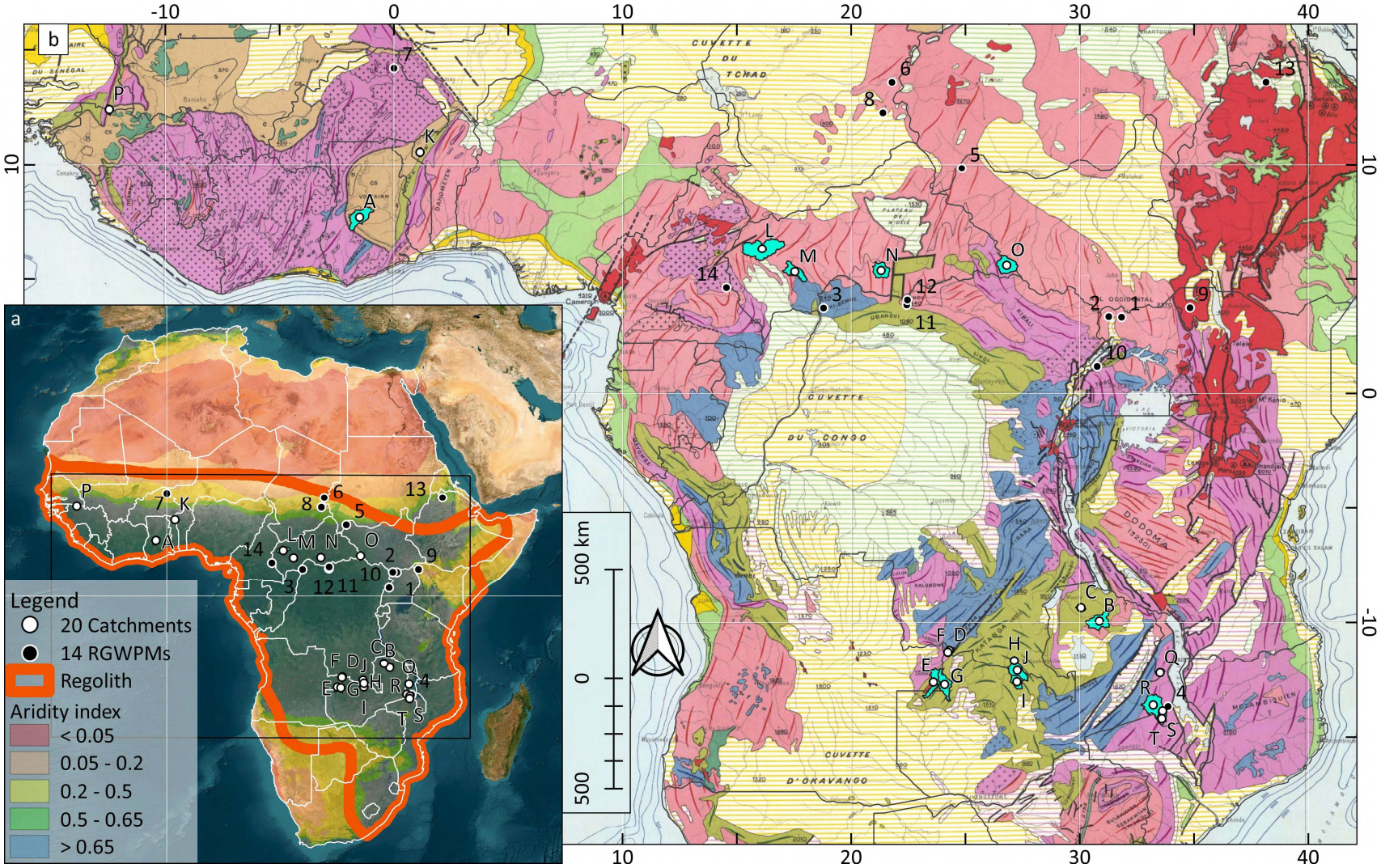

Fig. 5.1 *Caption on next page.*

Fig. 5.1 *Location of the 20 selected catchments with a gauging station used in this study.* ***a*** *map showing the locations of the catchments indicated by the white dots and labelled with capital letters in reference to Table 5.1 with the aridity index (Ai) and the extent of weathering environments (Regolith) modified from Tardy (1992).* ***b*** *map showing the locations of the catchments at a smaller scale but where the base map is the geological map of Furon (1958). The legend is given in Fig. 5.2. In both maps, the locations of the 14 RGWPM of Chapter 4 are represented with dots numbered according to Table 4.1.*

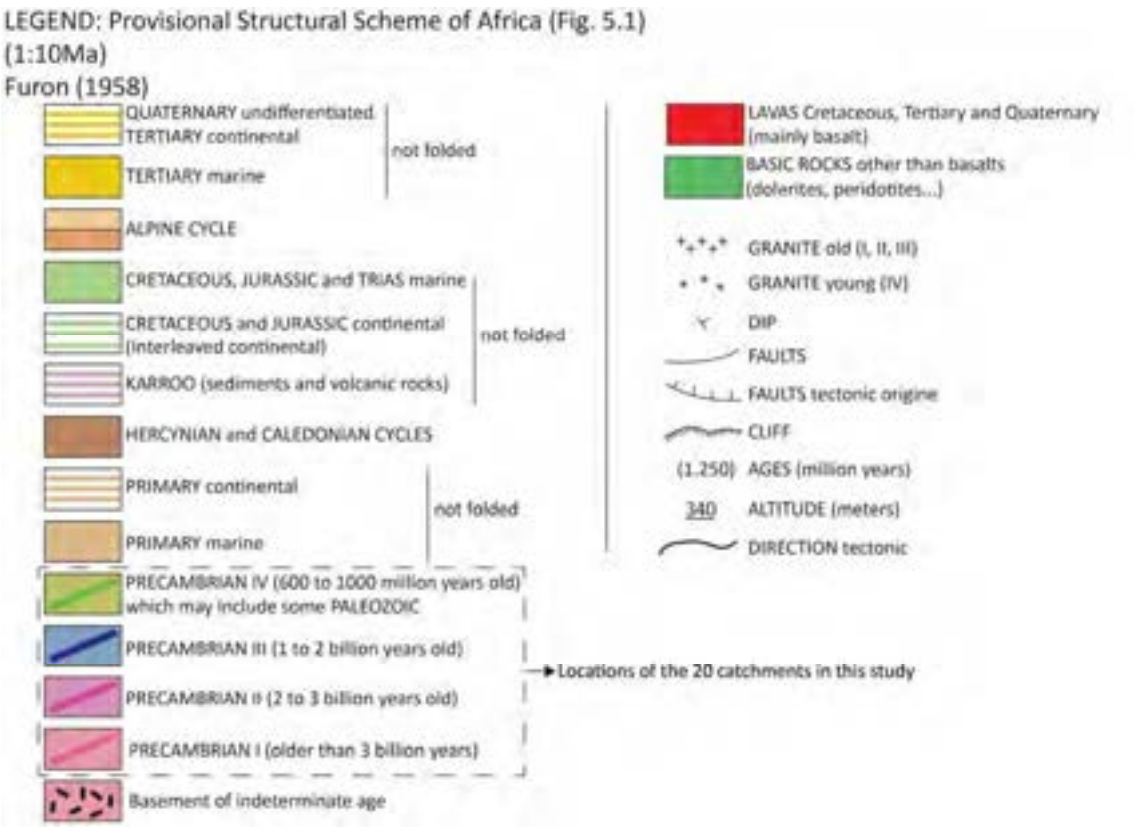

Fig. 5.2 *Adapted legend of the structural map of Furon (1958) partly displayed in Fig. 5.1b. All 20 catchments used in this study are located in formations that span the entire Precambrian Eon (stippled rectangle).*

The twenty catchments (Fig. 5.1a) are equally distributed in the northern and southern hemispheres with ten catchments in each hemisphere. All catchments are located in similar 'humid' environments with the Airidity Index (Ai) greater than 0.5 as shown in Fig. 5.1a. To illustrate that the catchment should have a developed the typical regolithic profile commonly found in Sub-Sahran Africa, the small map in Fig. 5.1a shows the extent of the continental scale weathered environments in Africa (Tardy, 1992). These environments are closely linked to the climatic conditions. Mild to warm temperatures and abundant precipitations are necessary to produce a substantial regolith as discussed in Appendix C.2.1. These climates are indeed those found where the aridity index presents a humid class.

In addition to the regolith, there must also be underlying hard rock to present hydrogeological conditions similar to those wished to be evaluated here (Appendix C.2.2). In Fig. 5.1b, the location of

the catchments is shown with a structural map of Africa. This map only shows the major geologic units and particularly clearly indicates the extent of the oldest units of the Precambrian. The legends of these units are given in Fig. 5.2 and highlighted by a dashed rectangle. The Precambrian rocks are plutonic or metamorphic rocks. Large areas such as the Central Cuvette in the Democratic Republic of the Congo or the Cuvette of Chad are certainly located at latitudes favourable to the development of a regolithic profile but are characterized by bassin Infilled with large quantities of uncosolidated materials of Quaternary age (Fig. 5.1b). The area surrounding these basins present rocks older than the Quaternary, i.e. Cretaceous and Jurassic formations. However, these formations are of continental origin and do not necessarily present a typical regolithic aquifer. The study of catchments at these locations (cuvettes and contiental formation) leads to an examination of a complicated multi-layered system on a continental scale, which is definitely beyond the scope of this study. This explains why the catchments are located on this belt of plutonic and metamorphic rocks that extends to arid climates and encircles the Democratic Republic of the Congo.

The general geological setting is presented in Fig. 5.1b with legend in Fig. 5.2 and the detailed geology of each catchment is summarized in Table 5.1. In this table, the first two columns refer to the letter used to label the catchment in Fig. 5.1b and the gauging GRDC station ID. The third column describes the geology of each site and is based on a qualitative analysis of geological maps each at a scale relevant to the catchment. The references and details of each map can be found in Appendix D. The last column of this table refers the geological Eon of each place discussed further up and found in Fig. 5.1 and 5.2.

Table 5.1 *Geology encountered in the 20 catchments used in this study. The first column of this table shows the letters used to label the catchments in the maps of Fig. 5.1. The second refers to the gauging station GRDC (Global Runoff Data Centre) ID. The third presents the specific geology at each site based on multiple geological maps. The references and the detail of each geological map is found in Appendix D. All the maps are georeferenced and given in a separate GIS project (Appendix D). The last column displays the Eon of each place and refer to Fig. 5.1 and 5.2.*

Catchment (Fig. 5.1)	GRDC Station ID	Geology (See Appendix D for further details)	Geological Eon (Fig. 5.2)
A	1531300	Sandstone, Shale, Mudstone	Hercynian
B	1547300	Granite, Gneiss, Quartzite	Pre. IV, I
C	1547340	Quartzite	Pre. IV
D	1591003	Sandstone, Shales, siltstones	Pre. III, II
E	1591100	Sandstone, Conglomerate, Calc-Dolomite, Silt, Quartzite, Carbonate, Basalt, Dolerite, Andesite	Pre. IV, II
F	1591110	Sandstone, Shales, Siltstones	Pre. II
G	1591235	Sandstone, Conglomerate, Calc-Dolomite, Silt, Quartzite, Carbonate	Pre. IV
H	1591400	Sandstone, Shales, Siltstones	Pre. IV
I	1591441	Granite, Gneiss, Sandstone, Shales, Siltstones	Pre. IV
J	1591481	Sandstone, Shales, Siltstones, Carbonate, Shale, Argillite	Pre. IV
K	1731450	Sandstone	Pre. IV
L	1737100	Granite, Gneiss	Pre. I
M	1749030	Granite, Gneiss, Quartzite, Mica-schist, comp. Till.	Pre. IIII, I
N	1749400	Quartzite, Mica-schist, Gneiss, granite	Pre. I
O	1749800	Mica-schist	Pre. II, I
P	1813650	Sandstone, Argillite	Pre. IV, II
Q	1992400	Semi-pelitic, Granite	Pre. II
R	1992490	Semi-pelitic, Sandstone	Pre. II
S	1992580	Semi-pelitic	Pre. II
T	1992600	Semi-pelitic, Sandstone, Granite	Pre. II

Noticeably in Table 5.1, the geology varies significantly from one catchment to another. However, it can be classified into plutonic and metamorphic rocks. Some rocks have a sedimentary origin such as the sandstones or shales for instance. According to the lithological description of each geological map (Appendix D), all these lithologies must have undergone a more or less intense metamorphism. Even the lithologies such as the conglomerates present all the characteristics of hard rocks. As

discussed previously all the catchments are located on formation that date back to the Precambrian and do not present large formation with a continental origin. In addition, all the catchments have been selected in order to not present significant zones of unconsolidated material such alluvial plains. This has been done based on high resolution satellite imagery because this type of information is not included in geological maps.

The 20 selected catchments with a gauging station are displayed in Appendix D. For each, the three mapped units, the geology and a satellite image with the drainage network are presented. Hereafter an example is given in Fig. 5.3. The catchment used here is the one labelled 1531300 in GRDC (Global Runoff Data Centre) and designated as B in Fig. 5.1. The extent of the three mapped hydrogeomorphological units is shown on the large map (Fig. 5.3a). The small map in Fig. 5.3b shows a satellite image with the drainage system that is of the dendritic type typical of regolithic environments. In the satellite image, it is also possible to notice that there is no urban infrastructure such as dams. The geology at this site is presented on the small map in Fig. 5.3c. The legend to this geological map refers to Appendix D of the Geological Map of Zambia, which indicates that the underlying hard rock geology consists of granite, gneiss, and quartzite.

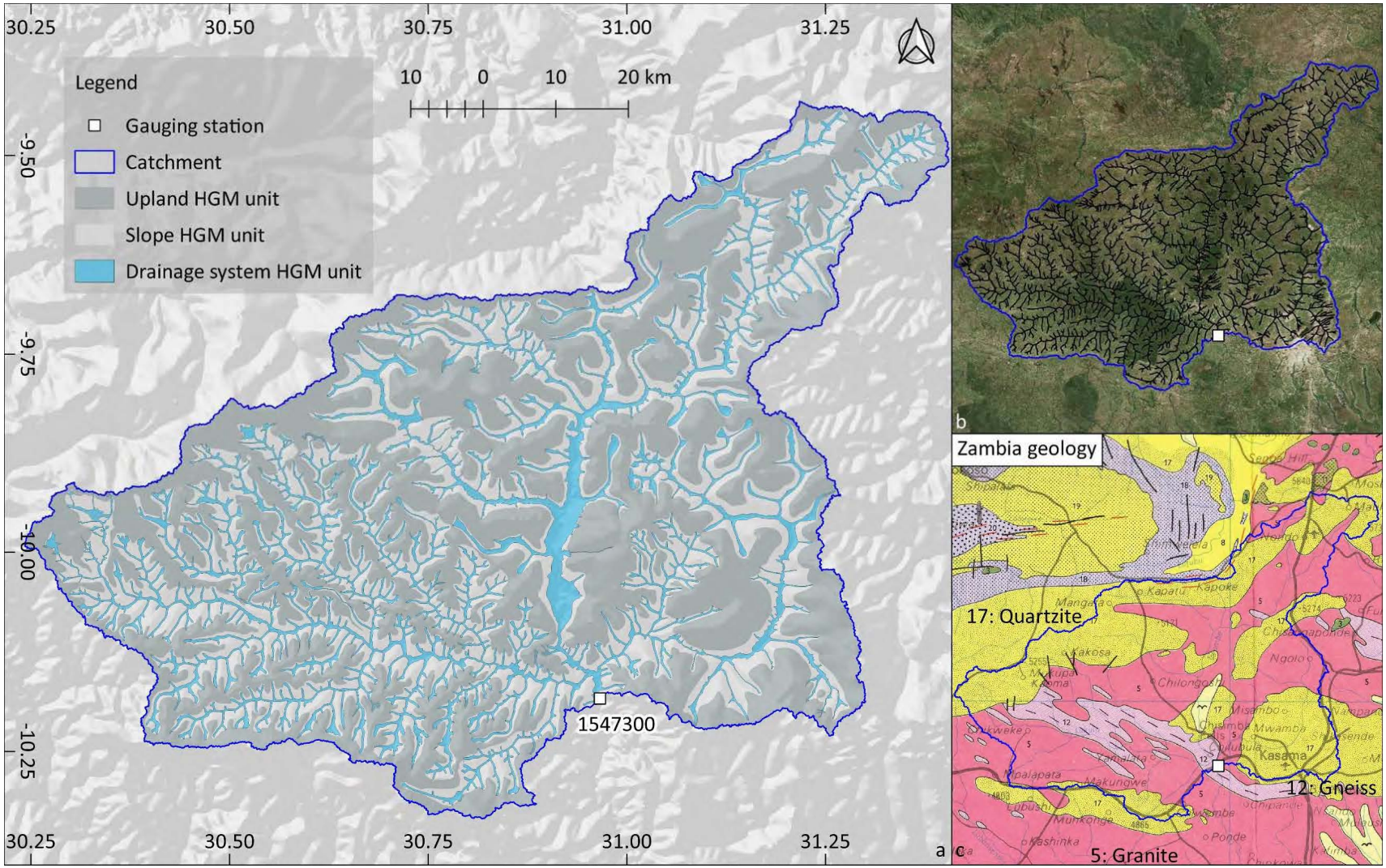

Fig. 5.3 *Caption on next page.*

Fig. 5.3 *Example illustrating the mapping of the hydrogeomorphological (HGM) landscape units of the 20 identified catchments. The catchment shown is in GRDC (Global Runoff Data Centre) labelled 1547300 and abbreviated B in Fig. 5.1.* ***a*** *Extent of the three units, i.e. upland (grey), slope (light grey) and drainage system (blue).* ***b*** *Satellite image with drainage network and* ***c*** *geology of Zambia with legend in Appendix D.*

5.3. Catchment water balance components

To estimate groundwater recharge in remote locations where data are scarce and no measuring instruments are installed (e.g. Fayer et al., 1996), the most convenient way to approximate it using the water balance method (e.g. Scanlon et al., 2006). The components required to solve the water balance for groundwater recharge are precipitation, evapotranspiration, and runoff. Precipitation and evapotranspiration are available from remote sensing products and runoff can be derived from discharge recorded at gauging stations by so-called hydrograph separation methods (e.g. Chapman et al., 1996), as described in detail in Appendix C.3.

The water balance of regolithic catchments can be simplified, as the water table is controlled by the topography, which means that the hydrogeological basin has the same area as the hydrological catchment (e.g. Lachassagne et al., 2021). This implies that all precipitation falling on the catchment which has not evapotranspired leaves it at one point, i.e. in and under the catchment outlet. All catchments were selected so as to control for human activity (e.g. agricultural, industrial, or urban extraction, or storage in dams or irrigation infrastructure) which could impact the water balance. The storage effect for groundwater is also neglected since long-term annual hydrological yearly means (Appendix C.3.3) are considered. Therefore, the water balance used here takes the simple form of:

$$P = ET + Q_0 + Q \tag{5.1}$$

where P is precipitation, ET evapotranspiration, Q surface water discharge at the catchment outlet and Q_0 axial groundwater flow. The discharge Q can be further subdivided into two components:

$$Q = R + Q_b \tag{5.2}$$

Where R is direct surface runoff and Q_b the base flow that is exfiltrating to the river upstream of the catchment outlet. Therefore, the total catchment groundwater recharge Q_i is:

$$Q_i = Q_b + Q_0 \tag{5.3}$$

Finally, according to Eq. 5.2 and 5.3, 5.1 is rewritten as follow:

$$P = ET + R + Q_i \tag{5.4}$$

Discharge data are obtained from gauging stations. These stations are provided by the Global Runoff Data Centre (GRDC). The gauging stations are selected on the basis of the previously defined catchment criteria. In addition, they are also selected on the condition that they present concise data over several years but that might not necessarily follow. However, a minimum 5 consecutive years without lacking data was defined. The catchment selection criteria defined in the previous chapter and the one that must be met by the gauging stations defined here are briefly summarized in Table 5.2.

Table 5.2 *Summary of criteria that must be met by the GRDC catchments to be used in the following analyses.*

1. Geological and hydrogeological setting criteria (catchment criteria)
Located in regolithic environments
Underlying hard rock
No alluvial plains
2. Natural water balance criteria (catchment criteria)
No surface water retention infrastructures
No intensive agriculture
No industrial withdrawals
3. Gauging stations time series criteria
No lacking data for several years
Minimum of 5 consecutive years

In order to assess the water balance of each catchment, each component is derived from an average of the annual means. This has the advantage of avoiding storage effects. To obtain annual means, the hydrological year characterized by the beginning and end of the rainy season is considered. All the discharge records plus the base flow and runoff for the 20 catchments are presented in the graphs in Appendix F.

The precipitation product used for this study comes from the Climate Hazards Group InfraRed Precipitation with Station data (CHIRPS) from the University of California at Santa Barbara and U.S. Geological Survey (Funk et al., 2014; 2015). The resolution of this product is 0.05 arc degrees, this means that close to the equator, the grid cells of this raster are approximately 5.5 km^2 in size. The raster is available from latitude 50°S to 50°N and at all longitudes. This resolution is currently the highest available for precipitation in the public domain. The data are available daily from 1981 to near-real time. Graphs showing precipitation for all catchments can be found in Appendix E and F.

The evapotranspiration product retained for this study (MOD16A2 Version 6) come from the Moderate Resolution Imaging Spectroradiometer (MODIS) on board the NASA Aqua satellite. The measurements of the sensors are used in an algorithm described by Mu et al. (2007) that has been revised by Cleugh et al. (2007) to generate evapotranspiration. It is produced thanks to the Penman-Monteith (P-M) equation (Monteith, 1965) with remotely sensed and daily meteorological reanalysis. The remotely sensed data comprise, amongst other, vegetation property dynamics, albedo, and land cover. This product provides global evapotranspiration every eight days. So that the 8-day measurements are extrapolated over the next 8 days. The resolution of the pixels is 500 m^2. Graphs showing evapotranspiration can be found in Appendix E.

In Appendix C.3, the remote sensing data products for precipitation and evapotranspiration are first presented. For both, a thorough review of the literature is carried out in order to justify the products that are retained for this study. In addition, for evapotranspiration data, there is a fairly long section devoted to the validation of the product, as it represents the component for which there is the least confidence. Finally, the data of the gauging station whose discharge records are used to estimate runoff and base flow by means of hydrograph separation (e.g. Chapman et al., 1996) is discussed and the most reliable method retained for this study i.e. Wittenberg (1999) is carefully assessed and presented.

5.4. Reference catchments data set: HGM units and water balance components

For the 20 selected reference catchments presented in Section 5.3, the hydrogeomorphological units were mapped and the water balance components retrieved (see Appendix C, D, E and F). These data are briefly summarised and compiled hereafter.

The graph in Fig. 5.4 illustrates, for the 20 catchments designated by the capital letters in reference to Fig. 5.1 and Table 5.1, the areas, and fractions of the three hydrogeomorphological (HGM) landscape units, i.e. upland, slope, and drainage system (Fig. 1.2). The areas (left axis) are given in km^2/1000 and are represented by stacked colour bars where the area of upland, slope and drainage system are shown in dark grey, light grey and blue, respectively. The fractions (right axis) of upland, slope and drainage system are illustrated by the solid, dashed, and dotted lines, respectively. The catchments are classified from left to right according to their upland fraction (solid line). The exact areas and fraction values are given in the table below the graph.

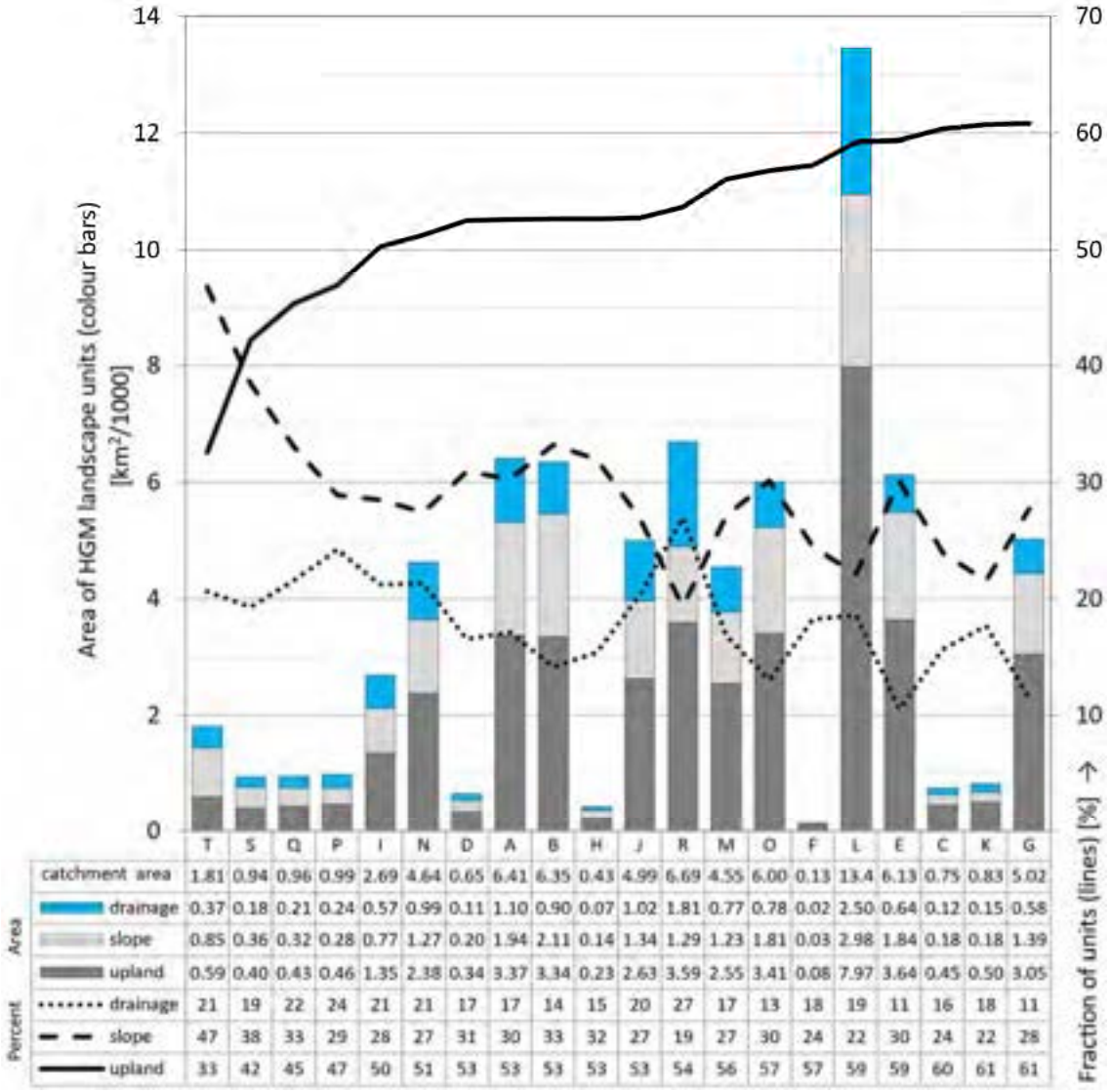

		T	S	Q	P	I	N	D	A	B	H	J	R	M	O	F	L	E	C	K	G
	catchment area	1.81	0.94	0.96	0.99	2.69	4.64	0.65	6.41	6.35	0.43	4.99	6.69	4.55	6.00	0.13	13.4	6.13	0.75	0.83	5.02
Area	drainage	0.37	0.18	0.21	0.24	0.57	0.99	0.11	1.10	0.90	0.07	1.02	1.81	0.77	0.78	0.02	2.50	0.64	0.12	0.15	0.58
	slope	0.85	0.36	0.32	0.28	0.77	1.27	0.20	1.94	2.11	0.14	1.34	1.29	1.23	1.81	0.03	2.98	1.84	0.18	0.18	1.39
	upland	0.59	0.40	0.43	0.46	1.35	2.38	0.34	3.37	3.34	0.23	2.63	3.59	2.55	3.41	0.08	7.97	3.64	0.45	0.50	3.05
Percent	drainage	21	19	22	24	21	21	17	17	14	15	20	27	17	13	18	19	11	16	18	11
	slope	47	38	33	29	28	27	31	30	33	32	27	19	27	30	24	22	30	24	22	28
	upland	33	42	45	47	50	51	53	53	53	53	53	54	56	57	57	59	59	60	61	61

Fig. 5.4 *Graph and table of the 20 catchments denoted by letters (letters refer to Fig. 5.1 and Table 5.1) of the areas and fractions of the hydrogeomorphological (HGM) landscape units, i.e. upland, slope, and drainage system. The areas are expressed in [km²/1000] and the fractions in percent. The areas are illustrated by bars and the fractions by lines. The catchments are ranked from the lowest to the highest upland fraction. The exact values of the areas and fractions are given in the table below the graph.*

According to Fig. 5.4, the catchments range from 0.13 km²/1000 (F) to 13.46 km²/1000 (L). However, without considering the largest (L), they generally vary between 0.13 km²/1000 (F) to 6.69 km²/1000 I. These catchments have been classified by their upland fraction (black line), not their total area, to illustrate that this unit is not proportional to the size of the catchment. In fact, in doing so the cumulated catchment area (bars) become randomly distributed. As for the slope and drainage fraction (dashed and dotted lines respectively), as the fraction of upland increases, they appear to vary randomly. Thus, subsequent analyses based on the hypotheses (Section 4.5) that groundwater

recharge could be correlated with the fraction of these units are not biased from the outset. For example, if there is indeed only diffuse recharge in the uplands and this unit was a function of the size of the catchment, then it could not be related to recharge since its fraction would always be the same whereas recharge in fact varies as presented afterwards. While the fraction of the upland varies between 30 and 60% (solid line), it is 20 to 40% for the slope (dotted line) and 10 to 20% for the drainage system.

In Fig. 5.5 the water balance components for the 20 catchments (capital letters) are presented. The components are, the base flow (Q_b), axial groundwater flow (Q_0), runoff (R) and evapotranspiration (ET) where the sum of the four gives precipitation (P). The stacked coloured bars referring to the left axis show the annual mean of the components in mm/year. Bars for Q_b (light blue) and Q_0 (dark blue), which when added together (Eq. 5.3) yield groundwater recharge (Q_i), are shown as positive. The values of Q_i are illustrated by the square markers. The bars showing ET (yellow) and R (orange) essentially represent catchment losses (L_s), i.e. the components which do not contribute to groundwater flow, therefore shown as negative values. The value of L_s are illustrated by the crosses. The fractions of Q_i and L_s relative to total precipitation are represented by the solid and dashed lines, respectively, and refer to the right axis. Catchments were ranked according to the percentage of Q_i. The exact values of the components in mm/year and the fractions of Q_i and L_s in % are given in the table below.

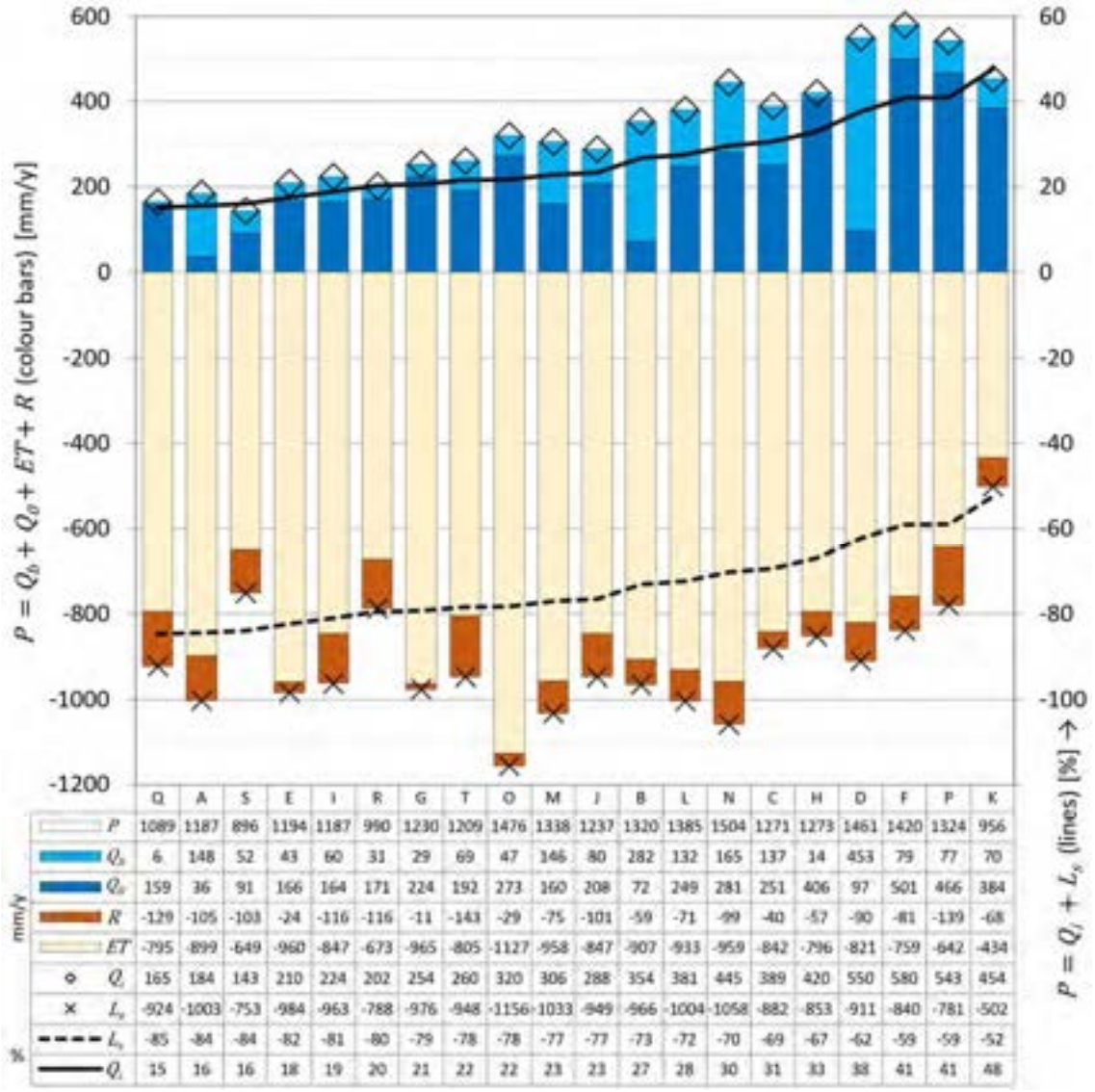

	Q	A	S	E	I	R	G	T	O	M	J	B	L	N	C	H	D	F	P	K
mm/y P	1089	1187	896	1194	1187	990	1230	1209	1476	1338	1237	1320	1385	1504	1271	1273	1461	1420	1324	956
mm/y Q_b	6	148	52	43	60	31	29	69	47	146	80	282	132	165	137	14	453	79	77	70
mm/y Q_0	159	36	91	166	164	171	224	192	273	160	208	72	249	281	251	406	97	501	466	384
mm/y R	-129	-105	-103	-24	-116	-116	-11	-143	-29	-75	-101	-59	-71	-99	-40	-57	-90	-81	-139	-68
mm/y ET	-795	-899	-649	-960	-847	-673	-965	-805	-1127	-958	-847	-907	-933	-959	-842	-796	-821	-759	-642	-434
mm/y Q_i	165	184	143	210	224	202	254	260	320	306	288	354	381	445	389	420	550	580	543	454
mm/y L_s	-924	-1003	-753	-984	-963	-788	-976	-948	-1156	-1033	-949	-966	-1004	-1058	-882	-853	-911	-840	-781	-502
% L_s	85	84	84	82	81	80	79	78	78	77	77	73	72	70	69	67	62	59	59	52
% Q_i	15	16	16	18	19	20	21	22	22	23	23	27	28	30	31	33	38	41	41	48

Fig. 5.5 *Graph and table showing the water balance components for the 20 catchments (capital letters in Fig. 5.1 and Table 5.1). The components with abbreviations are: base flow (Q_b), groundwater (Q_0), runoff (R) and evapotranspiration (ET) where the sum of the four gives precipitation (P). In the graph, the coloured bars referring to the left axis illustrate each component in mm/year. Total groundwater recharge (Q_i) and losses (L_s) in mm/year are indicated by square markers and crosses respectively. Fractions of Q_i and L_s to total precipitation are illustrated by solid and dashed lines respectively and refer to the right axis of the graph. The catchments were ranked according to the fractions of Q_i. The exact values of components and the fractions of Q_i and L_s are given in the table.*

According to the graph in Fig. 5.5, most of the precipitation is evapotranspired (yellow bars). Evapotranspiration is added to runoff (orange bars) and gives the amount of water essentially lost at the surface (L_s). The sum of losses (L_s) varies between 924 and 502 mm/year and represents arround 85—50 % of the total precipitation (dashed line).

The 20 catchments from which the HGM units and water balance components were compiled are all located in the typical regolithic environment of Sub-Saharan Africa. However, the size of the units and the water balance components show substantial variation from one catchment to another. This suggests a high degree of complexity where one interested in studying the relationship between HGM units and water balance components which requires a systematic analysis of all possible combinations, which is the object of the following chapter, using the described data set above.

5.5. Conceptual model of a regolithic landscape: relating water balance components with HGM units

In order to proceed with an analysis of the possible relationship between water balance components and HGM units, it is crucial to set the scene, by formulating a conceptual model, which can act as guidance in the following analysis. This was earlier presented in Fig. 1.2 but in this section, it is taken a step further where the processes occurring in the regolithic catchments, including groundwater recharge and the water balance components are put into perspective with the HGM concept of Winter (2001), presented in Section 2.4 (Fig. 2.1). For this purpose, the HGM concept shown in Fig. 2.1 presenting a cross-section, is now put into a 3D catchment perspective, as shown in Fig. 5.6, allowing visualisation and conceptualisation of the above-described data sets. This conceptual model is largely inspired by earlier research in the field of hydrogeomorphology, with pioneering work such as Dunne et al. (1975) and Dunne (1990), which focussed on 'reading' groundwater flow dynamics in HGM features. With these approaches having been developed in a period when morphological analysis was very cumbersome, since digital elevation models did not exist, it is highly relevant to revisit these well-established relationships in the framework of this study, by combining them with the now available data sets from remote sensing products.

According to the conceptual model shown in Fig. 5.6, effective precipitation P_{eff} (i.e. evapotranspiration ET minus precipitation P) infiltrates both on the upland and slope unit, while it is transformed exclusively into diffuse groundwater recharge Q_i on the upland and partially into Q_i and runoff R on the slope. The cumulated Q_i flows towards the drainage system unit and after crossing its perimeter c, either transforms into base flow Q_b by seeping into the drainage network (blue line) or continues as axial groundwater flow Q_0. Runoff is only generated on the slope and on the drainage system unit, added the surface runoff component to the base flow, measured at the gauging station as total discharge Q. A hydraulic conductivity K is stipulated for the regolith to illustrate that most of the water flows within the weathered layer. The thickness of the weathered layer is e. The variable m is the slope of the drainage system, which will subsequently also be used as

a proxy for the regional groundwater gradient, since erosional processes, such as the development of drainage systems are constrained by the groundwater table and its gradient.

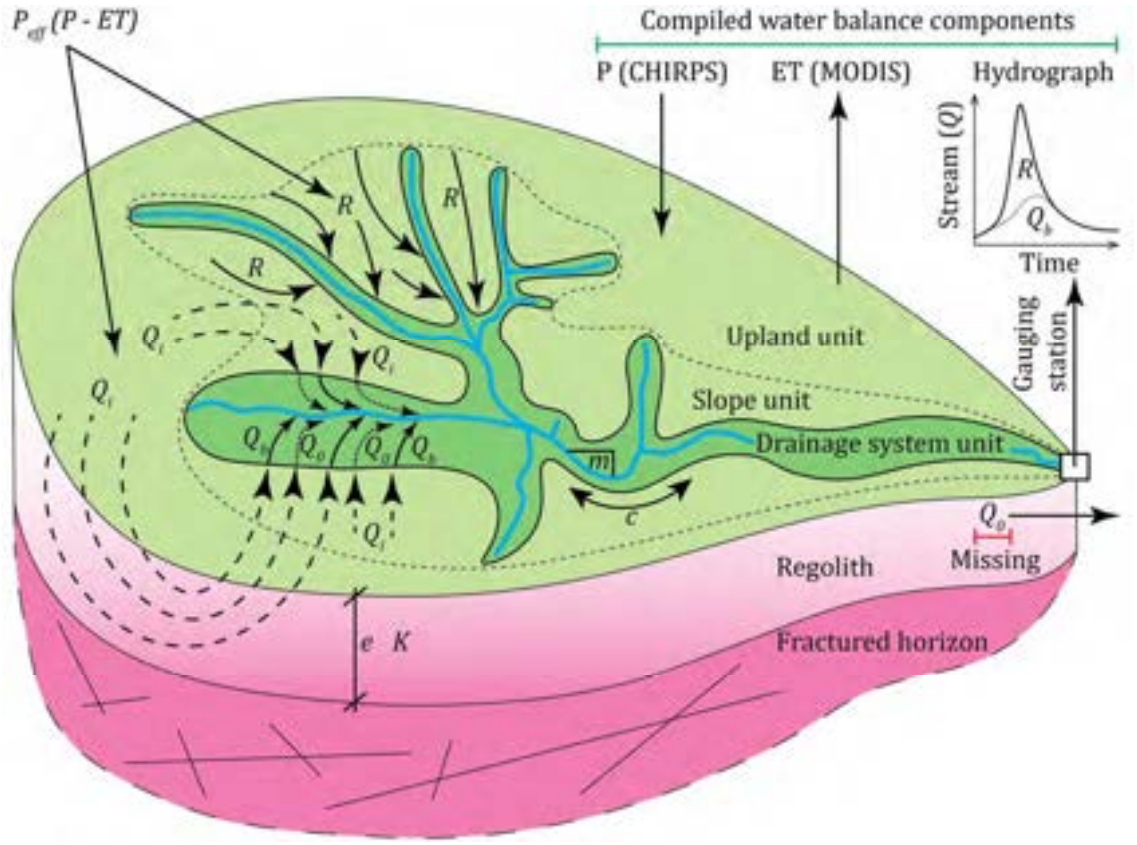

Fig. 5.6 *Illustration of an idealized regolithic catchment to embed the water balance in the hydrogeomorphological landscape unit concept (Winter, 2001). A portion of the effective precipitation P_{eff} falling on the upland and slope unit becomes groundwater recharge Q_i that infiltrated the weathered layer and flows (dashed arrows) towards the drainage system unit and becomes either base flow Q_b draining into the drainage (solid arrows) or groundwater flow Q_0 (dashed arrows). The portion of the P_{eff} that did not infiltrate becomes runoff R. P and ET are obtained from remote sensing products, and the discharge Q is measured at a gauging station and separated into Q_b and R by hydrograph separation techniques. The terms e and K are the thickness and hydraulic conductivity respectively of the regolithic aquifer. The terms m and c are the slope and perimeter respectively of the drainage system. The water components highlighted in green could have been recovered and compiled for this study and the red, i.e. Q_0 is missing.*

The regolithic environments have generally low hydraulic conductivities (Appendix C.2.2), with an average of approximately 3 x 10^{-6} m/s (Table C.1) and for the transmissivity it is 5 x 10^{-5} m^2/s (Table C.2), as deduced from literature values. This results in substantial hydraulic gradients depending on groundwater recharge, with the piezometric surface often close to the topography (Haitjema and Mitchell-Bruke, 2005). Since the water tables are high and sub-parallel to the topography in regolithic environments, the isopiezes are similar, though attenuated, to the iso-contours of the topography. Therefore, such aquifers are referred to be topographically controlled (e.g. Haitjema

and Mitchell-Bruke, 2005). This means that the hydrogeological basin equals the hydrological catchment (e.g. Lachassagne et al., 2021). In the regolithic environments, groundwater flows mainly in the weathered layer, overlying the (fractured) bedrock (Chilton and Smith-Carington, 1984). At the catchment scale, the thickness of the weathered layer varies from 20 to 40 m (Wright, 1992), but with an estimated average thickness of about 30 m (Appendix C.2.1), as suggested by Ollier et al. (1988).

Since regolithic aquifers are topographically controlled, this implies that where the aquifer intercepts the topography, there is necessarily exfiltration, and this occurs where the drainage has incised the landscape (Kirkby and Chorley, 1967; Fetter, 1980). This means that the drainage system results from a seasonally varying water table and gradient, consequently its slope represents the average hydraulic gradient (Montgomery and Dietrich, 1989; Dunne, 1990). As the aquifers are topographically controlled, the flow lines converge towards the drainage system (e.g. Dunne, 1969). This means that all the rainwater that was transformed into groundwater recharge, will eventually flow towards the drainage system, being the discharge areas, either transforming into base flow or axial groundwater flow (Dunne et al., 1975; Dunne, 1980). The axial groundwater flow, i.e. the part of the groundwater that does not discharge as base flow into the drainage system, also converges towards the drainage systems but leaves the system without being captured by measurements at the gauging station (Fig. 5.6). Since the entire drainage system essentially acts as discharge area, groundwater recharge can be neglected within the drainage HGM unit as it is largely saturated (Horton, 1945), thereby contributing as a whole to surface runoff. Conceptually, groundwater recharge therefore only takes place in the upland and slope HGM unit (Winter, 2004). However, in the slope HGM unit surrounding the drainage a fraction of the average precipitation also transforms into runoff because the saturation front fluctuates within this unit, since the water table is close to the surface (Dunne and black, 1970; Dunne and al., 1975).

The conceptual model shown in Fig. 5.6 illustrates how the effective precipitation P_{eff} is split amongst the different HGM units into runoff and groundwater recharge in regolithic aquifer systems. A systematic analysis of whether and which characteristics of the easily mapped HGM units can be used to estimate groundwater recharge on the catchment scale, given only P_{eff} from remote sensing products (but not discharge measurements), is the objective of the following two chapters, with the perspective of integrating the notion of sustainable groundwater potential into the revised RGWPM methodology.

In Chapter 6, the data set from the 20 reference catchments, i.e. the water balance components and HGM units are used in a cross-comparison analysis similar to that presented in Section 4.5, leading

to an empirical water balance-HGM unit relationship to estimate groundwater recharge on the catchment scale. The analysis suggests that indeed the HGM units reflect physical processes governing the different surface and subsurface processes. With the aim to integrate the notion of sustainable groundwater potential into the revised RGWPM methodology, the empirical groundwater recharge relationship was again applied to the Bidibidi case-study, calculating the sustainably extractable groundwater (defined at catchment-scale as 1/3 of groundwater recharge) along the entire drainage system and visualising three different sub-catchment sustainable cumulated extraction rate ranges. By doing this, sub-catchments were then isolated, and the actual extractions were compared to the sustainable groundwater potential, revealing sub-catchments which are over-exploited and others which still have a potential for further groundwater development.

In Chapter 7, the possible physical processes relating the HGM units to the water balance components to estimate groundwater recharge is explored using a simplified analytical approach, reflecting the above conceptual model (Fig. 5.6). A comparison of the groundwater recharge estimation derived from the empirical solution and the analytical approach are indeed coherent, thereby consolidating the initial intuition that easily mapped landscape features, such as the HGM units, reflected in the RGWPM units, can indeed inform on sustainable groundwater potential and not only, as in the initial RGWPM methodology (Section 2.4) on expected well yields.

Chapter 6

Analysing the relationship between water balance components and HGM landscape units to estimate gw. recharge: integrating sustainable groundwater potential into RGWPM

6.1. Introduction

From a general perspective, estimating groundwater recharge is a prerequisite to assess the sustainability of extractions by boreholes on a (sub)catchment-scale. For RGWPM, recharge estimation is essential to evaluate the sustainable groundwater potential (GWP). The concept of potential has so far been approached on the borehole-scale only, i.e. based on a yield threshold for a type of water supply (Section 2.4), disregarding surrounding boreholes. An estimate of the sustainable GWP is therefore necessary in areas that are already densely drilled. This must be considered in light of the increasing number of people in camps and settlements (Section 2.2). In such configurations, GWP zones may no longer yield what RGWPM forecasts over a long time-period.

The hydrogeomorphological (HGM) landscape units reflect the dominant surface and groundwater processes, i.e. runoff, recharge, or discharge as summarized in Fig. 1.2. but described in detail in Section 2.4. In Section 3.2, these units were considered sufficient for RGWPM to express the GWP. Afterwards, in Section 4.5, it was raised that there may be a relationship between the RGWPM units and recharge. For this purpose, the fourteen RGWPMs realized during the project were used. However, due to limited data, only the upland unit where exclusively diffuse recharge occurs could be evaluated, since a water balance could not be established on the catchment scale. The RGWPMs are all located in areas where only precipitation and evapotranspiration are available from remote sensing products. It was therefore only possible to make a preliminary assessment of the units where only one process is certain to occur, at that stage. Nevertheless, it was shown that there seems to be a correlation between the upland unit fraction with effective precipitation and the hydraulic conductivity associated to the dominant lithologies at each site. In order to further develop this idea and to determine the possible relationships between the upland and the other units, i.e. slope and drainage system, where recharge and runoff occur simultaneously, a systematic analysis could only be envisaged for catchments with known water balance components, being the reference catchments presented in the previous chapter.

The purpose of this chapter is to systematically analyse the possibilities of estimating groundwater recharge with the data of the water balance components and HGM units of the 20 reference catchments presented in Section 5.4. First, this data set is simply used in a cross analysis, to identify relationships. This analysis leads to an empirical relationship, expressing runoff as function of precipitation and the ratio between the upland and drainage units. The empirical expression for runoff is then introduced into the water balance equation to estimate groundwater recharge, based only on readily available remote sensing data of precipitation and evapotranspiration. While this first empirical relationship is reassuring under the assumption that the HGM units can indeed be used to quantify actual surface water and groundwater processes, it is explored in more detail in Chapter 7 through a physical model based on the groundwater flow equation adapted to use the units.

This chapter first presents the steps leading to the empirical solution that can be derived from the correlation between water balance components and HGM units of the 20 catchments to resolve runoff and thus groundwater recharge. Then, this solution is applied to the case-study in Bidibidi, for which groundwater recharge is estimated on the (sub)catchment scale using the established relationship, allowing identification of sub-catchments where the cumulated extractions exceed the estimated exploitable groundwater recharge (1/3 of groundwater recharge) indicating over-exploitation, and other sub-catchments, which indicate that extractions could be further developed. An amendment is thereby suggested to the revised RGWPM methodology, which allows to transform the estimated sub-catchment groundwater recharge into visualised sustainable groundwater potential on the sub-catchment scale. The amended methodology of the revised RGWPM is presented again for the Bidibidi case.

6.2. Analysis of water balance component-HGM units relationships

As already discussed in the previous chapter (Section 5.3), to quantify groundwater recharge in data-scarce regions, it is most convenient to use the water balance method with available precipitation and evapotranspiration data from remote sensing products (e.g. CHIRPS and MODIS, Appendix C.3). However, to solve the water balance, the runoff must be known, and without a gauging station, it cannot be estimated accurately (e.g. Blöschl, 2006). Therefore, in order to comment on either recharge or runoff, wherever this information is not available, they are assessed through the upcoming analysis via their presupposed relationship with the HGM units (Section 4.5).

The correlation between the HGM units and groundwater recharge or runoff obtained from the 20 reference catchments (Section 5.4) is presented in Fig. 6.1. In order to evaluate either runoff or recharge with the HGM units, all entities are normalized with respect to the catchment size, in order to compare their respective fractions. Similarly to the HGM units that are divided by the total

catchment area, both water balance components (i.e. runoff and recharge) are divided here by the system water input, either by precipitation or by effective precipitation. Figure 6.1 shows a matrix in the upper part that compares the fractions of recharge Q_i or runoff R with precipitation P (Q_i/P and R/P) and Q_i with effective precipitation P_{eff} (Q_i/P_{eff}) to the fractions and relative fractions of the fundamental HGM landscape units (Fig. 1.2). The relative fractions are understood as: upland/slope, upland/drainage, slope/drainage and finally (upland + slope)/drainage. In the matrix, the degree of correlation between recharge or runoff and the unit fractions is given by the Pearson correlation coefficient (Pearson, 1895) abbreviated r. The grade of r is shown as blue (positive) or red (negative) bars to visualize the correlation. For any combinations with r greater than 0.7, the data were plotted in the graphs below the matrix. The graphs were labelled from (a) to (f), referring to the lowest (0.72) to highest (0.92) r obtained in the matrix.

x/y HGM land. units		Q_i/P	R/P	Q_i/P_{eff}
1	upland fraction	0.28	-0.76	0.72
2	slope fraction	-0.36	0.29	-0.37
3	drainage fraction	0.06	0.86	-0.68
4	upland/slope	0.36	-0.40	0.46
5	upland/drainage	-0.02	-0.92	0.76
6	slope/drainage	-0.33	-0.50	0.30
7	(upl.+ slo.)/dra.	-0.14	-0.85	0.66

x = unknown (discharge measurments)

y = known (CHIRPS and MODIS)

Pearson correlation coefficient (r) = correlated (+) or anti-correlated (-)

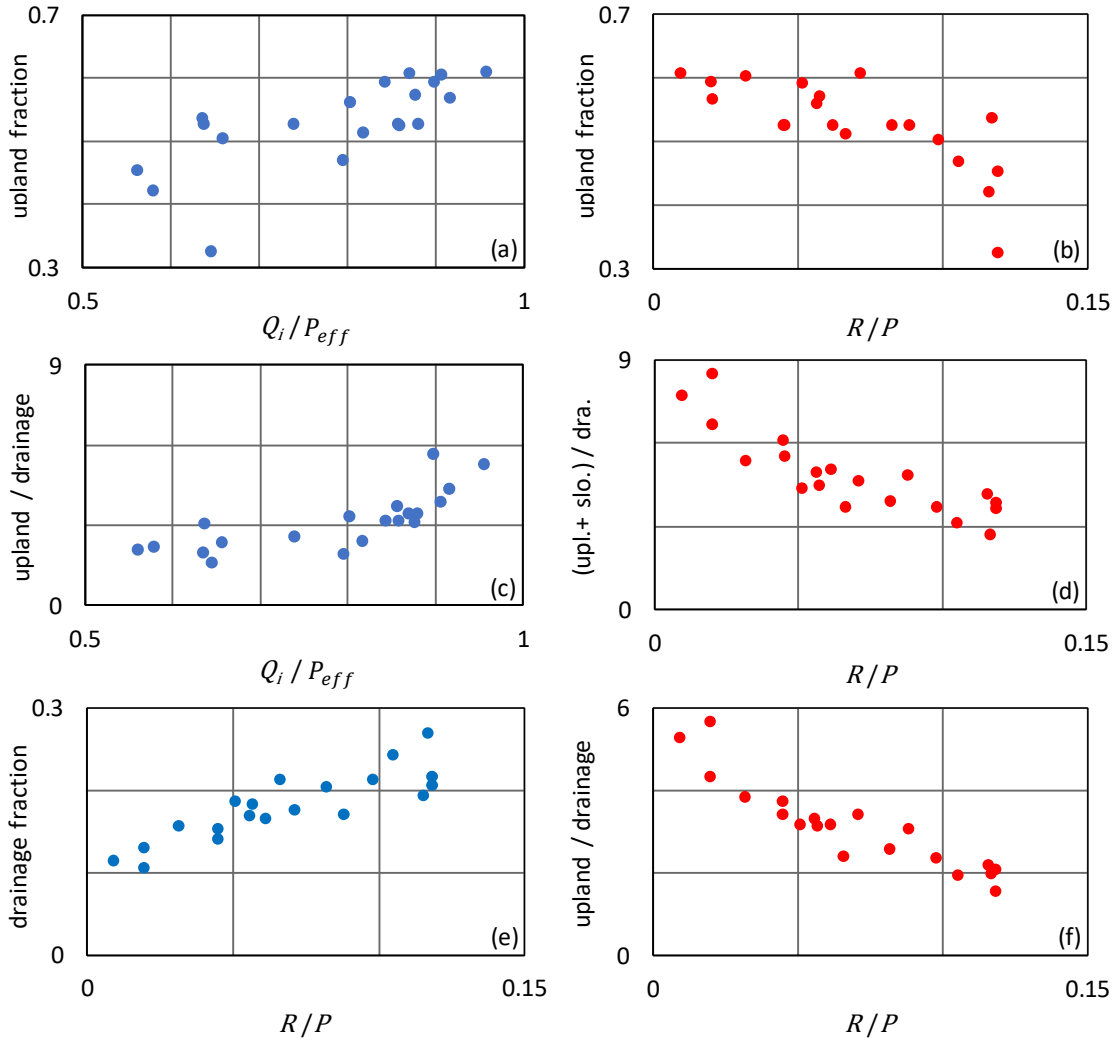

Fig. 6.1 *Correlation matrix and plots of the combination of the fraction of hydrogeomorphological (HGM) landscape units (Fig. 1.2.), i.e. upland slope, and drainage system, to groundwater recharge (Q_i) or runoff (R) over precipitation (P) or effective precipitation (P_{eff}). Q_i and R represent the unknown variable (x) and P and P_{eff} are known (y) with data from CHIRPS and MODIS. In the matrix, the degree of correlation is indicated by the Pearson coefficient (r). For a correlation of ±0.7, the data are plotted in the graph below the matrix. The graphs are labelled from (a) through (f) and refer to the correlation coefficient in the matrix.*

In Section 2.4 and 5.5, it was discussed that the HGM units indicate where different groundwater processes occur. In the upland unit, there is exclusively diffuse recharge. In the slope unit, there is recharge and runoff, while in the drainage unit, there is primarily runoff. Since the upland unit reflects only one groundwater process (diffuse recharge), it was stated earlier in Section 4.5 that the larger it is, the bigger the relative recharge capacity must be. This idea can be observed in the correlation matrix in Fig. 6.1 in row 1 where there is indeed a positive correlation between the upland fraction and Q_i over P or P_{eff}. The correlation for Q_i/P_{eff} is much higher (a positive r of 0.72) than the one for Q_i/P. This higher correlation makes sense since the portion that is evapotranspired must be subtracted from the precipitation to obtain the fraction that transforms to groundwater recharge in the upland. This correlation is plotted in Fig. 6.1a, it is not perfect, but it is clear that the Q_i/P_{eff} ratio increases as the upland unit gets larger.

Still in the first row of the matrix (Fig. 6.1), the upland unit fraction with R over P exhibit a significant anti-correlation with an r of -0.76. This is also consistent with the previous idea presented in Section 4.5 that the larger the upland unit fraction is, the higher the recharge and thus the lower the runoff further down in the landscape. The fraction R/P is plotted in Fig. 6.1b. It does appear that the data are somewhat less scattered than for Q_i/P_{eff} in Fig. 6.1a, but neither aligns perfectly.

According to the aforementioned, in both cases, a relationship appears between the Q_i or R ratios and the upland unit fraction but it is not perfect (row 1 of the matrix in Fig. 6.1). As far as Q_i is concerned it is for sure because there is also an important part of the precipitation that infiltrates in the slope unit. This is to some extent demonstrated by the weak correlations obtained with the fraction of the slope unit (row 2 of the matrix in Fig. 6.1) where neither groundwater recharge nor runoff can be properly captured, indicating that the processes there are far more complex to capture. However, the correlation becomes better when considering the drainage unit fractions (row 3 of the matrix in Fig. 6.1). In the drainage system, it is argued that one process, as in the uplands, prevails, namely runoff because it is mostly saturated. This is particularly well demonstrated between the drainage fraction and R/P which returns a high positive correlation (r = 0.86) and a decent alignment of the data (Fig. 6.1e) which indeed suggests that the greater the drainage unit fraction is, the more of P is transformed into R.

It is shown in Fig. 6.1 that the conceptual model, as described Section 5.5, may indeed, indicate where which groundwater-related processes typically occur. This is particularly the case for the upland and drainage unit where groundwater recharge and runoff occur as dominant processes, respectively (e.g. Figs. 6.1a and e), with slope unit playing an intermediate role. Thus, the relative fraction of the HGM units between them is at last discussed to capture the relevant relationships. In

Fig. 6.1, the last 4 rows of the matrix show the correlation for the upland/slope, upland/drainage, slope/drainage, and finally (upland + slope)/drainage. The fractions comprising exclusively slope, i.e. upland/slope and slope/drainage (row 4 and 6 in the matrix in Fig. 6.1) do not show any appropriate correlations. This is again attributed to the fact that in the slope unit, both Q_i and R might occur. However, the correlation for the fraction of upland/drainage with Q_i/P_{eff} is acceptable (r = 0.76) with an appropriate alignment of the data shown in Fig. 6.1c. This can also be observed with the fraction of (upland + slope)/drainage which shows a strong anti-correlation with R/P (r = -0.85) and a highly satisfactory alignment of the data in Fig. 6.1d indicating that indeed most of the runoff comes from the drainage unit alone.

Finally, according to the matrix in Fig. 6.1 the best anti-correlation (r = -0.92) is obtained with the unit fractions of upland/drainage and R/P. The data for this combination align very well as shown in Fig. 6.1f. Here, it is demonstrated that the larger the upland unit is relative to the drainage unit, the lower the runoff and inversely, the larger the drainage unit, the bigger the runoff fraction is. This indeed is in good agreement with the hydrogeomorphological concept (Section 2.4 and Section 5.5) in which it is stated that in the upland there is exclusively diffuse recharge and in the drainage system mostly runoff, where logically, as the fraction of upland gets smaller there is simply less precipitation infiltrating. If there is a better correlation with R/P than with Q_i/P, this is most certainly, related to the fact that the magnitude of runoff is directly related to the intensity of precipitation because as soon as it rains a fraction is immediately transformed into runoff and the remaining portion is first intercepted by vegetation before becoming Q_i making the correlation with Q_i/P_{eff} in Fig. 6.1c indeed greater.

The runoff data R used here are measured at gauging stations (Section 5.3). The locations of these stations are equivalent to the system outlet (Fig. 5.6) and their location determines the size of the catchment. Since for all 20 reference catchments there is a good correlation between R/P and upland/drainage unit (Fig. 6.1f), this means that whatever the size of the catchment (Fig. 5.4), the fraction of the landscape that ingests the precipitation and returns the runoff is always well captured by the HGM units. Hence, this suggests that this correlation can be used to express R for any type of regolithic catchment without gauging station, only using rainfall data for P from CHIRPS and the upland and drainage unit, which we know can be easily mapped. Consequently, this R can then be used in the water balance of Eq. 5.4 to be solve for Q_i which is demonstrated in the next section.

It can be concluded that with this simple analysis based on comparing HGM units with groundwater recharge or runoff fractions obtained from water balance analysis, surface processes are better captured than the subsurface ones. At this point, the reason for this result remains unanswered,

meaning that the entire water cycle cannot be explained by HGM units alone. It has to be kept in mind that the water balance components are all based on long-term averages, while units result from the integration of a long series of temporally highly variable events, which almost renders the above rather good correlations astonishing, implying that a regolithic landscape itself is somehow an 'average' or integrated reflection of the dynamic interplay between water inputs and hydraulic conductivity which translate into a dynamic equilibrium between physical and chemical weathering processes.

Since the above analysis allows for a good approximation of the runoff by means of precipitation and HGM units (Fig. 6.1f), groundwater recharge can now be estimated by simply deducting the runoff from the effective precipitation using the water balance equation, presented in the following section.

6.3. Empirical solution to estimate groundwater recharge at catchment scale based on readily available water balance data and mapped HGM units

The above evaluation of the relationships between HGM units and water balance components revealed the best correlation between upland/drainage units and precipitation (Fig. 6.1). Figure 6.2 shows the close-up of Fig. 6.1f of this relationship, i.e. between R/P and upland/drainage units. With this relationship it is possible to estimate R using the equation for the trend line and known variables, i.e. P, upland and drainage. A simple logarithmic function (Fig. 6.2, upper right corner) is found to be most appropriate. The coefficient of determination (R^2) of this function is high, being 0.9.

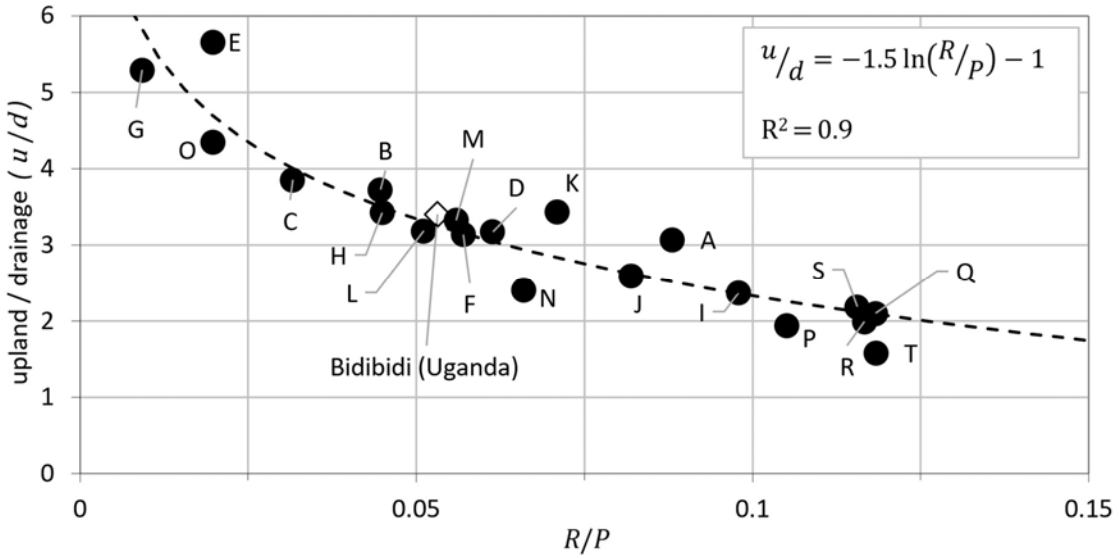

Fig. 6.2 *Relationship from Fig. 6.1f obtained from Runoff over precipitation (R/P) and upland over drainage (u/d) units. The data are from the 20 catchments indicated by the capital letters referring to Fig. 5.1. A logarithmic trend line runs through the data most successfully and is shown in the upper right corner. The case of Bidibidi (Uganda) has also been added as an example, but it is derived in Chapter 7.*

The function of the trendline obtained in the graph of Fig. 6.2 and given bellow is now used and solved for R:

$$^{u}/_{d} = -1.5 \ln(^{R}/_{P}) - 1 \tag{6.1}$$

where u is the surface of the upland and d the surface of the drainage.

So that R equals to:

$$R = e^{\left(-\frac{^{u}/_{d}+1}{1.5}\right)}P \tag{6.2}$$

With Eq. 6.2, runoff component R can now be obtained for any catchment for which upland and drainage units have been mapped and for which precipitation has been generated with CHIRPS. Equation 6.2 can now be used in the water balance Eq. 5.4 with the precipitation and evapotranspiration from MODIS to obtain an estimate of the groundwater recharge Q_i. Hence, Q_i can be expressed as follows:

$$Q_i = P - ET - e^{\left(-\frac{^{u}/_{d}+1}{1.5}\right)}P \tag{6.3}$$

With these empirical R and Q_i obtained from Eq. 6.2 and Eq. 6.3 respectively, they can now again be compared with the water balance components derived in Chapter 5. In Fig. 6.3a, the empirical R is first compared to that derived from discharge measurements taken at the gauging station using the

hydrograph separation technique (Section 5.3 and Appendix C.3.4). Afterwards in Fig. 6.3b the empirical Q_i is compared to the one obtained from the water balance calculations (Eq. 5.4) using now the empirical R from Eq. 6.2 and remote sensing for precipitation and evapotranspiration. The results of these comparisons show that an even better correlation is obtained for Q_i (Fig. 6.3b).

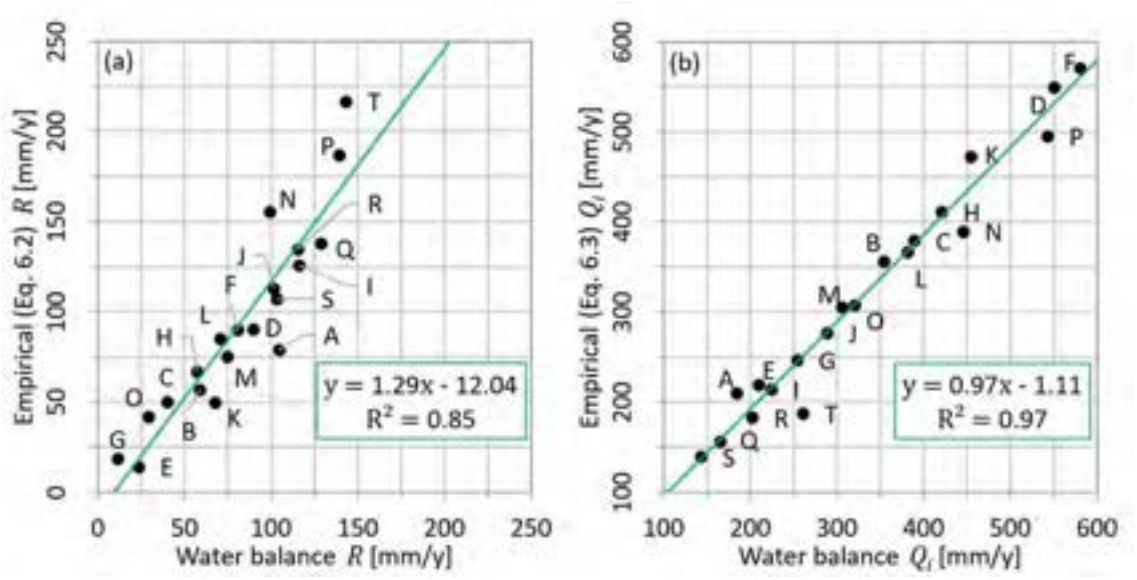

Fig. 6.3 a *empirical runoff R from Eq. 6.2 versus R derived from discharge measurements using the hydrograph separation technique (Section 5.3 and Appendix C.3.4).* ***b*** *empirical groundwater recharge Q_i obtained with Eq. 6.3 versus groundwater recharge Q_i derived from Eq. 5.4 with empirical R and precipitation and evapotranspiration from remote sensing summarized in Fig. 5.5.*

The results presented in Fig. 6.3a and b suggest that runoff and consequently groundwater recharge can be estimated almost equally well on a catchment scale with the HGM unit-precipitation empirical relationship (Fig. 6.2) as with existing gauging stations (Section 5.3). The highly relevant consequence of this result is that in data-scare areas for which revised RGWPM are established, the only additional step required to estimate groundwater recharge is the average annual catchment precipitation and evapotranspiration, based on CHIRPS and MODIS respectively, opening the way to introducing the notion of sustainable groundwater potential into the RGWPM methodology.

6.4. Introducing the notion of sustainable groundwater potential on a sub-catchment scale

According to the empirical solution described above, it is possible to easily evaluate the runoff R and thus the groundwater recharge Q_i for any specific catchment and sub-catchment, for which the basic characteristics of regolithic landscapes typical in Sub-Saharan environments is given. A catchment can originate from any defined point within the drainage system, and can therefore have

completely different sizes, but the assumption is made that the analogy with the derived runoff R established in Eq. 6.2 is still valid for any catchment size. For the reference catchments, the point defining the catchment size was the position of the gauging station, obviously located within the drainage system. As discussed earlier, in regolithic environments, water tables are topographically controlled (Section 5.5 and Appendix C.2.2), which means that the hydrologic catchment can be assimilated to the hydrogeological basin. Thus, if a borehole were to be drilled in the drainage unit, the associated groundwater capture zone must be situated within the hydrological catchment, with the position of the borehole defining its outlet. As refugee settings become more and more urban (with high population densities), where water supply has to be maximised and optimised aiming towards motorised systems, motorised boreholes should be drilled in the drainage unit, in order to capture as much groundwater as possible and having the highest probability of favourable hydraulic properties. Groundwater flow converges toward the drainage unit (Section 2.4, 5.5 and Appendix C.2.2), corresponding to medium or high GWP in the revised RGWPM methodology, suited for motorized systems.

In order to estimate the sub-catchment extraction of a borehole, the following 10 steps are proposed and illustrated in Fig. 6.4.

1. First produce a revised RGWPM (Section 3.2) allowing to identify the best location for a new borehole (Borehole #1) in a medium or a high GWP zone (drainage unit) not too far away, i.e. less than 10 km from the camp or settlement in order to remain within an economically viable water supply system (Section 2.2).
2. Generate a map of the drainage system and the corresponding catchment forming ‘upstream’ of the planned new borehole (Catchment #1).
3. Calculate the area of the upland, slope, and drainage unit (i.e. low, slope and medium plus high GWP) within Catchment #1.
4. Calculate the annual average precipitation and the evapotranspiration in Catchment #1 with CHIRPS and MODIS respectively.
5. Introduce the ratio of the mapped upland and drainage unit along with the precipitation and evapotranspiration into Eq. 6.3 to calculate the groundwater recharge for Catchment #1, defined by the position of the borehole.
6. In order to estimate the sustainable extraction for Catchment #1, or the sustainable groundwater potential, a third of the estimated groundwater recharge is retained, roughly corresponding to the maximum that can be extracted from a catchment by boreholes without leading to signs of depletion.

7. Identify other boreholes within Catchment #1 and take the sum of their yields to produce the current cumulative extraction from Catchment #1.
8. Deduct the cumulative extraction from the sustainable groundwater potential to obtain the maximum possible extraction for Borehole #1.
9. After drilling and pump testing, ensure that daily extractions do not exceed the sustainable maximum extraction of the borehole. Note that the daily sustainable extraction rate must not be confused with the 'safe well yield', which is a function of the hydraulic properties in the vicinity of the borehole only.
10. Finally, it must be considered that boreholes located downstream of Borehole #1 could be impacted because they may also depend on Catchment #1.

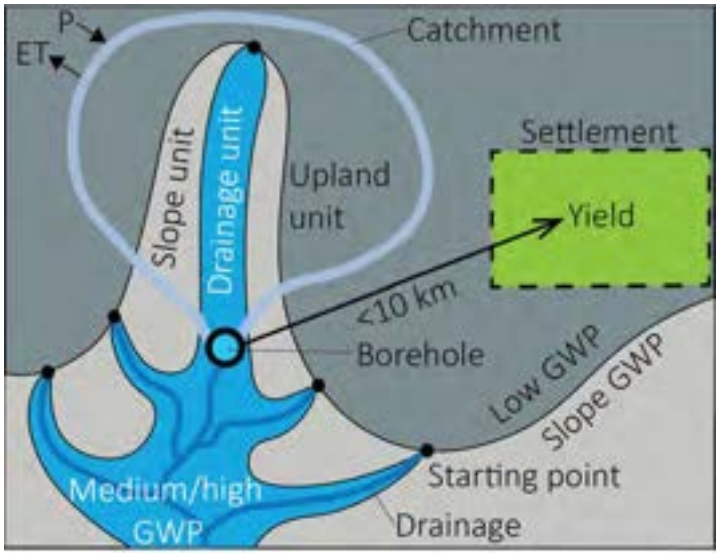

Fig. 6.4 *Illustration of the method for estimating the sustainable extractions from a sub-catchment. If there is only one borehole, this corresponds to the maximum sustainable extraction from that borehole. 1. Produce a revised RGWPM (Section 3.2). 2. Generate a sub-catchment from any given position of interest (e.g. new borehole). 3. Extract HGM units from RGWPM (upland, slope, and drainage unit) 4. Calculate sub-catchment groundwater recharge with Eq. 6.3 and divide by 3 to obtain sustainable sub-catchment groundwater potential.*

The above methodology can be used to introduce the notion of sustainable groundwater potential into the RGWPM methodology. To do so it is applied to the Bidibidi case-study by isolating the sub-catchments associated with the 15 high-yielding motorised boreholes and assessing the sustainable groundwater potential in order to identify those boreholes which are in a state of over or under-exploitation.

6.5. Introducing sustainable groundwater potential in the Bidibidi RGWPM case-study: assessment of groundwater sustainability on sub-catchment scale

In this section the groundwater recharge estimation method presented in Section 6.4 is evaluated using data from the 15 motorized systems in the settlement of Bidibidi in Uganda. In most cases (apart from two), there are no other motorised boreholes in the associated sub-catchments. Therefore, the names given to the sub-catchments are the same as the borehole names. The specificities of these boreholes can be found in the digital Appendix A. In order to introduce the notion of sustainable groundwater potential into the already existing revised RGWPM (Fig. 3.3) on a sub-catchment scale, for which the HGM units, corresponding to the WA classes have already been mapped, the sub-catchments are generated from the digital elevation model using the borehole positions as sub-catchment outlets. These HGM units are then used together with the precipitation and evapotranspiration in Eq. 6.3 to obtain the recharge, which, divided by three yields the sustainable groundwater potential. The locations of the boreholes with their respective catchments and HGM units are shown in Fig. 6.5. In Fig. 6.5, the same extension of the Bidibidi RGWPM (Fig. 2.3 or 3.3) is used but only the information relevant for the following analysis on the sub-catchment scale is shown. The base map shows the extension (dotted lines) of the Bidibidi RGWPM with the locations of the motorised boreholes (black dots) labelled with numbers, referenced to the UNHCR id in Table 6.1. The catchments forming upstream of each borehole are shown in light blue and the drainage lines in dark blue. In order to correctly display the units of each catchment, 5 squares labelled (a) to (e) indicate by an arrow close-ups of catchment groups. The three units, upland, slope, and drainage are shown in dark grey, light grey, and blue, respectively, and are designated as HGM units in the legend. It can be seen that there are only two sub-catchments, boreholes 9 and 15 which contain a second motorised system within the associated catchment, boreholes 3 and 9, each with their respective sub-catchments. For all other boreholes, the catchment extractions correspond to the extractions of the borehole defining the catchment outlet.

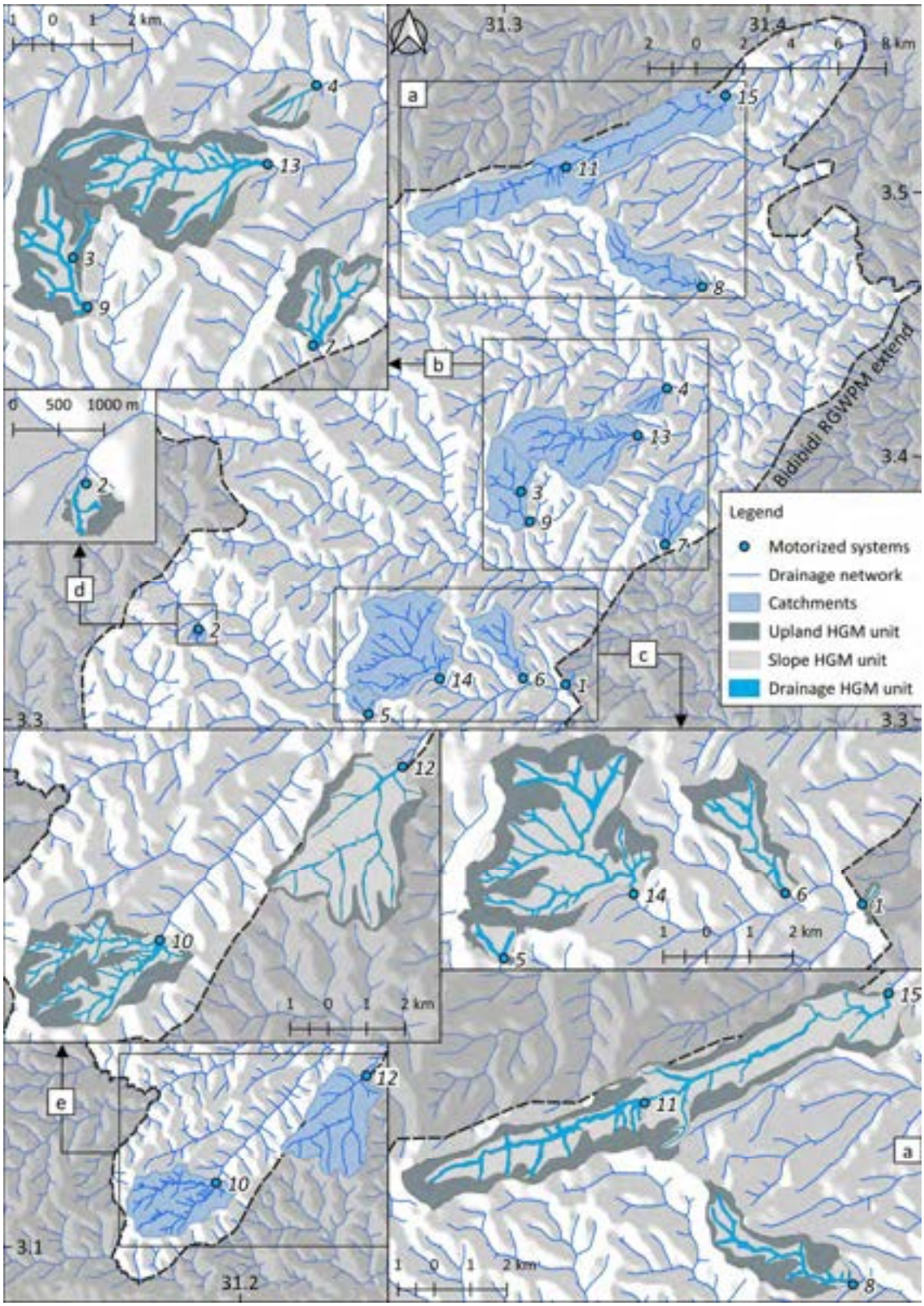

Fig. 6.5 *Caption on next page.*

Fig. 6.5 *RGWPM of Bidibidi revealing the hydrogeomorphological (HGM) units (Fig.1.2) within the catchments forming upstream of the 15 motorized boreholes used for assessment of the sustainable groundwater potential as described in Section 6.4. The base map shows the extent (dashed line) of the RGWPM (Fig. 2.3 or 3.3), the location of the boreholes as numbered (Table 6.1) and shown as black and blue dots, the drainage system (blue lines), and the catchment forming above each borehole (blue areas). The five close-ups labelled (a) through (e) show for groups of catchments the units of the upland, slope, and drainage contained in the sub-catchments.*

All 15 boreholes are located in the drainage unit (medium WA), which extraction rates defined by pumping tests, ranging from 5−80 m^3/h. Applying the method described in Section 6.4, with all the required elements available, and summarised in Table 6.1 for every sub-catchment/borehole (n° and Borehole id), yields the estimated groundwater recharge (Q_i) by use of Eq. 6.3. To solve Eq. 6.3, the average precipitation (P) and evapotranspiration (ET) were obtained and used homogeneously over the entire RGWPM domain (dotted line in Fig. 6.5) for all sub-catchments, as indicated in Table 6.1. The estimated sub-catchment groundwater recharge varies very little, ranging from 178−194 mm/year, as illustrated bellow the table in the box plot 6.1b. Since precipitation and evapotranspiration were kept constant in all calculations, the small variation of calculated groundwater recharge (Q_i) expressed as mm/year confirms that the HGM unit ratios vary very little from one sub-catchment to another (6.1a). To obtain the sustainable sub-catchment groundwater potential the groundwater recharge is multiplied by the sub-catchment size and divided by three ($Q_i/3$). The sustainable sub-catchment groundwater potential or $Q_i/3$ is classified in Table 6.1 from the smallest to the to the highest and expressed in m^3/h. For all catchments containing only one borehole, the last column, showing the borehole yield as measured by pump tests, can be directly compared to the sustainable groundwater potential of the sub-catchment $Q_i/3$, revealing whether the catchment is over-exploited (i.e. 'borehole yield' is greater than sustainable sub-catchment groundwater potential) or not.

Table 6.1 *Data used to estimate the yield of the 15 motorized systems at Bidibidi with the method presented in Section 6.4. The numbers (n°) refer to the catchments forming above the boreholes in Fig. 6.5 and the borehole id to Appendix A. The fraction of upland to drainage, precipitation (P) and evapotranspiration (ET) are used to calculate runoff (R) in mm/year with Eq. 6.2 or groundwater recharge (Q_i) with Eq. 6.3. After that Q_i is converted to m³/h with the size of the catchment (catch. Q_i) and divided by 3 to obtain the sustainable sub-catchment groundwater potential (catch. $Q_i/3$). At the bottom of the table, two box plots **a** and **b** show the distribution of the fraction of upland over drainage and Q_i in mm/year to emphasize that there is little variation from one catchment to another.*

n°	borehole id (UNHCR)	catch. [km²]	upland unit [km²]	slope unit [km²]	drainage unit [km²]	upland/drainage	P [mm/y]	ET [mm/y]	R [mm/y] (Eq. 6.2)	Q_i [mm/y] (Eq. 6.3)	catch. Q_i [m³/h]	catch. $Q_i/3$ [m³/h]	borehole yield [m³/h]
1	OxfamBH5	0.22	0.13	0.05	0.04	3.4			67	185	5	2	14
2	69232	0.27	0.13	0.10	0.04	3.5			61	192	6	2	6
3	44558	0.76	0.49	0.13	0.14	3.6			61	192	17	6	16
4	OxfamBH1	1.23	0.44	0.65	0.13	3.3			72	181	25	8	15
5	MSF BH1	1.25	0.62	0.45	0.18	3.5			65	188	27	9	5
6	69222	3.46	1.59	1.41	0.46	3.5			65	188	74	25	70
7	69224	3.98	1.85	1.58	0.56	3.3			72	181	82	27	60
8	69223	5.48	3.03	1.54	0.92	3.3	1271	1018	73	180	113	38	30
9	OxfamBH3	5.96	3.26	1.77	0.93	3.5			64	189	129	43	15
10	69408	8.99	4.32	3.42	1.25	3.4			66	187	192	64	10
11	69221	9.66	4.71	3.49	1.45	3.2			75	178	196	65	80
12	69407	10.86	2.21	7.98	0.67	3.3			72	180	224	75	14
13	OxfamBH2	11.72	5.67	4.48	1.58	3.6			59	194	259	86	16
14	69449	13.70	5.77	6.17	1.77	3.3			74	179	280	93	12
15	OxfamBH4	22.46	8.67	11.19	2.60	3.3			71	182	466	155	40
					Average	3.4	1271	1018	68	185			

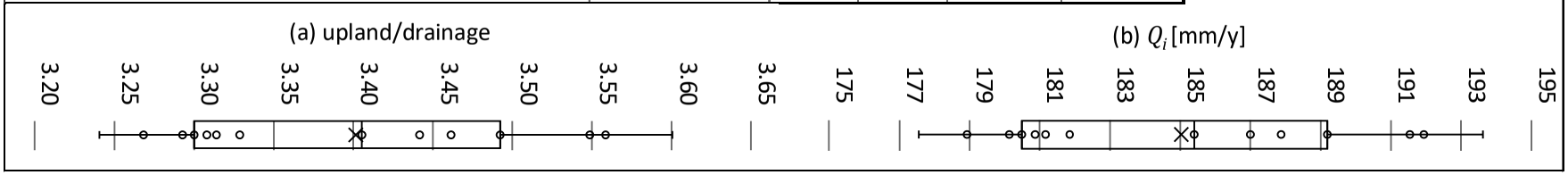

The above application of the method presented in Section 6.4 was illustrated on a real case-study, Bidibidi (Uganda). It is shown how groundwater recharge can be estimated very easily to obtain a sustainable groundwater potential for any sub-catchment. At this point, one could imagine applying this method at an earlier stage to assess whether drilling new boreholes in that area is sustainable or not. This method is further developed in this section, where it is illustrated how it can be used to assess the sustainability of the water supply at the settlement level, before proceeding with the spatial visualisation of the sustainable groundwater potential in the RGWPM methodology in the next section, thereby adding the so far missing dimension of water quantity and sustainability.

In order to evaluate the sustainability of a borehole and its water supply, the actual yields of the 15 boreholes in Bidibidi are compared to both the catchment groundwater recharge Q_i and the sustainable groundwater potential $Q_i/3$ in m^3/h obtained with the method described in Section 6.4 and summarized in Table 6.1. This is illustrated in Fig. 6.6 where the n° of the boreholes, corresponding to catchments are indicated on the lower axis and the sub-catchment extractions on the vertical axis. The catchment extractions are illustrated by red, orange, and green circles in order to present the state of exploitation (i.e. over, critical, and safe) in relation to the catchment groundwater recharge 'catch. Q_i' and the sustainable catchment groundwater potential $Q_i/3$, represented by red and green bars respectively. The boreholes were classified according to 'catch. Q_i'. Boreholes or catchment n°9 is downstream of borehole n°3 and borehole n°15 is downstream of borehole n°11 (Fig. 6.5). Therefore, the catchment extractions are the sum of the two boreholes contained in the catchments n°9 and n°15, respectively.

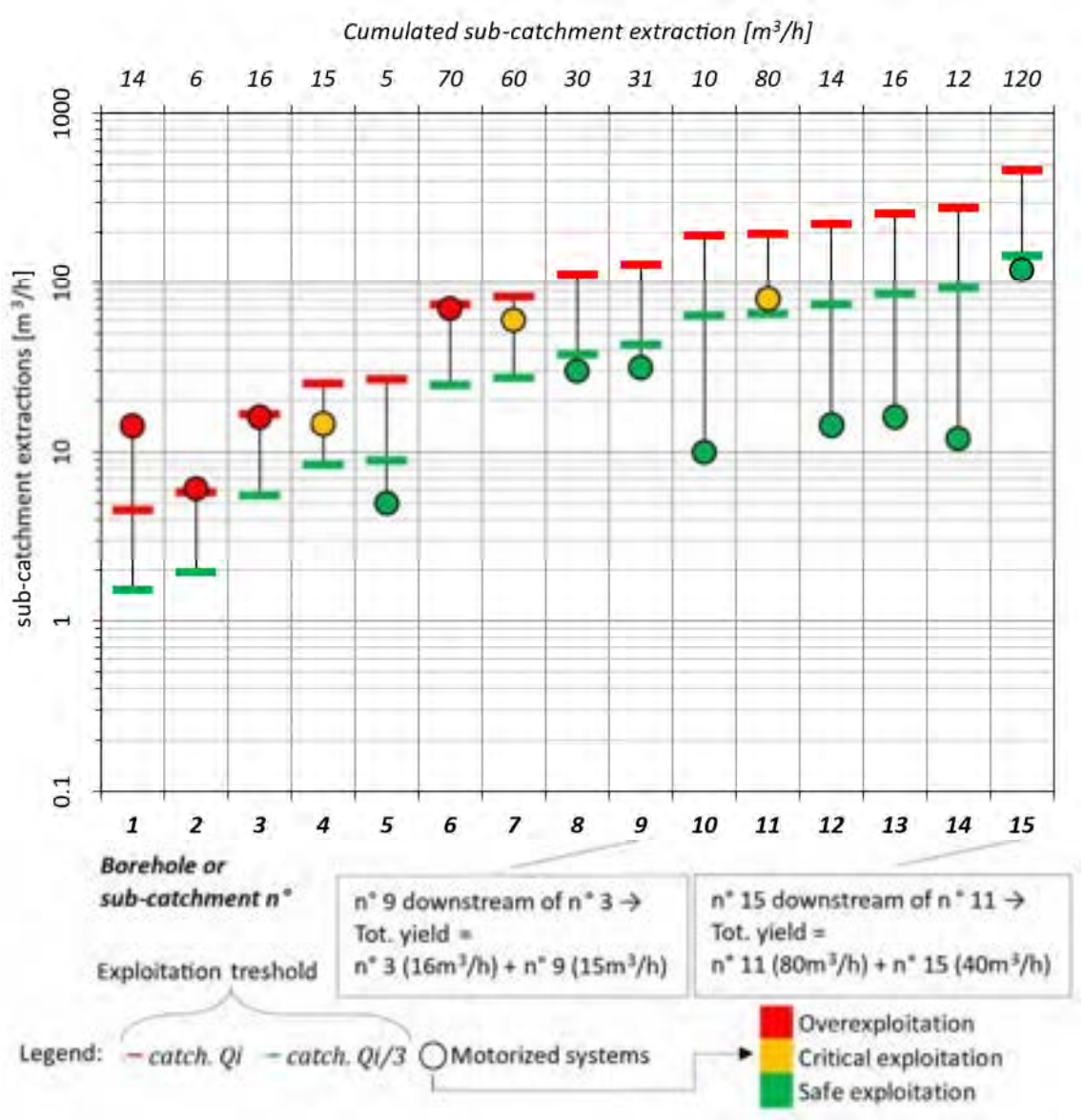

Fig. 6.6 *Comparison of the sub-catchment extractions, corresponding to boreholes yields of the 15 Bidibidi motorized systems with the groundwater recharge 'catch. Q_i' and sustainable groundwater potential $Q_i/3$ obtained by the method presented in Section 6.4, based on data shown in Table 6.1. The borehole or catchment n° in reference to Fig. 6.5 are shown on the lower axis and the catchment extractions in m³/h on the upper axis (Table 6.1). The actual catchment extractions are represented by circles while catch. Q_i and $Q_i/3$ are represented by red and green bars, respectively. If the yields are above, between or below the range catch. $Q_i - Q_i/3$, their circles are coloured red, orange and green, respectively, indicating their degree of sustainability.*

Through Fig. 6.6 the sustainability of the 15 sub-catchments can be discussed by assessing the position of the catchment extractions (circles) with respect to the calculated catchment groundwater recharge 'catch. Q_i' and the sustainable catchment groundwater potential 'catch. $Q_i/3$' (red and green bars, respectively). If the catchment extractions are below catch. $Q_i/3$, it means that

the extraction is lower than the sustainable catchment groundwater potential and can therefore be considered sustainable (green circles). If the catchment extractions are between catch. Q_i and $Q_i/3$, it means that the exploitation is critical (orange circles), withdrawing more than the sustainable groundwater potential but less than the annual groundwater recharge. If the catchment extractions exceed catch. Q_i, it simply means that more than the annual recharge is being withdrawn and therefore the current exploitation scheme is not sustainable (red circles).

The method presented in Section 6.4 to easily calculate catchment recharge 'catch. Q_i' for any location where there is a borehole, allows an assessment of the overall sustainability of the exploitation of the groundwater within the catchment (Fig. 6.6). In addition, it can also be used as a practical tool for management of the water resources and remediation of overexploitation. For example, considering those boreholes presented in Fig. 6.6, the pumping rates of boreholes located in the 4 overexploited catchments (red circles) can be reduced so that they fall below Q_i (red bar). To maintain the same volume of overall groundwater extraction (i.e. assuming this level of extraction is directly linked to the water supply needs of the area), the reduction for these four boreholes could then be redistributed and extracted from the sustainable catchments (green circles) while ensuring that they remain within the catch. Q_i and $Q_i/3$ range (red and green bars). This allows, at the settlement level, to continue to meet the required demand, but without over extracting certain sub-catchments. If the water distribution scheme were to be changed, this allows all systems to operate in the long term.

The method for estimating catchment recharge 'catch. Q_i' (Eq. 6.3) and sustainable groundwater potential is difficult to validate with the boreholes in Bidibidi (Fig. 6.6), since the implemented groundwater monitoring system that captured groundwater levels in each of the boreholes was disrupted and data therefore not available. However, should these data become available in the future, it would certainly be very useful to assess the predictability of the sustainable groundwater potential by means of the empirical relationship between HGM units and water balance components. Decisions on where to target groundwater monitoring equipment or activities could be informed by this assessment procedure as it can provide clear indication of catchments which are at higher risk than others.

6.6. Adding the notion of sustainable groundwater potential and groundwater recharge to the revised RGWPM methodology: case-study Bidibidi

The method presented in Section 6.4 aimed at introducing the notion of sustainable groundwater potential into the RGWPM methodology, which in its revised version (Chapter 3), did not allow to assess how many boreholes can be exploited sustainably in an area, but only estimate the expected

yield ranges one may encounter in the different mapped GWP zones. The relationship between precipitation, runoff and the HGM units has allowed to estimate groundwater recharge on the catchment scale and to define the sustainable groundwater potential as a third of the sub-catchment groundwater recharge, allowing to compare the exploitation with the sustainable extraction potential for any sub-catchment. Consequently, the next step is to represent groundwater recharge Q_i, defining the limit of over-exploitation on the RGWPM. Using the revised RGWPM methodology (Section 3.2), it is possible to identify GWP zones with a certain yield threshold for a single borehole based on water supply options. However, these thresholds are broad (Section 2.4), ranging from 5 to 50 m^3/h in the medium GWP zone. Therefore, it is intended to better spatially represent these two yield end members in addition to a single zone-wide threshold. This is done only for the medium GWP zone because it does not seem necessary to further investigate the low and slope GWP zones that are only suitable for hand pumps and already substantially assessed in Section 2.7 and 4.3. As for the high GWP zone, since it is rarely encountered and exists only very locally (Section 3.2), it is also excluded from this analysis.

In order to assess the 5 and 50 m^3/h yields along the medium GWP zone, it was deemed useful to work with the drainage system. In fact, this zone lies within the drainage system, i.e. the drainage hydrogeomorphological unit (Section 3.2). Groundwater recharge that occurs primarily on the upland and slope (low and slope GWP) is concentrated along the drainage (Section 5.5 and Appendix C.2.2). In order to spatially represent the location in the drainage system where recharge happen to become a certain volume, the size of the catchments needed to produce either flow rate by groundwater recharge has to be calculated. This is simply done by dividing these two flow rates in m^3/h by the groundwater recharge in mm/year to obtain a surface. After that, in any GIS software, one can easily generate the drainage system that initiates for a given catchment surface. For the following analysis, three recharge volumes, 5, 50 and 500 m^3/h, are chosen; for the first two, they represent the range of the medium GWP, and 500 m^3/h has been added to present an additional order of magnitude. These values are actually arbitrary and rather selected here as an example, in fact any specific value could be represented.

The aforementioned technique was applied to the settlement of Bidibidi (Section 2.5) and the result is shown in Fig. 6.7. In Bidibidi, according to Table 6.1, groundwater recharge Q_i [mm/year] does not vary a lot so that the average, i.e. 185 mm/year can be used to calculate the 3 catchment sizes producing 5, 50 and 500 m^3/h, respectively. After this, it is possible to generate the 3 drainage sections indicating where there is a groundwater recharge accumulation of 5, 50 and 500 m^3/h and for any section downstream of the 500 m^3/h section, it is simply assumed that the cumulated catchment extractions can be higher than 500 m^3/h. Depending on the density of boreholes and the

cumulated extractions within a catchment, it could very well be relevant to define other classes and extraction rates to be visualised in the RGWPM. In Fig. 6.7, the low and slope GWP zones of the revised RGWPM (Fig. 3.2) are reused but the previous medium and high GWP zone are replaced with the three drainage sections giving 5, 50 and >500 m^3/h and represented by light blue, blue and dark blue lines respectively and labelled in the legend as medium 1, 2 and 3. The 15 motorized systems with their respective catchments coloured green, orange and red according to the sustainability study performed in Fig. 6.6 are also added to the map in Fig. 6.7.

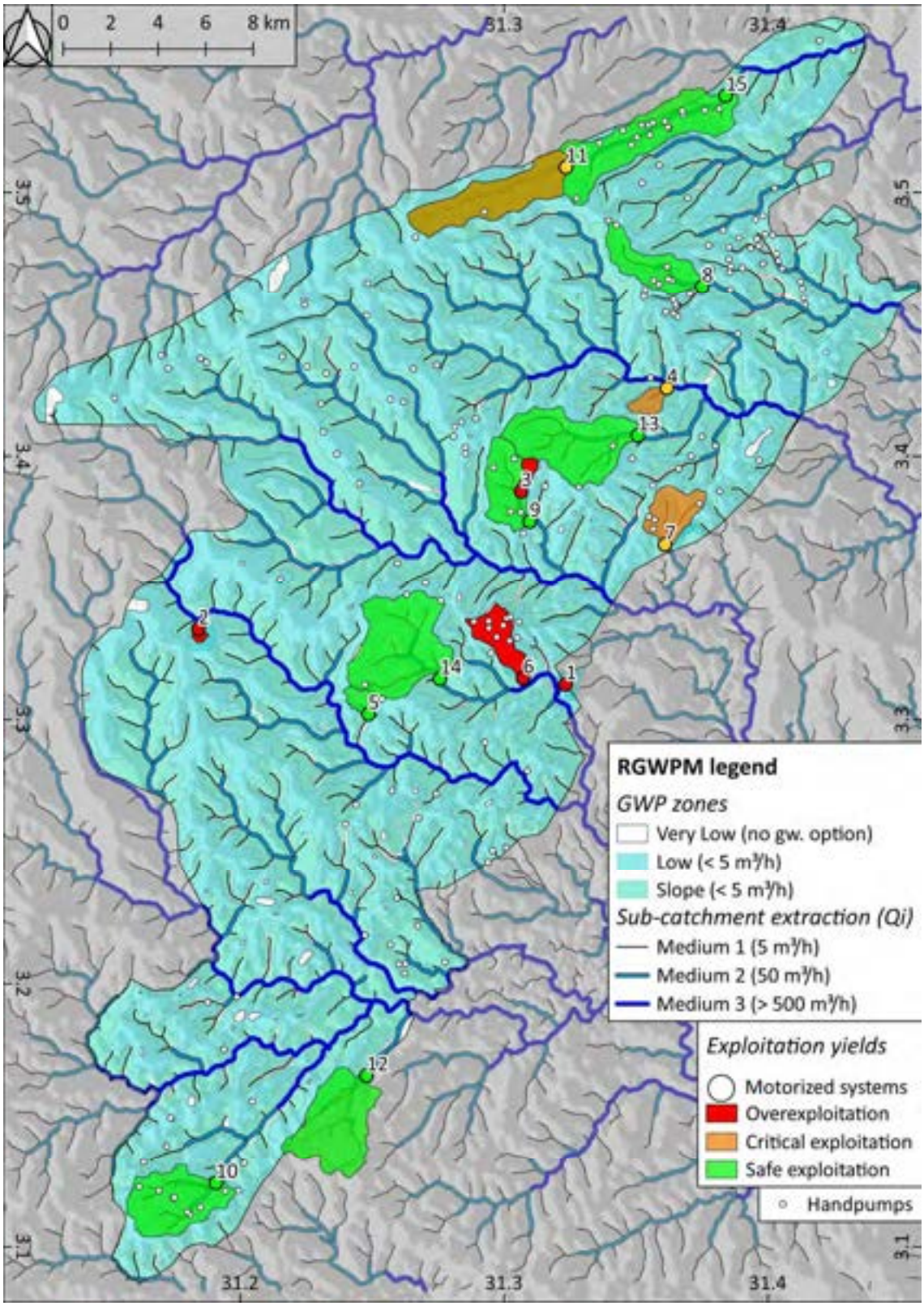

Fig. 6.7 *Caption on next page.*

Fig. 6.7 *Water balance integrated RGWPM of the settlement of Bidibidi based on Fig. 3.2 and the groundwater recharge method presented in this chapter. The low, slope, and high GWP zone of the previous revised RGWPM are reused and the medium GWP zone is refined with the recharge method presented in Section 6.4. The new medium GWP zone is subdivided into 1, 2, and 3 representing 3 yield ranges of 5, 50, and >500 m^3/h and shown on the map as light blue, blue, and dark blue lines respectively. The locations of the 15 motorized systems are indicated by green, orange, and red circles. The colours of the boreholes correspond to the sustainability study performed in Fig. 6.6. The catchments that form above the boreholes are also indicated and coloured according to the borehole circle to show where additional boreholes should not be implemented so as not to impact the existing systems. The white circles indicate the hand pumps.*

The revised RGWPM (Fig. 3.2) becomes now the water balance integrated RGWPM (Fig. 6.7) introducing the notion of groundwater recharge and sustainability zone is now believed to be relevant for coordinating the borehole siting of small motorized system more efficient than with the revised RGWPM methodology (Section 3.2). In fact, it is now shown where one might be more successful in implementing effectively boreholes sustainably yielding 5, 50 and >500 m^3/h, or how many boreholes with different discharge rates (according to local conditions) can be implemented and expected to be sustainable in a same sub-catchment. In addition, highlighting the existing state of sustainability of sub-catchments (green, orange, or red) clearly indicate where groundwater exploration should focus for further drilling campaigns.

In conclusion, on the map in Fig. 6.7, it can be seen that the 5 m^3/h drainage section of 'medium 1' always starts very close to the low GWP (upland). The low GWP is said to yield about 0.5 to 5 m^3/h (Section 2.4). The most possible place to find the maximum of 5 m^3/h in the low GWP, is indeed very likely to be at the beginning of the drainage system or starting point (Montgomery and Dietrich, 1988; Dietrich et al., 1986) where the groundwater flow starts to converge towards the drainage system (e.g. Dunne, 1969). It is therefore rather encouraging that with the very simple method presented in Section 6.4 a meaningful spatial representation of groundwater recharge and sustainable exploitation potential could be added in full coherence with the conceptual framework established early in this work, described in Section 2.4.

6.7. Conclusions

Through some preliminary evidence via the broader application of the revised RGWPM methodology (Section 3.2) to other camps and settlements (Chapter 4) it was observed that groundwater recharge may be correlated with characteristics of the mapped HGM units (Section 4.5). In order to evaluate this intuition, a thorough water balance analysis was carried out on 20 reference catchments across Sub-Saharan Africa (Section 5.4), with known water balance and HGM units. All catchments were selected to be located in similar climatic and lithological conditions of regolithic environments.

The objective of this chapter was to evaluate the possibility of finding a simple and practical way of introducing notions of water balance into the RGWPM methodology, requiring estimation of groundwater recharge with limited data, but using the already mapped HGM units of the revised RGWPM. Therefore, this first analysis simply consisted in cross comparing the water balance components and the HGM units of the 20 catchments, resulting in several relationships (Fig. 6.1). Yet, the best relationship was obtained between the fraction of runoff to precipitation versus the fraction of upland to drainage HGM unit (Fig. 6.2). In fact, if these two fractions are plotted against each other the data align astonishingly well, revealing a clear trend, suggesting that there is a physical explanation to this correlation. The relationship led to an empirical formulation (Eq. 6.2) that allowed runoff to be expressed as function of readily available data for any area, i.e. precipitation and HGM units, then introduced in a simple water balance to estimate recharge at the catchment scale (Eq. 6.3).

After deriving this empirical solution from the reference catchments, its application was evaluated on the 15 sub-catchments of motorized boreholes in Bidibidi. The methodology for applying the solution is the same, except that the catchment that forms upstream of a borehole location is used (Fig. 6.5). The unique aspect of regolithic environments is that the aquifers are topographically controlled so that the hydrogeological basin is the same as the hydrological catchment (Section 5.5 and Appendix C.2.2). This implies that all precipitation falling on the catchment that is not evapotranspired leaves the catchment as runoff or groundwater recharge at a single outlet. This means that if a borehole is placed in the drainage system, it could effectively capture most of the recharge. The sustainable catchment extractions, referred to as sustainable groundwater potential that were obtained with this approach allowed to evaluate the sustainability of each sub-catchment (Fig. 6.6). It turns out that among the 15 sub-catchments, 7 have a cumulated extraction rate that could lead to an unsustainable exploitation of the resource. On the other hand, the other 8 sub-catchments have a cumulated extraction rate in line with the capacity of the resource, even with a potential for further groundwater development, which could compensate for over-exploited catchments. Indeed, such an evaluation allows action to be taken at the camp or settlement level to modify the overall extraction scheme while still meeting the required demand.

Finally, the empirical solution was used to spatially transform the sub-catchment groundwater recharge into three different cumulated sub-catchment extraction rates (Fig. 6.7), allowing indirect visualisation of groundwater recharge in the water balance integrated RGWPM. The purpose of this step permits to better characterize the GWP of the RGWPM zones. Indeed, until now the potential is based on the exploitation rate and the type of water supply option, disregarding how many boreholes would be drilled within the same medium GWP zone, which is specifically addressed,

having the highest potential to induce over-exploitation. As the low and slope zones were found to be suitable only for hand pumps (Section 4.3), it has not been considered necessary to further assess them. Indeed, as the trend in the humanitarian sector is towards solarization/motorization of boreholes (Section 2.2). The zones that have proved capable of accommodating this type of supply are at least the medium zones. As for the high zone, since it only appears very locally and basically belongs to the same zone as the medium, i.e. the drainage unit, it is considered sufficient to simply extend the information from the medium to it. Eventually, with an average recharge obtained with the 15 borehole catchments and some basic GIS manipulations based on the drainage and ignition thresholds, it is possible to represent three zones along the drainage unit potentially producing 5, 10, and >500 m^3/h. This further distinction of the medium zone is shown to be useful for coordinating drilling activities but also relevant for assessing the exploitation status of a certain zone in relation to existing boreholes. Indeed, if the cumulative yield of the existing system located within a same catchment exceeds the estimated groundwater recharge or the sustainable groundwater potential, no additional boreholes should be considered.

The empirical solution was derived from a simple analysis based on the comparison of hydrogeomorphological landscape units with groundwater recharge and runoff fractions (Fig. 6.1). Based on this first analyse, it was concluded that the units better reflect the surface process leading to runoff, reason why the solution is based on runoff. This means that the hydrogeomorphological concept of Winter (2001) first described in 2.4, additionally reflects some well-founded physical processes discussed more thoughtfully in Section 5.5. However, it does not fully reflect the complexity of the subsurface since only a weak correlation between groundwater recharge and HGM units was observed. But having observed correlations, suggesting underlying physical processes, the following chapter will explore the conceptual model presented in Section 5.5, using a simple analytical approach, to mathematically describe both groundwater recharge and runoff processes in coherence with the conceptual model and to compare it to the observed data set from the reference catchments. This leads to a quantitative assessment of the empirical solution developed and introduced into the water balance integrated RGWPM methodology in this chapter.

Chapter 7

Groundwater recharge estimation on catchment scale combining HGM concept with analytical groundwater flow equation

7.1. Introduction

The RGWPM approach is primarily based on the hydrogeomorphological concept (Winter, 2001) that describes in which landscape unit groundwater or surface water processes are most likely to occur (Section 2.4 and 5.5). In addition, the landscape units can be used for the actual quantification of the processes. Indeed, in the previous chapter, an empirical solution based on the water balance components and HGM units of the 20 catchments (Section 5.4) has been derived for estimating groundwater recharge. Specifically, the relationship between runoff to precipitation fraction versus upland to drainage unit fraction was found to be the most successful. Since precipitation and HGM units can be easily identified, it is possible to extract runoff which can then be used in the water balance to derive recharge (Section 6.3). This solution was applied to estimate the recharge at the sub-catchments of the Bidibidi boreholes and provided insights into sustainable groundwater potential.

The solution in Section 6.3 to express groundwater recharge is built on actual catchment data (Section 5.4) but remains empirical (Eq. 6.3). An analytical approach that would eventually allow discussion of the validity of this simple solution would be reassuring and is therefore the purpose of this chapter. The framework for this analytical approach is the general HGM concept integrated into the conceptual hydrogeological model of regolithic environments previously presented in Fig. 5.6. Subsequently, after developing the approach, it is validated twice. First, by comparing the results to the water balance components of the 20 catchments. Secondly, by comparing the recharges found for the Bidibidi sub-catchments with the empirical solution with the one obtained with those of this additional analytical approach.

7.2. Conceptual HGM groundwater recharge model

The hydrogeomorphological concept of Winter (2001) defines which landscape units preferentially transform effective precipitation into groundwater recharge or runoff. On the upland unit, only diffuse recharge occurs. In the slope unit there is recharge and runoff, while in the drainage system unit, runoff is predominant. This concept has been embedded with the general water balance of the regolithic environments and the general functioning of the regolithic aquifer (Section 5.5 and

Appendix C.2.2) in a conceptual model presented in Fig. 5.6. This model was largely inspired by earlier work summarized by Dunne and al. (1975) and Dunne (1990) and serves as basis for the following analysis.

In the regolithic environments of Sub-Saharan Africa, the largest fraction of runoff is usually created when the subsurface is fully saturated (e.g. Lachassagne et al., 2021), which is dictated by the position of the water table (e.g. Horton, 1945). In these environments, water tables are topographically controlled (e.g. Lachassagne et al., 2021), which means that they are sub-parallel to the surface (e.g. Haitjema and Mitchell-Bruke, 2005). This implies that when the water table rises, it first comes into contact with the areas where the drainage has incised the landscape. This is where groundwater can exfiltrate (Kirkby and Chorley, 1967; Fetter, 1980) and where precipitation falling on this drainage area in contact with the water table becomes direct runoff (Horton, 1945). However, this necessarily means that the slope unit surrounding this part of the drainage is near to complete saturation (Dunne and Black, 1970; Dunne et al., 1975). This is because the water table is already close to the surface, and even more so in environments where it is topographically controlled. This implies that in this part of the slope, a fraction of the precipitation also becomes runoff (Dunne et al., 1975; Dunne, 1980). In such a configuration, the drainage system essentially represents the top of the water table and so its slope can be assimilated to the hydraulic gradient (Montgomery and Dietrich, 1989; Dunne, 1990).

In topography-driven hydrogeological landscapes, the water tables may only rise to the starting points of the drainage systems (Montgomery and Dietrich, 1988; Dietrich et al., 1986). Indeed, the starting points define the limit of the upland unit above which it is never oversaturated since there is only diffuse groundwater recharge (Winter, 2001). However, the water table only occasionally reaches the upland unit. Actually, subsurface water exfiltrating at the starting point is rarely observed (Kirkby and Chorley, 1967; Fetter, 1980). These areas are characterised by hollows formed by erosion that are only in some rare cases excavated, as for example during continuous large storms leading the water table to be very high, (Kirkby and Chorley, 1967). This idea is of course plausible, otherwise, these features would simply migrate uphill at each event and end up close to the crest. This means that in the slope unit, there is indeed always both diffuse groundwater recharge and runoff but the limit where runoff starts is changing depending on the climatic conditions (Chorley, 1957; Dunne and al., 1975).

The aforementioned is illustrated in Fig. 7.1 which is intended to present the conceptual model for defining the framework of the mathematical solution described in the next section. Figure 7.1 has been largely inspired by earlier works summarized in Dunne et al. (1975) and Dunne (1990). In the

upper part of Fig. 7.1 two cross-sections (a) are shown of an idealized aquifer embedded in the terminology of the hydrogeomorphological concept of Winter (2001) presented in Fig. 2.1. This aquifer is depicted during a low and high-water table situation numbered 1 and 2 respectively (right). The low corresponds to the beginning of the rainy season and the high to its end. Below the cross-sections is an illustration of the catchment of this aquifer (Fig. 7.1b) combining the low and high situations. In the cross-sections and the catchment, the upland unit is abbreviated as A and the slope and drainage system unit are jointly designated as B. In the cross-sections, the water table is indicated by a light blue line and where it intersects the topography it is highlighted by a stippled dark line to show where subsurface water exfiltrates into the drainage and where runoff occurs into both the slope and the drainage system unit (also see Fig. 5.6). Runoff and exfiltration, i.e. base flow, are designated as R and Q_b, respectively, while effective precipitation is abbreviated P_{eff} and axial groundwater flow as Q_0. This process is illustrated in the catchment where the level of the water table is represented by the light blue shape meant to indicate where it almost intersects the surface in the slope unit. Where the water table gets into contact with the surface, i.e. in the drainage unit, it is highlighted with a bold blue line. The dotted line shows how the water table migrates up and down over the year from low 1 to high 2 stages. The red dotted line marks the upper limit to which the water table can rise, i.e. the upland unit. The black lines (Fig. 7.1b) indicate the dry drainage lines because the water table has not yet reached them, and the black dots are the starting points marking the boundary with the upland unit (A) and the slope plus drainage system units (B), being the maximum extend of the seepage area during exceptional rainfall events.

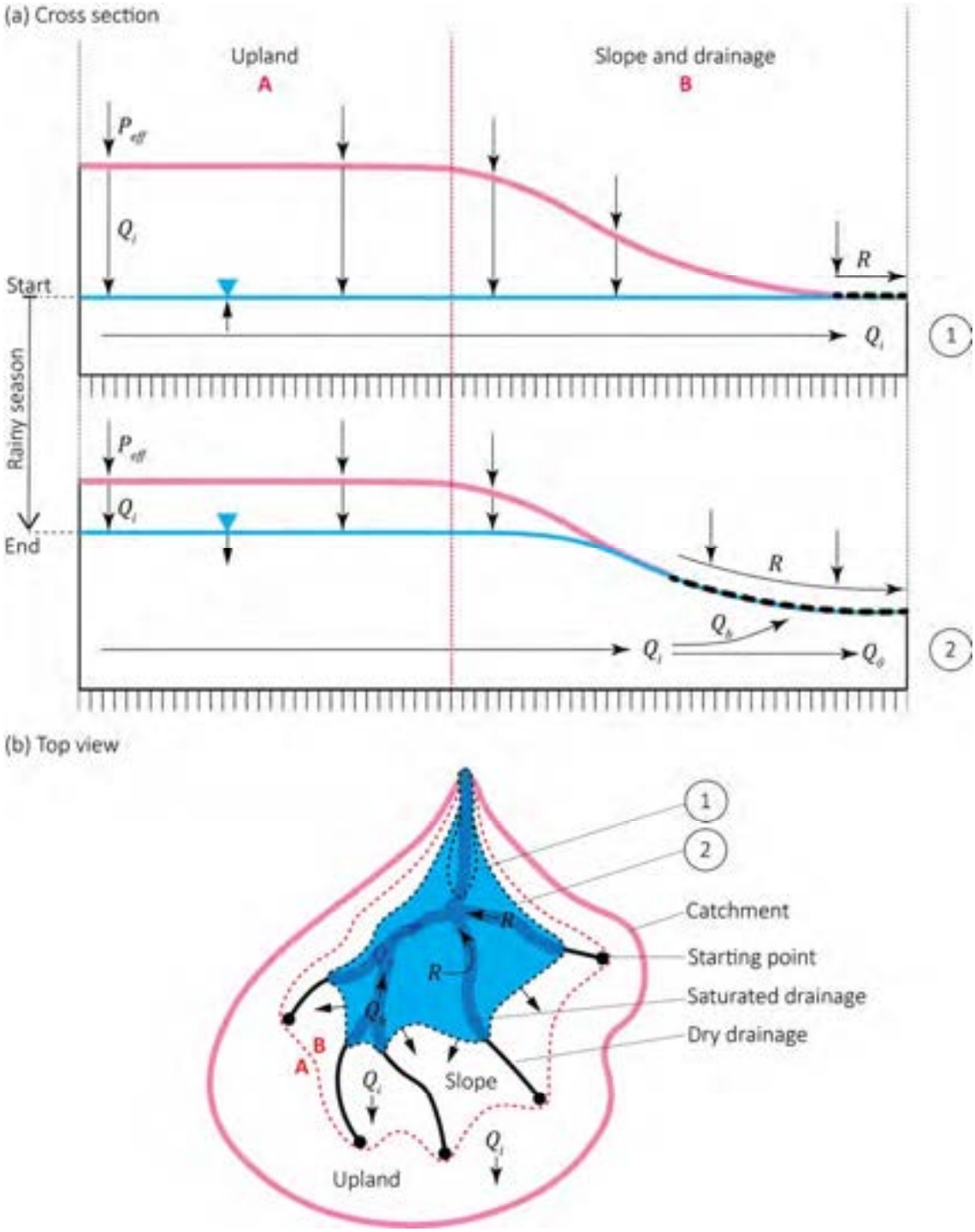

Fig. 7.1 *Caption on next page.*

Fig. 7.1 *Conceptual model of an aquifer describing the distribution of effective precipitation in runoff and groundwater recharge from a hydrogeomorphological perspective.* ***a*** *Cross sections of an idealised aquifer in a low and high-water table situation numbered 1 and 2 respectively.* ***B*** *Top view of the catchment of this aquifer.* A*: upland hydrogeomorphological unit;* B*: slope plus drainage hydrogeomorphological units;* P_{eff}*: effective precipitation*; Q_i*: groundwater recharge;* R*: runoff;* Q_b*: base flow;* Q_0*: axial groundwater flow. The blue line in* ***a*** *and surface in* ***b*** *represents the position of the water table. The black dashed lines illustrate the evolution of the water table from 1 and 2 situations and in* ***b*** *where it intersects with the topography (drainage system, i.e. black lines) it is highlighted by a bold blue line. The red dashed line marks the limit of the maximum the water table can reach, i.e.* A *unit in* ***a*** *and* A *unit or starting points (black dotes) in* ***b****.*

Based on the idea described above, to obtain an estimate of groundwater recharge it is sufficient to multiply effective precipitation by the area where the water table is low, i.e. on the upland and partly on the slope units. While it is easy to draw the upland unit based on satellite images (Section 2.4), it is impossible to obtain the fraction of the slope unit that is not in close contact with the water table. This fraction is therefore estimated in the following section. The objective here is to find from the available data, i.e. HGM units and effective precipitation, the location of the water table, which can then be extrapolated to the surface where water cannot infiltrate. For the mathematical model, it is assumed that all groundwater flows slowly due to the low hydraulic properties of the regolith (Appendix C.2.2). Therefore, in some way it accumulates to a greater extent than it immediately flows down within the slope towards the drainage system. In such a configuration, the water table reaches its maximum at the end of the rainy season. As formulated in Dunne (1990), the fraction of a specific rainfall event that managed to infiltrate is damped with the part of the previous events. So, that all the events become one single pulse of groundwater recharge reaching the water table indeed at the end of the rainy season (Youngs, 1958; Dunne, 1978; Sakura, 1983). Therefore, the hydrological year sum of effective precipitation can be used in a steady-state model describing the height of this water table. Consequently, conceptual model 2 (Fig. 7.1a) is used as a basis in the following section. The annual sums based on the hydrological year defined in Appendix C.3.3 that have been derived for the water balance components for the 20 catchments (Section 5.4) are subsequently used to validate this model.

7.3. Analytical expression of conceptual model

The conceptual model in Fig. 7.1a is translated into the technical sketch in Fig. 7.2 as a simplified 2D unconfined steady-state hydrogeological model. This allows describing the mathematical expression to assess the surface of the slope unit above the water table which is not saturated. This surface allows then to calculate the diffuse groundwater recharge to be added to that of the upland unit to obtain the overall groundwater recharge. The geometry of the model in Fig. 7.2 is simple. The topography is assumed to be flat on the upland unit (A) and uniformly inclined in the slope unit (B). In this sketch, the upland and slope plus drainage units are again abbreviated as A and B but marked

with an asterisk as A^* and B^* to emphasize that this is truly a 2D model where these units represent lengths for now. These lengths are subsequently converted to surfaces to work with the respective areas of the mapped units. In this model, the water table (blue line) is considered to be parallel to A^* (topographically controlled water tables, Section 5.5, and Appendix C.2.2) and therefore crosses B^* at a certain point which is inclined. The height of the water table is called H_0 and the thickness of the aquifer at the base of B^* is abbreviated h_0. Effective precipitation P_{eff} infiltrates over A^* and the fraction of B^* above H_0 which is B^* multiplied by a coefficient called α. This coefficient lies somewhere between 0 and 1. Therefore, the total length l where P_{eff} can infiltrate and become Q_i is $A^* + \alpha B^*$. After infiltrating along l, Q_i passes perpendicularly through the saturated thickness H_0. After H_0, the equipotential lines are assumed to be perpendicular to the base of the aquifer so that when the flow lines pass H_0, the consequence is that part of Q_i flows above h_0 and eventually exfiltrates as Q_b into B^*, specifically from a top view (Fig. 7.1b) into the drainage. The part of Q_i that flows into h_0 becomes Q_0. Therefore, the length L where exfiltration occurs and P_{eff} becomes R is equal to $(1-\alpha)B^*$. In this configuration, the hydraulic gradient between H_0 and h_0 is assimilated to essentially the slope of B^* (Montgomery and Dietrich, 1989; Dunne, 1990). This slope is expressed as m.

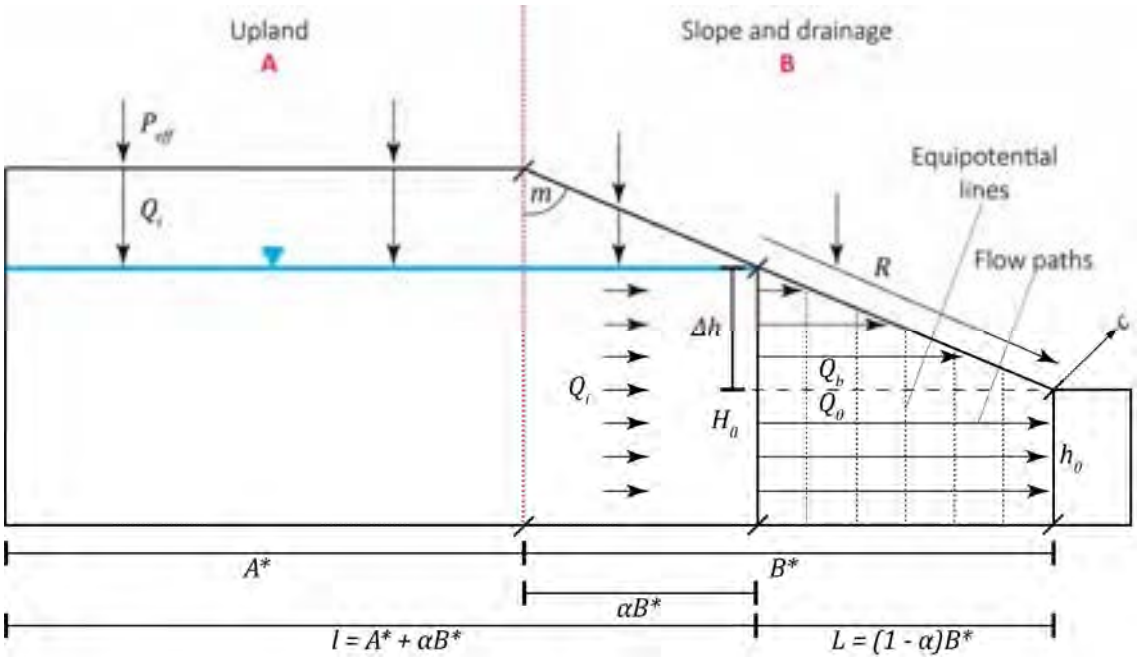

Fig. 7.2 *Technical sketch of the conceptual model in Fig.7.1a. The upland unit A is considered flat and the slope plus drainage unit B uniformly sloping. The surfaces of A and B are denoted as A^* and B^* to highlight that they represent lengths in this 2D model. The water table (blue line) elevation is abbreviated H_0 and marks the boundary between the upper part of B^* where P_{eff} infiltrates as Q_i and the lower part where it becomes runoff R. To express the fraction of B^* where recharge occurs it is multiplied by a coefficient α. Q_i crosses H_0 and if it is above or below the thickness of the aquifer h_0 becomes base flow Q_b or groundwater flow Q_0. The hydraulic gradient between H_0 and h_0 is the slope of the topography abbreviated m. The total length where there is Q_i is noted as l and the one where there is Q_b and R is indicated by L. l and L are expressed in terms of A^* and B^* with the coefficient α at the bottom of the sketch.*

According to Fig. 7.2, Q_i can be obtained by multiplying P_{eff} by l which is presented in Eq. 7.1. Here, the α in $(l = A^* + \alpha B^*)$ essentially represents the unknown that is sought in the subsequent mathematical development.

$$Q_i = Peff(A^* + \alpha B^*) \tag{7.1}$$

Given the 2D geometry of the model, Q_i is in L^2/T and can thus be expressed according to the Darcy's flow equation with the respective parameters in Fig. 7.2 as follows:

$$Peff(A^* + \alpha B^*) = KH_0 m \tag{7.2}$$

where K [L/T] is the hydraulic conductivity, H_0 [L] which is the height of the water table is defined as the fringe that Q_i crosses and m is the hydraulic gradient.

In Eq. 7.2, H_0 is unknown, but can be decomposed as follow:

$$H_0 = h_0 + \Delta h \tag{7.3}$$

With Δh that can be derived as follow:

$$\frac{\Delta h}{L} = \frac{\Delta h}{(1-\alpha)B^*} = m \tag{7.4}$$

So that Δh equals to:

$$\Delta h = m(1-\alpha)B^* \tag{7.5}$$

Introducing Eq. 7.5 into Eq. 7.3 yields:

$$H_0 = h_0 + m(1-\alpha)B^* \tag{7.6}$$

Equation 7.6 is now set in Eq. 7.2 and becomes:

$$Peff(A^* + \alpha B^*) = K(h_0 + m(1-\alpha)B^*)m \tag{7.7}$$

In order to work with the areas of the mapped landscape units (A and B) and express Q_i in L^3/T, the fictional lengths A^* and B^* must be converted to areas. It is assumed that multiplying these lengths by the perimeter of the drainage system unit should yield something fairly close to reality from a geometric perspective. Furthermore, when viewed from above, this perimeter in topographically controlled landscapes where groundwater converges on the drainage system (e.g. Dunne, 1969) represents the fringe that groundwater must necessarily cross (Dunne et al., 1975; Dunne, 1980). This has been especially highlighted in Fig. 5.6. Following this logic, the section of the 2D model thus unfolds in an accordion-like fashion along the drainage, resulting in a 3D model. According to Eq. 7.7, only B^* must be expressed as a surface. The perimeter of the drainage system (Fig. 5.6) is abbreviated to c and thus the surface of B can be expressed as:

$$B = B^* c \tag{7.8}$$

If Eq. 7.8 were to be introduced into Eq. 7.7 to express the left-hand side now with A and B in surface to get Q_i in L^3/T it yields:

$$Peff(A + \alpha B) = K\left(h_0 + \frac{m(1-\alpha)B}{c}\right)mc \tag{7.9}$$

In Eq. 7.9, the right side of Eq. 7.7 has been multiplied by c in order to formulate the fringe that the groundwater must cross, as mentioned above. For simplicity, Eq. 7.9 is developed as follows:

$$Peff(A + \alpha B) = Kh_0 mc + Km^2(1-\alpha)B \tag{7.10}$$

where the average thickness of the regolith is taken for h_0, approximated in the following according to the literature to 30 m (Appendix C.2.1).

Finally Eq. 7.10 is expressed for α with P_{eff} and K gathered as a fraction and becomes:

$$\alpha = 1 - \frac{\frac{p_{eff}}{K}(A+B) - h_0 mc}{B\left(m^2 + \frac{p_{eff}}{K}\right)} \tag{7.11}$$

In Eq. 7.11, with the exception of K, all terms are known. It might be possible to solve it at this point with literature values for K (Appendix C.2.2), but a simple method is developed below to obtain an average value that is thought to be closer to the reality of each location where this method is applied.

The coefficient α in Eq. 7.11 is a function of landscape units (here A and B), effective precipitation (P_{eff}) and hydraulic conductivity (K). The area of the landscape units can be assumed to remain fairly unchanged over time, but the precipitation may fluctuate. If this is the case, groundwater recharge is also affected. It is therefore possible to vary α in order to evaluate how P_{eff} and K alone are affected if A and B do not change. This coefficient α is a subrogate for the level of the water table since it indicates, when multiplied by B, the surface that is not in contact with the topography. This is illustrated in the figure below (Fig. 7.3) where three levels (WTL) are represented according to a maximum, minimum and actual α.

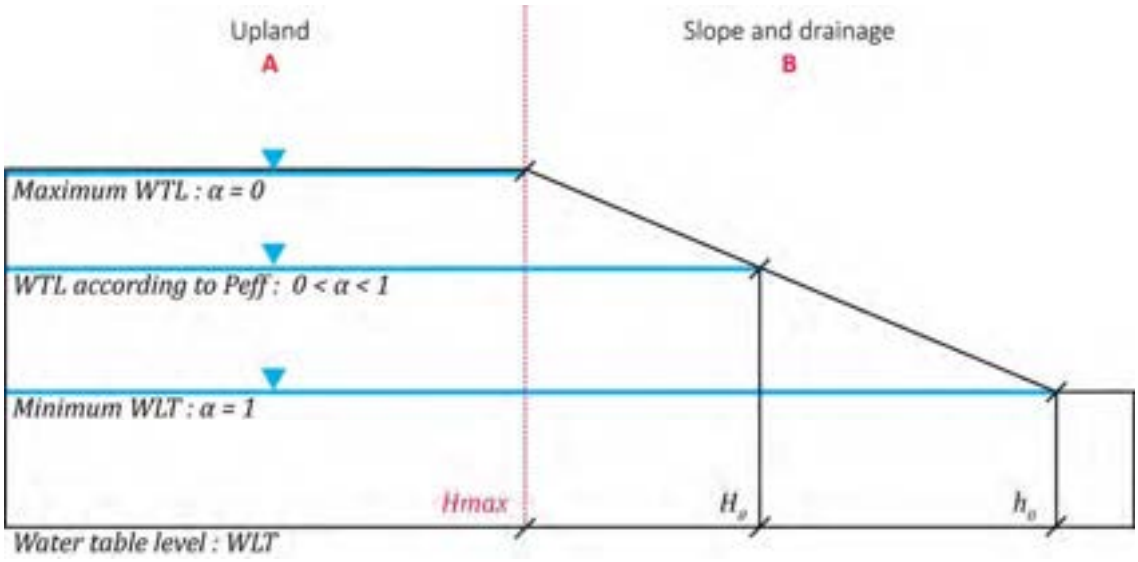

Fig. 7.3 *Illustration adapted from the technical sketch in Fig. 7.2 to present the location of the water table level (WLT) according to α from Eq. 7.11. α dictates the area in B where recharge occurs which translates to the area above the WTL. From Eq. 7.1 when α is 0 there is only recharge over A resulting in a WTL that rises almost to A at Hmax. When α is equal to 1 there is recharge over A and B (Eq. 7.1) so the WTL is at h_0. In reality the WTL fluctuates between the two extremes and crosses somewhere in B at H_0.*

The coefficient α varies between 0 and 1. If it is equal to 0, it means that P_{eff} can infiltrate only on A (Eq. 7.1); this translates into a P_{eff} event so large that it has completely saturated the aquifer and thus raised the water table almost to A at $Hmax$ (Fig. 7.3). On the other hand, if α is equal to 1, P_{eff} can infiltrate everywhere from A to B (Eq. 7.1). This situation may correspond to a very extended post-drought period. This means that the water table is at its lowest point and thus at h_0 (Fig. 7.3). For an average real P_{eff}, the water table rises somewhere in B as in Fig. 7.1a at H_0 and thus represents an average level between the two extremes. These extremes are only rarely reached. In fact, no unusual trends were noticed in the hydrograph and precipitation time series of the 20 catchments, nor were there any annual discharge or precipitation events that suddenly dramatically exceeded another year (Appendix F).

If α in Eq. 7.11 is either set to 0 or 1 (extremes) both resulting equations can be combined to express an average $\frac{p_{eff}}{K}$. In fact, the specific individual maximum or minimum precipitation and associated hydraulic conductivities cannot be known. This is not an issue because this average $\frac{p_{eff}}{K}$ can afterwards be used in Eq. 7.11 to get an average α representative of the average condition. The two equations when α is equal to 0 and 1 are shown below.

If $\alpha = 1$, Eq. 7.11 becomes:

$$\frac{p_{eff}}{K}(\alpha = 1) = \frac{h_0 mc}{A + B} \tag{7.12}$$

If $\alpha = 0$, Eq. 7.11 becomes:

$$\frac{p_{eff}}{K}(\alpha = 0) = \frac{m(mB + ch_0)}{A} \tag{7.13}$$

The average of Eqs. 7.12 and 7.13 is:

$$\frac{p_{eff}}{K}(\text{mean}) = \frac{1}{2}\left(\frac{m^2 B}{A} + h_0 mc\left(\frac{1}{A} + \frac{1}{A + B}\right)\right) \tag{7.14}$$

It is now possible to use $\frac{p_{eff}}{K}(\text{mean})$ in Eq. 7.11 to calculate an average α that can then be used in Eq. 7.1 with A and B and the average true effective precipitation measured with CHIRPS and MODIS to estimate Q_i.

To conclude, Eq. 7.11 has also been derived with $\alpha = 0.5$ to show that Eq. 7.14 has indeed a more complex origin and especially that in average condition P_{eff} does not simply infiltrate on exactly half the surface of B (Eq. 7.1). The equation for $\alpha = 0.5$ is:

$$\frac{p_{eff}}{K}(\alpha = 0.5) = \frac{m(Bm + 2ch_0)}{2A + B} \tag{7.15}$$

The aforementioned methodology to calculate Q_i can be summarised into the analytical approach as follows: first calculate $\frac{p_{eff}}{K}(\text{mean})$ with Eq. 7.14 then use it in Eq. 7.11 to get α which is set into Eq. 7.1 to obtained Q_i. This is applied in the upcoming two sections, first on the 20 reference catchments and afterward to the sub-catchment of the boreholes of Bidibidi.

7.4. Application to reference catchments and validation with water balance components

The analytical approach described above is applied to the 20 reference catchments presented in Chapter 5. Table 7.1 summarizes the required data of the catchments (abbreviated as capital letters referring to Fig. 5.1 and Table 5.1). These data are upland unit area (A), slope plus drainage unit area (B), drainage system slope (m), and effective precipitation (P_{eff}). In Table 7.1, the analytical Q_i (Analy. Q_i) is shown together with the Q_i (Wb. Q_i) from Fig. 5.5 obtained from the water balance (Eq. 5.4) with recovered components for the 20 catchments (Section 5.4). In order to compare the two, the last two columns of Table 7.1 show their fraction (Wb. Q_i / Analy. Q_i) and their difference (Wb. Q_i – Analy. Q_i) in mm/year.

Table 7.1 *Data of the 20 catchments (capital letters in reference to Table 5.1) needed to solve the analytical approach of Section 7.3 to determine groundwater recharge Q_i. The data used in the analytical approach (Section 7.3) are the upland unit area (A), slope plus drainage unit area (B), drainage system slope (m) in gradient, and effective precipitation (P_{eff}). The analytical Q_i (Analy. Q_i.) is shown next to the water balance Q_i (Wb. Q_i) from Fig. 5.5 obtained from the water balance (Eq. 5.4) with the water balance components of the 20 catchments (Section 5.4). The two are compared thanks their fraction (Wb. Q_i / Analy. Q_i) and their difference (Wb. Q_i – Analy. Q_i) in mm/year.*

catchment (Table 5.1)	catchment [km^2/1000] (Fig. 5.4)	A unit (upland) [km^2/1000]	B unit (Slo. + drai.) [km^2/1000]	c (drai. peri.) [km/1000]	m (Slope) [gradient]	P_{eff} [mm/y]	α	Analy. Q_i [mm/y]	Wb. Q_i [mm/y] (Fig. 5.5)	Wb. Q_i / Analy. Q_i	Wb. Q_i – Analy. Q_i [mm/y]
A	6.41	3.37	3.04	7.13	0.05	289	0.62	237	184	0.78	-53
B	6.35	3.34	3.01	5.70	0.05	413	0.64	343	354	1.03	11
C	0.75	0.45	0.30	0.31	0.03	429	0.66	371	389	1.05	18
D	0.65	0.34	0.31	0.77	0.04	640	0.61	521	550	1.06	29
E	6.13	3.64	2.49	5.44	0.03	233	0.60	195	210	1.07	14
F	0.13	0.08	0.06	0.15	0.04	661	0.61	550	580	1.06	30
G	5.02	3.05	1.97	5.44	0.04	265	0.59	223	254	1.14	31
H	0.43	0.23	0.20	0.45	0.04	478	0.62	391	420	1.08	30
I	2.69	1.35	1.34	3.37	0.04	340	0.61	274	224	0.82	-50
J	4.99	2.63	2.36	5.47	0.03	390	0.58	313	288	0.92	-24
K	0.83	0.50	0.33	1.04	0.03	522	0.58	435	454	1.04	19
L	13.46	7.97	5.49	24.10	0.04	452	0.57	372	381	1.02	9
M	4.55	2.55	2.00	6.74	0.04	380	0.58	310	306	0.98	-5
N	4.64	2.38	2.26	8.20	0.04	545	0.58	433	445	1.03	12
O	6.00	3.41	2.59	7.11	0.03	350	0.58	285	320	1.12	35
P	0.99	0.46	0.52	1.66	0.05	682	0.61	540	543	1.01	3
Q	0.96	0.43	0.52	1.43	0.06	294	0.63	234	165	0.71	-69
R	6.69	3.59	3.10	7.96	0.02	317	0.57	254	202	0.80	-52
S	0.94	0.40	0.55	1.18	0.03	246	0.60	190	143	0.75	-47
T	1.81	0.59	1.22	3.22	0.04	404	0.61	296	260	0.88	-36
						Average	**0.60**	**338**	**333**	**0.97**	**-5**

According to Table 7.1 the fraction (WB. Q_i / Analy. Q_i) of water balance derived to the analytical Q_i is consistently close to 1 with an average for the 20 catchments of 0.97. This high correlation is also reflected in their small differences. Although in specific cases the difference can be significant, such as for catchment Q, where the analytical Q_i is 69 mm/year higher than the water balance derived one, it can also be as low as 3 mm/year for catchment P. The overall average difference is -5 mm/year. These discrepancies are best illustrated in following graph in Fig. 7.4 where the Q_i from the analytical approach are plotted against those derived from the water balance.

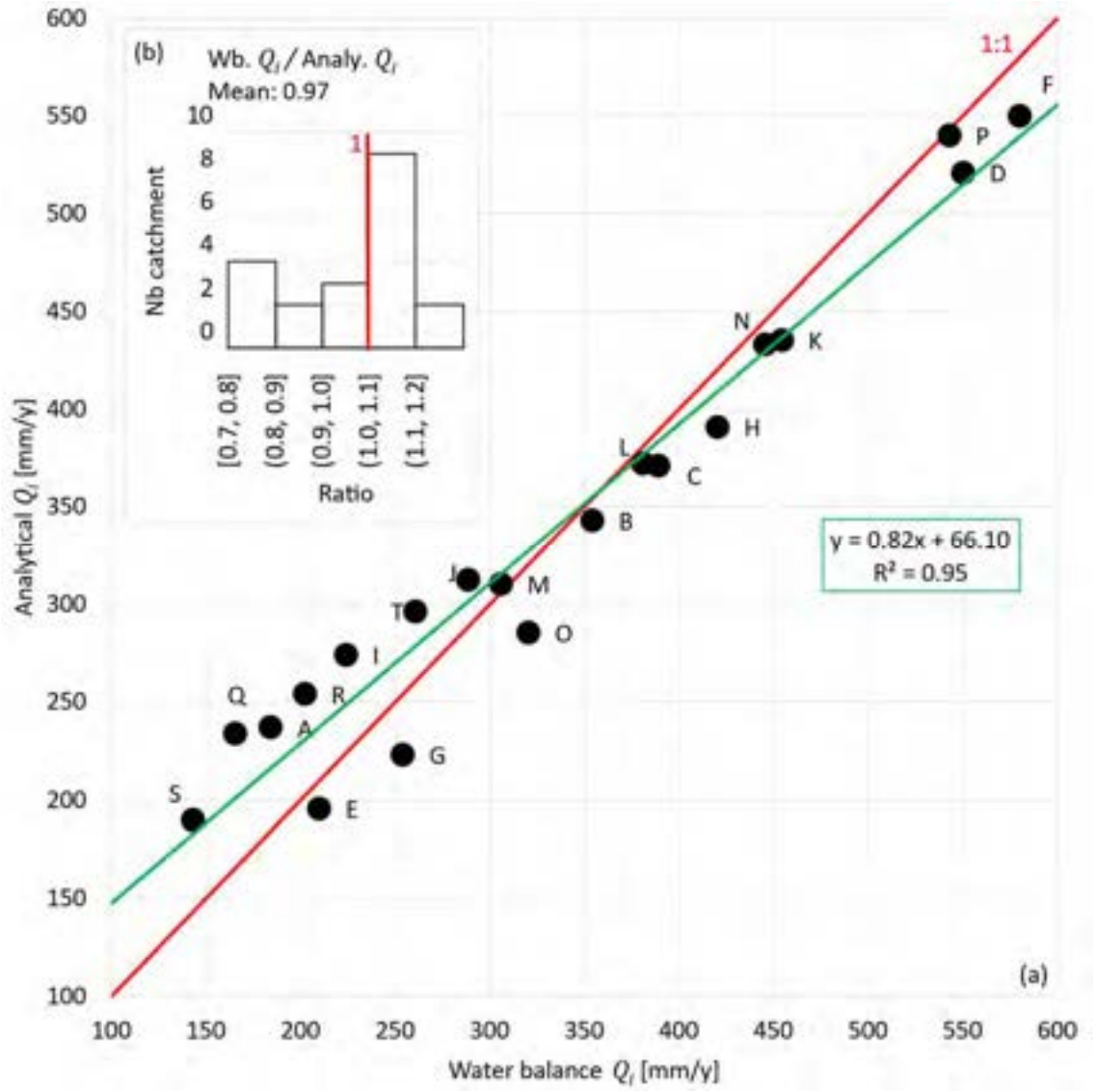

Fig. 7.4 *Graphs to compare the groundwater recharge Q_i obtained by the analytical approach described in Section 7.3 with that derived from the water balance using data of the 20 reference catchments (Section 5.4). The values are given in Table 7.1. In* ***a*** *the points are marked with capital letters referring to the catchment abbreviations in Table 5.1. The red line is a 1:1 line while the green line is a trend line that runs through the data with its function indicated in the green square. The small graph* ***b*** *labelled* WB. Q_i / Analy. Q_i *shows a histogram with a bin size of 0.1 presenting the ratios of water balance (WB.) to analytical (Analy.) Q_i.*

In Fig. 7.4a, the analytical versus the water balance derived Q_i line up properly and a relevant trend line crosses them. Indeed, the R^2 is 0.95 and the slope of the function is 0.82. Nevertheless, it appears that for small values, the analytical solution tends to overestimate while for large values, it tends to underestimate. As a result, the trend line is oblique to the 1:1 (red line) and intersects the y axis at 66.1 mm/year. However, when their fractions are compared in the bar graph Fig. 7.4b, it

appears that most of the calculated Q_i have an error relative to the measured Q_i less than or equal to a threshold of ±0.1. This is the case for 12 catchments while for the other 8 it is about ±0.2.

Since the analytical Q_i are very close to the water balance derived ones, but the relationship is not perfect (Fig. 7.4), the question arises as to the veracity of one or the other. The water balance derived Q_i are in fact obtained from a water balance comprising several components of different origins. These are remote sensing data for P_{eff} (i.e. CHIRPS and MODIS) and discharge measurements derived into runoff R (Appendix C.3). Alternatively, the analytical Q_i was not generated from a water balance, but the same P_{eff} is still needed and therefore the solution can certainly not perfectly simulate reality. Overall, although there may be some discrepancies, it seems appropriate to apply this analytical approach to get at least a first estimate of borehole catchment yields, which is done in the next section

7.5. Application to the sub-catchments of Bidibidi and cross-valid. with empirical solution

The analytical approach described in Section 7.3 is now applied to the 15 sub-catchments that form above the motorised boreholes in the settlement of Bidibidi to estimate the groundwater recharge at these sites. The location of these sub-catchments and the yields of the boreholes are shown in Fig. 6.4 and 6.6 respectively, while additional information has already been discussed in detail in Section 6.5. Some of the data described in Section 6.5 are reused here, which are the size of the upland, the slope, and the drainage unit contained in the sub-catchment. After estimating the recharge of the sub-catchments with the analytical approach, it can be compared to the one obtained with the empirical solution of Eq. 6.3. This provides an additional validation assessment to that of the 20 catchments discussed above. The data for this analysis are presented in Table 7.2. This table presents, for the 15 sub-catchments forming above the boreholes (n°) shown in Fig. 6.5 and referenced in Table 6.1, their respective upland unit area (A) and slope plus drainage unit area (B), drainage slope (m), and effective precipitation (P_{eff}) that are used in the analytical approach of Section 7.3. The Q_i obtained with the analytical approach (Analy. Q_i) are given in m^3/h and divided by three (Analy. Q_i/3) to get the potential extraction thresholds used afterwards in Fig. 7.6. Finally, the analytical and empirical Q_i are also expressed in mm/year in order to compare their fractions (Emp. Q_i / Analy. Q_i) and their differences (Emp. Q_i − Analy. Q_i).

Table 7.2 *Data of 15 sub-catchments that form above the motorised boreholes (n° in reference to Fig. 6.5) in the settlement of Bidibidi used in the analytical approach of Section 7.3 to estimate groundwater recharge Q_i. The data used in the analytical approach are upland unit area (A), slope plus drainage unit area (B), drainage system slope (m), and effective precipitation (P_{eff}). The Q_i obtained with the analytical approach (Analy. Q_i) are given in m³/h and divided by three (Analy. Q_i/3) to get the potential extraction threshold. Analy. Q_i is also expressed in mm/year next to the empirical Q_i (Emp. Q_i) obtained from Eq. 6.3 with their fractions (E. Q_i / A. Q_i) and their differences (Emp. Q_i − Analy. Q_i) in mm/year.*

n° (bh-catch.) (Fig. 6.4)	catchment [km²] (Table 6.1)	A unit (upland) [km²]	B unit (Slo. + drai.) [km²]	c (drai. Peri.) [km]	m (Slope) [gradient]	P_{eff} [mm/y]	α	Analy. Q_i [m³/h]	Analy. Q_i/3 [m³/h]	Analy. Q_i [mm/y]	Emp. Q_i [mm/y] (Table 6.1)	Emp. Q_i / Analy. Q_i	Emp. Q_i – Analy. Q_i [mm/y]
1	0.22	0.13	0.09	1.96	0.10		0.54	5	2	203	185	0.91	-18
2	0.27	0.13	0.14	1.89	0.11		0.56	6	2	195	192	0.98	-4
3	0.76	0.49	0.27	3.60	0.14		0.58	19	6	215	192	0.89	-23
4	1.23	0.44	0.78	6.07	0.15		0.62	27	9	191	181	0.94	-11
5	1.25	0.62	0.63	3.68	0.11		0.62	29	10	205	188	0.92	-17
6	3.46	1.59	1.87	12.53	0.14		0.63	80	27	202	188	0.93	-14
7	3.98	1.85	2.14	15.47	0.17		0.64	93	31	204	181	0.89	-23
8	5.48	3.03	2.45	19.13	0.15	253	0.62	131	44	210	180	0.86	-29
9	5.96	3.26	2.71	18.65	0.14		0.63	143	48	210	189	0.90	-21
10	8.99	4.32	4.67	47.90	0.14		0.59	204	68	199	187	0.94	-12
11	9.66	4.71	4.95	27.60	0.16		0.66	230	77	209	178	0.85	-31
12	10.86	2.21	8.65	37.35	0.13		0.67	230	77	185	180	0.97	-5
13	11.72	5.67	6.05	41.36	0.15		0.63	274	91	205	194	0.95	-11
14	13.70	5.77	7.93	50.23	0.13		0.63	310	103	198	179	0.90	-19
15	22.46	8.67	13.79	62.39	0.16		0.68	522	174	204	182	0.89	-22
						Average	**0.62**	**-**	**-**	**202**	**185**	**0.92**	**-17**

In Table 7.2 the groundwater recharge Q_i values obtained with the analytical solution (Analy. Q_i) are generally close to those obtained with the empirical one (Emp. Q_i) of Eq. 6.3. The values obtained with the analytical solution are in a similar range with an average of 202 mm/year. This was also the case for those obtained with the empirical solution already presented in Table 6.1, the average was 185 mm/year. This results in an average fraction *(*Emp . Q_i */* Analy. Q_i*)* being good since it is 0.92 and the average difference *(*Emp. Q_i − Analy. Q_i*)* is -17 mm/year. As for the 20 catchments the analytical Q_i is always slightly overestimated. If the values of the analytical approach were plotted against the empirical ones, since both are close, it results in a cloud of points and so do not present a proper relation as in Fig. 7.4. Therefore, to discuss the results of the two solutions a bit more, their normal distribution is presented in the following figure (Fig. 7.5).

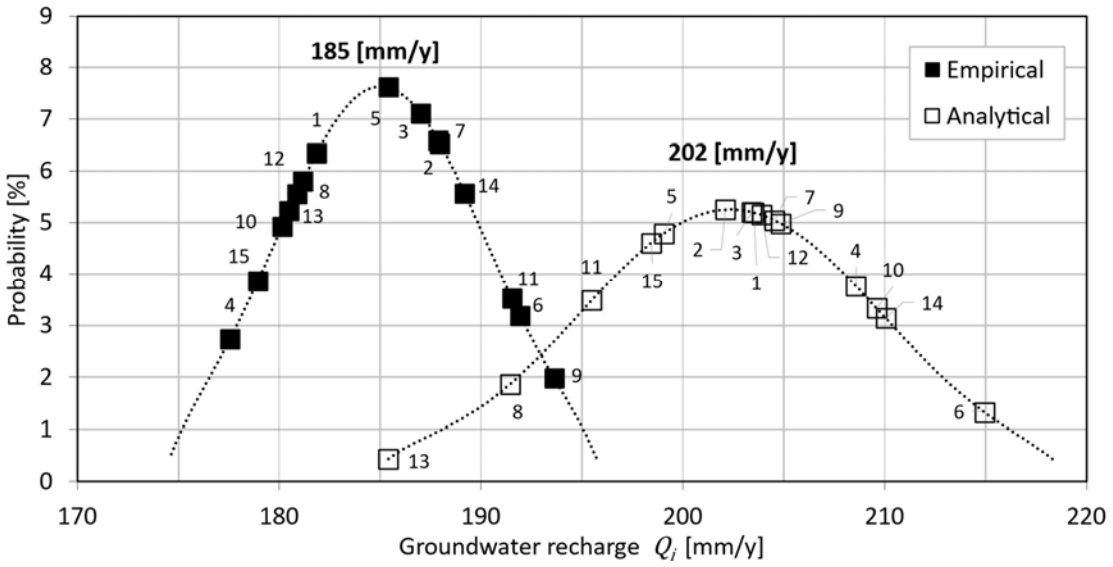

Fig. 7.5 *Normal distribution of groundwater recharge Q_i obtained at the 15 sub-catchments that form above the motorised boreholes of Bidibidi with the empirical solution (left) discussed in Section 6.3 and the analytical approach (right) presented in this chapter. The numbers next to the markers refer to the list of boreholes or catchments in Table 6.1.*

In Fig. 7.5, the two curves show the distribution of groundwater recharge values Q_i obtained with the empirical (Eq. 6.3) and analytical approach. The analytical approach returns generally higher values. Indeed, the curve is shifted to the right compared to the empirical one. In addition, the bell shape of the analytical curve is flatter and wider than that of the empirical solution. The curve for the empirical solution is actually more centred around its mean of 185 mm/year while the values for the analytical solution present a larger range. It may be possible to make some adjustments to the analytical approach to produce values closer to the empirical one. However, this would mean that the empirical solution is fully trusted. In order to evaluate either solution, a more thorough analysis than that presented here is needed. This could be done through groundwater modelling, for

example. This could not be achieved during the course of the project and thus makes it one of the perspectives for further research.

Although the analytical approach tends to slightly overestimate the groundwater recharge compared to the empirical one (Fig. 7.5), this is thought to have little consequences when viewed from a sub-catchment water balance perspective. This is shown in Fig. 7.6 which is based on a simplification of Fig. 6.6. The purpose of Fig. 6.6 was to discuss the sustainability of the 15 sub-catchments in Bidibidi. This was done by comparing their sub-catchment extractions to the recharge that was obtained at their sub-catchment with the empirical solution. Figure 7.6 displays the cumulated sub-catchment extractions as white dots, the sub-catchment Q_i or $Q_i/3$ obtained with the empirical solution (Table 6.1) as plain green and red bars respectively and the analytical values of Q_i or $Q_i/3$ (Table 7.2) are shown as green and red dashed bars respectively.

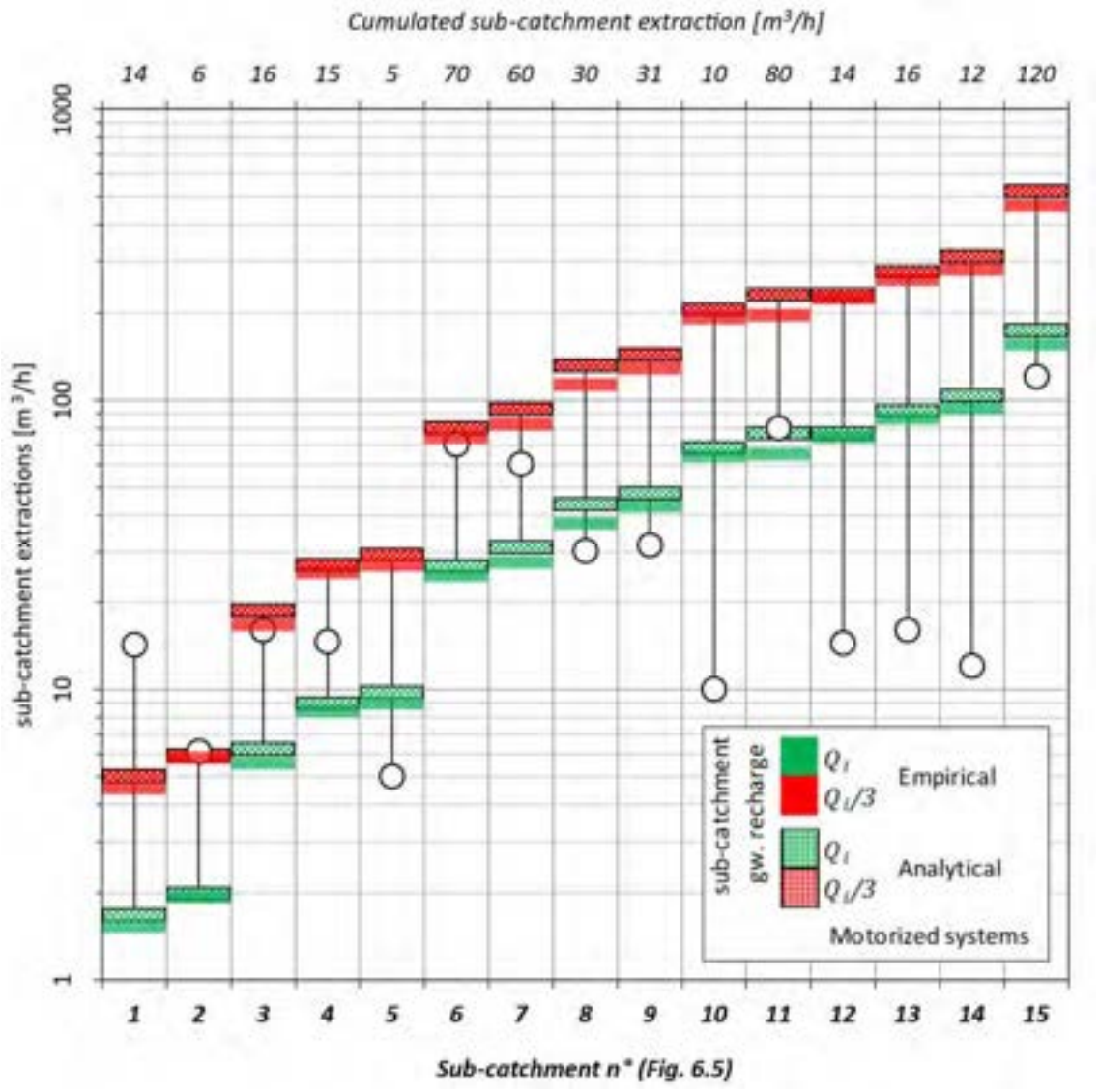

Fig.7.6 *Modified graph of Fig. 6.6 showing the cumulated sub-catchment extraction of the 15 Bidibidi motorized boreholes in perspective with the estimated groundwater recharge Q_i at their sub-catchments with the empirical solution of Eq. 6.3 and analytical approach of Section 7.3. The sub-catchments n° in reference to Fig. 6.5 and Table 6.1 are shown on the lower axis and the cumulated sub-catchment extraction in m³/h on the upper axis. The individual cumulated sub-catchment extractions are represented by circles while the Q_i and $Q_i/3$ are represented by green or red bars for those obtained with the empirical solution and by green or red dotted bars for those obtained with the analytical approach. The data are found in Table 6.1 and 7.2.*

In Fig. 7.6 the estimated groundwater recharge values Q_i with the empirical solution of Eq. 6.3 and analytical approach of Section 7.3 are very close. Both methods seem appropriate to assess the sustainability of sub-catchments. Again, as in Fig. 6.6, if the sub-catchment extraction falls below the two green bars, one can conclude that its exploitation is sustainable, while if it is situated between the green and red bars, it means that it needs to be closely monitored and the exploitation certainly

not increased. Finally, if the sub-catchment extraction is higher than one of the red bars, i.e. if it extracts more than the recharge, it means that the resource is definitely overexploited.

In conclusion, if the analytical approach tends to overestimate the groundwater recharge (Fig. 7.5 and 7.6) compared to the solution of Eq. 6.3, one might, to stay within the realm of safety, prefer the former option. Therefore the water balance integrated RGWPM (Fig. 6.7) where the medium GWP has been refined based on the groundwater recharge estimated with the empirical method must not be further developed here. However, in practice to get a better idea and to be sure that the first method worked well, one can use the analytical approach as a verification.

7.6. Perspectives to assess hydraulic conductivity by means of hydrogeomorphological landscape units

In this chapter, it is shown that both the empirical solution of Eq. 6.3 and the analytical approach of Section 7.3 are appropriate for estimating groundwater recharge since they return similar values at the catchment and at the sub-catchment scale (e.g. Figs. 7.4, 7.5, and 7.6). Though it is possible to estimate recharge at the sub-catchment scale with either solution with respect to hydraulic conductivity, there is undeniably no better option than the pumping test. Therefore, with respect to estimating the hydraulic conductivity at the sub-catchment scale, no further action is taken here. However, estimation of hydraulic conductivity at the catchment scale could have great potential for future research. Indeed, to model an area where data are scarce and no pumping tests have been performed, it is crucial to have a good initial estimate of hydraulic conductivity.

The analytical approach presented in this chapter can be used to derive the hydraulic conductivity at the catchment scale since it is based on the groundwater flow equation. The last equation i.e. Eq. 7.14 which is used to obtain $\frac{p_{eff}}{K}(\text{mean})$ can be solved for $K(mean)$ and so becomes:

$$K(mean) = \frac{2\, p_{eff}(mean)}{\left(\frac{m^2 B}{A} + h_0 mc\left(\frac{1}{A} + \frac{1}{A+B}\right)\right)} \tag{7.16}$$

As a reminder, $p_{eff}(mean)$ is simply the average annual effective precipitation over a hydrologic year (Appendix C.3.3). In order to test Eq. 7.16 it is applied to the 20 reference catchments. The parameters of the 20 reference catchments needed for solving 7.16 are listed in Table 7.1. The result is presented in the following figure (Fig. 7.7) which shows two hydraulic conductivity box plots. The box plot on the left is obtained with the hydraulic conductivities of the 20 reference catchments and the one on the right is obtained from the literature values for regolith hydraulic conductivity presented in Appendix C.2.2.

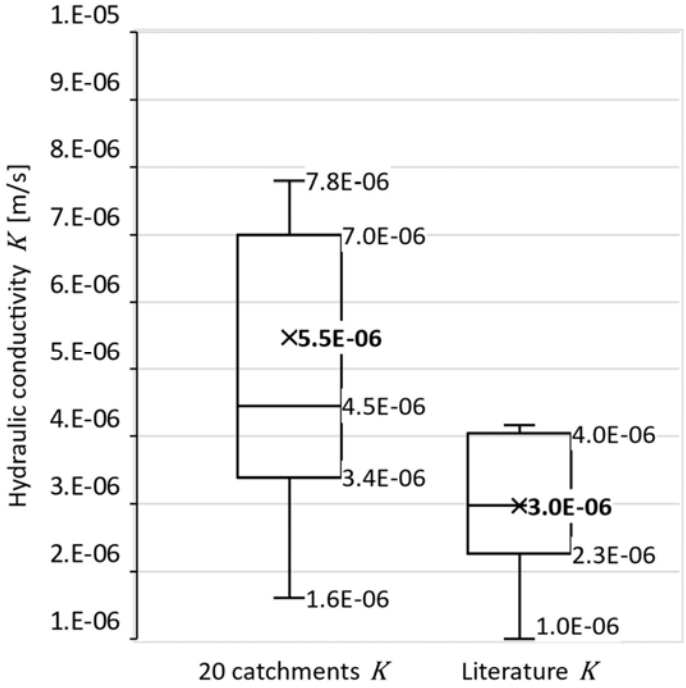

Fig. 7.7 *Two box plots showing the hydraulic conductivities of the 20 reference catchments (Section 5.4) and the hydraulic conductivities for the regolithic environments from literature values. The hydraulic conductivities for the 20 catchments are derived from Eq. 7.16 and the hydraulic conductivities for the literature are taken from* Appendix C.2.2.

From Fig. 7.7, both box plots have similar hydraulic conductivities, which are in the same order of magnitude, i.e. 10^{-6} m/s. The minimum and maximum of the 20 catchments box plot cover almost the entire 10^{-6} m/s order of magnitude. The hydraulic conductivities of the 20 catchments are generally higher. The lower quartiles are close, but the upper quartile of the 20 catchments box plot is almost twice as high. However, both medians and means (indicated by crosses) are quite close. However, the medians and means for the 20 catchments are about 1.5 times higher.

On the whole, the results discussed here on the basis of Fig. 7.7 are acceptable. It is rather reassuring, for the first, that the range of hydraulic conductivity of the 20 catchments is partially consistent with that of the literature values, and for the second, that the medians and means are not too far apart. The literature values are also to be taken with caution. Thus, it is not possible to validate the hydraulic conductivities of the 20 catchments much more than by other techniques such as modelling. Unfortunately, this topic could not be addressed during this project. Therefore, evaluation of this method to obtain these hydraulic conductivities in a more reflective manner, either through field data and/or modelling, is considered one of the main perspectives for future research.

7.7. Conclusions

Although the revised RGWPM methodology (Section 3.2) can be used to indicate the best location for a borehole, the sustainability of newly drilled or existing systems cannot be guaranteed by the methodology alone. However, based on several assumptions in light of the early chapters (Section 4.5), it was suggested that the underlying principle of the hydrogeomorphological landscape unit concept Winter (2001) forming the core of the methodology could, in addition to indicating where surface and subsurface water processes occur, be used to actually quantify the processes. In order to evaluate this idea, data were required. Therefore, the water balance components for 20 catchments in Sub-Saharan Africa have been derived (Section 5.4). These data first led to the expression of an easily applicable empirical solution based on HGM units and water balance components to estimate first runoff and then groundwater recharge (Section 6.3) for catchments. The problem with this empirical solution is that it ingests all of the recovered data and could not be validated in an unbiased manner. Although this method has been applied to the sub-catchments of the Bidibidi boreholes, with a reasonably good correlation (Section 6.5), it is difficult to get a clear picture of catchment recharge. The objective of this chapter was therefore to develop, on the basis of the hydrogeomorphological concept an analytical approach to further evaluate the empirical solution.

The analytical approach developed in this chapter is based on the groundwater flow equation adapted to the HGM units (Fig. 7.1 and 7.2). This analytical approach simulates properly the groundwater recharge for the 20 catchments (Fig. 7.4) and supports the recharge estimated at the sub-catchments of the Bidibidi boreholes with the empirical solution (Eq. 6.3). It was observed that the empirical solution, compared to the analytical approach, gives slightly lower sub-catchment groundwater recharge (Fig. 7.5 and 7.6). Thus, as a precaution, the empirical solution should be used for a first estimation and the analytical solution used to confirm the results.

In addition, since the analytical solution is based on the groundwater flow equation, it can also be used to estimate the hydraulic conductivity. The hydraulic conductivities of the 20 catchments were estimated and compared to literature values (Fig. 7.7). However, due to limited data, this approach could not be evaluated in depth. As it could be very useful for research that, for example, aims at modelling in data-scarce areas, further development of this approach is therefore one of the perspectives of this study.

To conclude and summarize the insights of this chapter and previous ones, the overall concept of hydrogeomorphology is integrated with all data retrieved or created in Fig. 7.8. Figure 7.8 shows a partially modified graph of Fig. 6.2. The graph in Fig. 6.2 showed the best relationship obtained from the HGM units and water balance components fraction of the 20 catchments (Fig. 6.1). This best

relationship is that of the Upland unit / drainage system unit versus Runoff / Precipitation and allowed for the extraction of an appropriate trend line which is shown in Fig. 7.8 as a dashed line. This trend line was used to express the empirical solution (Eq. 6.3) to first calculate catchment runoff from the available data, i.e. precipitation and HGM units, and then to express catchment groundwater recharge with the water balance equation. Added to this graph (Fig. 7.8) are the lithologies encountered in each of the 20 catchments (capital letters), which were first presented in Table 5.1. Finally, the circles around the points have a diameter proportional to the fraction of runoff to hydraulic conductivity R/K. The hydraulic conductivities are obtained from Eq. 7.16 and presented in Fig. 7.7. The hydraulic conductivity is put into a fraction with the runoff so that its size can be viewed in perspective with the other fractions (i.e. Upland unit/drainage system unit and runoff/precipitation).

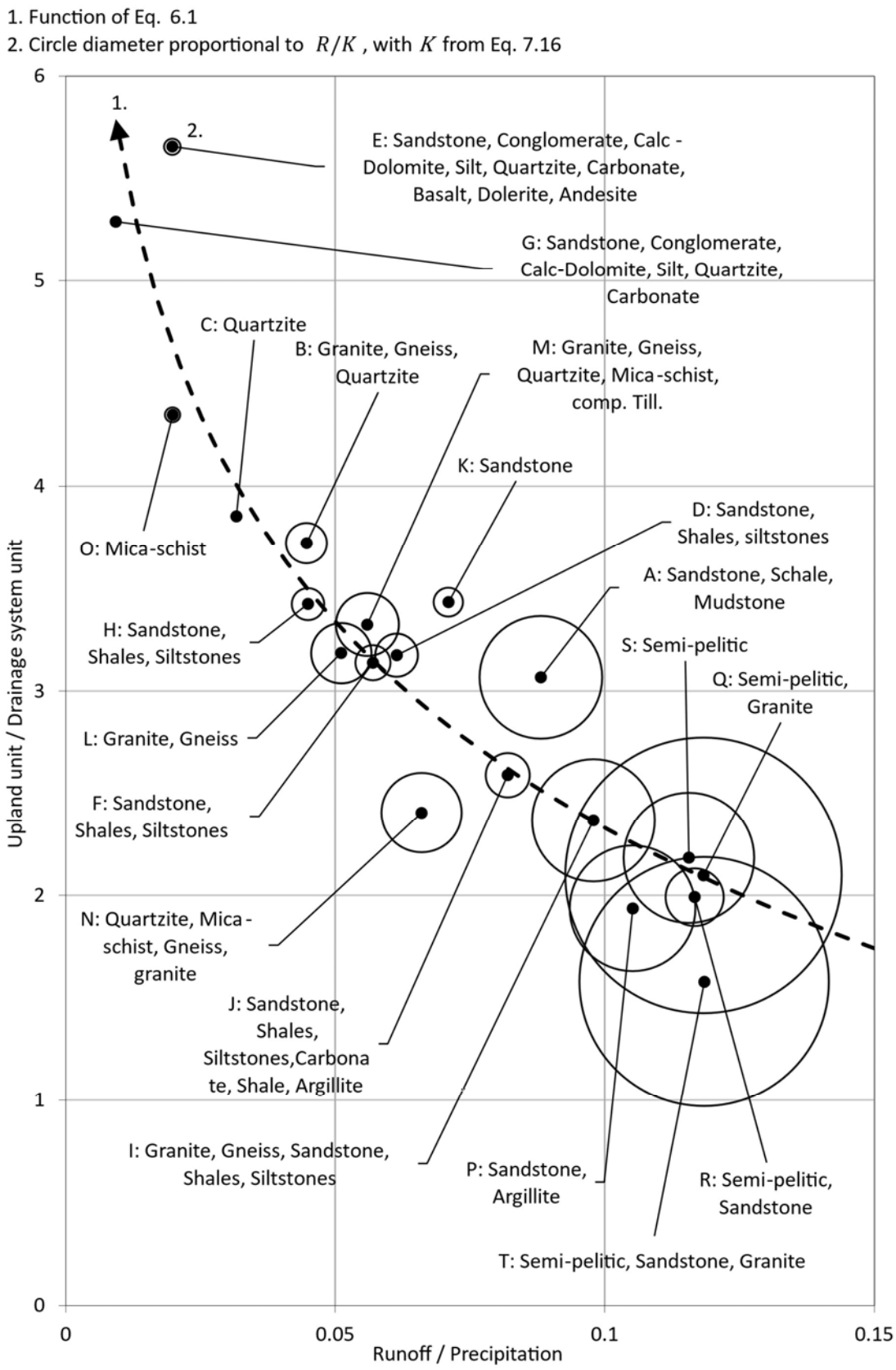

Fig. 7.8 *Caption on next page.*

Fig. 7.8 *Graph partially based on Fig. 6.2 that showed the relationship between runoff over precipitation (R/P) and upland over drainage unit from the 20 catchments (Section 5.4). This relationship led to the function in Eq. 6.1 shown here as a dashed line. This function was used to express the empirical solution of Eq. 6.3 for the estimation of recharge. Capital letters refer to the 20 catchments and for each the lithologies in Table 5.1 are shown. The circles surrounding the points have a diameter proportional to the runoff over the hydraulic conductivity, i.e. R/K with K obtained from Equation 7.16.*

Figure 7.8 shows the correlation discussed in Section 6.2, that as runoff increases relative to precipitation, the fraction of upland relative to drainage unit decreases. This was attributed to the fact that, since there is only diffuse recharge in the upland unit, the smaller it is relative to the drainage unit where there is primarily runoff, the greater the runoff, so the trend line decreases to the right. While groundwater recharge may be a function of upland unit size, it is necessarily a function of hydraulic conductivity. This is indeed illustrated in Fig. 7.8 with the size of the R/K circles increasing toward the right. This means that the runoff relative to the hydraulic conductivity becomes more important. If the runoff increases, it necessary means that the hydraulic conductivity must become smaller. Furthermore, if one examines the lithologies, it can be qualitatively determined that their presupposed hydraulic properties also decrease towards the right. In fact, one starts at the top with sandstones, conglomerates and quartzites and ends with pelitic and clayey lithologies. Between the two, there are granites and other hard rocks. From Fig. 7.8, as already hypothesized in Section 4.5, it does appear that more permeable lithologies tend to produce larger uplands probably because they are more exposed to chemical weathering due to a higher groundwater recharge.

The observations that can be drawn from Fig. 7.8 are certainly impartial. In fact, 5 types of data of completely different origin are mixed together, namely the landscape units derived from the DEM and satellite images, the precipitation of the CHIRPS, the runoff of the gauging station, the hydraulic conductivity of the analytical solution and the lithologies of the geological maps.

From Fig. 7.8, there is no doubt that the landscape synthesizes all the processes that occur on the surface and subsurface. It begins with the climatic conditions that give rise to a certain amount of precipitation that, before being rendered by plant activities, is transformed into a surplus or effective precipitation which then conditions all surface and subsurface water processes. This effective precipitation is divided into runoff and groundwater recharge. The amount of runoff is dictated by the amount of water that can be absorbed by the subsurface, i.e. recharge. The amount of recharge is necessarily a function of the hydraulic properties (Freeze, 1969). On the other hand, the infiltrated water dictates the biochemical processes that alter the rocks and thus also conditions the permeability (Twidale, 1990). In fact, the amount of weathered material forms the body that transmits most of the groundwater (e.g. Lachassagne et al., 2021) and thus refers to the hydraulic

properties of the landscape. These properties drive the size of the different HGM units, in turn reflecting how the landscape ingests precipitation.

Chapter 8

Conclusion

8.1. Discussion and limitation

The objective of the RGWPM methodology, as repeated throughout this work, was to provide a simple tool for humanitarian actors to identify optimal areas for local-scale geophysical investigations during drilling campaigns, highlighting the probabilities for different water supply options, i.e. hand pumps or small to large motorised systems. In order to achieve this objective, a somewhat tortuous workflow arose, leading from the original RGWPM mapping methodology, based on classical spatial overlay of variables, partially based on simplistic hydromorphological concepts, to the boiled-down revised RGWPM methodology, which only relies on the hydromorphological concept of Winter (2001).

Introducing hydrogeomorphological analysis into the methodology was the way chosen to address the problem of data-scarcity, while remaining consistent with fundamental physics of groundwater processes. With the revised RGWPM methodology, cross-validated with available but rather poor data sets, the objective of an easily implemented and rapid tool was achieved, while high-lighting the inherent limitation of not including any information on sustainability of exploitation schemes. At that point in the workflow, the actual research component of this study plugged in, by systematically establishing relationships between hydrogeomorphological units and groundwater recharge, leading to the 'water balance integrated RGWPM', allowing assessment of sustainable exploitation on sub-catchment scales, being the main result of this study.

In the wake of this work and to achieve the operational objectives of providing a practical mapping tool rapidly, many basic assumptions and a high degree of simplification, e.g. limiting its applicability to regolithic landscapes, were the price to pay to achieve rapidity and to fill the gap arising from data scarcity. Confronting the presented RGWPM methodologies with the common siting strategy of 'drill where people are', i.e. without any notion of groundwater processes, leading to low 'drilling success rates', justifies the simplistic but physical-based RGWPM mapping approaches, essentially implying that they are certainly better than nothing. However, using such RGWPM maps will always require keeping in mind the underlying limitations and assumptions, which are discussed in the following.

A fundamental question which arises from the presented RGWPM methodologies, is how to addresses uncertainty in RGWPM. Since uncertainty cannot be easily quantified due to the inherent lack of (high quality) data in the studied sites, and the resulting maps resulting from a mixture of

data of very different types and resolution combined within a conceptual framework, it is appropriate at this point to separate the different sources of uncertainty which interact. The uncertainties can be subdivided into three sources, the first one related to data and their resolution, the second one to the mapping methodology itself, and the third one to conceptual framework.

The most obvious sources of uncertainty associated to the data sets, consisting of digital elevation models (DEM) and remote sensing data for precipitation (CHIRPS) and evapotranspiration (MODIS), are related to the spatial resolution. For the latter two the spatial resolution is 5.5 km and 500 m respectively, leading to higher errors the smaller the catchments under investigation are. The different temporal resolutions, daily and 8-day, respectively, combined with the problem of cloud coverage for evapotranspiration lead to errors in the water balance analysis, with higher errors in areas with higher cloud coverage, leading to missing snap-shots and reducing the annual cumulated values.

The resolution of the DEM (usually 30 m), on the other hand, has a major impact on the construction of the HGM landscape units. Qualitatively and comparatively, the 'flatter' a landscape is, the higher the errors induced by the DEM analysis will be, often requiring cross-validation with satellite imagery, i.e. to identify starting points of drainage systems.

Another important source of uncertainty is related to field data retrieved in humanitarian contexts to cross-validate the RGWPM methodology. While the hand pump type of water supply is still favoured in rural areas of Sub-Saharan Africa, there is a shift towards the implementation of motorised systems. Despite this transition, the collection of drilling data is still not standardised by the various humanitarian agencies nor by most national governments. This leads to the loss of a lot of information just after the drilling is finished. However, if data is collected, it is still very questionable. This leads to the second major drawback of this work, validating hypotheses based on poor quality borehole data and in particular on indicated yields. These yields are estimated at the time of drilling or evaluated a posteriori in a more detailed manner by means of a pumping test. In both cases, there is considerable uncertainty about what this information represents in the long term.

The second source of uncertainty is related to the mapping methodology itself. Being an expert method, the question of reproducibility is fundamental and has not been addressed in this work. Although clear instructions are given to 'construct' the upland HGM landscape unit (i.e. low WA), inherently linked to the errors of the DEM, it is more difficult to give well-founded instructions for the drainage HGM landscape unit (i.e. medium WA). It obviously follows the drainage system, but the necessary manual mapping of the lateral extension remains imprecise at this point. Although this

drawback is somewhat alleviated for the maps themselves by the fact that geophysical campaigns will investigate areas across this unit and not limit themselves to the exact position of the area, it may have a major impact on the ratio between upland and drainage, forming the basis for the empirical approach for groundwater quantification. It therefore seems necessary to address this hidden but important source of uncertainty and find relevant criteria in the methodology as how to map the drainage unit systematically.

The third major source of uncertainty is related to the conceptual framework and assumptions underlying the methodology. Restricting the RGWPM methodology to regolithic landscapes in Sub-Saharan environments has somewhat alleviated the uncertainty related to natural environments, resulting from complex interaction of the lithosphere with the atmosphere, biosphere, and hydrosphere, by attempting to keep the variable 'lithosphere' constant. Hence, boiling down these complex processes taking place over long time-periods and integrating them all in the analysis of the landscape as it appears as a snap-shot in time, i.e. 'now', may be close to the limit of what can be considered as scientific rigour. The results from the hydrogeomorphological-water balance analysis in particular, which comprise the uncertainty and errors of all the possible sources of uncertainty, therefore, need to be handled with considerable reluctance. The empirical relationship between HGM and water-balance components to quantify groundwater recharge, as an example, incorporates all sources of uncertainty in addition to neglecting conceptually important landscape forming processes, such as overland flow. Since the analysis was conducted for multiple areas, and errors will have been introduced for all sites, the observed patterns are still believed to actually point towards physical relationships, while the errors associated to the actual 'numbers' are difficult to quantify. Hence, although the hydrogeomorphological-water balance analysis which form the basis of the conceptual framework led to surprisingly good results to estimate recharge and sustainability on sub-catchment scale, far more in-depth research is required, including systematic cross-validation. The field of hydrogeomorphology is huge and detailed and systematic analysis have been developed by many researchers, especially decades ago, when digital elevation models and therefore massive landscape analysis were not at hand. Although the concepts applied in this work only scratch the surface of this vast area of research, the results clearly indicate that there is great potential to re-examine it with modern means and a hydrogeological perspective.

While it is hoped that the RGWPM methodologies and approaches to estimating groundwater recharge developed in this work will be implemented in future humanitarian interventions, it will take some time to fully understand the implications of the three main sources of uncertainty described above, namely the available data, the mapping methodology and the conceptual framework. In addition, continuous validation is obviously necessary as natural resources and water

demand are constantly changing. For now, the choice is between doing nothing or trying to do something with the little information available. Nevertheless, it must be concluded here that overall, this work has shown that better results regarding the implementation of boreholes in humanitarian operations can be achieved, which is in fact a gain in itself to already make a statement about mitigating these uncertainties.

8.2. Perspectives

In conclusion, two possible research directions are suggested. The first involves further research to follow up on this study. The second could focus on applying some of the findings based on hydrogeomorphological principles in a more practical way.

Water scarcity is often attributed to the climatic and/or hydrogeological context. Camps and settlements are often located on top of hills. Since the usual strategy is to drill close to the people, this tends to lead to low-yielding boreholes. In such cases, water scarcity is artificially assigned to a location. It would be interesting to explore to what extent the results of this study can be used as an indicator to distinguish 'natural water scarcity' from 'man-made water scarcity'. By generating RGWPMs in advance, one can already predict the type and number of water supplies that a specific location can potentially accommodate to meet at least the minimum standards.

This study was carried out after identification of the need for a groundwater potential mapping methodology adapted to humanitarian contexts. Therefore, it seems important to investigate the possibility of designing methodologies similar to the one presented in this study for other types of aquifers than regolithic e.g. porous, sedimentary (also karstic) and to altogether different climatic conditions. More generally, it would be interesting to know to which extent the results of this work are applicable to aquifers that are not topographically controlled.

A key aspect would be to make more extensive use of different geomorphological features and indices. In this study, only hydrogeomorphological units, i.e. surfaces, were used. The use of lengths, e.g. of landscape unit perimeters, but especially of the drainage network, seems favourable for establishing a relationship similar to the empirical solution for example. To this end, the use of the Horton-Strahler numbers (Horton, 1945; Strahler, 1952 and 1957) seem promising.

Follow-up research to this study that should be evaluated as a priority concerns the empirical and analytical solutions for the estimation of groundwater recharge. Indeed, what has been particularly highlighted at the end of this study is that if the empirical solution is applicable, it is not necessarily required to use the analytical one. However, the analytical solution which is based on the groundwater flow equation incorporates the hydraulic conductivity. Currently, the hydraulic

conductivity can only be derived from pumping tests, having the possibility to estimate it with remote sensing data and a simple formula is promising. In particular, for modelling in locations where data are scarce. This approach to obtaining hydraulic conductivity could be evaluated in locations where many pumping tests have been performed or by modelling a number of real catchments for comparison.

Finally, regolithic environments were the focus of this study. However, it would be worthwhile to investigate and apply the tools developed in this study in less chemically eroded environments. For example, in a hard rock alpine landscape. The last glaciation mechanically shaped the landscape. The hydrogeomorphological concept used in this study is certainly not applicable as such, but the effect of the water certainly takes over quickly. It would therefore be interesting to study how long it takes after a glacial period for the concept to be applicable. This would for instance make it possible to study past and future climate change only throughout the landscape.

References

Abatzoglou, J. T., Dobrowski, S. Z., Parks, S. A., & Hegewisch, K. C. (2018). TerraClimate, a high-resolution global dataset of monthly climate and climatic water balance from 1958–2015. *Scientific Data*, *5*(1), 170191. https://doi.org/10.1038/sdata.2017.191

Abdalla, F. (2012). Mapping of groundwater prospective zones using remote sensing and GIS techniques: A case study from the Central Eastern Desert, Egypt. *Journal of African Earth Sciences*, *70*, 8–17. https://doi.org/10.1016/j.jafrearsci.2012.05.003

Abdelmoneim, H., Soliman, M. R., & Moghazy, H. M. (2020). Evaluation of TRMM 3B42V7 and CHIRPS Satellite Precipitation Products as an Input for Hydrological Model over Eastern Nile Basin. *Earth Systems and Environment*, *4*(4), 685–698. https://doi.org/10.1007/s41748-020-00185-3

Aguilar, A., Flores, H., Crespo, G., Marín, M., Campos, I., & Calera, A. (2018). Performance Assessment of MOD16 in Evapotranspiration Evaluation in Northwestern Mexico. *Water*, *10*(7), 901. https://doi.org/10.3390/w10070901

Ahnert, F. (1977). Some comments on the quantitative formulation of geomorphological processes in a theoretical model. *Earth Surface Processes*, *2*(2–3), 191–201. https://doi.org/10.1002/esp.3290020211

Aksoy, H., & Wittenberg, H. (2011). Nonlinear baseflow recession analysis in watersheds with intermittent streamflow. *Hydrological Sciences Journal*, *56*(2), 226–237. https://doi.org/10.1080/02626667.2011.553614

Alazard, M., Boisson, A., Maréchal, J.-C., Perrin, J., Dewandel, B., Schwarz, T., Pettenati, M., Picot-Colbeaux, G., Kloppman, W., & Ahmed, S. (2016). Investigation of recharge dynamics and flow paths in a fractured crystalline aquifer in semi-arid India using borehole logs: implications for managed aquifer recharge. *Hydrogeology Journal*, *24*(1), 35–57. https://doi.org/10.1007/s10040-015-1323-5

Allen, R. (1998). Crop evapotranspiration-Guidelines for computing crop water requirements-FAO Irrigation and drainage paper 56. *Fao, Rome*, *300*(9), D05109.

Allen, R. G., Pereira, L. S., Howell, T. A., & Jensen, M. E. (2011). Evapotranspiration information reporting: I. Factors governing measurement accuracy. *Agricultural Water Management*, *98*(6), 899–920. https://doi.org/10.1016/j.agwat.2010.12.015

Amrit, K., Singh, S., & Singh, R. M. (2016). Estimation of natural groundwater recharge using MIKE11 NAM Model. *Indian Journal of Soil Conservation*, *44*(2), 216-220.

Anderson, M. C., Kustas, W. P., Norman, J. M., Hain, C. R., Mecikalski, J. R., Schultz, L., González-Dugo, M. P., Cammalleri, C., D'Urso, G., Pimstein, A., & Gao, F. (2011). Mapping daily evapotranspiration at field to continental scales using geostationary and polar orbiting satellite imagery. *Hydrology and Earth System Sciences*, *15*(1), 223–239. https://doi.org/10.5194/hess-15-223-2011

Araújo, A.G., Perevalov, O. V., Jukov, R. A. (1988). *1:1 million scale carta geológica de Angola*. Instituto nacional de geologia, Republic of Angola.

Arciniega-Esparza, S., Breña-Naranjo, J. A., & Troch, P. A. (2017). On the connection between terrestrial and riparian vegetation: the role of storage partitioning in water-limited catchments. *Hydrological Processes*, *31*(2), 489–494. https://doi.org/10.1002/hyp.11071

Arnold, J., Muttiah, R., Srinivasan, R., & Allen, P. (2000). Regional estimation of base flow and groundwater recharge in the Upper Mississippi river basin. *Journal of Hydrology*, *227*(1–4), 21–40. https://doi.org/10.1016/S0022-1694(99)00139-0

Arnold, J. G., & Allen, P. M. (1999). AUTOMATED METHODS FOR ESTIMATING BASEFLOW AND GROUND WATER RECHARGE FROM STREAMFLOW RECORDS. *Journal of the American Water Resources Association*, *35*(2), 411–424. https://doi.org/10.1111/j.1752-1688.1999.tb03599.x

Ashouri, H., Hsu, K.-L., Sorooshian, S., Braithwaite, D. K., Knapp, K. R., Cecil, L. D., Nelson, B. R., & Prat, O. P. (2015). PERSIANN-CDR: Daily Precipitation Climate Data Record from Multisatellite Observations for Hydrological and Climate Studies. *Bulletin of the American Meteorological Society*, *96*(1), 69–83. https://doi.org/10.1175/BAMS-D-13-00068.1

Aubinet, M., Vesala, T., & Papale, D. (Eds.). (2012). *Eddy covariance: a practical guide to measurement and data analysis*. Springer Science & Business Media.

Awange, J. L., Hu, K. X., & Khaki, M. (2019). The newly merged satellite remotely sensed, gauge and reanalysis-based Multi-Source Weighted-Ensemble Precipitation: Evaluation over Australia and Africa (1981–2016). *Science of The Total Environment*, *670*, 448–465. https://doi.org/10.1016/j.scitotenv.2019.03.148

Bates, D. A. (1954). *1:1 million scale geological map of Ghana*. Geological Survey, Republic of Ghana.

Balek, J. (1977). Hydrology and water resources in tropical Africa. Development In Water. *Sciences*, *8*.

Barnes, B. S. (1939). The structure of discharge-recession curves. *Transactions, American Geophysical Union*, *20*(4), 721. https://doi.org/10.1029/TR020i004p00721

Beck, H. E., Zimmermann, N. E., McVicar, T. R., Vergopolan, N., Berg, A., & Wood, E. F. (2018). Present and future Köppen-Geiger climate classification maps at 1-km resolution. *Scientific Data*, *5*(1), 180214. https://doi.org/10.1038/sdata.2018.214

Bense, V. F., Gleeson, T., Loveless, S. E., Bour, O., & Scibek, J. (2013). Fault zone hydrogeology. *Earth-Science Reviews*, *127*, 171–192. https://doi.org/10.1016/j.earscirev.2013.09.008

Berry, L., & Ruxton, B. P. (1959). Notes on weathering zones and soils on granitic rocks in two tropical regions. *Journal of Soil Science*, *10*(1), 54–63. https://doi.org/10.1111/j.1365-2389.1959.tb00665.x

Biswal, B., & Marani, M. (2010). Geomorphological origin of recession curves. *Geophysical Research Letters*, *37*(24). https://doi.org/10.1029/2010GL045415

Bloomfield, K., & Manson, T.P.R. (1966). *1:1 million scale geological map of Malawi*. Bulletin of the Geological Survey, Republic of Malawi.

Blöschl, G. (2006). Rainfall-runoff modeling of ungauged catchments. *Encyclopedia of hydrological sciences*. John Wiley & Sons, Ltd. https://doi.org/10.1002/0470848944.hsa140

Boast, R. (1990). Dambos: a review. *Progress in Physical Geography: Earth and Environment*, *14*(2), 153–177. https://doi.org/10.1177/030913339001400201

Boisson, A., Maréchal, J. C., Perrin, J., Dewandel, B., & Ahmed, S. (2015). Impact of Vertical Geological Structure and Water Table Depletion on Indian Crystalline Aquifers. In *Engineering Geology for Society and Territory - Volume 3* (pp. 583–587). Springer International Publishing. https://doi.org/10.1007/978-3-319-09054-2_117

Braun, J., Mercier, J., Guillocheau, F., & Robin, C. (2016). A simple model for regolith formation by chemical weathering. *Journal of Geophysical Research: Earth Surface*, *121*(11), 2140–2171. https://doi.org/10.1002/2016JF003914

Brutsaert, W. (2005). *Hydrology*. Cambridge University Press. https://doi.org/10.1017/CBO9780511808470

Brutsaert, W., & Nieber, J. L. (1977). Regionalized drought flow hydrographs from a mature glaciated plateau. *Water Resources Research*, *13*(3), 637–643. https://doi.org/10.1029/WR013i003p00637

Bryan, R.B. and Yair, A., eds., 1982, Badland geomorphology and Piping, Norwich, U.K., GeoBooks, 408 pp

Bullock, A. (1988). *Dambos and discharge in central Zimbabwe* (Doctoral dissertation, University of

Southampton).

Chang, C.-T., Wang, H.-C., & Huang, C. (2018). Assessment of MODIS-derived indices (2001–2013) to drought across Taiwan's forests. *International Journal of Biometeorology*, *62*(5), 809–822. https://doi.org/10.1007/s00484-017-1482-2

Chapman, T. (1999). A comparison of algorithms for stream flow recession and baseflow separation. *Hydrological Processes*, *13*(5), 701–714. https://doi.org/10.1002/(SICI)1099-1085(19990415)13:5<701::AID-HYP774>3.0.CO;2-2

Chapman, T., & Maxwell, I. A. (1996, May). Baseflow separation-comparison of numerical methods with tracer experiments. In *National Conference Publication-Institution of Engineers Australia NCP* (Vol. 2, pp. 539-546). Institution of Engineers, Australia.

Chardon, D., Grimaud, J.-L., Beauvais, A., & Bamba, O. (2018). West African lateritic pediments: Landform-regolith evolution processes and mineral exploration pitfalls. *Earth-Science Reviews*, *179*, 124–146. https://doi.org/10.1016/j.earscirev.2018.02.009

Chávez, J. L., Gowda, P. H., Howell, T. A., & Copeland, K. S. (2009). Radiometric surface temperature calibration effects on satellite based evapotranspiration estimation. *International Journal of Remote Sensing*, *30*(9), 2337–2354. https://doi.org/10.1080/01431160802549393

Chen, B., & Krajewski, W. F. (2015). Recession analysis across scales: The impact of both random and nonrandom spatial variability on aggregated hydrologic response. *Journal of Hydrology*, *523*, 97–106. https://doi.org/10.1016/j.jhydrol.2015.01.049

Chilton, P. J., & Foster, S. S. D. (1995). Hydrogeological Characterisation And Water-Supply Potential Of Basement Aquifers In Tropical Africa. *Hydrogeology Journal*, *3*(1), 36–49. https://doi.org/10.1007/s100400050061

Chilton, P. J., & Smith-Carington, A. K. (1984). *Characteristics of the weathered basement aquifer in Malawi in relation to rural water supplies* (pp. 57-65). *IAHS Press*.

Chorley, R. J. (1957). Climate and geomorphology. *J Geol*, *65*(6), 628-638.

Chorley, R. J. (1962). *Geomorphology and general systems theory* (Vol. 500). Washington, DC: US Government Printing Office.

Chorley RJ, Schumm SA, Sugden DE (1984) Geomorphology. Methuen, London

Coates, D. R. (1990). Geomorphic controls of groundwater hydrology. *Special Paper-Geological Society of America*, (252), 341-356.

Compaore, G., Lachassagne, P., & TRAVI, Y. (1997). Evaluation du stock d'eau des altérites: Expérimentation sur le site granitique de Sanon (Burkina Faso). *IAHS-AISH Publication*, *241*.

Dept of Geological Survey and Mines of Uganda (DGSM) (2004). 1:2 million scale geology map of Uganda.

Degano, M. Florencia, et al. "Assessment of the potential evapotranspiration MODIS product using ground measurements in the Pampas." 2018 IEEE Biennial Congress of Argentina (ARGENCON). IEEE, 2018.

Degano, M. F., Rivas, R. E., Carmona, F., Niclòs, R., & Sánchez, J. M. (2021). Evaluation of the MOD16A2 evapotranspiration product in an agricultural area of Argentina, the Pampas region. *The Egyptian Journal of Remote Sensing and Space Science*, *24*(2), 319–328. https://doi.org/10.1016/j.ejrs.2020.08.004

Dewandel, B., Lachassagne, P., Wyns, R., Maréchal, J. C., & Krishnamurthy, N. S. (2006). A generalized 3-D geological and hydrogeological conceptual model of granite aquifers controlled by single or multiphase weathering. *Journal of Hydrology*, *330*(1–2), 260–284. https://doi.org/10.1016/j.jhydrol.2006.03.026

Dewandel, B., Maréchal, J. C., Bour, O., Ladouche, B., Ahmed, S., Chandra, S., & Pauwels, H. (2012). Upscaling and regionalizing hydraulic conductivity and effective porosity at watershed scale in deeply weathered crystalline aquifers. *Journal of Hydrology*, *416–417*, 83–97. https://doi.org/10.1016/j.jhydrol.2011.11.038

Dewandel, B., Jeanpert, J., Ladouche, B., Join, J.-L., & Maréchal, J.-C. (2017). Inferring the heterogeneity, transmissivity and hydraulic conductivity of crystalline aquifers from a detailed water-table map. *Journal of Hydrology*, *550*, 118–129. https://doi.org/10.1016/j.jhydrol.2017.03.075

Díaz-Alcaide, S., & Martínez-Santos, P. (2019). Review: Advances in groundwater potential mapping. *Hydrogeology Journal*, *27*(7), 2307–2324. https://doi.org/10.1007/s10040-019-02001-3

Diem, J. E., Hartter, J., Ryan, S. J., & Palace, M. W. (2014). Validation of Satellite Rainfall Products for Western Uganda. *Journal of Hydrometeorology*, *15*(5), 2030–2038. https://doi.org/10.1175/JHM-D-13-0193.1

Dietrich, W. E., Wilson, C. J., and Reneau, S. L., 1986, Hollows, colluvium, and landslides in soil-mantled landscapes, in Abrahams, A., D ed., Hillslope processes: Winchester, Massachusetts, Allen and Unwin Inc., p. 361-388.

Dinku, T., Ceccato, P., Grover-Kopec, E., Lemma, M., Connor, S. J., & Ropelewski, C. F. (2007).

Validation of satellite rainfall products over East Africa's complex topography. *International Journal of Remote Sensing*, *28*(7), 1503–1526. https://doi.org/10.1080/01431160600954688

Dinku, T., Ceccato, P., & Connor, S. J. (2011). Challenges of satellite rainfall estimation over mountainous and arid parts of east Africa. *International Journal of Remote Sensing*, *32*(21), 5965–5979. https://doi.org/10.1080/01431161.2010.499381

Dinku, T., Funk, C., Peterson, P., Maidment, R., Tadesse, T., Gadain, H., & Ceccato, P. (2018). Validation of the CHIRPS satellite rainfall estimates over eastern Africa. *Quarterly Journal of the Royal Meteorological Society*, *144*(S1), 292–312. https://doi.org/10.1002/qj.3244

Donigian, A. S., Imhoff, J. C., & Bicknell, B. R. (1983). Predicting water quality resulting from agricultural nonpoint source pollution via simulation: HSPF [Hydrologic Simulation Program-Fortran]

Dralle, D. N., Karst, N. J., Charalampous, K., Veenstra, A., & Thompson, S. E. (2017). Event-scale power law recession analysis: quantifying methodological uncertainty. *Hydrology and Earth System Sciences*, *21*(1), 65–81. https://doi.org/10.5194/hess-21-65-2017

Drysdall, A. R., Thieme, H. G., Johnson, L. (1974). *1:1 million scale geological map of the Republic of Zambia*. Prepared for publication by the Government of the United Kingdom (Directorate of Overseas Surveys) for the Government of the Republic of Zambia.

Dupuit, J. (1857). Mouvement de l'eau à travers les terrains perméables. *CR Hebd. Seances Acad. Sci*, *45*, 92-96.

Dupuit, J. (1863). *Etudes théoriques et pratiques sur le mouvement des eaux dans les canaux découverts et à travers les terrains perméables avec des considérations relatives au régime des grandes eaux, au débouché à leur donner, et à la marche des des alluvions dans les rivières à fond mobile*. Dunod, éditeur.

Domenico, P. A. i FW Schwartz (1990). *Physical and chemical hydrogeology*.

Dunne, T. 1969: *Runoff production in a humid area*. Johns Hopkins University, Baltimore, PhD thesis (249 pp.) Also published 1970 as US Department of Agriculture Report ARS 41-160 (108 pp.)

Dunne, T. (1978). Field studies of hillslope flow processes. *Hillslope hydrology*, 227-293.

Dunne, T. (1980). Formation and controls of channel networks. *Progress in Physical Geography*, *4*(2), 211-239.

Dunne, T. (1990). Hydrology, mechanics, and geomorphic implications of erosion by subsurface flow. *Groundwater geomorphology: The role of subsurface water in earth-surface processes and*

landforms, *252*, 1-28.

Dunne, T. and Black, R. D. 1970a: An experimental investigation of runoff processes in permeable soils. Water Research 6, 478-90. 1970b: Partial-area contributions to storm runoff in a small New England watershed. Water Resources Research 6, 1296-1311.

Dunne, T., Moore, T., & Taylor, C. H. (1975). Recognition and prediction of runoff-producing zones in humid regions. *Hydrol. Sci. Bull*, *20*(3), 305-327.

Eckhardt, K. (2005). How to construct recursive digital filters for baseflow separation. *Hydrological Processes*, *19*(2), 507–515. https://doi.org/10.1002/hyp.5675

Eckhardt, K. (2008). A comparison of baseflow indices, which were calculated with seven different baseflow separation methods. *Journal of Hydrology*, *352*(1–2), 168–173. https://doi.org/10.1016/j.jhydrol.2008.01.005

Ehlers, J., Gibbard, P. L., & Hughes, P. D. (Eds.). (2011). *Quaternary glaciations-extent and chronology: a closer look* (Vol. 15). Elsevier.

Elewa, H. H., & Qaddah, A. A. (2011). Groundwater potentiality mapping in the Sinai Peninsula, Egypt, using remote sensing and GIS-watershed-based modeling. *Hydrogeology Journal*, *19*(3), 613–628. https://doi.org/10.1007/s10040-011-0703-8

Ettazarini, S. (2007). Groundwater potentiality index: a strategically conceived tool for water research in fractured aquifers. *Environmental Geology*, *52*(3), 477–487. https://doi.org/10.1007/s00254-006-0481-0

Evans, J. P., Forster, C. B., & Goddard, J. V. (1997). Permeability of fault-related rocks, and implications for hydraulic structure of fault zones. *Journal of Structural Geology*, *19*(11), 1393–1404. https://doi.org/10.1016/S0191-8141(97)00057-6

Fairbridge, R. W., & Finkl Jr, C. W. (1980). Cratonic erosional unconformities and peneplains. *The Journal of Geology*, *88*(1), 69-86. https://doi.org/10.1086/628474

Farquharson, F. A. K., & Bullock, A. (1992). The hydrology of basement complex regions of Africa with particular reference to southern Africa. *Geological Society, London, Special Publications*, *66*(1), 59–76. https://doi.org/10.1144/GSL.SP.1992.066.01.03

Fayer, M. J., Gee, G. W., Rockhold, M. L., Freshley, M. D., & Walters, T. B. (1996). Estimating Recharge Rates for a Groundwater Model Using a GIS. *Journal of Environmental Quality*, *25*(3), 510–518. https://doi.org/10.2134/jeq1996.00472425002500030016x

Fetter, C. W. (1980). Applied Hydrogeology, Charles Merrill pub. *Co. A. Bell and Howell company, Columbus, Ohio, 488p*.

Fetter, C. W. (2018). *Applied hydrogeology*. Waveland Press.

Fleming, K., & Awange, J. L. (2013). Comparing the version 7 TRMM 3B43 monthly precipitation product with the TRMM 3B43 version 6/6A and Bureau of Meteorology datasets for Australia. *Australian Meteorological and Oceanographic Journal*, *63*(3), 421-426.

Foppen, J. W., Lutterodt, G., Rau, G. C., & Minkah, O. (2020). Groundwater flow system analysis in the regolith of Dodowa on the Accra Plains, Ghana. *Journal of Hydrology: Regional Studies*, *28*, 100663. https://doi.org/10.1016/j.ejrh.2020.100663

Forchheimer, P. (1986). Uber die ergiebigkeit von brummen, Anlagen und Sickerschlitzen. *Zeitsch Archit. Ing. Ver., Hannover*, *32*, 539-563.

Freeze, R. A. (1969). The mechanism of natural ground-water recharge and discharge: 1. One-dimensional, vertical, unsteady, unsaturated flow above a recharging or discharging ground-water flow system. *Water Resources Research*, *5*(1), 153-171.

Freeze, R. A., & Cherry, J. A. (1979). *Groundwater*. Prentice-hall.

Freeze, R. A., & Witherspoon, P. A. (1967). Theoretical analysis of regional groundwater flow: 2. Effect of water-table configuration and subsurface permeability variation. *Water Resources Research*, *3*(2), 623–634. https://doi.org/10.1029/WR003i002p00623

Frohlich, K., & Wittenberg, H. (1994). Determination of groundwater recharge by baseflow separation: regional analysis in northeast China. *IAHS Publications-Series of Proceedings and Reports-Intern Assoc Hydrological Sciences*, *221*, 69-76.

Funk, C. (2014). A quasi-global precipitation time series for drought monitoring. *US Geological Survey data series*, *832*(4), 1-12.

Funk, C. (2015). The climate hazards infrared precipitation with stations—a new environmental record for monitoring extremes. *Scientific data*, *2*(1), 1-21.

Furon, R. 1958. Esquisse Structural Provisoire de l'Afrique. A.A.G.S.

Gee, G. W., & Hillel, D. (1988). Groundwater recharge in arid regions: Review and critique of estimation methods. *Hydrological Processes*, *2*(3), 255–266. https://doi.org/10.1002/hyp.3360020306

Gowda, P. H., Chavez, J. L., Colaizzi, P. D., Evett, S. R., Howell, T. A., & Tolk, J. A. (2008). ET mapping for agricultural water management: present status and challenges. *Irrigation Science*, *26*(3), 223–237. https://doi.org/10.1007/s00271-007-0088-6

Guerschman, J. P., Van Dijk, A. I. J. M., Mattersdorf, G., Beringer, J., Hutley, L. B., Leuning, R., Pipunic, R. C., & Sherman, B. S. (2009). Scaling of potential evapotranspiration with MODIS data reproduces flux observations and catchment water balance observations across Australia. *Journal of Hydrology*, *369*(1–2), 107–119. https://doi.org/10.1016/j.jhydrol.2009.02.013

Gupta, M., Sorooshian, S., & Yapo, P. O. (1999). Status of automatic calibration for hydrologic models: Comparison with multilevel expert calibration. *Journal of hydrologic engineering*, *4*(2), 135-143.

Gupta, M., Srivastava, P. K., Islam, T., & Ishak, A. M. Bin. (2014). Evaluation of TRMM rainfall for soil moisture prediction in a subtropical climate. *Environmental Earth Sciences*, *71*(10), 4421–4431. https://doi.org/10.1007/s12665-013-2837-6

Haitjema, H. M., & Mitchell-Bruker, S. (2005). Are Water Tables a Subdued Replica of the Topography? *Ground Water*, 050824075421008. https://doi.org/10.1111/j.1745-6584.2005.00090.x

Heath, R. C. (1984). *Ground-water regions of the United States* (Vol. 2242). US Department of the Interior, Geological Survey.

Herzog, A., Hector, B., Cohard, J., Vouillamoz, J., Lawson, F. M. A., Peugeot, C., & Graaf, I. (2021). A parametric sensitivity analysis for prioritizing regolith knowledge needs for modeling water transfers in the West African critical zone. *Vadose Zone Journal*, *20*(6). https://doi.org/10.1002/vzj2.20163

Hijmans, R. J., Cameron, S. E., Parra, J. L., Jones, P. G., & Jarvis, A. (2005). Very high resolution interpolated climate surfaces for global land areas. *International Journal of Climatology*, *25*(15), 1965–1978. https://doi.org/10.1002/joc.1276

Hill, J. L. & Kidd, C. H. R. 1980. Rainfall—runoff Relationship for 47 Malawi Catchments. Report TP7, Water Resources Branch, Malawi.

Hirpa, F. A., Gebremichael, M., & Hopson, T. (2010). Evaluation of High-Resolution Satellite Precipitation Products over Very Complex Terrain in Ethiopia. *Journal of Applied Meteorology and Climatology*, *49*(5), 1044–1051. https://doi.org/10.1175/2009JAMC2298.1

Horton, R. E. (1945). Erosional development of streams and their drainage basins; hydrophysical approach to quantitative morphology. *Geological society of America bulletin*, *56*(3), 275-370.

Howard, A. D. (1967), Drainage analysis in geologic interpretation: A summation, Am. Assoc. Pet. Geol. Bull., 51, 2246-2259.

Hutton, G., Haller, L., Water, S., & World Health Organization. (2004). *Evaluation of the costs and benefits of water and sanitation improvements at the global level* (No. WHO/SDE/WSH/04.04). World Health Organization.

Houston, J. (1992). Rural water supplies: comparative case histories from Nigeria and Zimbabwe. *Geological Society, London, Special Publications*, *66*(1), 243–257. https://doi.org/10.1144/GSL.SP.1992.066.01.12

Houston, J. F. T., & Lewis, R. T. (1988). The Victoria Province Drought Relief Project, II. Borehole Yield Relationships. *Ground Water*, *26*(4), 418–426. https://doi.org/10.1111/j.1745-6584.1988.tb00407.x

Huffman, G. J. (2019). GPM IMERG Early precipitation L3 half hourly 0.1 degree x 0.1 degree V06. *Goddard Earth Sciences Data and Information Services Center (GES DISC): Greenbelt, MD, USA*.

Huffman, G. J., Adler, R. F., Arkin, P., Chang, A., Ferraro, R., Gruber, A., Janowiak, J., McNab, A., Rudolf, B., & Schneider, U. (1997). The Global Precipitation Climatology Project (GPCP) Combined Precipitation Dataset. *Bulletin of the American Meteorological Society*, *78*(1), 5–20. https://doi.org/10.1175/1520-0477(1997)078<0005:TGPCPG>2.0.CO;2

Huffman, G. J., Adler, R. F., Bolvin, D. T., & Nelkin, E. J. (2010). The TRMM Multi-Satellite Precipitation Analysis (TMPA). In *Satellite Rainfall Applications for Surface Hydrology* (pp. 3–22). Springer Netherlands. https://doi.org/10.1007/978-90-481-2915-7_1

Jackson, G. (1968). The vegetation of Malawi. II. The Brachystegia woodlands X. Brachystegia with evergreen understory. *The Society of Malawi Journal*, 11-19.

Karimi, P., & Bastiaanssen, W. G. M. (2014). Spatial evapotranspiration, rainfall and land use data in water accounting–Part 1: Review of the accuracy of the remote sensing data. *Hydrol. Earth Syst. Sci. Discuss*, *11*(1), 1073-1123

Karimi, P., & Bastiaanssen, W. G. M. (2015). Spatial evapotranspiration, rainfall and land use data in water accounting – Part 1: Review of the accuracy of the remote sensing data. *Hydrology and Earth System Sciences*, *19*(1), 507–532. https://doi.org/10.5194/hess-19-507-2015

Karlsen, R. H., Bishop, K., Grabs, T., Ottosson-Löfvenius, M., Laudon, H., & Seibert, J. (2019). The role of landscape properties, storage and evapotranspiration on variability in streamflow recessions in a boreal catchment. *Journal of Hydrology*, *570*, 315–328. https://doi.org/10.1016/j.jhydrol.2018.12.065

Kim, H. W., Hwang, K., Mu, Q., Lee, S. O., & Choi, M. (2012). Validation of MODIS 16 global terrestrial evapotranspiration products in various climates and land cover types in Asia. *KSCE Journal of Civil Engineering*, *16*(2), 229–238. https://doi.org/10.1007/s12205-012-0006-1

King, L. C. (1963). South African scenery. 3rd edn. rev.

King, L. C. (1967). King. Morphology of the earth. Edinburgh (Oliver & Boyd), 726 pp., 247 figs. Price: 105s. *Mineralogical magazine and journal of the Mineralogical Society*, *36*(279), 461-462.balek

Kirkby, M. J., & Chorley, R. J. (1967). Throughflow, overland flow and erosion. *International Association of Scientific Hydrology. Bulletin*, *12*(3), 5–21. https://doi.org/10.1080/02626667709493533

Kirchner, J. W. (2009). Catchments as simple dynamical systems: Catchment characterization, rainfall-runoff modeling, and doing hydrology backward. *Water Resources Research*, *45*(2). https://doi.org/10.1029/2008WR006912

Kummerow, C., Simpson, J., Thiele, O., Barnes, W., Chang, A. T. C., Stocker, E., Adler, R. F., Hou, A., Kakar, R., Wentz, F., Ashcroft, P., Kozu, T., Hong, Y., Okamoto, K., Iguchi, T., Kuroiwa, H., Im, E., Haddad, Z., Huffman, G., Nakamura, K. (2000). The Status of the Tropical Rainfall Measuring Mission (TRMM) after Two Years in Orbit. *Journal of Applied Meteorology*, *39*(12), 1965–1982. https://doi.org/10.1175/1520-0450(2001)040<1965:TSOTTR>2.0.CO;2

Kyatengerwa, C., Kim, D., & Choi, M. (2020). A national-scale drought assessment in Uganda based on evapotranspiration deficits from the Bouchet hypothesis. *Journal of Hydrology*, *580*, 124348. https://doi.org/10.1016/j.jhydrol.2019.124348

Lachassagne, P., Dewandel, B., & Wyns, R. (2021). Review: Hydrogeology of weathered crystalline/hard-rock aquifers—guidelines for the operational survey and management of their groundwater resources. *Hydrogeology Journal*, *29*(8), 2561–2594. https://doi.org/10.1007/s10040-021-02339-7

Langbein, W. B. (1938). Some channel-storage studies and their application to the determination of infiltration. *Transactions, American Geophysical Union*, *19*(1), 435. https://doi.org/10.1029/TR019i001p00435

Laws, K. B., Janowiak, J. E., & Huffman, G. J. (2004). P2. 2 Verification of rainfall estimates over Africa using RFE, NASA MPA-RT, and CMORPH.

Leopold, L. B., Wolman, M. G., & Miller, J. P. (1964). Fluvial processes in geomorphology WH Freeman and Co. *San Francisco 522pp*.

Linsley, R. K., Kohler, M. A., & Paulhus, J. L. (1975). Hydrology for engineers.

Linsley, R. K., Kohler, M. A., & Paulhus, J. L. (1982). Hydrology for engineers: McGraw Hi11 Book.

Lyne, V., & Hollick, M. (1979, September). Stochastic time-variable rainfall-runoff modelling. In *Institute of Engineers Australia National Conference* (Vol. 79, No. 10, pp. 89-93). Barton, Australia: Institute of Engineers Australia.

Mäckel, R. (1973). Dambos: A study in morphodynamic activity on the plateau regions of Zambia. *CATENA*, *1*, 327–365. https://doi.org/10.1016/S0341-8162(73)80018-9

Maidment, R., Black, E., & Young, M. (2017). TAMSAT Daily Rainfall Estimates (Version 3.0).

Maidment, R., Grimes, D. I. F., Allan, R. P., Greatrex, H., Rojas, O., & Leo, O. (2013). Evaluation of satellite-based and model re-analysis rainfall estimates for Uganda. *Meteorological Applications*, *20*(3), 308–317. https://doi.org/10.1002/met.1283

Maidment, R., Grimes, D., Black, E., Tarnavsky, E., Young, M., Greatrex, H., Allan, R. P., Stein, T., Nkonde, E., Senkunda, S., & Alcántara, E. M. U. (2017). A new, long-term daily satellite-based rainfall dataset for operational monitoring in Africa. *Scientific Data*, *4*(1), 170063. https://doi.org/10.1038/sdata.2017.63

Mamédov, V., & Bouféév, Y. (2006). *1:500,000 carte géologique de la Guinée*. Ministère de mines, de la géologie et de l'environement, Republic of Guinea.

Mandal, U., Sahoo, S., Munusamy, S. B., Dhar, A., Panda, S. N., Kar, A., & Mishra, P. K. (2016). Delineation of Groundwater Potential Zones of Coastal Groundwater Basin Using Multi-Criteria Decision Making Technique. *Water Resources Management*, *30*(12), 4293–4310. https://doi.org/10.1007/s11269-016-1421-8

McFarlane, M. J. (1989). Dambos–their characteristics and geomorphological evolution in parts of Malawi and Zimbabwe, with particular reference to their role in the hydrogeological regime of surviving areas of African surface. In *Proceedings of the groundwater exploration and development in crystalline basement aquifers workshop, Commonwealth Science Council Technical Paper* (Vol. 273, pp. 254-302).

Maignien, R. (1965). 1:1 million scale carte pédologique du sénégal. ORSTOM.

Maillet, E. T. (1905). *Essais d'hydraulique souterraine & fluviale*. A. Hermann.

Melton, M. A. (1957). An analysis of the relations among elements of climate, surface properties, and geomorphology. Columbia Univ New York.

Mestraud, J.-L. (1964). *1:500,000 scale carte géologique de la république Centreafricaine*. Bureau de recherches géologiques et minières, Republic of the Congo.

Monteith, J. L. (1965). Radiation and Crops. *Experimental Agriculture*, *1*(4), 241–251. https://doi.org/10.1017/S0014479700021529

Montgomery, D. R., & Dietrich, W. E. (1988). Where do channels begin? *Nature*, *336*(6196), 232-234.

Montgomery, D. R., & Dietrich, W. E. (1989). Source areas, drainage density, and channel initiation. *Water resources research*, *25*(8), 1907-1918.

Moore, R. D. (1997). Storage-outflow modelling of streamflow recessions, with application to a shallow-soil forested catchment. *Journal of Hydrology*, *198*(1–4), 260–270. https://doi.org/10.1016/S0022-1694(96)03287-8

Moriasi, J. G. Arnold, M. W. Van Liew, R. L. Bingner, R. D. Harmel, & T. L. Veith. (2007). Model Evaluation Guidelines for Systematic Quantification of Accuracy in Watershed Simulations. *Transactions of the ASABE*, *50*(3), 885–900. https://doi.org/10.13031/2013.23153

Motovilov, Y. G., Gottschalk, L., Engeland, K., & Rodhe, A. (1999). Validation of a distributed hydrological model against spatial observations. *Agricultural and Forest Meteorology*, *98–99*, 257–277. https://doi.org/10.1016/S0168-1923(99)00102-1

Mu, Q., Zhao, M., & Running, S. W. (2011). Improvements to a MODIS global terrestrial evapotranspiration algorithm. *Remote Sensing of Environment*, *115*(8), 1781–1800. https://doi.org/10.1016/j.rse.2011.02.019

Nash, J. E., & Sutcliffe, J. V. (1970). River flow forecasting through conceptual models part I — A discussion of principles. *Journal of Hydrology*, *10*(3), 282–290. https://doi.org/10.1016/0022-1694(70)90255-6

Nathan, R. J., & McMahon, T. A. (1990). Evaluation of automated techniques for base flow and recession analyses. *Water Resources Research*, *26*(7), 1465–1473. https://doi.org/10.1029/WR026i007p01465

Okamoto, K. i., Ushio, T., Iguchi, T., Takahashi, N., & Iwanami, K. (n.d.). The global satellite mapping of precipitation (GSMaP) project. *Proceedings. 2005 IEEE International Geoscience and Remote Sensing Symposium, 2005. IGARSS '05.*, *5*, 3414–3416. https://doi.org/10.1109/IGARSS.2005.1526575

Ollier, C. D. (1988). Deep Weathering, Groundwater and Climate. *Geografiska Annaler: Series A,*

Physical Geography, *70*(4), 285–290. https://doi.org/10.1080/04353676.1988.11880258

Pain, C. F., Scott, K. M., & Pain, C. F. (2008). Regolith description and mapping. *Regolith Science. CSIRO Publishing: Melbourne, Australia*, 281-306.

Partridge, T. C., & Maud, R. R. (1987). Geomorphic evolution of southern Africa since the Mesozoic. *South African Journal of Geology*, *90*(2), 179–208.

Peschechera, G., Tarantino, E., & Fratino, U. (2018). Crop water requirements estimation at irrigation district scale from remote sensing: a comparison between MODIS ET product and the analytical approach. In K. Themistocleous, D. G. Hadjimitsis, S. Michaelides, V. Ambrosia, & G. Papadavid (Eds.), *Sixth International Conference on Remote Sensing and Geoinformation of the Environment (RSCy2018)* (p. 48). SPIE. https://doi.org/10.1117/12.2326147

Peters-Lidard, C. D., Houser, P. R., Tian, Y., Kumar, S. V., Geiger, J., Olden, S., Lighty, L., Doty, B., Dirmeyer, P., Adams, J., Mitchell, K., Wood, E. F., & Sheffield, J. (2007). High-performance Earth system modeling with NASA/GSFC's Land Information System. *Innovations in Systems and Software Engineering*, *3*(3), 157–165. https://doi.org/10.1007/s11334-007-0028-x

Péwé, T. L. (1990). Land subsidence and earth-fissure formation caused by groundwater withdrawal in Arizona; a review. *Groundwater geomorphology: the role of subsurface water in earth-surface processes and landforms, edited by: Higgins, CG and Coates, DR, Geol. Soc. Am., spec. paper*, *252*, 219-233.

Programme, U. N. E. (n.d.). *World Atlas of Desertification: Second Edition*. https://wedocs.unep.org/20.500.11822/30300

Purcell, P. G. (2018). Re-imagining and re-imaging the development of the East African Rift. *Petroleum Geoscience*, *24*(1), 21–40. https://doi.org/10.1144/petgeo2017-036

Ramoelo, A., Majozi, N., Mathieu, R., Jovanovic, N., Nickless, A., & Dzikiti, S. (2014). Validation of Global Evapotranspiration Product (MOD16) using Flux Tower Data in the African Savanna, South Africa. *Remote Sensing*, *6*(8), 7406–7423. https://doi.org/10.3390/rs6087406

Roques, C., Rupp, D. E., de Dreuzy, J. R., Longuevergne, L., Jachens, E. R., Grant, G., ... & Selker, J. S. (2022). Recession discharge from compartmentalized bedrock hillslopes. *Hydrology and Earth System Sciences*, *26*(16), 4391-4405.

Rodell, M., Houser, P. R., Jambor, U., Gottschalck, J., Mitchell, K., Meng, C.-J., Arsenault, K., Cosgrove, B., Radakovich, J., Bosilovich, M., Entin, J. K., Walker, J. P., Lohmann, D., & Toll, D. (2004). The Global Land Data Assimilation System. *Bulletin of the American Meteorological Society*, *85*(3), 381–394.

https://doi.org/10.1175/BAMS-85-3-381

Sakura, Y. (1983). Role of capillary water zone in groundwater recharge Observation of rain infiltration by lysimeter. *Japanese Journal of Limnology (Rikusuigaku Zasshi)*, *44*(4), 311-320.

Saha, S. (2011). NCEP climate forecast system version 2 (CFSv2) 6-hourly products. *Research Data Archive at the National Center for Atmospheric Research, Computational and Information Systems Laboratory*, *10*, D61C1TXF.

Scanlon, B. R., Keese, K. E., Flint, A. L., Flint, L. E., Gaye, C. B., Edmunds, W. M., & Simmers, I. (2006). Global synthesis of groundwater recharge in semiarid and arid regions. *Hydrological Processes*, *20*(15), 3335–3370. https://doi.org/10.1002/hyp.6335

Scheidegger, A. E. (1973). Hydrogeomorphology. *Journal of Hydrology*, *20*(3), 193–215. https://doi.org/10.1016/0022-1694(73)90061-9

Scherrer, C., Schweitzer, R., Bünzli, MA. et al. Rapid groundwater potential mapping in humanitarian contexts: improving borehole implementation in basement environments. Hydrogeol J 29, 2033–2051 (2021). https://doi.org/10.1007/s10040-021-02352-w

Schicht, R. J., & Walton, W. C. (1961). *Hydrologic budgets for three small watersheds in Illinois*. Illinois State Water Survey.

Scotese, C. R. (1991). Jurassic and Cretaceous plate tectonic reconstructions. Palaeogeography, Palaeoclimatology, Palaeoecology, 87(1-4), 493-501. https://doi.org/10.1016/0031-0182(91)90145-H

Senay, G. B., Bohms, S., Singh, R. K., Gowda, P. H., Velpuri, N. M., Alemu, H., & Verdin, J. P. (2013). Operational Evapotranspiration Mapping Using Remote Sensing and Weather Datasets: A New Parameterization for the SSEB Approach. *JAWRA Journal of the American Water Resources Association*, *49*(3), 577–591. https://doi.org/10.1111/jawr.12057

Sharannya, T. M., Al-Ansari, N., Deb Barma, S., & Mahesha, A. (2020). Evaluation of Satellite Precipitation Products in Simulating Streamflow in a Humid Tropical Catchment of India Using a Semi-Distributed Hydrological Model. *Water*, *12*(9), 2400. https://doi.org/10.3390/w12092400

Shaw, S. B. (2016). Investigating the linkage between streamflow recession rates and channel network contraction in a mesoscale catchment in New York state. *Hydrological Processes*, *30*(3), 479–492. https://doi.org/10.1002/hyp.10626

Shaw, S. B., & Riha, S. J. (2012). Examining individual recession events instead of a data cloud: Using a modified interpretation of dQ/dt–Q streamflow recession in glaciated watersheds to better inform

models of low flow. *Journal of Hydrology*, *434–435*, 46–54. https://doi.org/10.1016/j.jhydrol.2012.02.034

Schumm, S. A., Dumont, J. F., & Holbrook, J. M. (2000). *Active tectonics and alluvial rivers* (Vol. 276). Cambridge: Cambridge University Press

Sidle, R. C., & Onda, Y. (2004). Hydrogeomorphology: overview of an emerging science. *Hydrological Processes*, *18*(4), 597–602. https://doi.org/10.1002/hyp.1360

Sikakwe, G. U. (2020). Geospatial applications in delineating groundwater prospect zones in a hard rock terrain: an integrated approach. *Environmental Earth Sciences*, *79*(21), 487. https://doi.org/10.1007/s12665-020-09235-5

Strahler, A. N. (1952). Hypsometric (area-altitude) analysis of erosional topography. *Geological society of America bulletin*, *63*(11), 1117-1142.

Strahler, A. N. (1957). Quantitative analysis of watershed geomorphology. *Eos, Transactions American Geophysical Union*, *38*(6), 913-920.

Tallaksen, L. M. (1995). A review of baseflow recession analysis. *Journal of Hydrology*, *165*(1–4), 349–370. https://doi.org/10.1016/0022-1694(94)02540-R

Tang, G., Zeng, Z., Long, D., Guo, X., Yong, B., Zhang, W., & Hong, Y. (2016). Statistical and Hydrological Comparisons between TRMM and GPM Level-3 Products over a Midlatitude Basin: Is Day-1 IMERG a Good Successor for TMPA 3B42V7? *Journal of Hydrometeorology*, *17*(1), 121–137. https://doi.org/10.1175/JHM-D-15-0059.1

Tardy, Y. (1992). *Diversity and terminology of lateritic profiles* (pp. 379–405). https://doi.org/10.1016/B978-0-444-89198-3.50020-9

Taylor, R., & Howard, K. (1998). The dynamics of groundwater flow in the regolith of Uganda.

Taylor, R., & Howard, K. (2000). A tectono-geomorphic model of the hydrogeology of deeply weathered crystalline rock: Evidence from Uganda. *Hydrogeology Journal*, *8*(3), 279–294. https://doi.org/10.1007/s100400000069

Teixeira, J., Chaminé, H. I., Espinha Marques, J., Carvalho, J. M., Pereira, A. J. S. C., Carvalho, M. R., Fonseca, P. E., Pérez-Alberti, A., & Rocha, F. (2015). A comprehensive analysis of groundwater resources using GIS and multicriteria tools (Caldas da Cavaca, Central Portugal): environmental issues. *Environmental Earth Sciences*, *73*(6), 2699–2715. https://doi.org/10.1007/s12665-014-3602-1

Thiéblemont D, Liégeois JP, Fernandez-Alonso M, Ouabadi A, Le Gall B, Maury R, Michard A (2016) Geological map of Africa at 1:10M scale. Geological map, CGMW-BRGM, Orléans, France.

Tóth, J. (1963). A theoretical analysis of groundwater flow in small drainage basins. *Journal of Geophysical Research*, *68*(16), 4795–4812. https://doi.org/10.1029/JZ068i016p04795

Twidale, C. R. (1990). Weathering, soil development, and landforms. *Groundwater geomorphology—the role of subsurface water in Earth-surface processes and landforms: Geological Society of America, Special Paper*, *252*, 29-50.

United Nations Environment Programme (UNEP) (1997). *World Atlas of Desertification: Second Edition*. https://wedocs.unep.org/20.500.11822/30300

UNHCR (2017a) WASH Uganda: WASH situational and gap analysis. https://data2.unhcr.org/en/documents/details/63327. Accessed August 27, 2020

UNHCR (2017b) UGA factsheet Bidibidi gap analysis. https://data2.unhcr.org/en/documents/details/6496. Accessed August 27, 2020

UNHCR (2020) Global trends in forced displacement. https://www.unhcr.org/statistics/unhcrstats/5ee200e37/unhcr-global-trends-2019.html. Accessed August 27, 2020

UNHCR (2020) Global trends in forced displacement. Unpublished at the end of the writing of this thesis.

UNHCR (2021a) Clean energy challenge. The UN Refugee Agency. https://www.unhcr.org/clean-energy-challenge.html. Accessed March 2021

UNHCR (2021b) WASH GIS portal. http://wash.unhcr.org/wash-gis-portal/. Accessed March 29, 2021.

Van Liew, M. W., Veith, T. L., Bosch, D. D., & Arnold, J. G. (2007). Suitability of SWAT for the conservation effects assessment project: comparison on USDA agricultural research service watersheds.

Vasconcelos, P. M., Brimhall, G. H., Becker, T. A., & Renne, P. R. (1994). analysis of supergene jarosite and alunite: Implications to the paleoweathering history of the western USA and West Africa. *Geochimica et Cosmochimica Acta*, *58*(1), 401–420. https://doi.org/10.1016/0016-7037(94)90473-1

Velpuri, N. M., Senay, G. B., Singh, R. K., Bohms, S., & Verdin, J. P. (2013). A comprehensive evaluation of two MODIS evapotranspiration products over the conterminous United States: Using point and gridded FLUXNET and water balance ET. *Remote Sensing of Environment*, *139*, 35–49.

https://doi.org/10.1016/j.rse.2013.07.013

Vinukollu, R. K., Wood, E. F., Ferguson, C. R., & Fisher, J. B. (2011). Global estimates of evapotranspiration for climate studies using multi-sensor remote sensing data: Evaluation of three process-based approaches. *Remote Sensing of Environment*, *115*(3), 801–823. https://doi.org/10.1016/j.rse.2010.11.006

Vogel, R. M., & Kroll, C. N. (1992). Regional geohydrologic-geomorphic relationships for the estimation of low-flow statistics. *Water Resources Research*, *28*(9), 2451–2458. https://doi.org/10.1029/92WR01007

Voss, C. I. (2022). Editor's Message: The 2021 Editors' Choice articles. *Hydrogeology Journal*, *30*(1), 1-2.

Whitlow, J. R. (1980). Morphology of two different vleis on the highveld of Zimbabwe Rhodesia. *Rhodesia agricultural journal*.

Willaime, MM. P., & Volkoff, B. (1967). *1:1 million scale carte pédologique du Dahomey*. ORSTOM.

Winter, T. C. (2001). THE CONCEPT OF HYDROLOGIC LANDSCAPES. *Journal of the American Water Resources Association*, *37*(2), 335–349. https://doi.org/10.1111/j.1752-1688.2001.tb00973.x

Wittenberg, H. (1994). Nonlinear analysis of flow recession curves. *IAHS Publications-Series of Proceedings and Reports-Intern Assoc Hydrological Sciences*, *221*, 61-68.

Wittenberg, H. (1999). Baseflow recession and recharge as nonlinear storage processes. *Hydrological Processes*, *13*(5), 715–726. https://doi.org/10.1002/(SICI)1099-1085(19990415)13:5<715::AID-HYP775>3.0.CO;2-N

Wright, E. P. (1992). The hydrogeology of crystalline basement aquifers in Africa. *Geological Society, London, Special Publications*, *66*(1), 1–27. https://doi.org/10.1144/GSL.SP.1992.066.01.01

Wyns, R., Dewandel, B., & Lachassagne, P. (2015). Origine de la fracturation des aquifères de socle: quels sont les facteurs qui contrôlent les propriétés de l'horizon fissuré? Origin of fracturation in hard-rock aquifers: what are the factors that control the properties of the fissured horizon. *Proceedings of Hard-Rock Aquifers: Up-to-date Concepts and Practical Applications (Aquifères de socle: le point sur les concepts et les applications oprationnelles).-20th Technical Days of the International Association of Hydrogeologists French Chapter*.

WWAP (UNESCO World Water Assessment Programme) (2019) The United Nations World Water Development Report 2019: Leaving No One Behind. UNESCO, Paris.

Xie, P., & Arkin, P. A. (1996). Analyses of Global Monthly Precipitation Using Gauge Observations, Satellite Estimates, and Numerical Model Predictions. *Journal of Climate*, *9*(4), 840–858. https://doi.org/10.1175/1520-0442(1996)009<0840:AOGMPU>2.0.CO;2

Xu, Y., & Beekman, H. E. (2019). Review: Groundwater recharge estimation in arid and semi-arid southern Africa. *Hydrogeology Journal*, *27*(3), 929–943. https://doi.org/10.1007/s10040-018-1898-8

Ye, S., Li, H.-Y., Huang, M., Ali, M., Leng, G., Leung, L. R., Wang, S., & Sivapalan, M. (2014). Regionalization of subsurface stormflow parameters of hydrologic models: Derivation from regional analysis of streamflow recession curves. *Journal of Hydrology*, *519*, 670–682. https://doi.org/10.1016/j.jhydrol.2014.07.017

Youngs, E. G. (1958). Redistribution of moisture in porous materials after infiltration: 1. Soil science, 86(3), 117-125.

Zhang, Y., Leuning, R., Hutley, L. B., Beringer, J., McHugh, I., & Walker, J. P. (2010). Using long-term water balances to parameterize surface conductances and calculate evaporation at 0.05° spatial resolution. *Water Resources Research*, *46*(5). https://doi.org/10.1029/2009WR008716

Zhuo, W., Fang, S., Gao, X., Wang, L., Wu, D., Fu, S., Wu, Q., & Huang, J. (2022). Crop yield prediction using MODIS LAI, TIGGE weather forecasts and WOFOST model: A case study for winter wheat in Hebei, China during 2009–2013. *International Journal of Applied Earth Observation and Geoinformation*, *106*, 102668. https://doi.org/10.1016/j.jag.2021.102668

Appendix A: RGWPMs and databases of Bidibidi and Uganda

Maps and data relative to Bidibidi and Uganda on digital format

1. RGWPM of Bidibidi (Fig. 2.3).
2. Revised RGWPM of Bidibidi (Fig. 3.3).
3. Hydrogeomorphological map of Bidibidi (Fig. 6.4).
4. Water balance integrated RGWPM of Bidibidi (Fig. 6.6).
5. Existing boreholes in Bidibidi and additional information, i.e. for some existing boreholes, the borehole completion reports, and pumping tests are available.
6. Pumping test interpretations for 80 boreholes in Bidibidi and Adjumani.
7. Newly drilled boreholes in Uganda and additional information, i.e. borehole completion reports, pumping test interpretations and borehole camera inspections.

Appendix B: RGWPMs carried out in Sub-Saharan Africa

1. The individual GIS projects for the 14 RGWPMs, the borehole database used for validation, the climatic and geological settings are given in digital format.
2. The 14 RGWPMs are presented in the following maps. In these maps, the boreholes are labelled with numbers in reference to the digital tables and the legend of each map is common and given below.

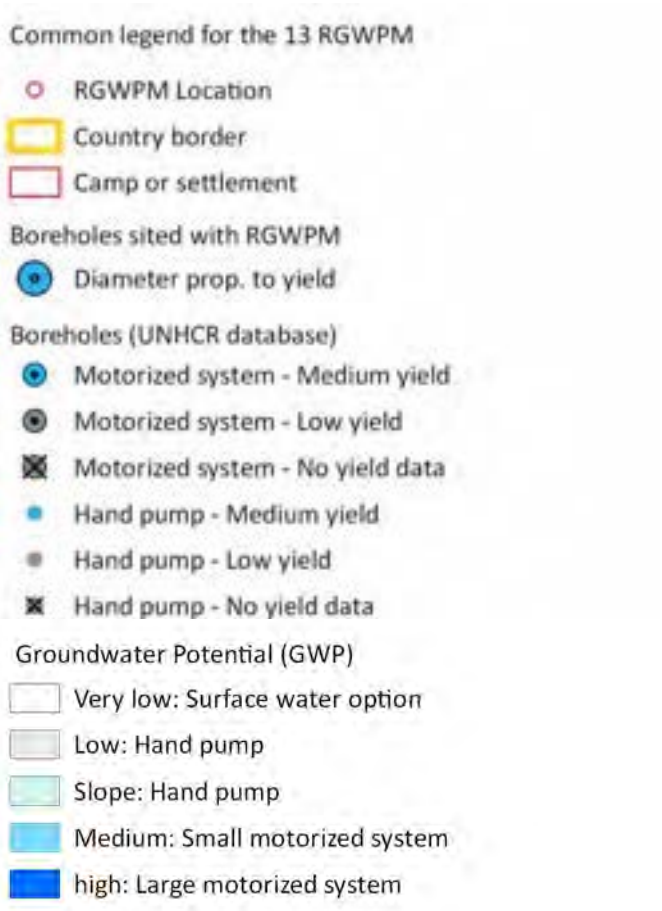

Legend for the 14 RGWPMs.

Burkina-Faso—Goudebou.

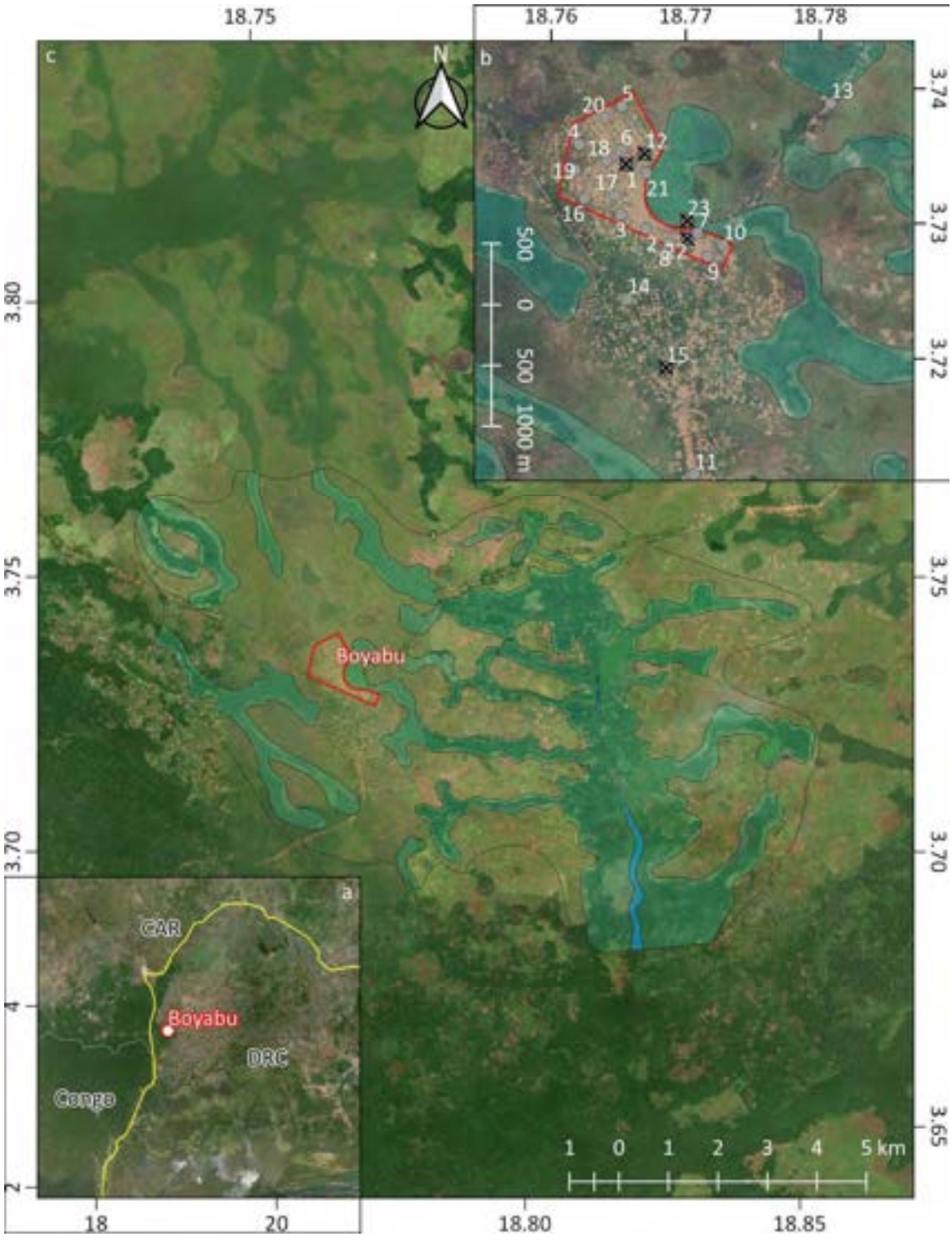

Democratic Republic of the Congo (DRC)—Boyabu.

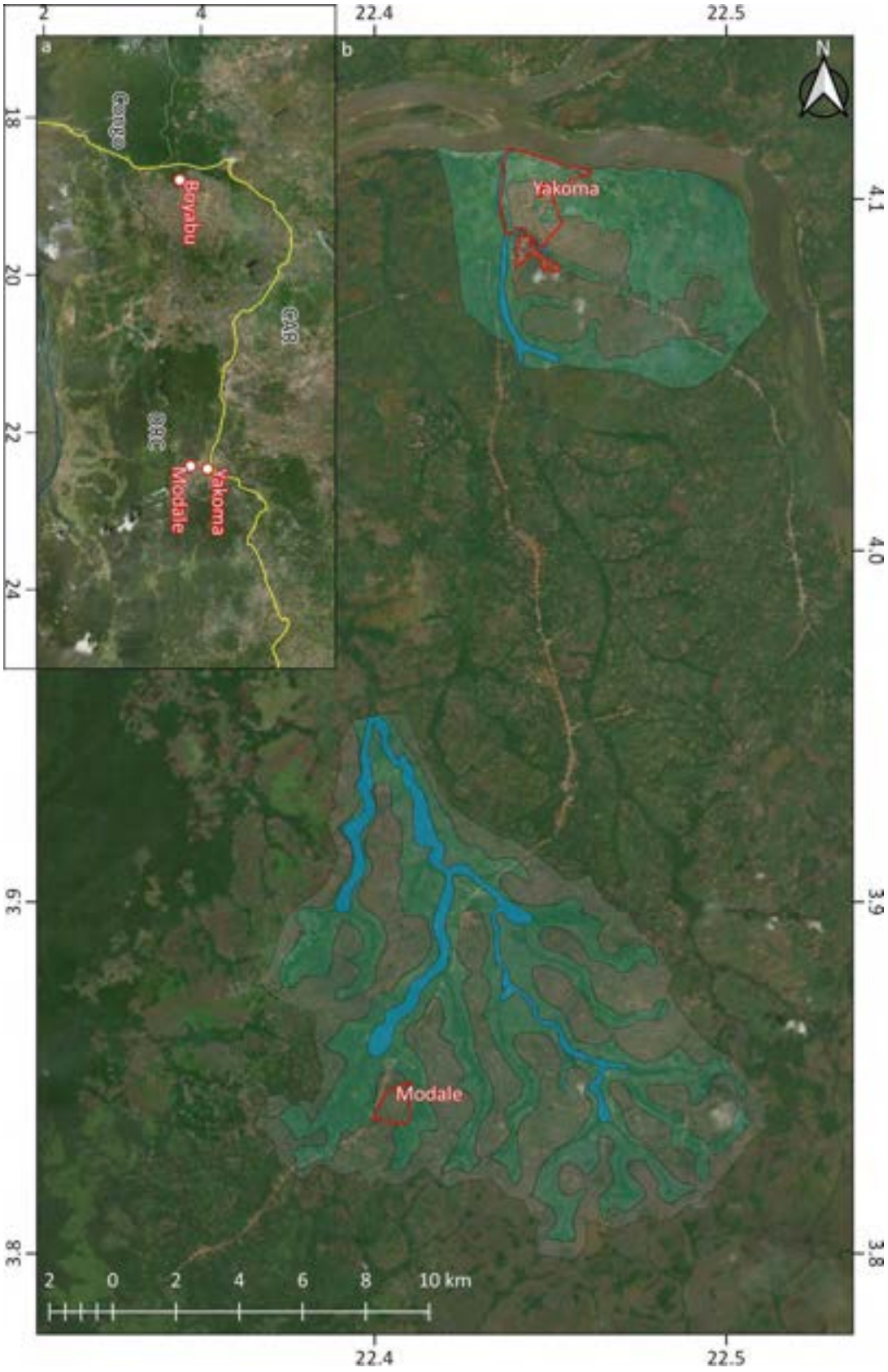

DRC—Modale and Yakoma.

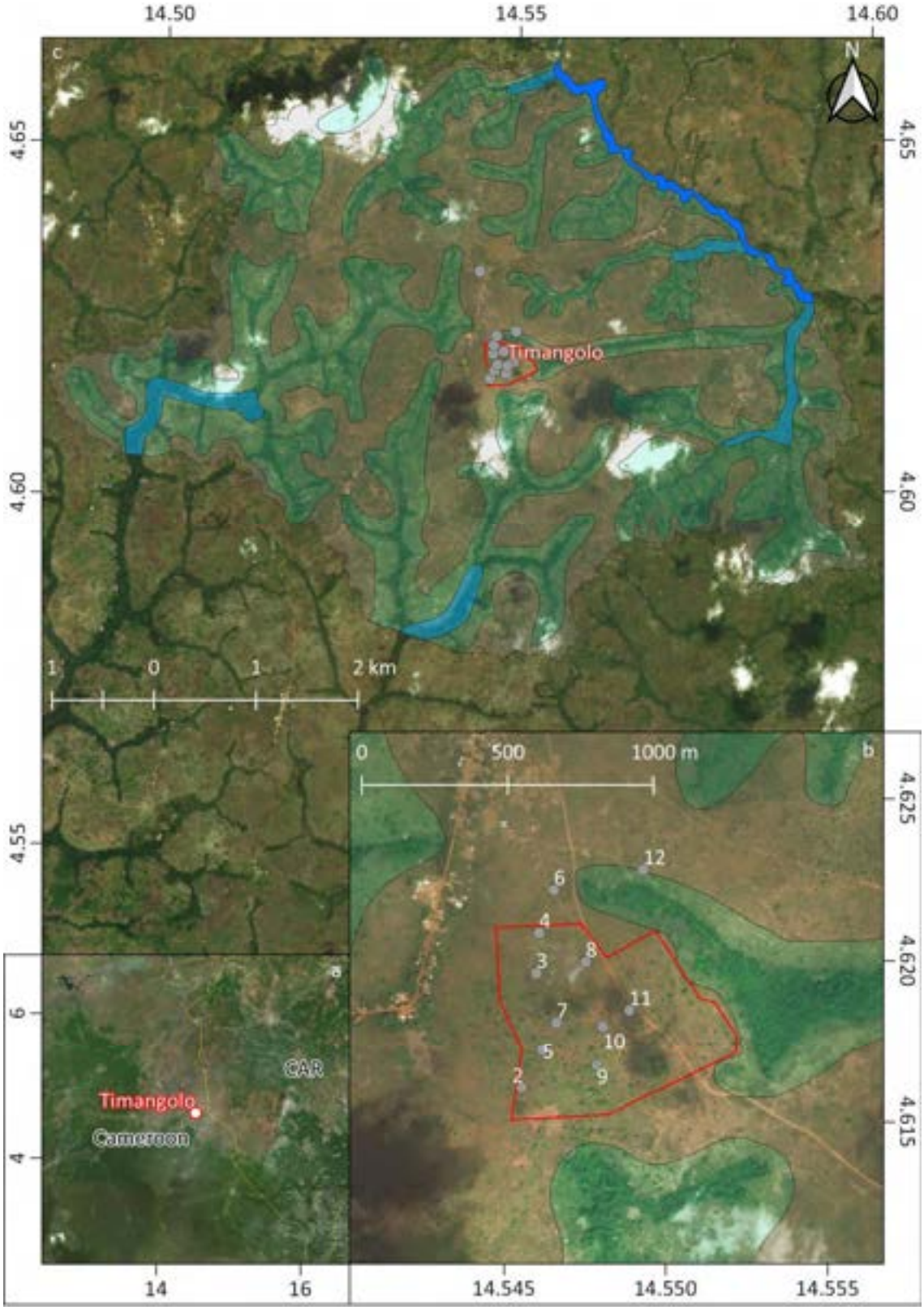

Cameroon—Timangolo.

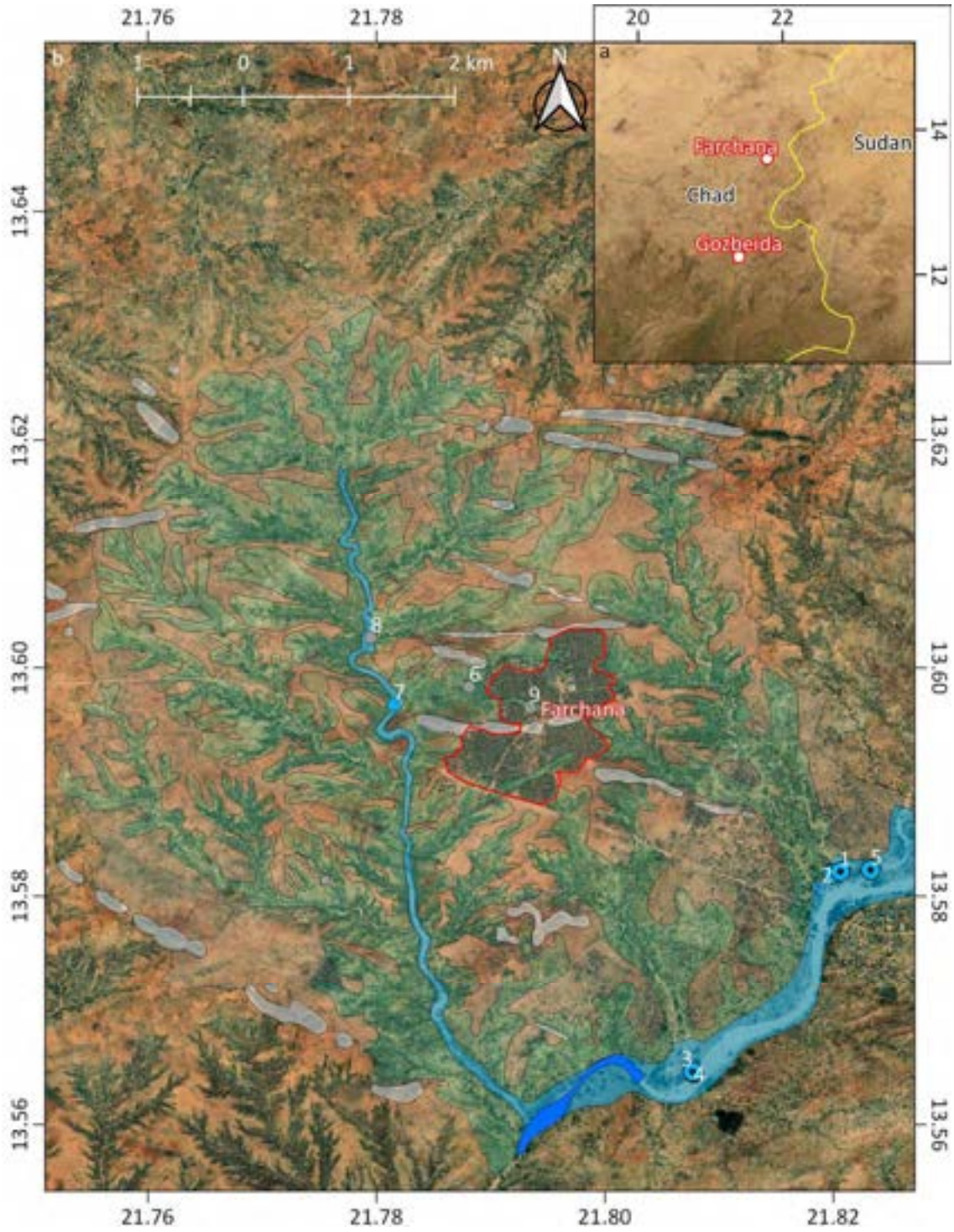

Chad—Farchana.

Chad—Goz Beida.

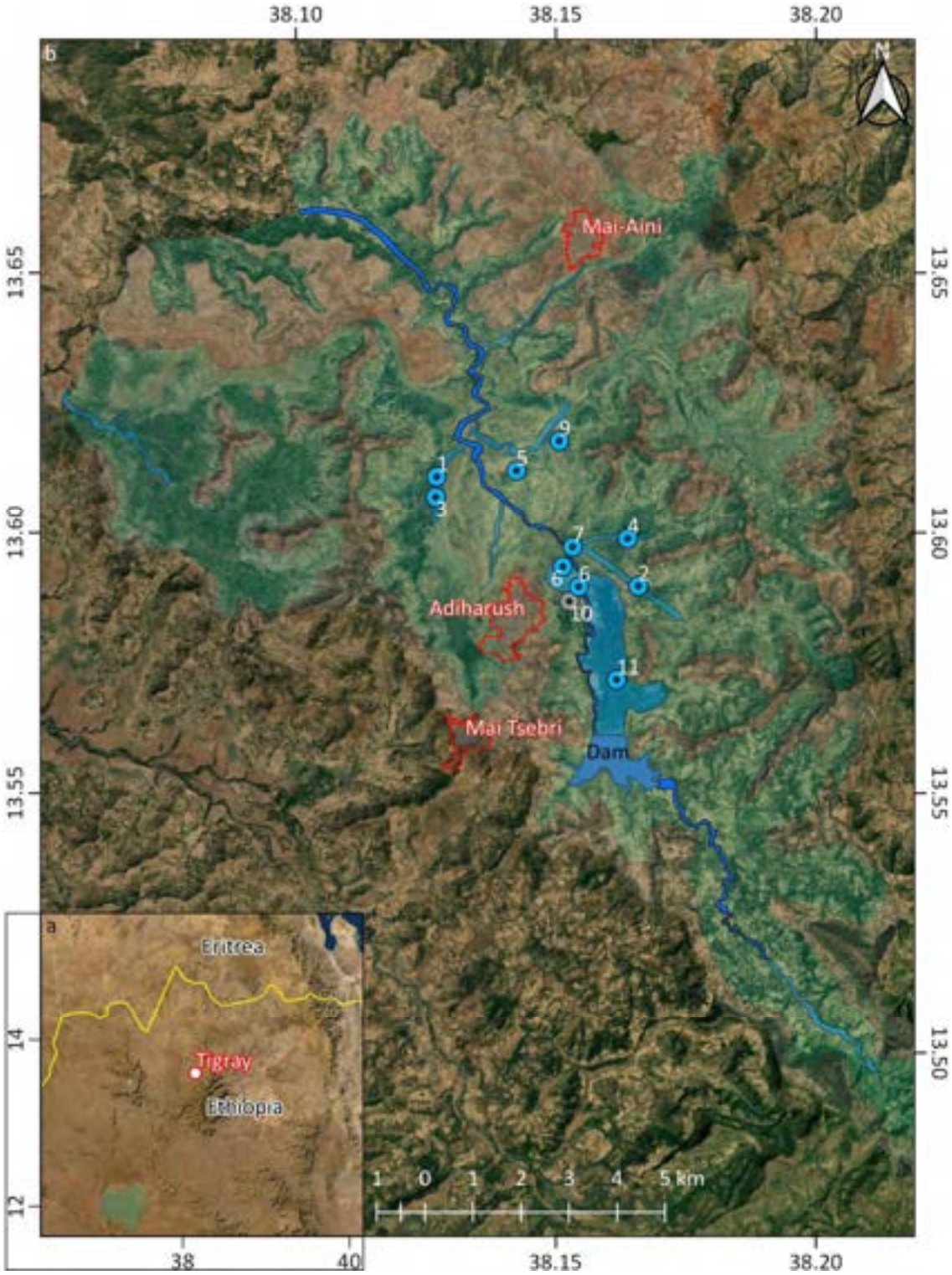

Ethiopia—3 camps in Tigray.

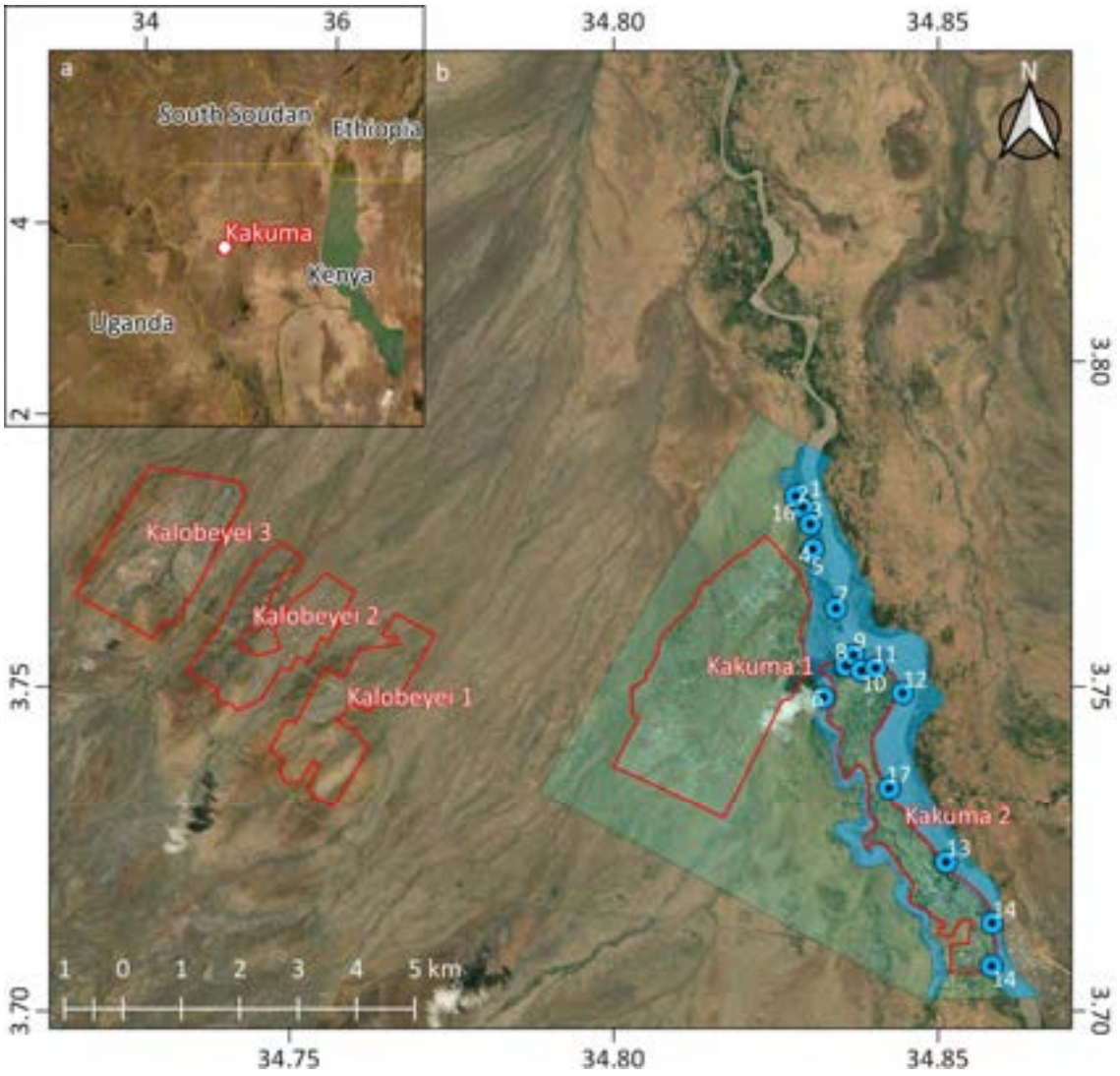

Kenya—Kakuma.

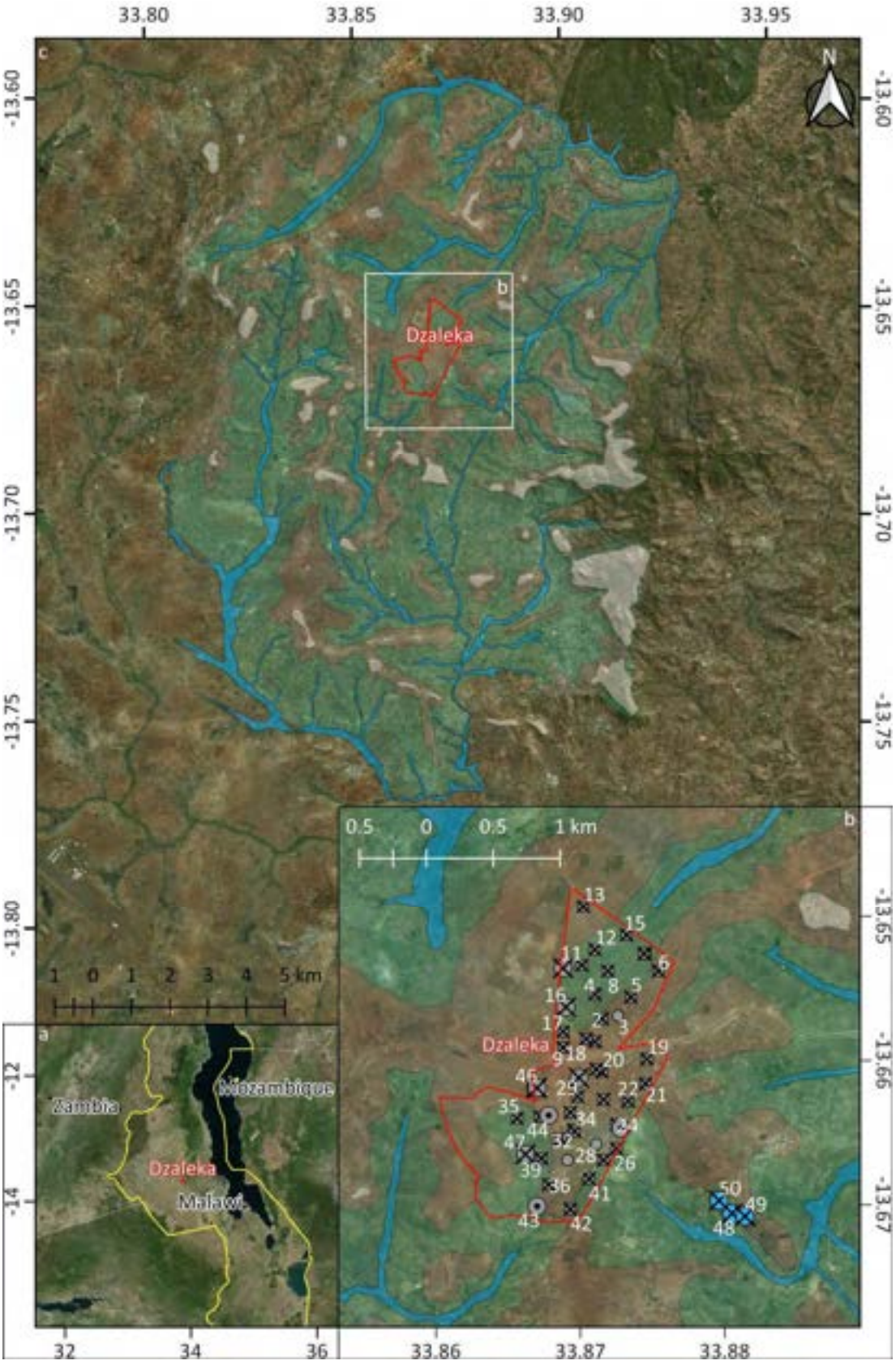

Malawi—Dzaleka.

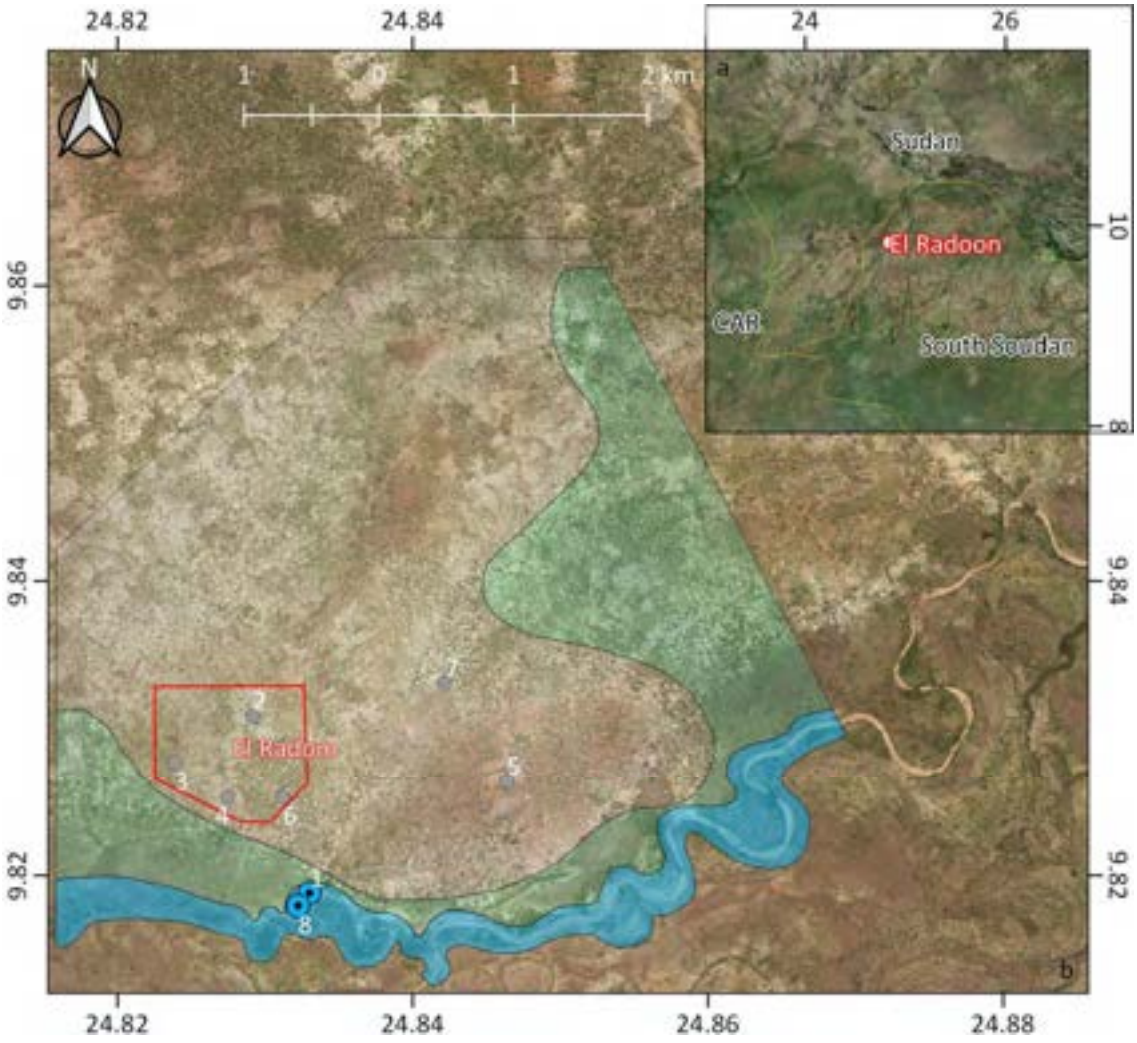

South Sudan—El Radoon.

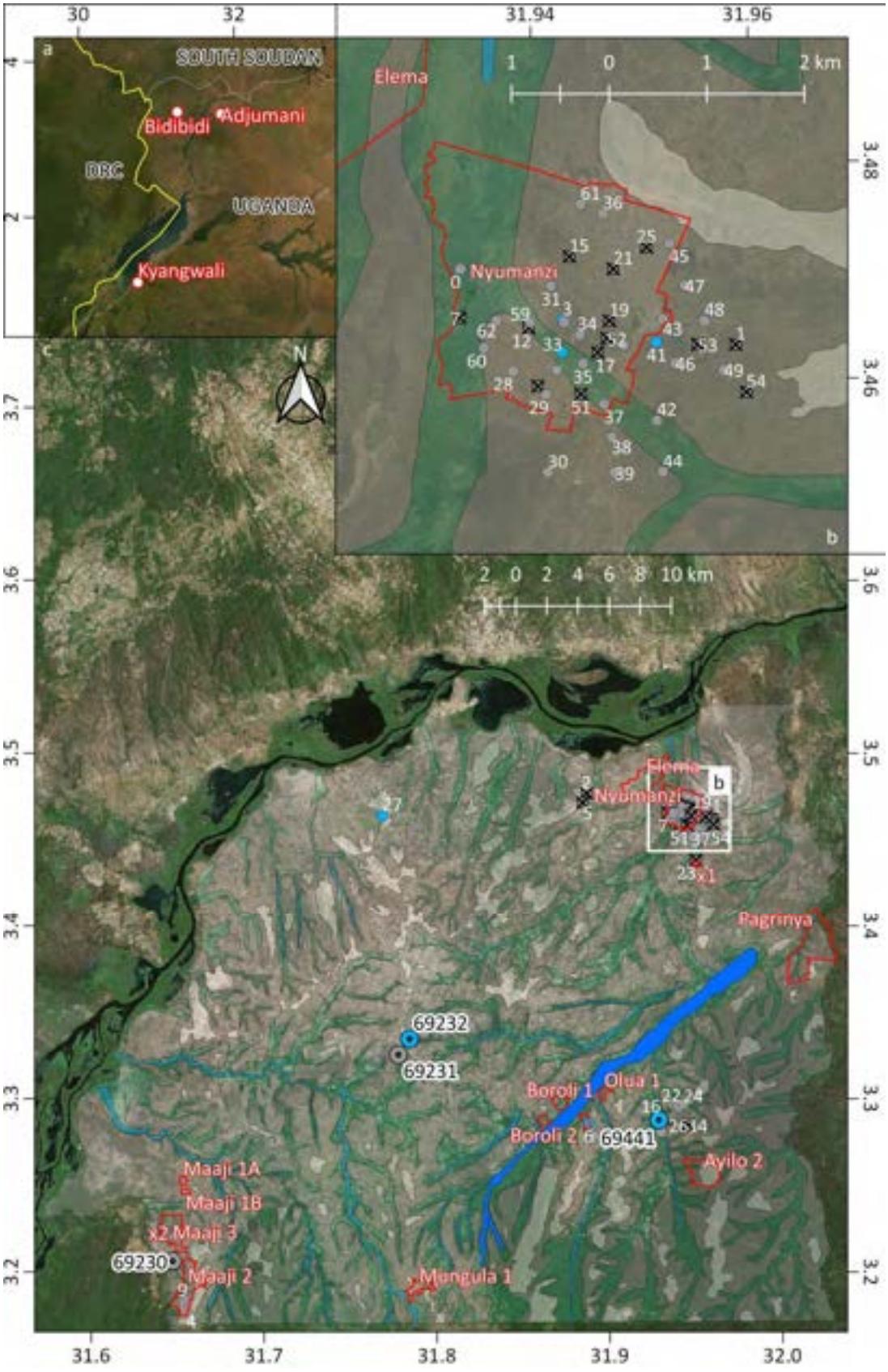

Uganda—Adjumani.

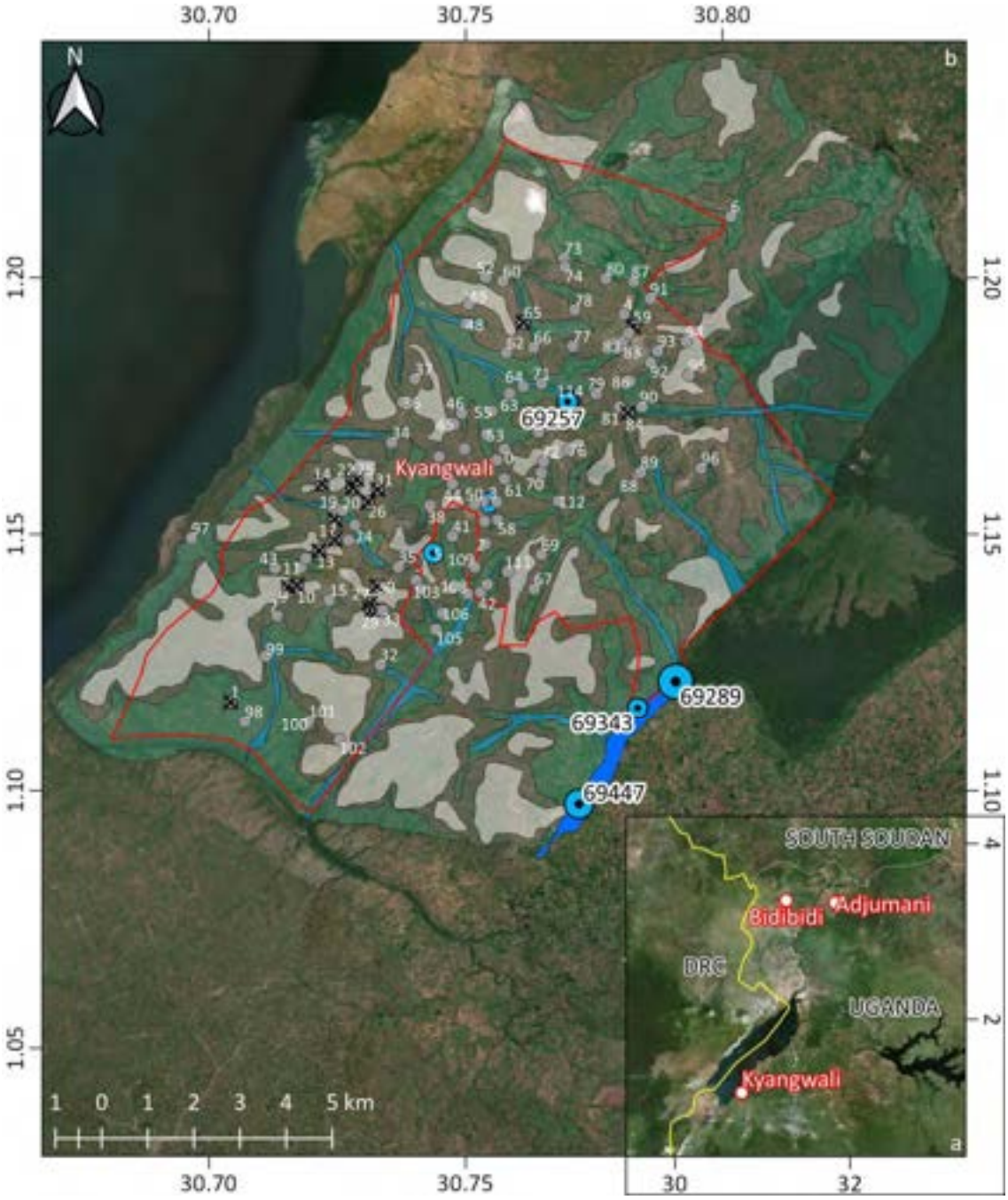

Uganda—Kyangwali.

Appendix C: Water balance components evaluation in data-scares regolithic environments (Supplementary documentation to Chapter 5)

C.1. Introduction

This appendix chapter is intended to provide additional information to that in Chapter 5. In Chapter 5, the data of the 20 catchments, i.e. the hydrogeomorphological units and the water balance components, used in Chapters 6 and 7 are briefly presented. In the interest of streamlining, the information presented below had to be simplified. It is primarily a description of how the water balance components were obtained. Nevertheless, this must be documented. Furthermore, such a data evaluation in these regolithic environments has never been done at this scale, which is an additional reason to detail all the steps. Indeed, this chapter can also serve as a basis for other work involving this type of data.

The 20 catchments used in this study are all located in the typical regolithic environments of Sub-Saharan Africa. Chapter 5 begins with a brief description of each catchment, focusing primarily on the lithologic setting (Section 5.2). However, the specifics of these environments have also been simplified to stay on topic. Therefore, this chapter also provides additional information that is referred to in Chapters 5 through 7. The origin, hydrogeology, and hydrogeomorphology are discussed first.

The information provided on regolithic environments is particularly useful later in this chapter. Some parameters from the literature such as regolith hydraulic properties are used in Section C.3.2.2 in the groundwater flow equation to evaluate the groundwater component. It is used here to assess the validity of the evapotranspiration component by solving the water balance for it with the components with the highest confidence, i.e. precipitation and stream discharge. Indeed, this remotely sensed evapotranspiration seems to have reliability problems according to the literature.

After presenting the regolithic environments, the water balance components are discussed. For precipitation and evapotranspiration, remote sensing products had to be used. For each component, a literature review is performed to discuss their validity and to present the most appropriate products to be used in data-scarce regions of Sub-Saharan Africa. Finally, the most reliable methods for analysing discharge records to obtain runoff and base flow by hydrograph separation are presented.

C.2. Hydro-geo(morpho)logical characteristics of the regolithic environments

This section presents a review of the literature on the regolithic environments. Although the most relevant information on this topic has already been presented in Sections 2.4 and 5.5, a supplement is provided here because a number of additional concepts and parameters on origin, hydrogeology, and hydrogeomorphology are needed to support Chapters 5 through 7, and some parameters will be used later in this chapter.

C.2.1. Origin and geology

Regolith is formed by water-induced weathering of rock (e.g. Taylor and Howard, 1998; Scott and Pain, 2008). It can be primary or secondary. If it is primary, it is the result of weathering of the rock it overlies. Secondary means that it has been transported and deposited further away from the source of weathering (e.g. Chardon, 2018). Both depend mainly on tectonic activity (e.g. Tardy, 1992). For example, the main erosive response to uplift is gravitational and mechanical (Ahnert, 1977). This process generates instability, and the steep topography allows for greater runoff and more material to be transported. It is during periods of tectonic calm, when chemical alteration takes over, that the typical regolith profile is formed (Berry and Ruxton, 1959).

The typical regolith profile extends between 3 and 100 m depth before encountering unweathered rocks (e.g. Chardon, 2018). Depending on the authors and especially on the area of interest, a different number of layers can be distinguished within the regolith itself. Indeed, hydrogeologists such as Tardy and Howard (2000) discuss two main layers, the ferricrete or the laterites above a thick undifferentiated unconsolidated layer. On the other hand, authors interested in the processes leading to a regolith consider more layers. For example, Chardon (2018) distinguishes four, i.e. from the surface to the unweathered rock: ferricrete, Fe-carapace, mottled clays and saprolite. The first three layers are characterised by having no longer earlier rock structures. The fourth layer, the saprolite, has preserved structures such as schistosity or bedding. The first definition of Tardy and Howard (2000) is preferred here.

Regolithic environments are mainly associated with tropical shields. These shields are found in equatorial Africa, Australia, India, and South America. They can extend over very large areas and so can the regolith. Indeed, Tardy (1992) has presented a world map showing the distribution of regolithic environments indicating that they never extend beyond 30°N and 30°S. In the case of Africa, the limits are rather 15°N and 30°S (Fig. 5.1).

Shields are associated with low tectonic activity. But they must be located in areas subject to an equatorial climate for deep weathering to occur, i.e. abundant precipitation and warm temperatures

are needed (Braun et al., 2016). Meteoric water percolating into the subsurface is first rendered acidic by the bio-chemical activity occurring in the topsoil before it can alter the fresh rock below (Scott and Pain, 2008). It mainly dissolves alkaline minerals (Braun et al., 2016). The most soluble elements are displaced and the others eventually re-precipitate. This is the case for the ferritic and aluminium oxides (e.g. Vasconcelos et al., 1994).

Once formed, for a regolith to be maintained, there must be no significant tectonic activity nor glaciation or aeolian erosion (Taylor and Howard, 1998). The last glaciations that reshaped parts of the earth began in the Quaternary (e.g. Ehlers et al., 2011) but did not affect Africa. The extension was mostly limited to Europe and North America. Only isolated mountain glaciers may have appeared sporadically e.g. Mount Kenya (e.g. Ehlers et al., 2011). However, aeolian erosion strongly affects large areas of Africa. It is of course most visible in arid to hyper-arid regions where landforms such as dunes are characteristic of this type of erosion. A milder climate and abundant precipitation are needed to prevent the soil from drying out and to allow the wind to pick up the weathered particles. This is the main reason why regolith is generally found in tropical regions (Taylor and Howard, 1998).

The right climatic and tectonic activity must be present over a long period of time for alteration to occur. According to Taylor and Howard (1998), the shields of Africa are located in environments that present these perfect conditions. After the Late Palaeozoic glaciation, there was a trend of increasing temperature and humid conditions throughout the Mesozoic. This type of climate remained more or less the same until the Pleistocene, when the temperature decreased again. This climatic stability was accompanied by a certain tectonic calm (Scotese, 1991). After the break-up of Gondwana at the end of the Jurassic, the African continent remained more or less where it is today and enjoys a tropical climate since then.

Not all regions of equatorial Africa experienced exactly the same climatic and tectonic conditions throughout the entire Mesozoic. Thus, some places have inherited their landscape through alternating weathering and stripping (Partridge and Maud, 1987). For example the western part of Uganda, where the settlements of Bidibidi are located (Fig. 2.3), underwent some stripping during the Paleogene due to colder conditions, as well as some stripping at the end of the Neogene due to rift opening. However for the eastern part, e.g. in Adjumani there was only this episode of stripping of the Paleogene (Taylor and Howard, 1998). This time period (more or less entire Mesozoic) corresponds to the observation of Fairbridge and Finkl (1980) that arround 10^7 and 10^8 years are needed to get a deep weathering profile.

C.2.2. Hydrogeology

A number of authors, as Lachassagne et al. (2021), Chilton and Smith-Carington (1984) or Taylor and Howard (2000), have described the hydrogeological processes of the regolithic environment in great detail. All agree that groundwater flows mainly in large regional aquifers in the regolith and little in the fractured bedrock. According to Freeze and Cherry (1979) fractured bedrock can have locally high hydraulic conductivities (10^{-4} m/s), but on a regional scale they become very low (10^{-8} m/s). This might be because the fractures are not connected, so that water percolating from the regolith into these fractures is trapped there (Alazard et al., 2016).

It is commonly agreed that the regolith at the catchment scale is uniformly distributed (Taylor and Howard, 2000), it is also found to have similar thickness ranges everywhere. This observation is highlighted by lots of authors, e.g. Dewandel et al. (2012) who have made a particular review on this topic, but it was also described earlier by Ollier et al. (1988) who report that it is generally of the order of 30 metres.

In addition to the simple geometry of regolithic aquifers, their hydrogeologic properties, i.e. hydraulic conductivity, transmissivity, and porosity, are in a similar range wherever these parameters have been evaluated. The regolith hydraulic conductivity values from several studies are summarised in Table C.1 which was partially modified from Taylor and Howard (2000) and Dewandel et al. (2012). These studies are selected because the authors describe in great detail their study site and the type of pumping test they performed. Only studies conducted in Sub-Saharan Africa are listed in Table C.1.

Table C.1 *Hydraulic conductivity (K) of regolith at six locations in Sub-Saharan Africa retrieved from literature. It ranges between 1.00E-06 and 4.17E-06 m/s and the average is 2.69E-06 m/s.*

K [m/s] (Geo. mean)	N. of sites	Location	Authors
3.00E-06	64	Masvingo, Zimbabwe	Houston and Lewis (1988)
1.00E-06	8	Sano, Burkina Faso	Compaore et al. (1997)
4.00E-06	6	Africa	Wright (1992)
2.95E-06	4	Aroca, Uganda	Taylor and Howard (2000)
4.17E-06	1 (Modelling)	Ouémé, Benin	Herzog et al. (2021)
2.69E-06	80	Bid. and Adj., Uganda	This study (Appendix A)
1.00E-06	4.17E-06	Minimum and maximum K [m/s]	
2.69E-06		Mean K [m/s]	

As with hydraulic conductivity, mean transmissivities for the regolith were retrieved from the literature and summarised in Table C.2. A total of 10 sites across Sub-Saharan Africa are again well documented.

Table C.2 *Transmissivity (T) values of regolith at 10 locations in Sub-Saharan Africa retrieved from literature. It varies 2.43E-05 and 6.91E-05 m^2/s and the average is 5.03E-05 m^2/s.*

T [m^2/s] (Geo. mean)	N. of sites	Location	Author
5.79E-05	8	Zimbabwe/Malawi	Wright (1992)
6.37E-05	134	Livulezi, Malawi	Chilton and Foster (1995)
2.43E-05	81	Dowa, Malawi	Chilton and Foster (1995)
6.02E-05	64	Masvingo, Zimbabwe	Chilton and Foster (1995)
3.94E-05	27	Masvingo, Zimbabwe	Chilton and Foster (1995)
5.32E-05	6	Malawi/Zimbabwe	Chilton and Foster (1995)
5.56E-05	40	Mukono, Uganda	Chilton and Foster (1995)
6.91E-05	4	Aroca, Uganda	Taylor and Howard (2000)
3.47E-05	3	Dodowa, Ghana	Foppen et al. (2020)
4.51E-05	80	Bid. and Adj., Uganda	This study (Appendix A)
2.43E-05	6.91E-05	Minimum and maximum T [m^2/s]	
5.03E-05		Mean T [m^2/s]	

The main purpose of Table C.1 and C.2 is to emphasize that neither the hydraulic conductivity nor the transmissivity varies greatly from one place to another. In fact, the order of magnitude is the same for both, since the hydraulic conductivity ranges from 1.00E-06 to 4.17E-06 m/s with an average of 2.69E-06 m/s and the transmissivity varies from 2.43E-05 to 6.91E-05 m^2/s with an average of 5.03E-05 m^2/s.

Since the bedrock has a low hydraulic conductivity (Freeze and Cherry, 1979) it consequently has a low effective porosity. Most of the water flows at the interface of the regolith and the unaltered rock because it is composed of loose material. A comprehensive case study by Dewandel et al. (2012) estimated the general saturated porosity to be around 1.5%. Two other studies, again by Dewandel et al. (2012, 2017) and reported later in Lachassagne et al. (2021), clearly support the estimate of 1.5% at the bottom of the weathered layer where the largest part of the groundwater flows and thus where most of the change in groundwater storage take place.

The regolithic environments have low hydraulic properties as shown in Table C.1 and C.2, leading to important hydraulic gradients (Haitjema and Mitchell-Bruke, 2005). According to Lachassagne et al (2021), they are superior to 1%. This already leads to the piezometric surface being close to the

topography, but it is even further accentuated if infiltration is high (Haitjema and Mitchell-Bruke, 2005). For example, the ratio of infiltration to effective precipitation found for several catchments in Malawi is between 46% and 96% (Hill and Kid, 1980); the same has been documented in Zimbabwe (Farquharson and Bullock, 1992) where this ratio is also between 50% and 98%. Taylor and Howard (2000) report, for example, that for a deeply weathered catchment in central Uganda (Aroca), infiltration reaches 120 mm/year for an effective precipitation of 125 mm/year.

Since the water tables are high and sub-parallel to the surface, the isopiezes on the surface are similar to the iso-contour of the topography. These aquifers are therefor considered to be topographically controlled (e.g. Haitjema and Mitchell-Bruke, 2005). This means that the hydrogeological basin has the same surface as the hydrological catchment (e.g. Lachassagne et al., 2021).

C.2.3. Hydrogeomorphology

According to McFarlane's (1989) studies in Malawi, the formation of regolithic landscapes can be understood as a description of what happens with water. Its theory contrasts with the work of King (1963; 1967) who assumed that they were the result of massive peneplanation induced by strong surface runoff. McFarlane (1989) presents a radically different formation process of these landscapes by arguing that the main actor in peneplanation is infiltration. This has also been demonstrated by Bullock (1988) in Zimbabwe. Both describe surface runoff as having little impact on the formation of these landscapes.

In the revised RGWPM methodology presented in Section 3.2, all the steps to obtain the WA zone based on the hydrogeomorphological landscape units are described (Winter, 2001). These units are the upland (low WA), slope (slope WA) and the lowland (high WA) unit. Within the slope unit forms the drainage system (medium WA) which is not only a one-dimension path but also has a variable lateral extension, making it a unit or a zone. In the regolithic environment the drainage system represents one of the main and certainly most distinctive geomorphological features (e.g. McFarlane, 1989).

The drainage system is formed by mechanical erosion and chemical weathering of the regolith (Boast, 1990). Mechanical erosion is mainly attributed to streams that ascend and descend during the year (Mäckel, 1973). During the rainy season, heavy rainfall can make the subsoil saturated upon the limit of the upland, so that the stream moves upwards. During the dry season, the stream initiates further downstream. This idea of mechanical erosion was most likely coupled with chemical weathering. McFarlane (1989) suggests that it is the original fractures and faults allowing easier

alteration that are the main actor of its formation. The streams pass preferably through fractures and faults in which infiltration is facilitated, thereby allowing greater weathering arround these structures. This explains the sometimes-important lateral extension of the drainage system, induced by this 'melting' of the regolith.

The mapping of the upland and slope unit are well described in Section 2.4 and can be automated however in order to properly map the drainage system unit, it must be drawn manually. This is not a problem because it is easily identified with satellite images thanks to the type of vegetation that grows preferentially in it, such as grass (Balek, 1977; Jackson, 1968). The reasons for this reduced form of vegetation are, according to Whitlow (1980), attributed to the waterlogged conditions found there, preventing the growth of larger plants.

C.3. Products and methods to quantify water balance components in data-scarce regions

Hereafter, the remote sensing products for precipitation and evapotranspiration are first presented. For both, a review of the literature is carried out in order to justify the products that are retained for this study. In addition, for evapotranspiration data, there is a fairly long section devoted to the validity of the product, as it represents the component for which there is the least confidence. Afterwards, the data of the gauging station which are the discharge records used to estimate runoff and base flow by hydrograph separation are discussed. Finally, a review of the literature on hydrograph separation is presented before discussing the most reliable method.

C.3.1. Remote sensing products of precipitation

Precipitation can be measured at weather stations and presents the most reliable data. But in remote locations, as it is often the case for most places in Africa, this type of measurement is usually not available (Maidment et al., 2017). Atmospheric modelling is a way of coping with this data scarcity (e.g. Peters-Lidard et al., 2007). However, increasingly, precipitation is being estimated using sensors on satellites and to date a small number of products offer this information. They have of course already been widely used and several of these products have been validated for Africa, (e.g. Awange et al., 2019), and even some for Uganda (Diem et al., 2014; Maidment et al., 2013).

Recently, several global precipitation products have been made available to a wider audience than climatologists. Only the best known and most widely used products in Africa which have been reasonably well validated are briefly presented to justify the selection of the one used in this study. The ones presented here are among the most accessible and least time-consuming to process, which

is why well-known products such as NOAA's (National Oceanic and Atmospheric Administration) are not mentioned here.

A notable satellite that measured precipitation is the one of the Tropical Rainfall Measuring Mission (TRMM) (Kummerow et al., 2000). It was a joint mission caried out by NASA and the Japan Aerospace Exploration Agency (JAXA). TRMM produced two products available the 3B43 and the 3B42. The first are monthly precipitation estimate and the second are 3-hourly estimates. Both have a resolution of 0.25 arc degrees and the data are available from 1998 to 2019. The sensor onboard the TRMM measures microwave energy emitted by the earth in order to estimate the amount and different state of water in the atmosphere. Another sensor onboard the TRMM, the Precipitation Radar, gives insights on the cloud structures. These data are used along the Global Precipitation Climatology Centre (GPCC) rain gauge analysis (e.g. and Huffman, 2010). Both daily TRMM products are slightly overestimated compared to ground truth data (Gupta et al., 2014). Similar results have been shown by Fleming and al. (2013) and Tang et al. (2016). Various studies carried out by Dinku et al. (2007; 2011) or Hirpa et al. (2010) over complex topographies of Ethiopia have also proven TRMM to perform well.

Another widely used product is from the Famine early warning system or simply FEWS-Net project produced by USAID in partnership with NASA and NOAA. The algorithm producing these data is called African Rainfall Estimation Version 2 later updated into RFE2 (Laws et al., 2003). The later algorithm uses data from two radar sensors (AMSU-B and SSM/I) and one infrared sensor (GPI) onboards METEOSAT 2-9 missions. The measurements are calibrated with daily data of 2000 rain gauging stations. Satellite and radar estimates are mainly used to evaluate the size of rainfall distributions and gauging stations are used to evaluate the magnitude of events. The algorithm associates by likelihood estimation methods (Xie & Arkin, 1996) the grid near the gauging station with the measured value and depends increasingly on the distance to the satellite measurements. This daily product has a resolution of 0.1 degree. The correlation of these daily data with respect to ground truth data is very low (0.5) but it seems that the quality somewhat becomes better if longer time periods are considered for which a correlation of 0.7 to 0.9 can be reached if annual data are considered. However, on an annual average, the error range can still be large because it is between 2% and 19% (Karimi et al., 2014).

The following paragraph briefly presents two products that have the advantage to be easily available and are considered here as rather useful in order to have a rough overview of the precipitation distribution. The first is the WorldClim product from Hijmans and al. (2005). This dataset is produced by an enormous amount of weather station from all arround the world that have been used to

interpolate a continuous layer. This makes this data unique compared to the others that mostly or partly rely on satellite imagery. The monthly data are available at a high resolution of 0.5 arc minute. The monthly data are produced from an average of the years 1970-2000, so that values of a specific month for a specific year cannot be selected. The second product is the one of OpenLandMap. This product partially uses data from WorldClim along two other sources including climatic modelling. The resolution is 0.5 arc minute. As for WorldClim, the data are available monthly and have been averaged over the period 2007 to 2019.

Not being able to select a specific period is a major drawback, as more and more products appear with hourly data. Furthermore, as it will be discussed later, the discharge of several rivers is going to be used, which is of course closely related to the rainfall intensity of the measured period.

Recently, numerous products have been made available. Although less literature is published about them, they are listed below to present the range of products that are readily available. It is certain that some of them will soon become very popular as they offer hourly and high spatial resolution data. They are listed here with the product name followed by the period of availability data and resolution.

- ERA5 (Copernicus), 1979-2020, monthly, daily, and hourly, 0.25 arc degrees.
- TerraClimate (Abatzoglou, et al,. 2018), 1958-2020, monthly, 2.5 arc minutes.
- GSMaP (Okamoto, et al,. 2005), 2014 to present, three-hourly intervals, 0.1 arc degrees.
- GLDAS (Rodell et al,. 2004), 2000 to present, hourly,0.25 arc degrees.
- GPM (Huffman, 2019), 2000 to present, half hourly, 0.1 arc degrees.
- CFSV2 (Saha, 2011), 1979-present, six-hourly, 0.2 arc degrees
- PERSIANN-CDR (Ashouri et al., 2015), 1983-present, daily, 0.25 arc degrees.

The future flagship, but not yet easily available, is likely to be TAMSAT (Maidment et al., 2017). Indeed, it has an exceptionally high resolution of 0.0375°. This product, like most others, is also based on thermal infrared precipitation products and stations. Moreover, this product has a very good correlation with ground data like the next product presented here (CHIRPS) which has almost the same resolution.

The last precipitation product being discussed here and the one used for this study comes from the Climate Hazards Group InfraRed Precipitation calibrated with Station data (CHIRPS) from the University of California at Santa Barbara and U.S. Geological Survey (Funk et al., 2014; 2015). The

spatial resolution of this product is 0.05 arc degrees, this means that close to the equator, the grid cells of this raster are approximately 5.5 km^2 in size. The raster is available from latitude 50°S to 50°N for all longitudes. This resolution is currently the highest available for precipitation in the public domain. The data are available daily from 1981 to near-real time.

The CHIPRS products are created with three inputs and based on thermal infrared precipitation measurements methods like the one of the African Rainfall Estimation from FEWS-Net mentioned earlier or the products of the NOAA. CHIRPS utilizes the Tropical Rainfall Measuring Mission Multi-Satellite Precipitation Analysis version 7 (TMPA 3B42 v7) (Huffman et al., 2010) in order to transform cold clouds into precipitation (Funk et al., 2015). In the tropics, cold clouds, i.e. ≤ 235°K are indicating precipitation. The data are ultimately calibrated with rain gauges by several interpolations (Funk et al., 2015).

C.3.1.1. Summary of available remote sensing products of precipitation

Of all the above discussed products, one might hesitate between CHIPRS and TRMM for the use in data scares regions because they have been calibrated with ground data. Indeed, the FEWS-net product is becoming obsolete for the former and the latter have an extremely low daily validity. Other monthly products such as those from WorldClim are useful for a quick assessment as the time period cannot be chosen. The CHIRPS and TRMM products are generally equally suitable (Sharann et al., 2020). Both yield good results at larger scales, e.g. for the Blue Nile Basin and the East Nile Basin (Abdelmoneim et al., 2020). In this work, CHIRPS is chosen because it has a higher spatial resolution than TRMM, which is considered better to capture rainfall invents on the rather small catchments under consideration.

C.3.1.2. Discussion of the validity of CHIRPS

Dinku et al (2018) conducted a study to evaluate CHIPRS in selected regions of eastern Africa. It was conducted in Ethiopia, Kenya and Tanzania and thus covers a wide range of climatic and topographic regions such as mountainous, coastal, and desert areas. Their study compares data from a large number of weather stations, i.e. 1200, to the CHIRPS acquisitions. They argue that the problem of validating this product is related to the fact that CHIRPS already ingests a large number of weather stations so that other station that are not used by the algorithm have to be encountered to assess the validity. The study made all kinds of different statistical comparisons. Here, in order to briefly summarise their results, only the bias values are discussed. The monthly and daily biases for Ethiopia are 0.96 and 0.89, respectively and for Tanzania it was 0.89 and 1.03, respectively. For Kenya, they only show the monthly bias of 1.13.

Maidment et al (2017) also used daily station measurements to validate the CHIRPS product and other satellite images. In total, they compared seven precipitation products, namely two products from TAMSAT, CHIRP (CHIRPS without station), CHIRPS, ARC, RFE, TMPA-3B42 and CMORPH. They conducted this study for Mozambique, Niger, Nigeria, Uganda, and Zambia. In total, they used 265 stations. As in the above study, only the bias between the satellite images and the station is presented here. The daily bias is 0.75 for Mozambique, 0.87 for Niger, 1.03 for Nigeria, 1.17 for Uganda and 1.01 for Zambia. According to Dinku et al. (2018), the rather large error in Uganda comes from the small amount of data (2000-2005 measurements from 56 stations), so this error is mitigated. Finally, the general assessment for all countries returns a bias of 0.96. This last value is not only exceptionally good, but according to the study, it is the best met for all 7 products.

C.3.2. Remote sensing products of evapotranspiration

The main remote sensed evapotranspiration products readily available for Africa are provided by TerraClimate and two by MODIS, i.e. MOD16A2 V105 and MOD16A2 Version 6. As with precipitation, they are briefly discussed and presented hereafter with a rationale for the choice of MOD16A2 Version 6. Other well-known approaches to generating evapotranspiration data, based on the satellite acquisition of the Advanced Spaceborne Thermal Emission and Reflection Radiometer (ASTER) or that of the LandSat mission, are not discussed here. They capture both very high-resolution images of at least 30 m and provide relevant information on evapotranspiration (e.g. Allen et al., 2011, Gowda et al., 2008). The problem with these two products is that it is complicated and time consuming to convert the thermal bands meaningfully into actual evapotranspiration. Moreover, for both, an image is only taken every two and four weeks. This is therefore not suitable for the resolution of the water balance on a catchment scale. In fact, the temporal frequency should be higher in order to extrapolate as little as possible. This is just one example where MODIS outperforms this type of product by providing weekly evapotranspiration.

The TerraClimate product (Abatzoglou et al., 2018) is based on a model that allows to generate monthly evapotranspiration data among other variables such as precipitation, as mentioned in the previous section. It is mainly the authors who developed the product who discuss its validity. But one can still conclude that their product correlates reasonably well with ground data. The algorithm behind the model is assisted by the monthly climatological normals of WorldClim mentioned earlier but integrating data from CRU Ts4.0 and the Japanese 55-year Reanalysis (JRA55). The model is based on a simple one-dimensional soil water balance. The monthly data are available from 1958 to near present, and the requested time span can be modelled. Although it is possible to go back in

time exceptionally far, the major problem here is that the resolution is only 2.5 arc minutes. (~4 km at the equator)

The measurements of the Moderate Resolution Imaging Spectroradiometer (MODIS) on board the NASA Aqua satellite are used in an algorithm described by Mu et al. (2007) that has been revised by Cleugh et al. (2007) to generate two evapotranspiration products. These two are named MOD16A2 V105 and MOD16A2 Version 6 that both provide global evapotranspiration data every eight days. The first has a resolution of 1 km^2 and the second of 500 m^2. Both products are produced based on the Penman-Monteith (P-M) equation (Monteith, 1965) with remotely sensed and daily meteorological reanalysis. The remotely sensed data comprise, amongst other, vegetation property dynamics, albedo, and land cover. The first product (MOD16A2 V105) can be generated from 2000-2014 and the second (MOD16A2 Version 6) from 2001-present.

According to literature (e.g. Kim et al., 2012) it appears that the quality of the MOD16A2 V105 product is questionable. However, if one exclusively analysis biomes and climates close to those of Africa, satisfactory results are nevertheless found. The following results are obtained by comparing it to several weather stations measurements made during the year. For example, in the USA, Velpuri et al. (2013) showed that an R^2 of 0.70 and 0.71, respectively, for cropland and savannah woodland can be obtained. They also showed that for other climates that might be similar to those found in Africa, the R^2 can be lower than 0.6. Studies in semi-arid to arid regions (e.g. Ramoelo et al., 2014) suggest that evapotranspiration can be simulated very well in some years with an R^2 of up to 0.85 but in other years only at 0.26. Aguilar et al. (2018) showed that in northern Mexico at Rayòn and El Mogor that during 2008-2010 the R^2 was 0.86 and 0.44 respectively. Degano et al (2018), showed that for a location in Argentina in the Pampa region between 2012-2014, the R^2 was 0.86. Thus, overall heterogeneous results.

The review Degano et al. (2021) summarises all sensitivity analyses performed so far on MOD16A2 V105. They concluded that six studies were worth looking at. This opens the discussion as to whether this product has been properly evaluated. Furthermore, only one study has been conducted in Africa (Ramoelo et al., 2014), so this product is in serious need of further testing.

As discussed, next, the MOD16A2 V105 and MOD16A2 Version 6 present similar data qualities. therefore, the latest will be used for the subsequent analysis since it has a higher spatial resolution. Hereafter, for linguistic simplicity, when referring to the evapotranspiration product of MOD16A2 Version 6, it will be abbreviated as MODIS.

To date, four studies by Aguilar et al. (2018), Chang et al. (2018), Peschechera et al. (2018) and Degano et al. (2021) have evaluated MODIS under different climatic conditions. The conclusions of these studies can be summarized as follows: (1) the product underestimates evapotranspiration in semi-arid areas, (2) due to the limited research carried out to date, the potential of this product cannot be properly assessed and (3) without being able to compare this product with ground truth data, it cannot be taken for granted. Finally, (4) the spatial error is transmitted to each pixel, so that if ground truth data are available, MODIS can be spatially corrected.

C.3.2.1. Discussion of the validity of MODIS

As discussed above, the spatial and temporal resolution of MODIS exceeds that of all other remotely sensed evapotranspiration products. Nevertheless, some authors who have dealt with it, and in particular those presented in the previous section, do not always report it very positively, sometimes presenting significant errors when comparing it to 'reality'. Reality is either understood as various near meteorological ground measurements converted to evapotranspiration (e.g. Allen, 1998) or modelling, i.e. solving the water balance for evapotranspiration. None of them provide a practical solution for direct use or simple correction. Therefore, in the following section, the direct use of MODIS data in data scarce regions is explored.

Before presenting how the validity of MODIS is assessed in this study, a brief overview of the general ways this product is evaluated is discussed. The ways it is evaluated may be one of the reasons for the discrepancies raised by some. Most authors evaluating MODIS are in fact comparing this remote sensing product, i.e. a raster with point data. Others attempt to solve the water balance for evapotranspiration but may perhaps oversimplify it.

Evapotranspiration can be measured at an Eddy Covariance flux tower (e.g. Aubinet, 2012). If one compares such point measurement to a pixel of 500 m, i.e. the resolution of the MODIS sensor, the errors will obviously be significant (Gowda et al., 2008). In fact, over 0.25 km^2 the climate, depending mainly on the topography and, above all, the type of vegetation, can vary significantly.

The study by Kim et al., 2012 is considered a good example to illustrate this point data to pixel value comparison. They do not work in Africa but in Asia. They compare the 8-day value of MODIS with measurements from weather stations. A total of 17 stations are used in their study and they are well distributed across Asia. However, almost none of the measurements correlate with MODIS. The measuring stations are located in very different climatic settings and vegetation types. As none of the stations correlate with MODIS, the problem is certainly not related to a specific location. One would have thought that, for example, the emission of a specific type of vegetation might have been

more or less well captured by the MODIS sensor. Or that the geographical location, e.g. latitude and longitude, could also have an influence on the sensor. So that indeed, the problem is certainly related to this evaluation methodology. Their study is based on more or less long-term evapotranspiration measurements, which could be a cause of error, as discussed in the next paragraph.

The study by Ramoelo et al. (2014) is similar to that of Kim et al., 2012, but was conducted in South Africa and is based on comparing annual evapotranspiration measurements. In short, they show that there is a different error for each year. This is rather surprising since the MODIS satellite passes over the same locations about once a week. As far as the error is concerned, this is probably again the problem of comparing point measurements with pixel data, but it does not explain why there is a difference from year to year. One possible explanation is that at specific times MODIS fails to capture certain images. This could be due to cloud cover that sometimes blurs the terrestrial emission. A study by Zhuo et al. (2022) in north-eastern China, emphasizes the importance of using 'clear sky' images in order to obtain good results.

This first way of evaluating, i.e. comparing point measurements with pixel values, is arguably a questionable approach. However, if one were to take the results of this approach at face value, one is not really interested here in the ability of MODIS to be solved at a point but at a catchment scale. Indeed, a point measurement does not capture the cumulative heterogeneities in a catchment that are ultimately useful for this study to solve the water balance at the catchment scale. This suggests another way of validating MODIS, which is through the resolution of the catchment-scale water balance.

A relevant study of Velpuri and al. (2013) using the simple equation: $P = ET + Q + \Delta S$ to find an evapotranspiration (ET) to be compared with MODIS, is discussed to illustrate this approach, but more importantly to highlight why this can lead to important errors. This very simple equation has the advantage that if the storage change (ΔS) can be neglected, it can be solved easily, if the other terms of precipitation (P) and the river flow (Q), can be measured. This study takes place in the USA and uses hundreds of catchments with areas comprised between 500,000 and 4000 km^2. In the end, the authors report that when the calculated evapotranspiration for these catchments is compared to MODIS, it results in a R^2 of 0.7.

The way Velpuri and al. (2013) solve the water balance for evapotranspiration was done by many others, such as Zhang et al. (2010) or Senay et al. (2013), but their results are not presented here as they use the information from MODIS through a more complicated meteorological modelling which will not be covered here. These authors are assuming that the change in water storage after a

certain time can be neglected. All three studies consider that the hydrological year is sufficient for this. However, the major component of the water balance that is not included in this equation is the axial groundwater flow passing the measuring station, through the riverbed. From a hydrogeological perspective, it does not make much sense not to consider this component as it can be significant Indeed, a wadi perfectly illustrates this phenomenon because there is very little surface water flow during the year and only occasionally after certain extreme storm events there is runoff, so that most of the time the gauging station runs dry although axial groundwater flow still takes place.

The literature review by Velpuri and al. (2013) highlighted five relevant studies on using the water balance to assess MODIS (Anderson et al., 2011; Guerschman et al., 2009; Mu et al., 2011; Senay et al., 2013; Vinukollu et al., 2011b). Although they partly use MODIS information in more complex climatic modelling, they are not going to be discussed. The main objective for this study is to understand whether the raw results such as the one used by Velpuri and al. (2013) mentioned above can be used directly and without complex modelling in order to be useful in a rapid groundwater potential approach in data scares regions.

C.3.2.2. Assessing the validity of MODIS with HGM model

Evapotranspiration data was analysed using MODIS (MOD16A2 Version 6) for the 20 catchments each time for a period of 10 years. This criterion was used to first check if, as mentioned before, in certain years some acquisitions might have been missed due to cloud cover. This was also done to understand the frequency and magnitude and see if they are the same each year. The results for the 20 catchments are presented in Appendix E. For each of them, evapotranspiration and precipitation were plotted. An example is shown in Fig. C.1 for catchment J (1591481) in Fig. 5.1. In this example, it can be noticed that evapotranspiration has a sinusoidal frequency that follows the intensity of precipitation. This nice frequency can be observed at every catchment (Appendix E). In the example bellow (Fig. C.1), evapotranspiration was always captured every 8 days. This is not the case for all catchments. Sometimes a certain image was missing in some years. Thus, these years were simply not considered. However, sometimes for several years, one image was missing, so to have several years in order to obtain a meaningful average, MODIS had to be completed. This is simply done by linear interpolation through the missing days. The positive aspect is that there were never several consecutive missing images, but always one. Thus, the interpolation is not overly extrapolated. Ultimately, even though some images are missing all the catchment present evapotranspiration data that seem appropriate and so are evaluated hereafter.

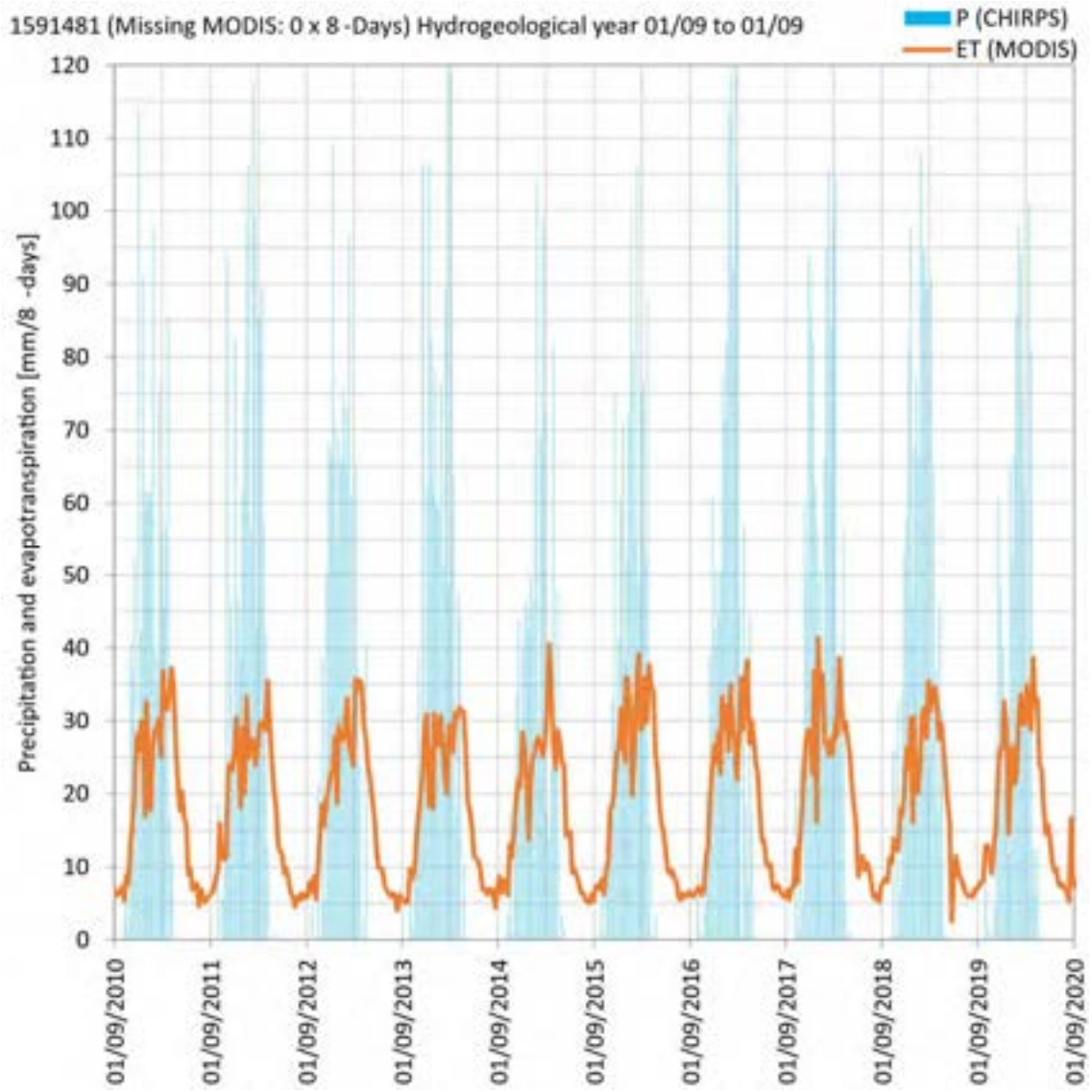

Fig. C.1 *Example illustrating the evapotranspiration and precipitation derived from MODIS and CHIRPS respectively for catchment J (1591481) in Fig. 5.1. The intent is to illustrate the 10-year trend to demonstrate that the frequency and magnitude remains constant from year to year to discuss the data of MODIS. The evapotranspiration and precipitation for the 20 catchments are all illustrated in Appendix E.*

With limited data, the only alternative to assess the validity of MODIS is to use the water balance at the catchment scale i.e. Eq. 5.1 by calculating an evapotranspiration which can then be used for comparison. This is going to be done with the water balance components of the 20 catchments. In addition, some hydrogeomorphological principles and the landscape units mapped for each catchment are also going to be used. The data useful for solving the water balance for evapotranspiration at the catchment scale are precipitation from CHIRPS (Section C.3.1), stream flow described afterwards in Section C.3.4 and groundwater flow. As mentioned above, the latter term is found to be neglected in most studies (e.g. Velpuri and al., 2013), so it is intended to be included

here. To obtain it, the groundwater flow equation, shown below in Eq. C.1 is going to be used and simply solved with the typical hydraulic properties and parameters of the regolithic aquifers.

$$Q_0 = \frac{KeS\Delta H}{L} = \frac{TS\Delta H}{L} \qquad (C.1)$$

where Q_0 is the groundwater flow in [L^3/T], K [L/T] the hydraulic conductivity, e [L] the aquifer thickness, S [L] the cross-section, $\frac{\Delta H}{L}$ the hydraulic gradient and the transmissivity T [L^2/T] which is equal to K times e.

Fortunately, the regolithic environments present similar hydrogeological characteristics. In fact, it is discussed in Section C.2.2 that the main aquifer transmitting most of the groundwater is contained in the regolith, which is a uniform layer covering more or less fractured bedrock. On a regional scale, the fractured bedrock does not transmit much water because it is compartmented so that if one is interested at the groundwater flow it can be neglected (e.g. Lachassagne et al., 2021).

The first parameters of equation Eq. C.1, i.e. K, e and T were given in Table C.1 and C.2. However, the hydraulic gradient, $\frac{\Delta H}{L}$ and the cross-section S have to be estimated. The hydraulic gradient has been documented by a number of authors and was summarized by Lachassagne et al. (2021), but it is possible to measure it easily. Indeed, regolithic aquifers are topographically controlled, this means that where the hydraulic head intercepts the topography, there is exfiltration. This occurs where the drainage has incised the landscape. This means that the drainage system essentially represents the top of the water table and so represents the average hydraulic gradient as discussed in Section 5.5. The average slope of the drainage system is derived from the digital elevation model (DEM). This gradient is denominated hereafter as m.

The last term to deduce for solving Eq. C.1 is the cross-section S. As the aquifers are topographically controlled, the flow lines converge towards the drainage system before being concentrated along it (e.g. Dunne, 1969; Dunne and al., 1975 and Dunne, 1980). This means that all the water that infiltrated, whether it has drained, i.e. the base flow or not in the drainage system, must have entered it at some point. The part of the infiltration that does not drain into the drainage system flows through it and therefore represents the part that escapes at the gauging station (Section 5.5). Infiltration can be neglected in the drainage system as it is largely saturated and therefore only considered in the upland and slope (Section 5.5). In section C.2.3 it is discussed that in regolithic environments the drainage system has a certain lateral extension, making it an area. Therefore the perimeter of the drainage system represents the cross-section S in Eq. C.1. This term is abbreviated to c.

The aforementioned is illustrated in Fig. C.2 with a conceptual catchment model already shown in Fig. 5.6 that merges the hydrogeomorphological landscape unit concept (Winter, 2001) with the topographically controlled regolithic aquifer system. While the effective precipitation P_{eff} (i.e. evapotranspiration ET minus precipitation P) falls on the upland or slope, it is transformed exclusively into groundwater recharge Q_i on the upland and partially into Q_i and runoff R on the slope. The fraction that has infiltrated flows towards the drainage system unit and, after crossing its perimeter c, either becomes base flow Q_b by seeping into the drainage network (blue line) or axial groundwater flow Q_0 that is channelled underneath the drainage system, which is the fraction that is calculated in the subsequent analysis. Runoff from the slope and effective precipitation falling on the drainage system unit is added to the base flow and captured at the gauging station as total discharge Q. In Fig. C.2, K represent typical hydraulic conductivity for the regolithic aquifers while e represents the thickness of the weathered layer.

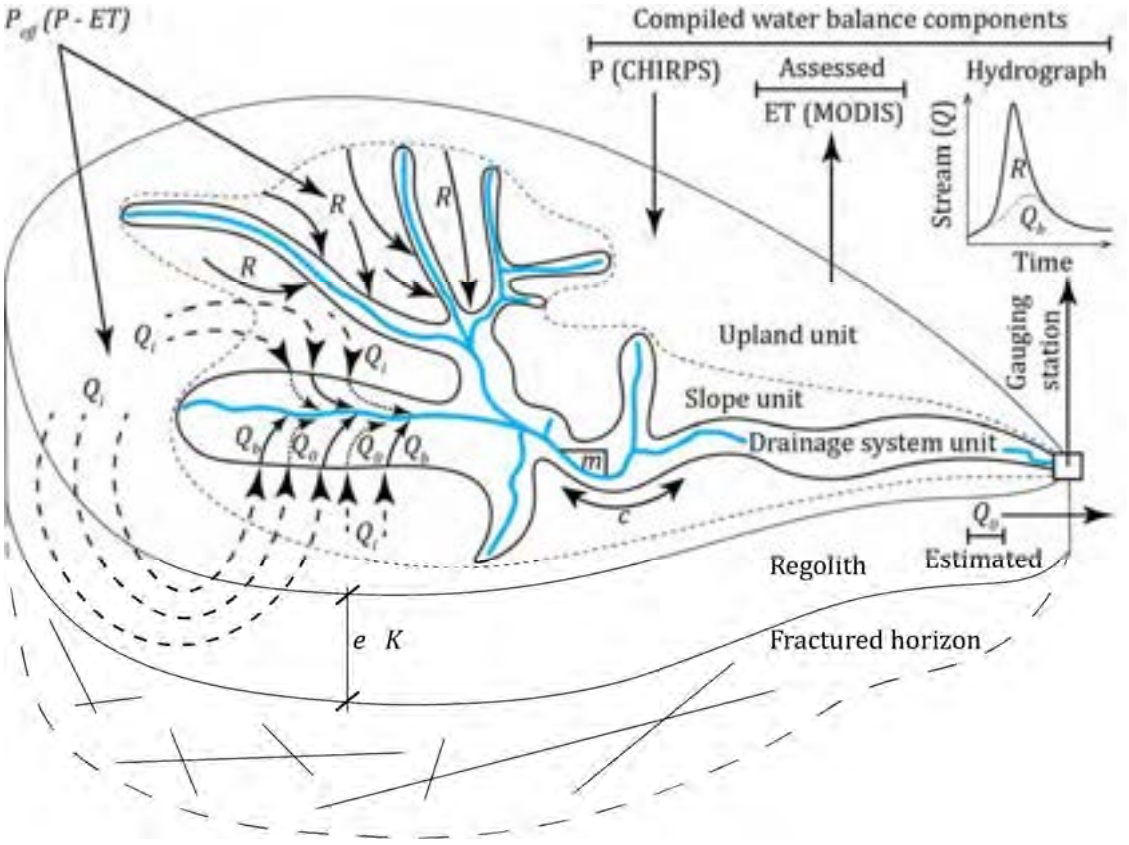

Fig. C.2 *Conceptual catchment model merging the hydrogeomorphological landscape unit concept (Winter, 2001) and the topographically controlled aquifer system of regolithic environments. This model is used to estimate the groundwater component Q_0 with the groundwater flow equation (Eq. C.1) which is then used in the water balance (Eq. 5.1) with the other components (P and Q) to get the evapotranspiration ET. This ET is finally compared to that of MODIS for evaluation. The technicities of this model are already extensively described in Section 5.5.*

In Eq. C.1 if one sets the typical hydraulic conductivity K, the transmissivity T from Table C.1 and C.2, the regolith thickness e of 30 m (Section C.2.2), the measured perimeter of the drainage system c used as the cross-section S and the slope m of the drainage as the hydraulic gradient $\frac{\Delta H}{L}$ it becomes:

$$Q_0 \left[\frac{\mathrm{m}^3}{\mathrm{y}}\right] = (2.69\mathrm{E}-06 \left[\frac{\mathrm{m}}{\mathrm{s}}\right] * 60 * 60 * 24 * 365) * 30\ [\mathrm{m}] * c\ [\mathrm{m}] * m\ [-] \qquad (C.2)$$

and for the transmissivity:

$$Q_0 \left[\frac{\mathrm{m}^3}{\mathrm{y}}\right] = (5.03\mathrm{E}-05 \left[\frac{\mathrm{m}^2}{\mathrm{s}}\right] * 60 * 60 * 24 * 365) * c\ [\mathrm{m}] * m\ [-] \qquad (C.3)$$

After estimating with Eq. C.2 and C.3 the groundwater Q_0 for the 20 catchments it is then used in the water balance (Eq. 5.1) to obtain ET with P and Q. This ET can then be compared to that obtained with MODIS. This is presented in the following two figures (Fig. C.3 and C.4) where the first shows the evapotranspiration (method 1) obtained from Q_0 calculated with a hydraulic conductivity (Eq. C.2) and the second (method 2) from Q_0 calculated with a transmissivity (Eq. C.3). For both figures (Figs. C.3 and C.4), the main graph shows the calculated evapotranspiration on the y-axis against the MODIS values on the x-axis by means of the black dots. The dotted black line is the trend line, and the red line is a 1:1 line. The small graph labelled MODIS/calc. shows a histogram with a bin size of 0.1 representing the ratios of MODIS to calculated evapotranspiration.

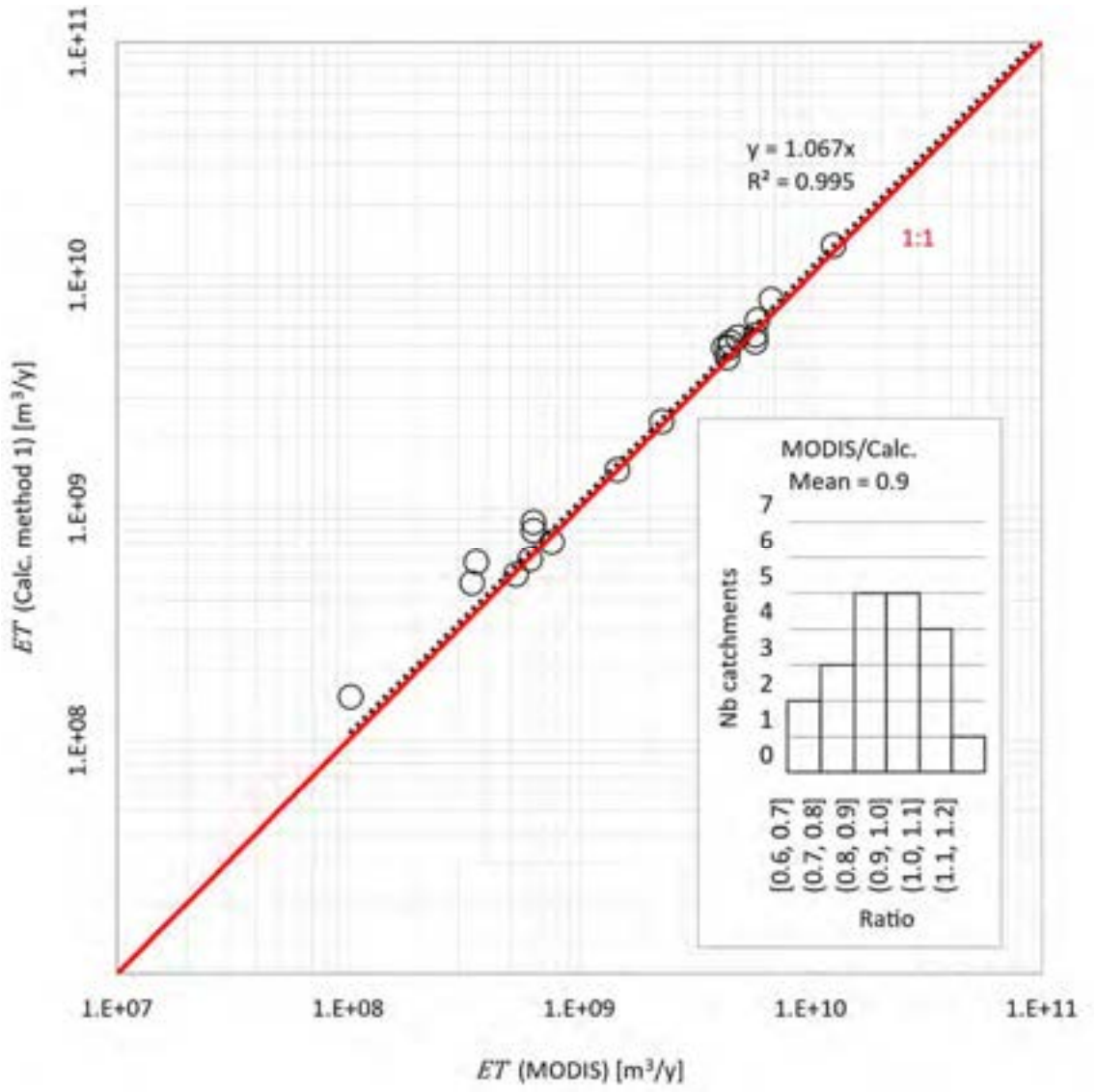

Fig. C.3 *Comparison of MODIS and calculated evapotranspiration for the 20 catchments (black circles). The calculated evapotranspiration (Calc. method 1) is obtained from the water balance of Eq. 5.1 with CHIPRS data for precipitation (Section C.3.2.1), stream flow measurements recorded at the gauging station (Section C.3.4) and groundwater derived from Eq. C.1. The black dashed line is the trend line through the evapotranspiration data and the red one is a 1:1 line. The small graph labelled MODIS/Calc. shows a histogram with a bin size of 0.1 representing the ratios between MODIS and calculated evapotranspiration.*

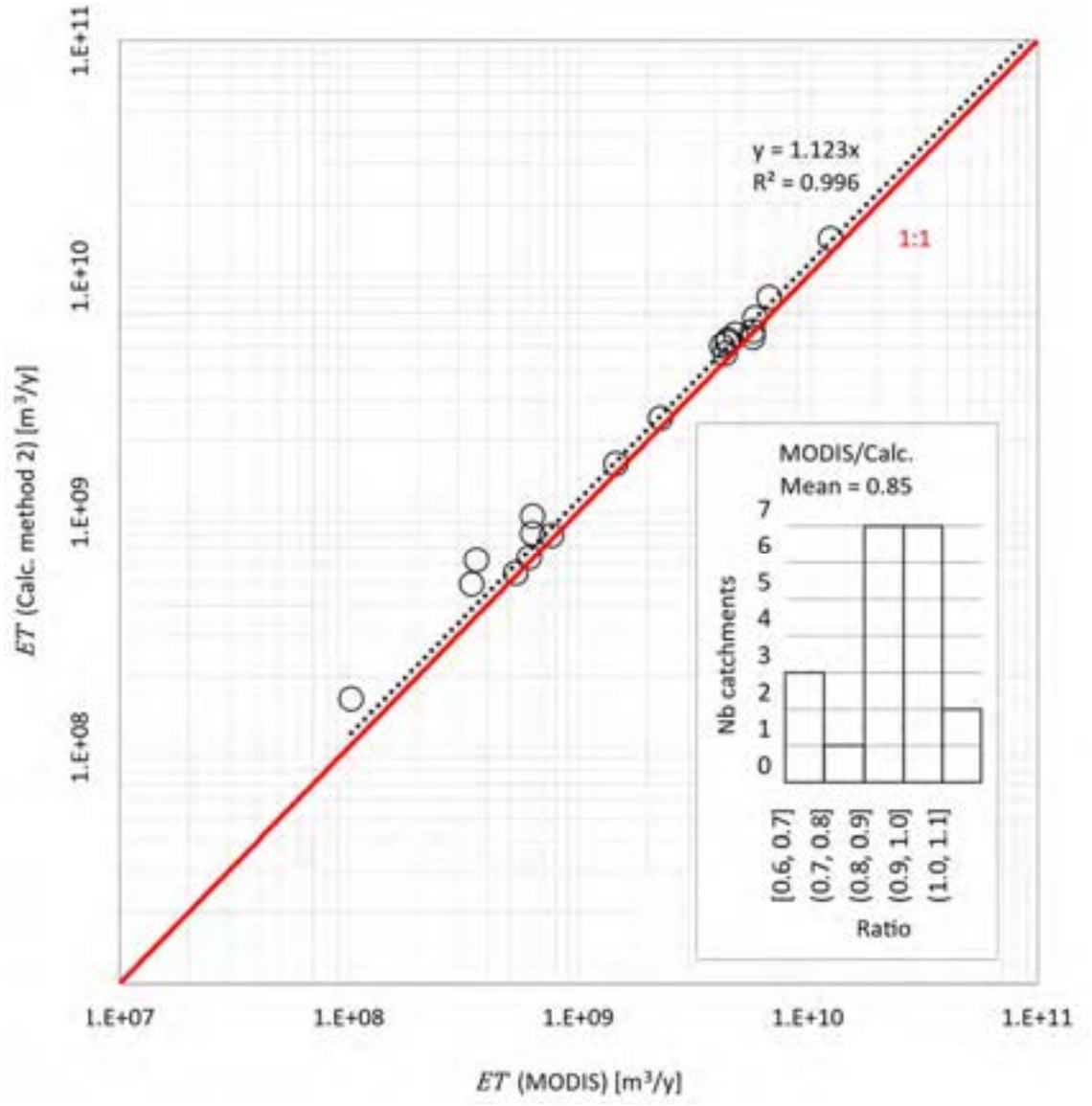

Fig. C.4 *Comparison of MODIS and calculated evapotranspiration for the 20 catchments (black circles). The calculated evapotranspiration (Calc. method 2) is obtained from the water balance of Eq. 5.1 with CHIPRS data for precipitation (Section C.3.1), stream flow measurements recorded at the gauging station (Section C.3.4) and groundwater derived from Eq. C.3. The black dashed line is the trend line through the evapotranspiration data and the red one is a 1:1 line. The small graph labelled MODIS/Calc. shows a histogram with a bin size of 0.1 representing the ratios between MODIS and calculated evapotranspiration.*

In both Figs. C.3 and C.4, the trend line (black dotted line) is fixed to intercept the origin. The rationale for this choice is that evapotranspiration is the sum of plant transpiration, saturated zone evaporation and evaporation from open water bodies (e.g. Scanlon et al., 2006). Since only catchments where there is no visible indication of surface water are considered (Section 5.2), the only way to evapotranspire water is through plants and the saturated zone. For a plant to transpire water, it must first percolate through the soil to be absorbed by the roots before being sent to the

leaves. The same applies to evaporation of water from the saturated zone, provided there is soil. In other words, without soil, there is no evapotranspiration. Over outcropping bedrock and cities, MODIS indeed returns a zero value. Furthermore for regolithic enviroments in term of water balance, if there is no soil, this necessarily means that there is no infiltration, hence no groundwater term, which means that evapotranspiration is also equal to 0 since runoff will simply be equal to precipitation.

The relationship between MODIS and calculated evapotranspiration data is reasonably good in both cases (Figs. C.3 and C.4). This is best illustrated by the slope of the trend line first for Fig. C.3 where it is 1.067 and Fig. C.4 where it is 1.123. In addition, the coefficient of determination (R^2) is for both cases almost 1, indicating a perfect relationship. The small histogram in the lower corners, show that the ratio between MODIS and calculated is for the first method better cantered arround 1 while it is more shifted to the left for the second method. This means the second method tends to generally slightly overestimate evapotranspiration. However, for both the average ratios are very good being 0.90 and 0.85. It is possible to go further by using the guidelines for assessing the accuracy of catchment modelling of Moriasi et al. (2007), considered as a reference in this subject. Two famous evaluation methods, namely Nash-Sutcliffe efficiency (NSE) and percentage bias (PBIAS), are among others recommended statistical indicators, but ones that, according to a literature review by Moriasi et al. (2007) the most relevant. In brief, the NSE shows how observation versus simulations is aligned on 1:1 where the highest possible score is 1 (Nash and Sutcliffe, 1970). The PBIAS, is an indicator of the simulation to be larger or smaller than the observation where the best score is 0 but if it is positive or negative, simulation is, respectively, underestimated or overestimated (Gupta et al., 1999). Both indicators are used for evaluating plots. As for the ratio mentioned in the beginning, the observation is attributed to the evapotranspiration of MODIS and the simulation to the calculated one. For the first graph, one obtains a NSE of 0.99 and for the second 0.98. According to Gupta et al. (1999) if it is higher than 0.8 it means that the model is efficient and according to Motovilov et al. (1999) one of 0.75 means it is good. For the PBIAS, in the first case a value of –7.32% is found and for the second a value -12.62%. According to Van Liew et al. (2007) a PBIAS between ±10 and 15% means that the model is good. All these values are summarized in Table C.3.

Table C.3 *Summary of the two methods for calculating evapotranspiration that is compared to the one measured by MODIS. The methods are based on the water balance of Eq. 5.1 including the groundwater component calculated with Eq. C.2 and C.3.* ET, P, Q *are evapotranspiration, precipitation, and discharge respectively,* K *(Table C.1) the hydraulic conductivity,* e *the thickness of the regolith,* c *the perimeter of the drainage system,* m *the slope of the drainage system considered as the hydraulic gradient,* T *the transmissivity (Table C.2). The other columns present the statistical values obtained from the comparison, i.e. the slope of the trend line through the data, the correlation coefficient* R^2*, the ratio, the Nash-Sutcliffe efficiency (NSE) and the percentage bias (PBIAS).*

Method	Equation of water balance	Slope	R^2	Ratio	NSE	PBIAS (%)
1	$ET = P - Q - K * e * c * m$	1.067	0.995	0.90	0.99	-7.32
2	$ET = P - Q - T * c * m$	1.123	0.996	0.85	0.98	-12.62

The objective of this section was to assess the validity of the evapotranspiration data predicted by MODIS with the goal of determining whether it can be used as it is. The literature review found that the accuracy of MODIS is questionable, but also that little research has evaluated it properly. It was concluded, in general, that the assessment methods are questionable. Indeed, MODIS evapotranspiration averaged over a large pixel is usually compared to measurements taken at a meteorological station. This approach is by definition inconsistent since the two evapotranspiration are derived from different dimensions, namely a point and an area. The other widely used approach is to solve the water balance for evapotranspiration with precipitation and discharge measurements. Authors (e.g. Velpuri and al., 2013) doing this do not include or neglect the axial groundwater flow component. It is believed that not considering this component returns overestimated evapotranspiration values compared to MODIS measurements. Therefore, this section was devoted to studying the accuracy of MODIS differently yet based on the water balance approach since one is working here with catchment data. Two methods based on the water balance (Eq. 5.1) that is solved for evapotranspiration are used here with data from the 20 catchments. These data are precipitation, discharge, and the calculated axial groundwater flow. The latter component was calculated using the groundwater flow equation adapted to the hydrogeomorphological model described in Section 5.5 and either solved with the hydraulic conductivity or the transmissivity i.e. Eq. C.2 and C.3 respectively. In the end, both models perform astonishingly well with the one based on the hydraulic conductivity slightly better, meaning that not only does MODIS correctly estimate evapotranspiration at the catchment scale, but the groundwater flow equation adapted to the hydrogeomorphological model indeed properly simulates the groundwater component for the 20 catchments.

C.3.3. Stream discharge records and hydrological year

Discharge data for the 20 catchments are obtained from gauging stations. These stations are provided by the Global Runoff Data Centre (GRDC). The gauging stations are selected on the basis of the previously defined catchment criteria (Section 5.2). In addition, they are also selected on the condition that they present concise data over a certain number of years. A minimum was defined for this study as 5 years of consecutive data. In order to assess the water balance of each catchment, each term is derived from an average of the annual means. This has the advantage of avoiding storage effects. To obtain annual means, the hydrological year had to be defined with regards to the beginning and end of the rainy season.

The hydrologic event is reflected in the river by a bell-shaped curve in the water level. An event may not last more than a year, but its start and end depend on location. The 20 catchments across Africa are all located in similar climates but scattered in the northern and southern hemispheres. While in the north the rainy season runs from January to June, in the southern hemisphere it is the dry season. From October to March, the tropical rain belt is located in the southern hemisphere and thus there is a dry season in the northern hemisphere. From April to September, the rain belt moves northwards, and the south therefore experiences a dry season (e.g. Farquharson and Bullock, 1992). The start of the event in both hemispheres must therefore be set in these two dry periods. When working with river data, it often happens that the water continues to flow even during the dry season. The base flow is eventually delayed in relation to the runoff. To be consistent with rainfall, it is suggested to start the hydrological year at the end of the dry seasons. This allows time for the river to dry out completely and not to let the remaining base flow from the previous event interfere with the new event. For the northern hemisphere, events are defined to occur from March to March and for the southern hemisphere from September to September.

C.3.4. Hydrograph separation methods for runoff and base flow evaluation

The flow of a river can be divided into two terms (Eq. 5.2). The fraction of water that immediately reaches the river after a rainfall, i.e. runoff, and the delayed part of the rainfall that infiltrated known as base flow. In fact, a fraction of the discharge comes from the aquifer through which the river makes its way. It is by exfiltration from the aquifer through the banks and bed of the stream that groundwater is discharged. This is particularly visible during extended periods of droughts when the rivers are still flowing. However, during rainy periods, when the stream swells to its maximum, it is also apparent that the total flow cannot be explained by rainfall alone and that another source must contribute. In many cases, it can be observed that very soon after even a small rainfall event, the flow increases considerably. This is the results of an increase in infiltration, which leads to a rise

in the hydraulic head in the aquifer. This surge in pressure will push the existing water in the system towards the stream (e.g. Chapman and Maxwell, 1996).

Base flow and runoff can be assessed by using river flow, derived by the so-called hydrograph separation techniques. There are numerous of these technics, and it is a vast field of research. Here, only the two most common are discussed. From a mathematical point of view, they are justifiable because they are based on physical observation of aquifer dynamics and have been widely studied and compared in recent years. These techniques consider that the aquifer acts as a linear or non-linear reservoir that drains into the river. Only the latter technique is used in this work, the other is presented because it is necessary to justify this choice. A good way to do this is to develop both mathematically to discuss the effectiveness of each because ultimately there is no other way of knowing whether the simulated base flow or runoff are correct as they cannot actually be measured in a river.

C.3.4.1. Linear hydrograph separation with recursive filters

A widely used technic nowadays is to use recursive filters for separating the base flow from the total flow. This technique compared to the ones used later, has the great advantage to be easily implemented in a spread sheet because it does not require complex algorithm. This methodology is based on the idea that the hydrograph can be considered as a frequency spectrum. The base flow compared to the runoff is delayed and discharged smoothly due to the storage processes occurring in the aquifer. Considering this, the spectrum of the hygrograph can be separated in order to obtain two different frequencies. The low frequencies will be associated to the base flow and the highs, or the nervous part of the hygrograph corresponds to the runoff.

Since the base flow is associated to the low frequencies of the hygrograph it can be extracted applying a low-pass filter. A low-pass filter is a filter that only keeps frequencies lower than a selected threshold, this threshold is known as the cut-off frequency (Lynn and Hollick, 1979). The frequency response depends on the type of filter. Eckhardt (2008) is one of the main authors who discusses the validity and compares the different filtering methods. In the study of Eckhardt (2005), all steps leading to existing filters are summarized and developed. This led Eckhardt (2005) to propose his own solution which is the most used. Therefore, the structure of this section is largely based on the work of Eckhardt (2005 and 2008).

One starts by defining the problem as follow:

$$Q_t = R_t + Q_{bf_t} \tag{C.5}$$

where, Q_t is the total flow, R_t the runoff, Q_{bf_t} the base flow at a given time.

The first type of filter is a one parameter recursive digital filter frequently used in signal processing and permit dividing the total flow of a hydrograph into runoff and base flow (Lynn and Hollick, 1979). This filter is commonly named Lynn – Hollick filter. Equation C.6 presents this filter. This filter is constrained in order that the base flow cannot be superior to the stream flow. Also, it is a forward filter.

$$R_t = aR_{t-1} + \frac{1+a}{2}(Q_t - Q_{t-1}) \tag{C.6}$$

where, a is the filter parameter.

While the Lynn – Hollick filter has been extensively used for instance by Nathan and McMahon (1990), Arnold and Allen (1999) and Arnold et al. (2000) it is criticized by Chapman (1991) who argues that it generates an incorrect streamflow or base flow when the runoff equals to zero. Therefore, Chapman (1991) proposes the following version:

$$Q_{bf_t} = aQ_{bf_{t-1}} + \frac{1-a}{2}(R_t + R_{t-1}) \tag{C.7}$$

Equation C.7 is now valid during dry periods where there is no runoff but where the river is only fed by groundwater. In this case this equation simply becomes:

$$Q_{bf_t} = aQ_{bf_{t-1}} \tag{C.8}$$

At this stage the parameter a has to be determined but there is no information available on base flow at this time, so it is necessary to work with stream flow data. Langbein (1938) proposes that during the recessions where streamflow exclusively consist of base flow that Eq. C.8 is the same as:

$$Q_t = aQ_{t-1} \tag{C.9}$$

If Eq. C.9 has the form of a linear equation, it means that if Q_t and Q_{t-1} are plotted against each other, a can be determined as it represents the slope. This leads to the major assumption of all filter methods, the ones shown further up and the following that will be described. In all solutions it is assumed that the aquifer acts as a linear reservoir. At this stage the streamflow data during a recession corresponding to base flow have not been defined yet. This will be discussed further below

in detail because it represents another significant issue of the methodology. For the moment, the two other types of filters are presented.

According to Chapman and Maxwell (1996) similar results are obtained with the simplification of Eq. C.7 into C.10.

$$Q_{bf_t} = \frac{a}{2-a} Q_{bf_{t-1}} + \frac{1-a}{2-a} Q_t \qquad (C.10)$$

Finally, the last filter presented is the one of Eckhardt (2005). The development of this filter is presented in detail in his article. Eckhardt (2005) bases its solution on Eq. C.10 to come up with the following filter:

$$Q_{bf_t} = \frac{(1-BFI_{max}) - aQ_{bf_{t-1}} + (1-a)BFI_{max}Q_t}{1-aBFI_{max}} \qquad (C.11)$$

where, BFI_{max} stands for the base flow index which is the ration of the long-term base flow over the streamflow.

Equation C.11 is now compared to the other filters a two-parameter filter with the recession constant a and the BFI_{max}. While a can be encountered with the already mentioned recession analysis based on Eq. C.10, the BFI_{max} must be somehow estimated. Eckhardt (2005) suggests three values of BFI_{max} according to the dynamics of the river and the geology.

1. $BFI_{max} = 0.8$ for a perennial stream with a porous aquifer
2. $BFI_{max} = 0.5$ for an ephemeral stream with a porous aquifer
3. $BFI_{max} = 0.25$ for a perennial stream with hard rock aquifer

The solution of Eckhardt compared to the other digital filters, uses another parameter, i.e. BFI_{max} that can be associated to a type of aquifer. This solution must therefore simulate the base flow more realistically than the other filters that do not integrate parameters related to stream nor aquifer types. The three values of BFI_{max} have been identified thanks to several case studies. However, since the base flow cannot be compared to actual data, this parameter is strongly related to expert judgment. In fact, for example, ephemeral streams are considered by Eckhardt (2005) as such if they are dry for at least 10% of the year, which is entirely arbitrary.

The main problem after extracting the base flow is that it is difficult to validate. This means that the solution used must be particularly convincing or that the theoretical mathematical expression of the applied formula integrates observations and/or is based on physical dynamics of the aquifer. In both cases, it appears that digital filters do not meet these conditions. Eckhardt's (2005) solution,

compared to the other ones, aims at integrating parameters whose values can be adapted to the type of system. However, the mathematical expression of a digital filter is not based on the physical processes of the aquifer.

C.3.4.2. Hydrograph separation with non-linear storage/discharge relationship

The second method for separating runoff and base flow from total flow is based on the non-linearity of the storage and infiltration processes. This method, compared to the previous one, has a solid mathematical basis, as presented in this chapter, and is therefore preferred for this study. The literature reveals that four authors have made significant contributions to this technique, namely Maillet, Boussinesq, Coutagne and Wittenberg which are referenced bellow. Among those, the latest devoted most of his work to this subject. In addition, Wittenberg (1999) presents an extremely well-structured description of the previous authors' solution that led to the most widely used method. The reader is therefore forewarned that this chapter has a similar structure and that the following equations also take the same form as those proposed by Wittenberg (1999).

At the end of a rainfall event, it takes some time for all the surface water to reach the river. This can be seen in the hydrograph before the river reaches its local maximum, after which the flow decreases until it converges to a base level. This decay is commonly referred to as the recession curve. If no more surface water flows into the river, it means that the river is only fed by the aquifer. Therefore, this base level is exclusively composed of groundwater. A closer look at these recessions gives an idea of the dynamics of the aquifer.

The behaviour of the recession curve reflects the storage and recharge/discharge characteristics of the aquifer. In fact, there is an infinite range of possible interpretations, but perhaps the most obvious one to illustrate this is that a very rapid recession compared to a recession that extends over a long period of time would indicate an aquifer with lower storage or lower permeability. If this is translated into discharge/infiltration implications, it means that a rapid decay of the recession could indicate that the aquifer is more prone to surface runoff where all the water after a rainfall event is quickly delivered to the stream. On the contrary, a slow decrease in recession could indicate that infiltration is high, explaining the longer delay as the water, before being released into the river, has to work its way through the pores and fractures of the aquifer.

The method presented hereafter needs two initial inputs before one can proceed with the hydrograph separation. One has to know the beginning and the minimal length of the recession. Almost every author agrees that several days of stream flow data have to be removed after a peak in the hydrograph in order to define the beginning of the recession. The underlying reason according to

Brutsaert and Nieber (1977) based on the work of Linsley et al. (1982) and Walton and Schicht (1961) is to minimize the effect of isolated showers that could occur in specific places of the catchment. This has to be understood that not the entire catchment has been uniformly wetted during a rainfall event and that the fraction of precipitation that ended in the river does not properly represent the entire mechanism of the catchment transforming the fraction of precipitation into runoff and base flow. In fact, Arciniega-Esparza (2017) nicely state that this time after the storm event has to be considered in order to exclude the storm-runoff effect in the storage-discharge relationship. The major contributors to base flow separation suggest the following: Vogel and Kroll (1992) remove the first 30% of days after a storm event. Brutsaert and Nieber (1977) remove the first 3-4 days and the last 2 days of the recession. Kirchner (2009) on his side is the only one that does not remove any day after a storm event. Aksoy and Wittenberg (2011) remove the first 2 days. In more recent works, Karlsen et al. (2019) also remove the first two days of the recession. In this study, 1 day of streamflow data are removed after a peak in the hygrograph. This choice is based on the fact that it is consistent with the recession model used here and with the last three authors (Kirchner, 2009; Aksoy and Wittenberg, 2011; Karlsen et al., 2019) who remove 0 and 2 days respectively.

The three main reasons for setting a minimum length of recession duration are summarised in Dralle et. al (2017). The first and probably most widely accepted is that it suppresses noise from short events (Ye et al., 2014). However, Chen and Krajewski (2015) discuss that the minimum duration should also not be set too long in order to capture the full range of low-flow processes. Finally, Shaw (2016) refers to data quality issues related to sample size. With regard to a specific duration, the solution of the main contributors to the hygrograph separation is again presented. Vogel and Kroll (1992) suggest that the minimum duration of the recession should be 10 days. Brutsaert and Nieber (1977) suggest removing 6-7 days. While Kirchner (2009) states that only one day should be removed. Finally, Aksoy and Wittenberg (2011) argue that 5 days should be the minimum duration. In order to be consistent with the author's solution used here (Wittenberg, 2011), a minimum duration of 5 days is chosen. This is also in line with more recent work such as Shaw and Riha, (2012) Biswal and Marani (2010) who have generally chosen a minimum of 4-5 days of recession. More recently, Dralle et al (2017) set a minimum of 4 days. Therefore, 5 days is a good consensus because it is between the basic work such as Brutsaert and Nieber (1977) and with the most recent work and finally the same as for Aksoy and Wittenberg (2011) whose model is used in this study.

The widely accepted conceptual model of groundwater flow in a river is based on Dupuit-Boussinesq solution. The model takes the form of a rectangle describing a perfectly horizontal unconfined aquifer. This aquifer rests on a continuous impermeable layer. The aquifer is delimited on one side

by an impermeable boundary and on the other side by a stream. Initially, it is assumed that the aquifer is fully saturated and that the water table is curvilinear between the impermeable boundary and the stream. The non-linear Boussinesq differential equation for aquifers has been extensively used since Maillet (1905) to describe recession curves by the form of:

$$Q_t = Q_0 \cdot \exp(-t/k) \qquad (C.12)$$

where, Q_t in [L/T] or [V/T] is the discharge in the stream at a given time, Q_0 the initial discharge and k [-] the retention constant. The retention constant k can be understood as a sort of reservoir constant that dictates the rate at which the aquifer discharges.

In the sub-mentioned solution, if a lumped analysis is carried out over the entire data set, the relationship between the storage and discharge is proportional. The storage is linearly proportional to the discharge because the aquifer acts as a linear reservoir due to the exponential function. Thus, Eq. C.12 can be translated into:

$$S = kQ \qquad (C.13)$$

where, S is the storage is in [V].

This implies that if $logQ_t$ is plotted against t a straight line can be drawn (e.g. Barnes, 1939). The value of k can be encountered while using the slope of the function obtained thanks this line. However, very often, the logarithmic plot of the recession curves is concave. This means that the relationship between the storage and the discharge is non-linear. This observation has indeed been widely recognized by numerous hydrologists and especially the ones working with recession curves for describing the dynamics of streams during rainless periods where a cursory literature review revealed e.g. Brutsaert (2005), Linsley et al. (1982), Tallaksen (1995) and Wittenberg, (1999). The latter, in order to cope with this non-linearity proposed a new solution. It is the one used in this work and is detailed hereafter. Wittenberg (1994) and Moore (1997) pointed out that the parameter k does not remain constant when considering different ranges of recession curves. In fact, k rather increases if one analyses longer periods of recession curves. This is due to the fact that this decline tends to be stretched over a longer period before converging to a minimum.

In order to cope for non-linearity, Wittenberg (1999) generalizes the linear storage-discharge relation by adding an exponent b to the discharge Q so that Eq. C.13 becomes:

$$S = aQ^b \qquad (C.14)$$

where Q is in m^3/s, a has the special dimension of $m^{3-3b}s^b$. But if Q is expressed as a height over a length with a unit time step of one day such as mm/d, then S is in mm and a in $mm^{1-b}d^b$.

In the following section the derivation of the recession equation of the nonlinear reservoir is presented. This derivation is found in Wittenberg (1999) but has been found practical to present here because it allows to properly understand the underlying physic of this technique. Equation C.13 is combined with the equation of continuity of a reservoir whereas inflow is neglected and only discharging:

$$\frac{dS}{dt} = -Q \qquad (C.15)$$

The combination of Eq. C.14 and C.15 leads to:

$$abQ^{(b-1)}\frac{dQ}{dt} = -Q \qquad (C.16)$$

Integrating Eq. C.16 between t_0 to t and Q_0 to Q_t takes the form of:

$$\int_0^t -dt = \int_{Q_0}^{Q_t} ab\, Q^{b-2} dQ \qquad (C.17)$$

With $b \neq 1$ otherwise it would take the form of the linear reservoir mentioned above:

$$\frac{b-1}{ab}|-t|_0^t = \left|Q^{b-1}\right|_{Q0}^{Qt} \qquad (C.18)$$

This finally becomes:

$$\left(\frac{Q_0}{Q_t}\right)^{1-b} = 1 + \frac{1-b}{ab} Q_0^{1-b} t \qquad (C.19)$$

Or:

$$Q_t = Q_0 \left[1 + \frac{(1-b)Q_0^{1-b}}{ab} t\right]^{1/(b-1)} \qquad (C.20)$$

The parameter a and b can now be calibrated in order that equation (C.20) returns the actual recession flow. Wittenberg (1994) suggest using an iterative least-square method according to Chen (2015) that tested three different of those methods, the following one performs the best.

$$a = \frac{\sum(Q_{i-1} + Q_i)\Delta t}{2\sum(Q_{i-1}^b - Q_i^b)} \qquad (C.21)$$

where Q_i is the discharge at a time i of an actual flow recession.

In Eq. C.21, parameter a is simply solved by systematically varying parameter b at each iteration step in order that the calculated outflow equals to the value the recession at this step. Ultimately the values of a and b giving the minimal sum of square deviation over the entire data set are kept.

The following figure (Fig. C.6) shows an example of the results of the above-mentioned fitting techniques for gauging station no. 1591481. (All recession curves obtained for each gauging station are provided in digital format in Appendix F). It will appear to the reader that by examining the entire set of recessions, that all are subject to non-linearity and so that the model used here is adequate. Furthermore, it will also be apparent that the R^2, Wi and NS correlations are always very high. In fact, special care has been taken to select only those gauging stations whose recessions can be correctly simulated. Otherwise, the whole procedure would not be valid because if the parameter a and b do not allow proper simulation of recession, the later described base flow separation is not correct.

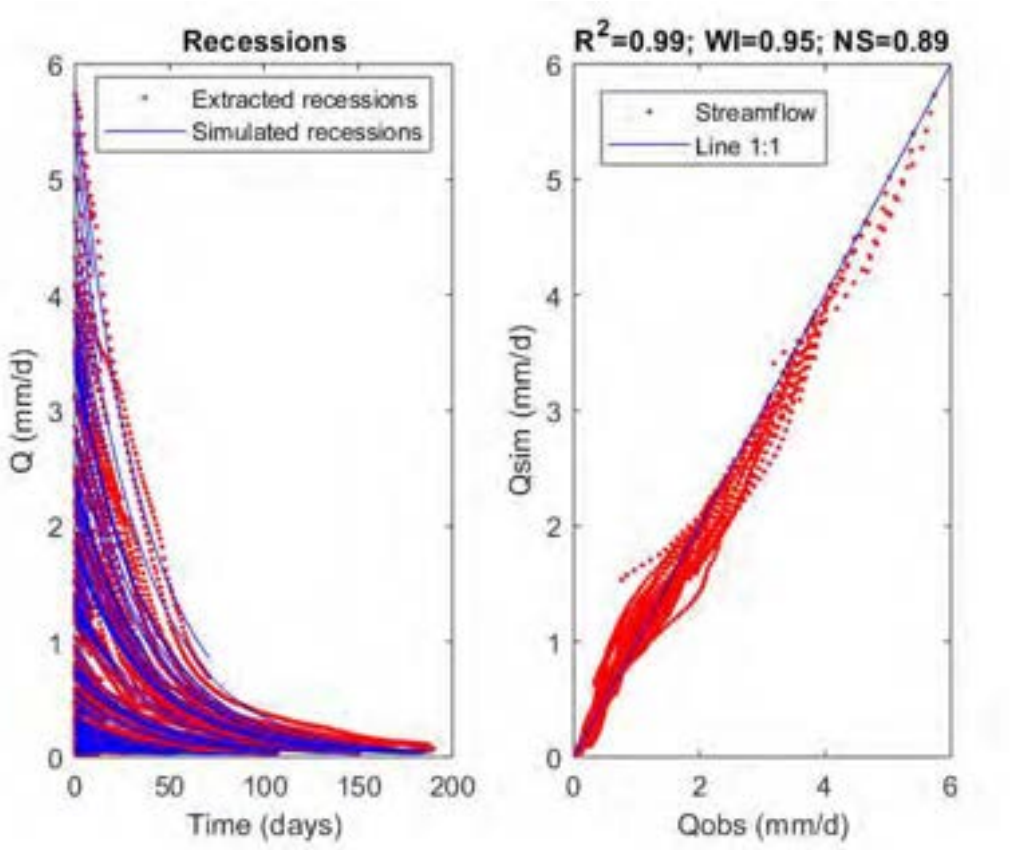

Fig. C.6 *Example of simulated recessions versus actual hydrograph data and correlation coefficient between observed and simulated hydrograph points both obtained from the fitting techniques based on Eq. C.21. This example comes from gauging station no. 1591481 and all other recession are given digital in Appendix F.*

In many studies, a and b are termed recession parameters and are considered as a subrogation of the aquifer properties (e.g. Roques et al., 2022). Here a and b are only used to solve the separation of base flow from total flow as described above. Once the value of a and b presenting the best fit are encountered, they are used for the base flow separation. The same method than the one used by Fröhlich and al. (1994) for a linear reservoir is applied. The separation begins at the last value of

the recession and propagates towards the beginning of the hydrograph. In other words, the calculation is done by going back in time. This is achieved by simply inverting equation Eq. C.20 to obtain $Q - \Delta t$ where Δt is in days as it is usually the case while working with hydrograph data and all our gauging station measure the total flow in days so that Eq. C.16 becomes:

$$Q_{t-\Delta t} = \left[Q_t^{b-1} + \frac{\Delta t(b-1)}{ab} \right]^{1/(b-1)} \qquad (C.22)$$

Now the problem of the base flow intersecting the total flow has yet to be solved. For this purpose, when the reversed calculated base flow intersects the total flow, the previous value of base flow is retained as a maximum. The values of the rising base flow between the next recession (backwards) and the mentioned maximum are calculated thanks the previous recession for one time step forward (Wittenberg, 1999).

All the hydrograph separations of the 20 catchments are given in Appendix F. To conclude this section, an example of base flow separation is presented in Fig. C.7. The lower part of the graph shows the stream flow and the base flow. The daily precipitation obtained with CHIRPS is also shown in the upper part of the graph. Here one can see that during the dry season the flow decreases and at a certain point it is equal to the base flow. This is the time of year when the river is exclusively fed by the aquifer. During the rainy season, there is a clear difference between the base flow and the river discharge. The difference between the two represents runoff.

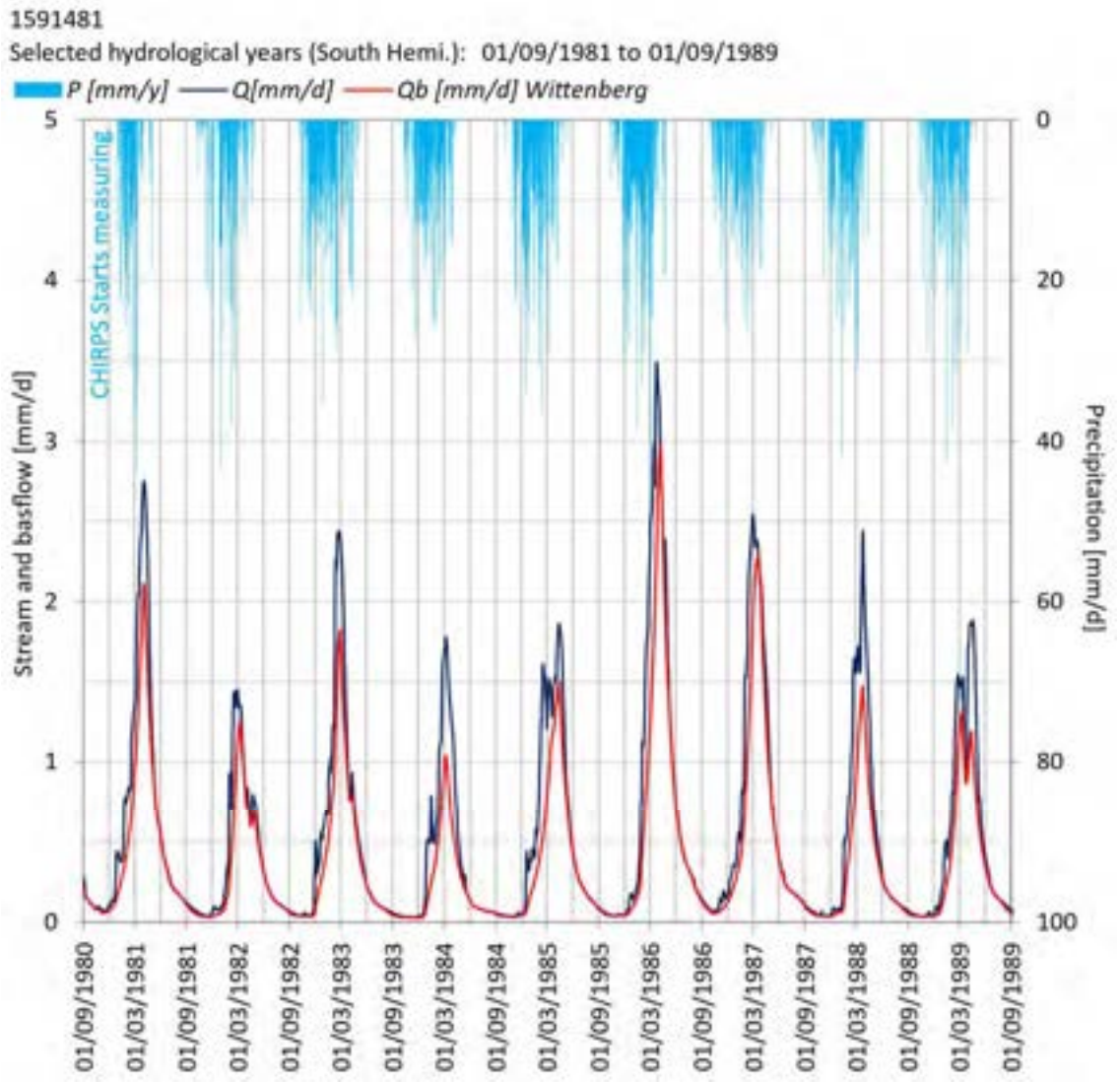

Fig. C.7 *Example of a hydrograph separation obtained with the method of Wittenberg (1999). The lower curve shows the river level and base flow (left y-axis) while the upper bars show the precipitation (right y-axis) derived from CHIRPS. This example comes from gauging station no. 1591481 and all other hydrograph separations are given in Appendix F.*

Appendix D: HGM maps and geological settings of the reference catchments

1. The individual GIS projects of the 20 reference catchments are given in digital format.
2. The Geological maps and settings of the 20 reference catchments referred in the HGM maps are first presented.
3. The HGM maps of the 20 reference catchments are presented after the geological maps and settings. In each map, the three mapped HGM units, the geology and a satellite image with the drainage network are presented. The catchments are labelled according to the GRDC id and referenced as capital letters in Table 5.1.

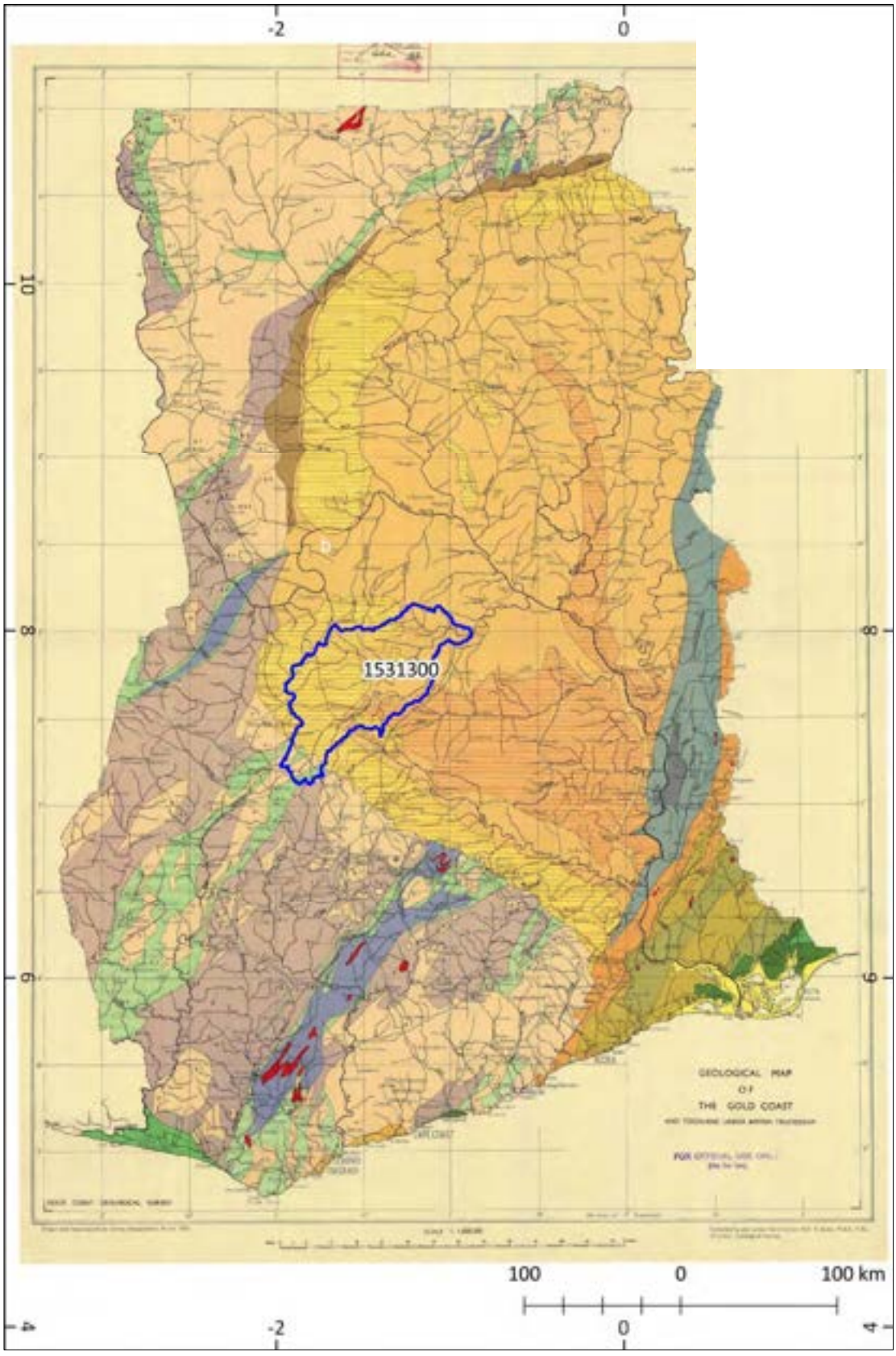

Geological map of Ghana (Bates, 1955) with catchment 1531300-A.

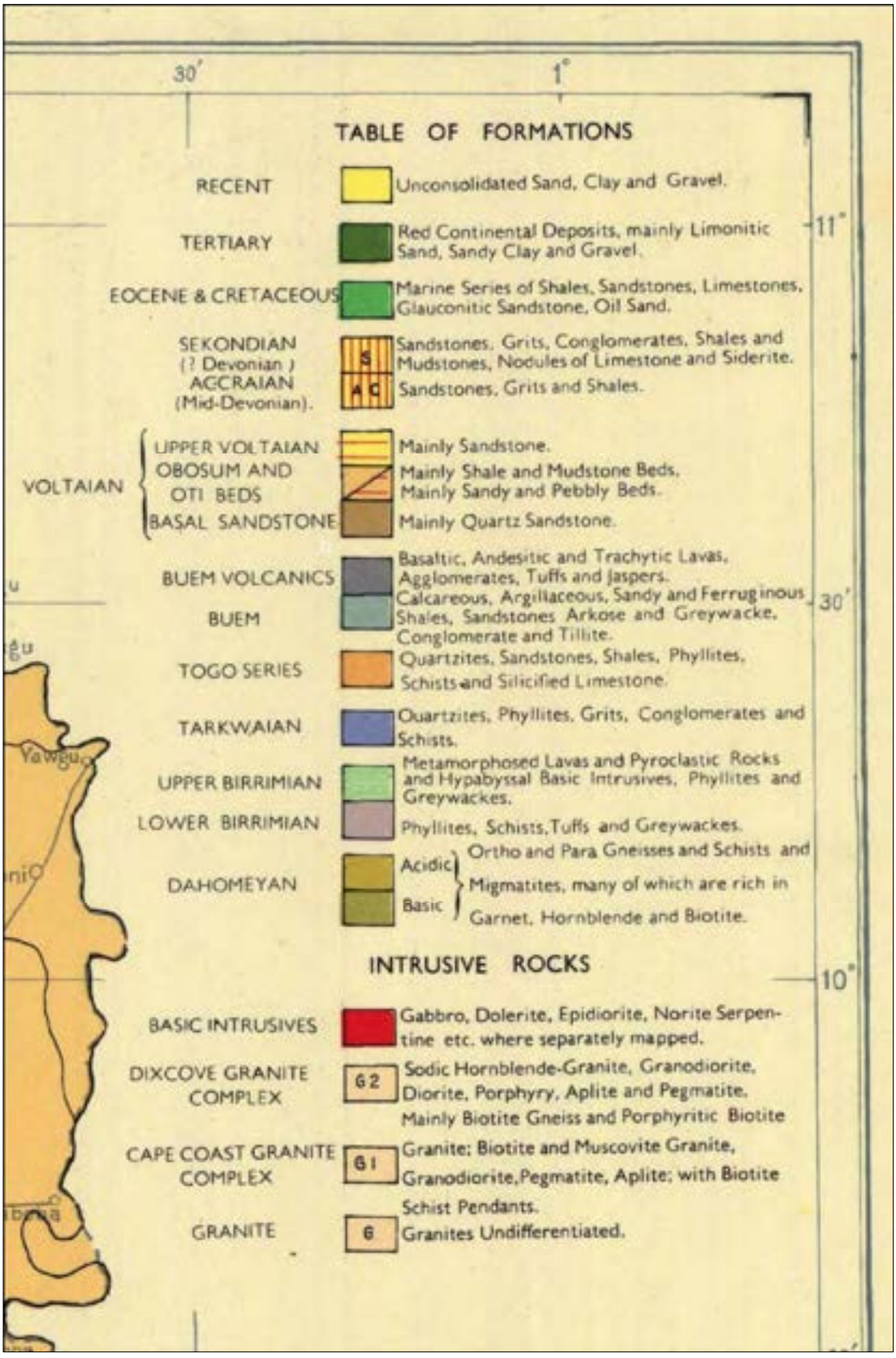

Legend to geological map of Ghana (Bates, 1955).

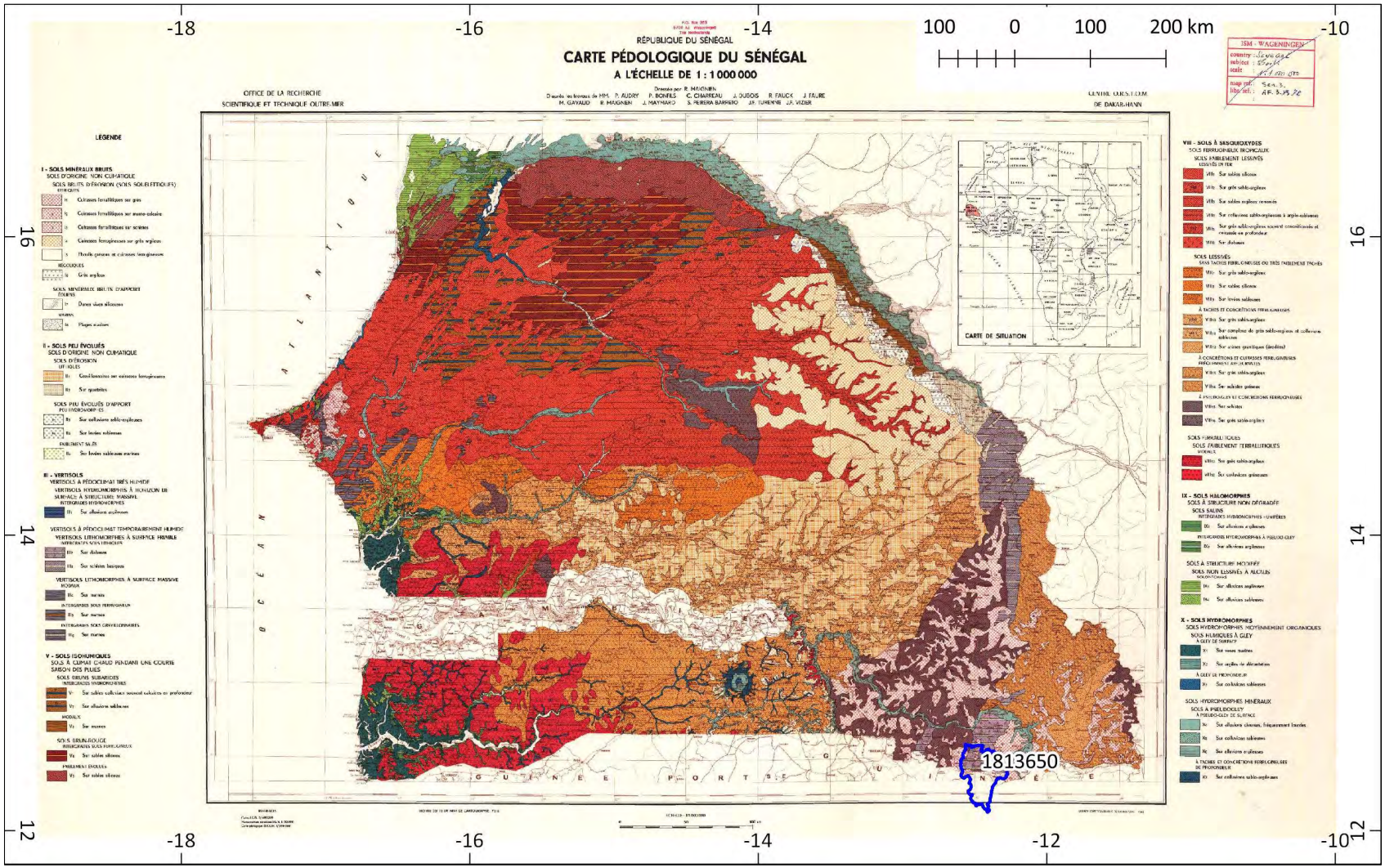

Geological map of Senegal (Maignien et al., 1965) with catchment 1813650-P.

Legend to geological map of of Senegal (Maignien et al., 1965).

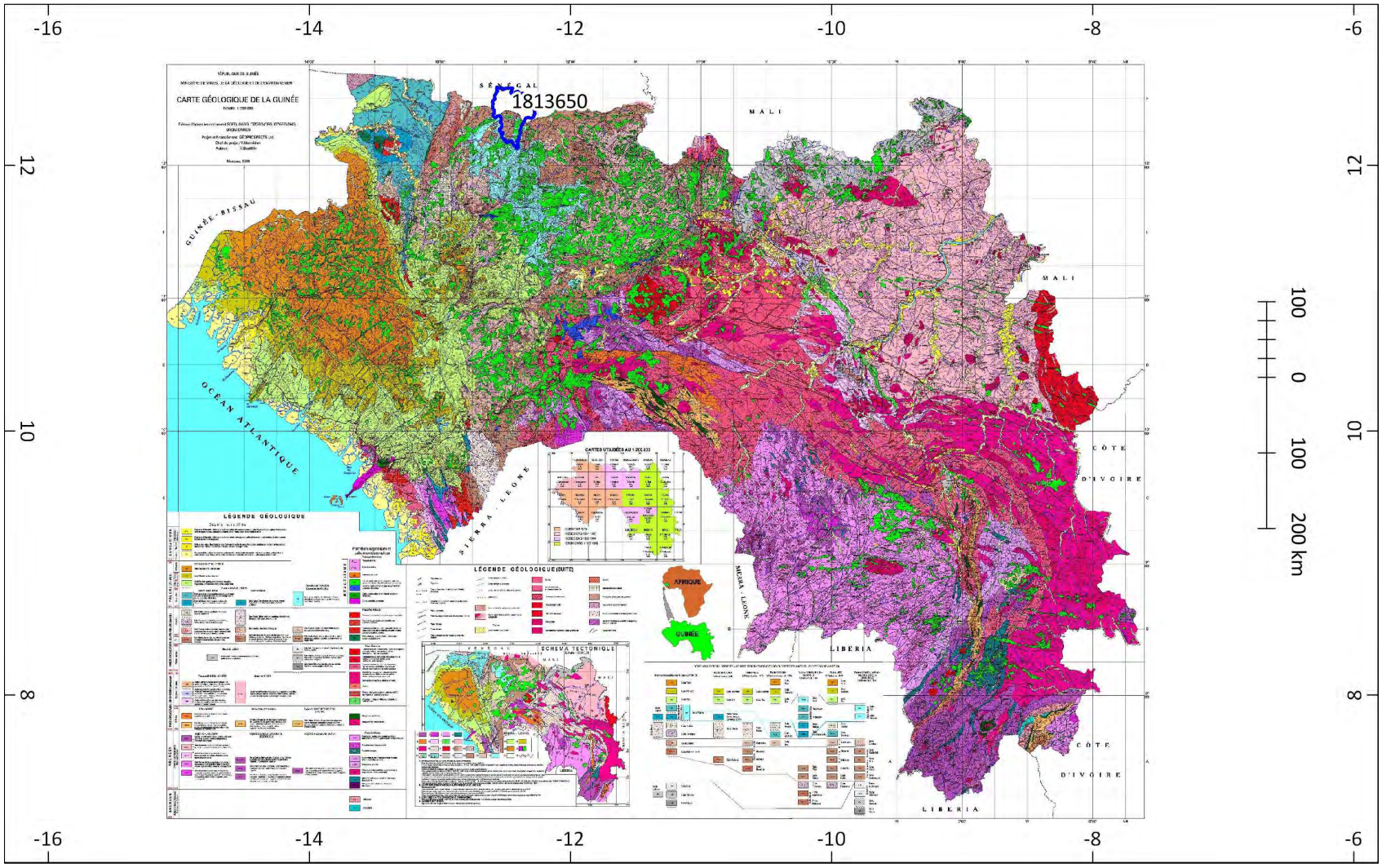

Geological map of of Guinea (Mamédov and Bouféév, 2006) with catchment 1813650-P.

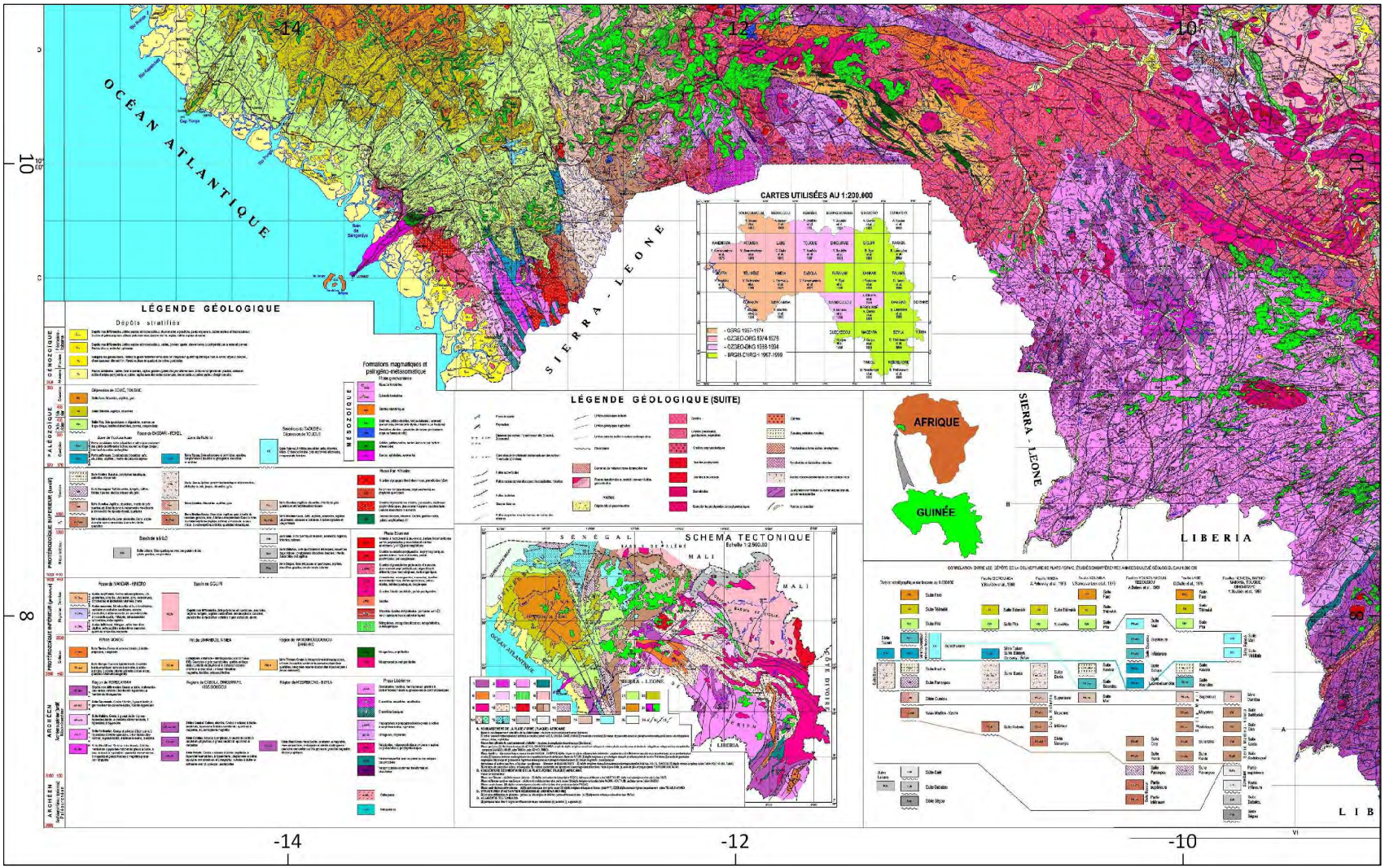

Legend to geological map of of Guinea (Mamédov and Bouféév, 2006).

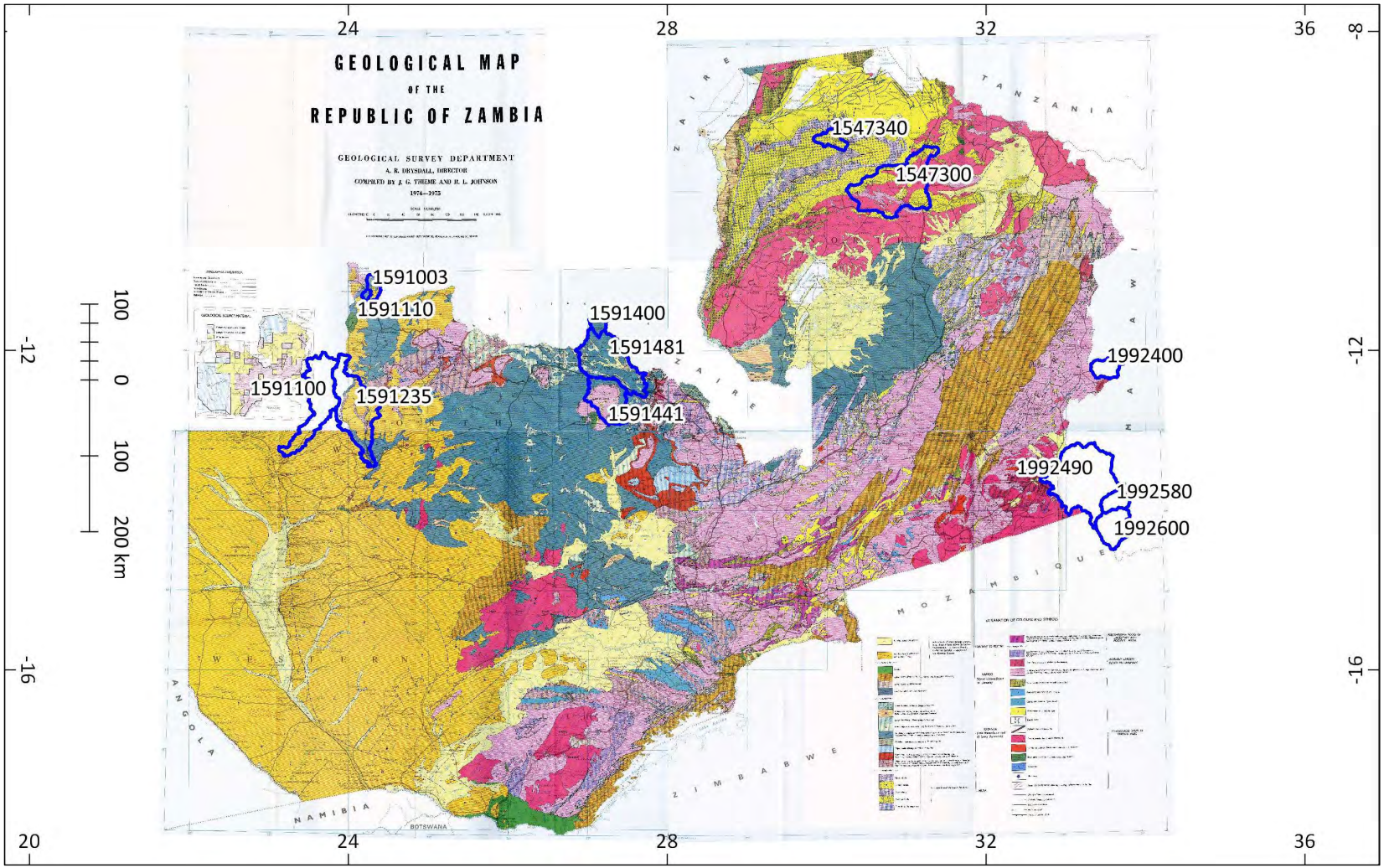

Geological map of Zambia (Drysdall et al., 1974) with catchments 1547300—B, 1547340—C, 1591003—D, 1591100—E, 1591110—F, 1591235—G, 1591400—H, 1591441—I, 1591481—J, 1992400—Q, 1992490—R, 1992580—S and 1992600—T.

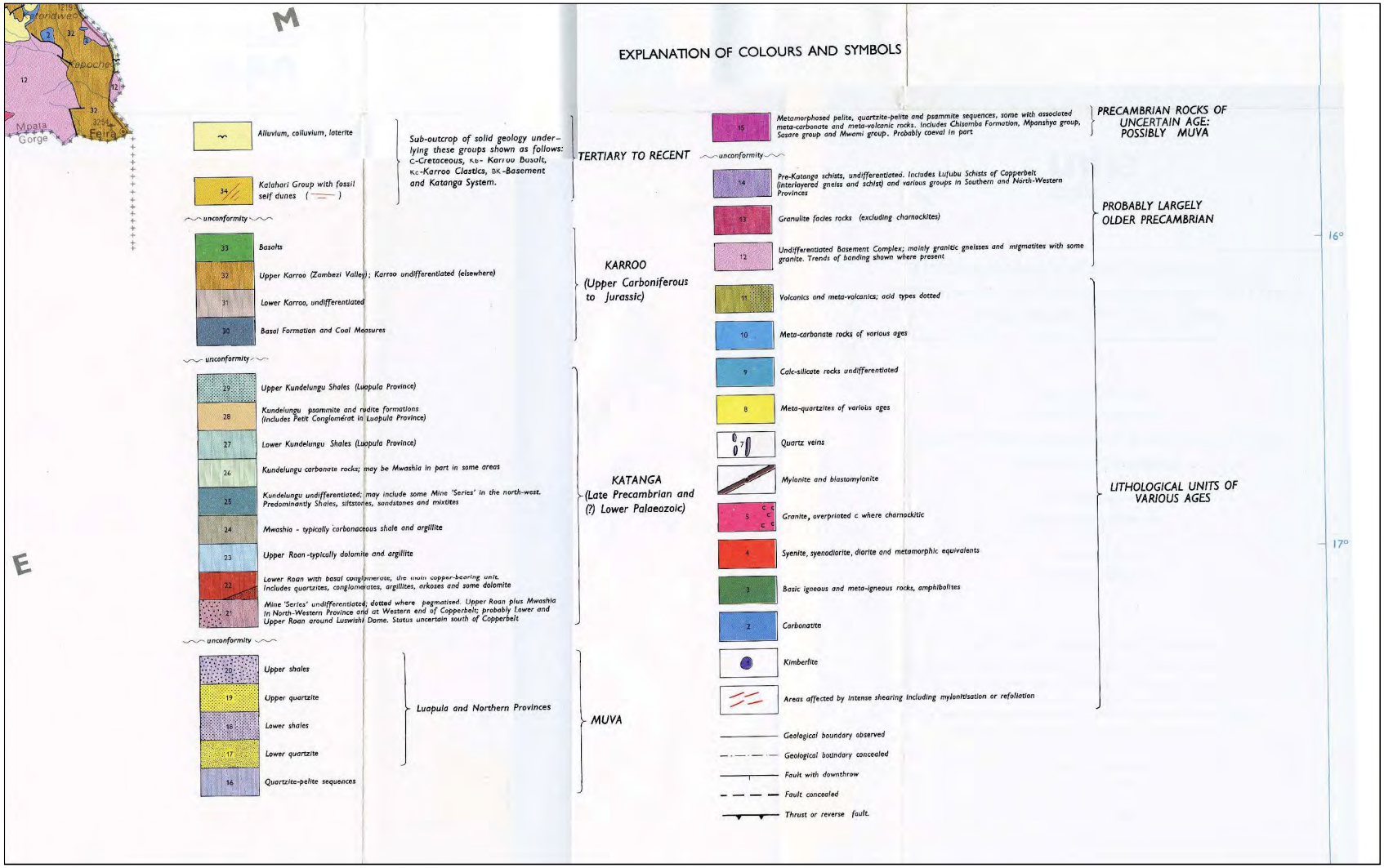

Legend to geological map of Zambia (Drysdall et al., 1974).

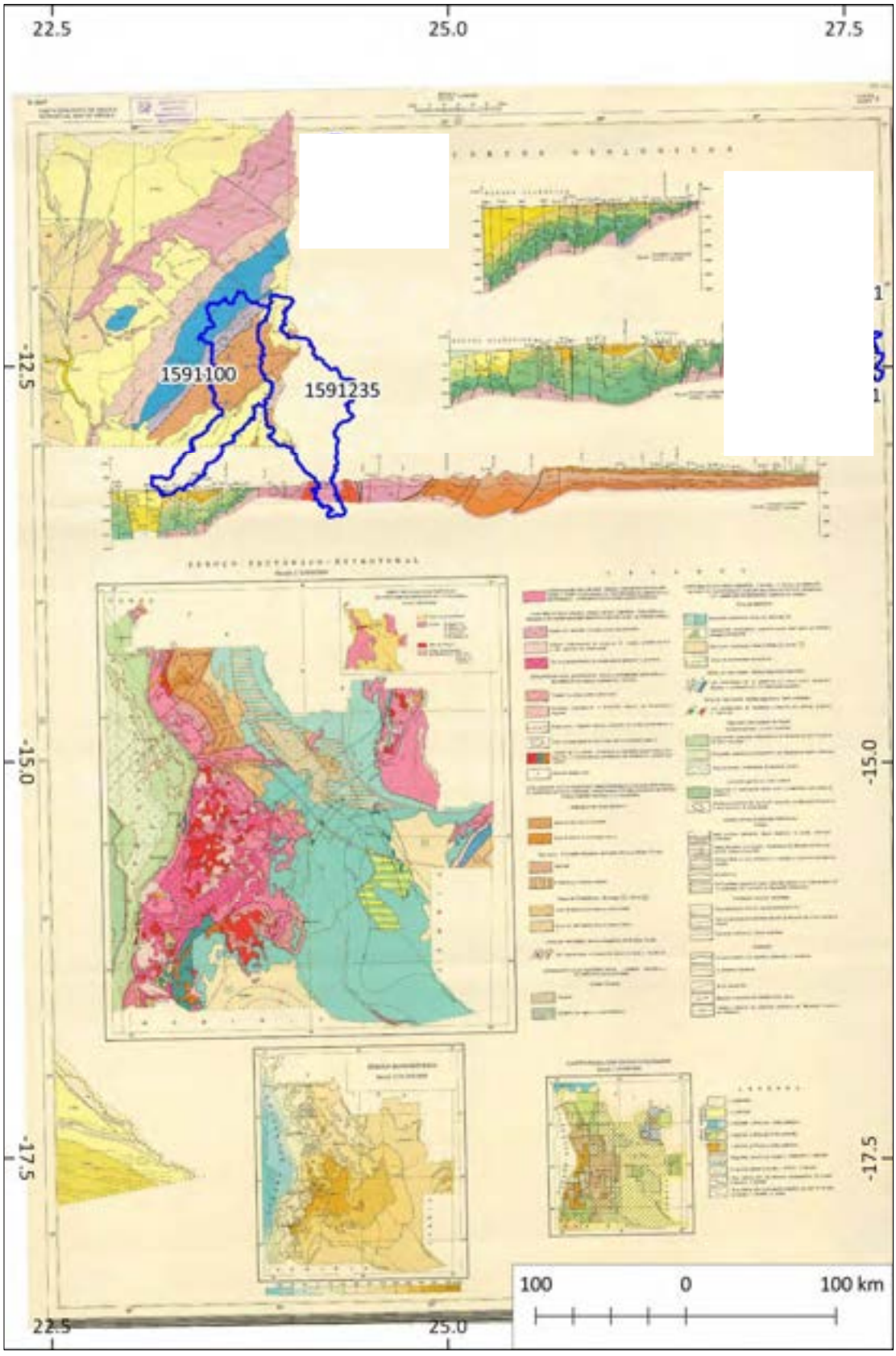

Geological map of Angola (Araújo et al., 1988) with catchments 1591100—E and 1591235—G.

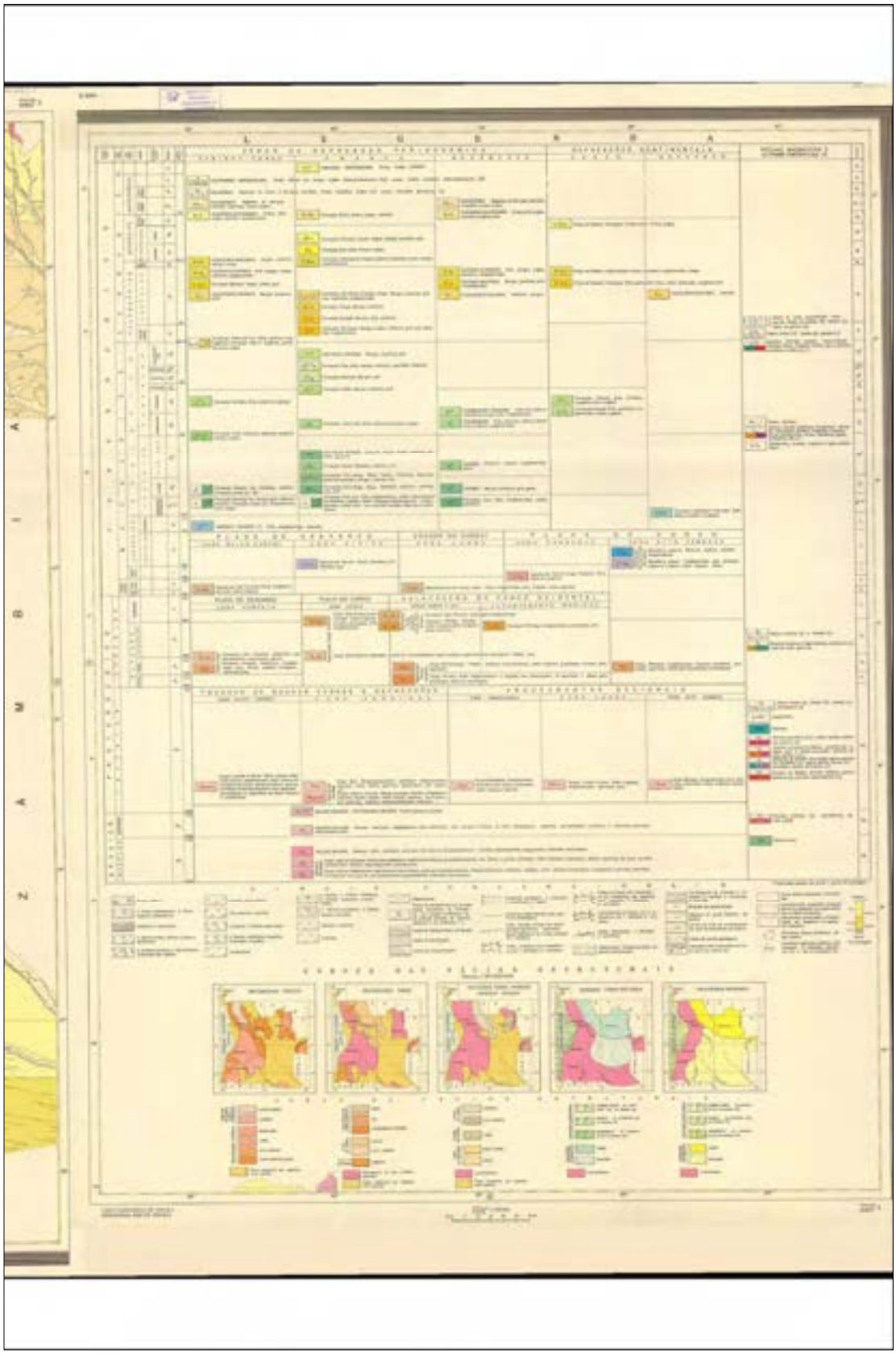

Legend to geological map of Angola (Araújo et al., 1988).

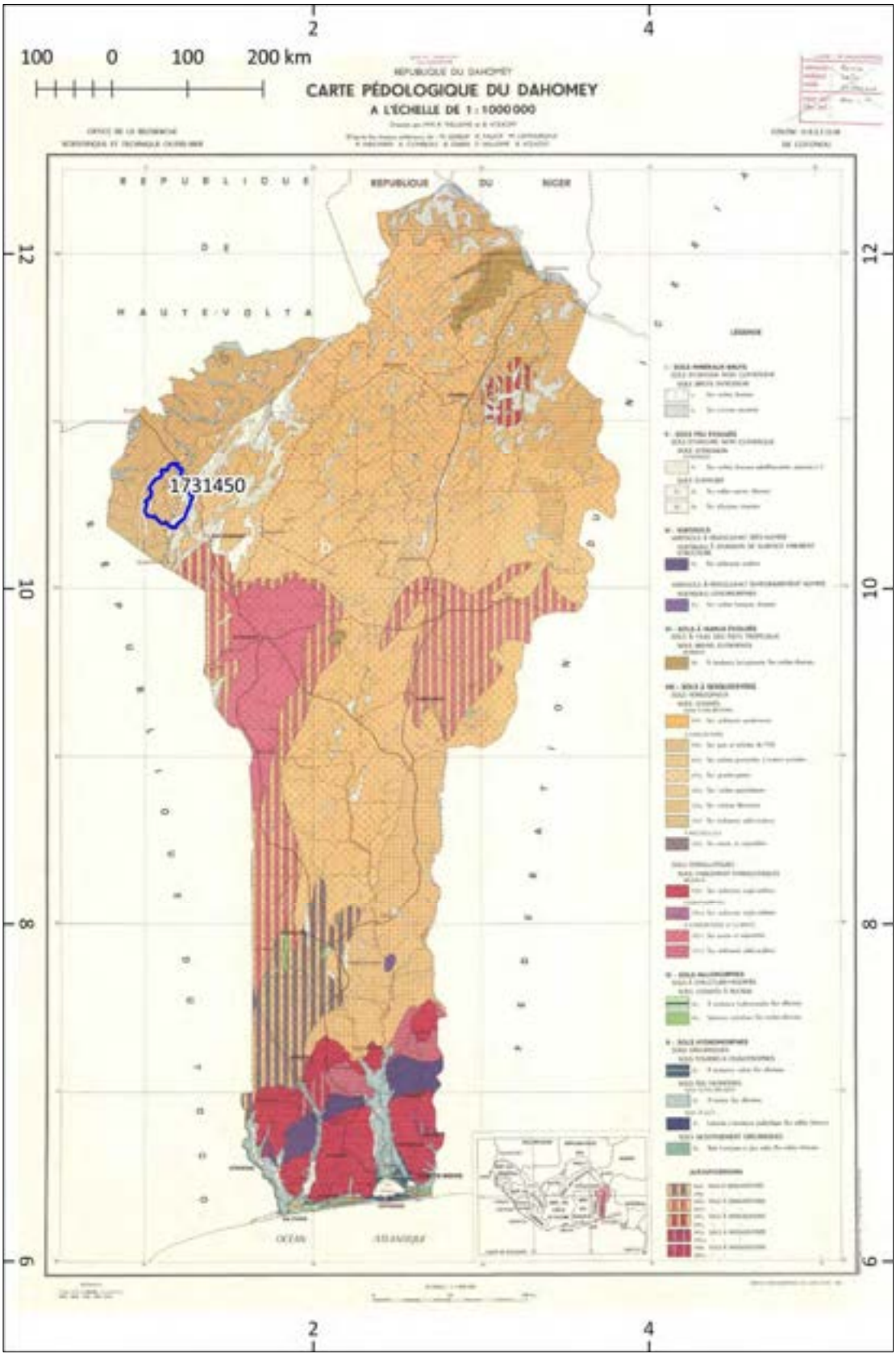

Geological map of Benin (Willaime et al., 1967) with catchment 1731450–K.

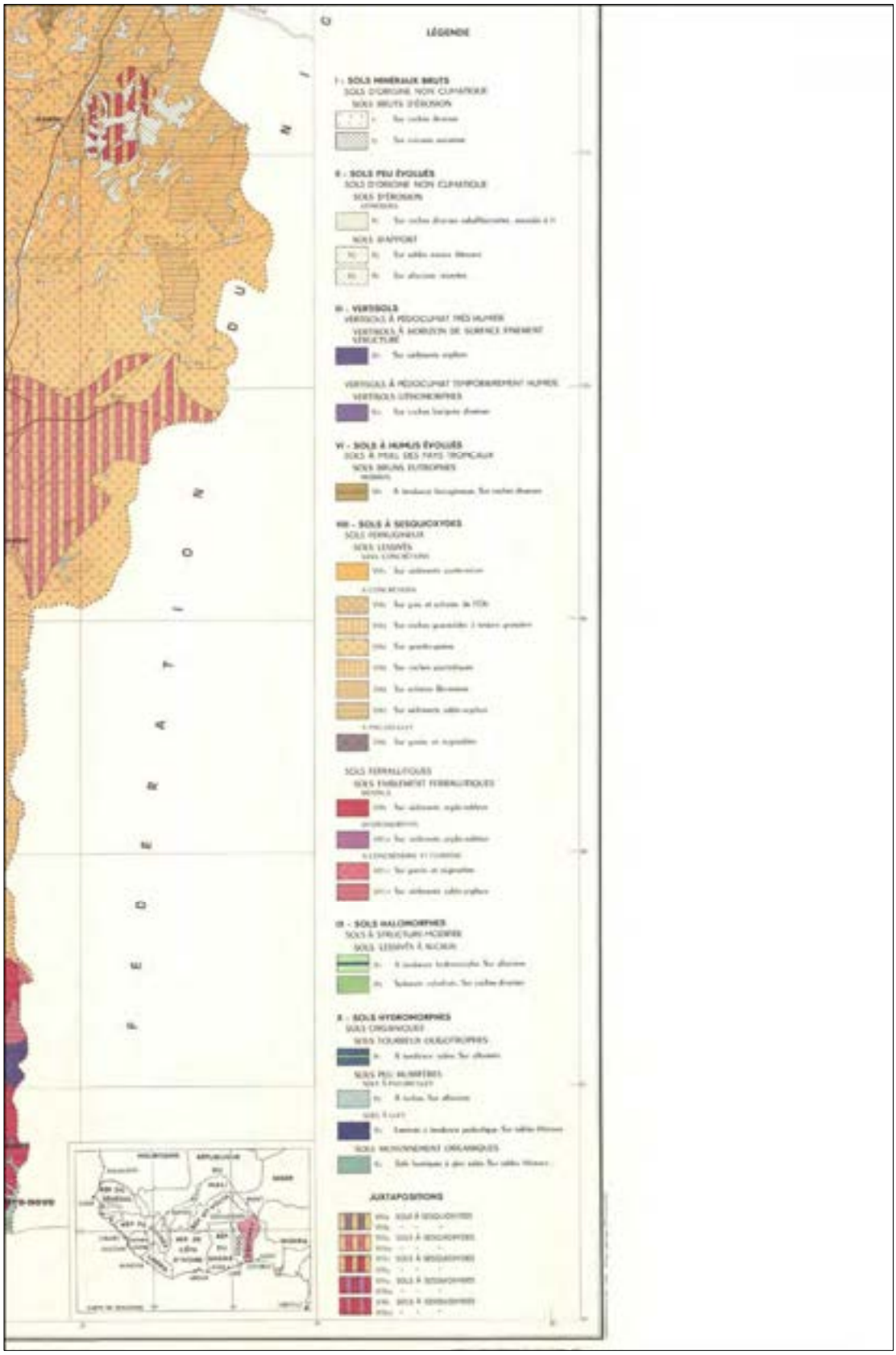

Legend to geological map of Benin (Willaime et al., 1967).

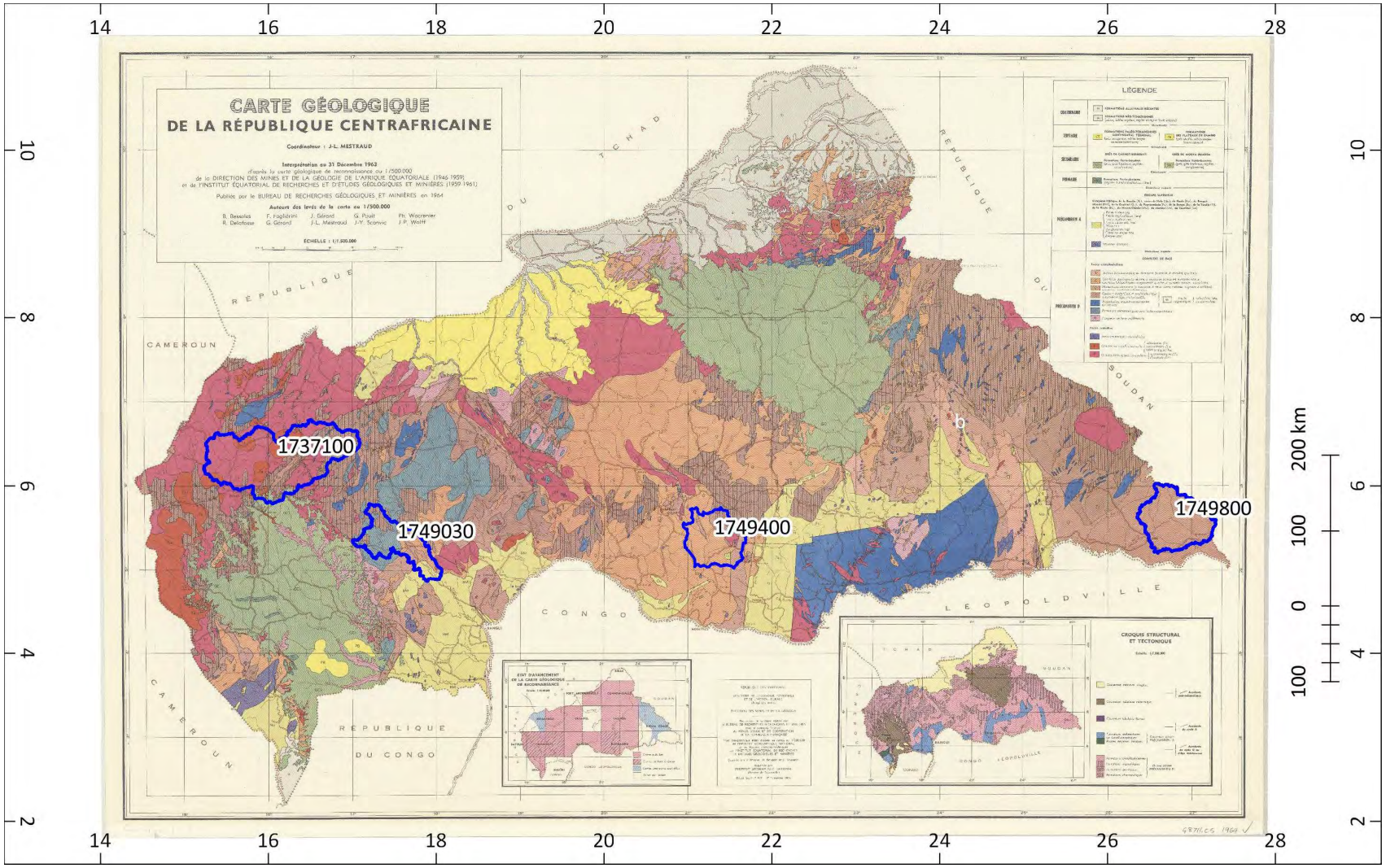

Geological map of CAR (Mestraud et al., 1963) with catchments 1737100—L, 1749030—M, 1749400—N and 1749800—O.

legend to Geological map of CAR (Mestraud et al., 1963).

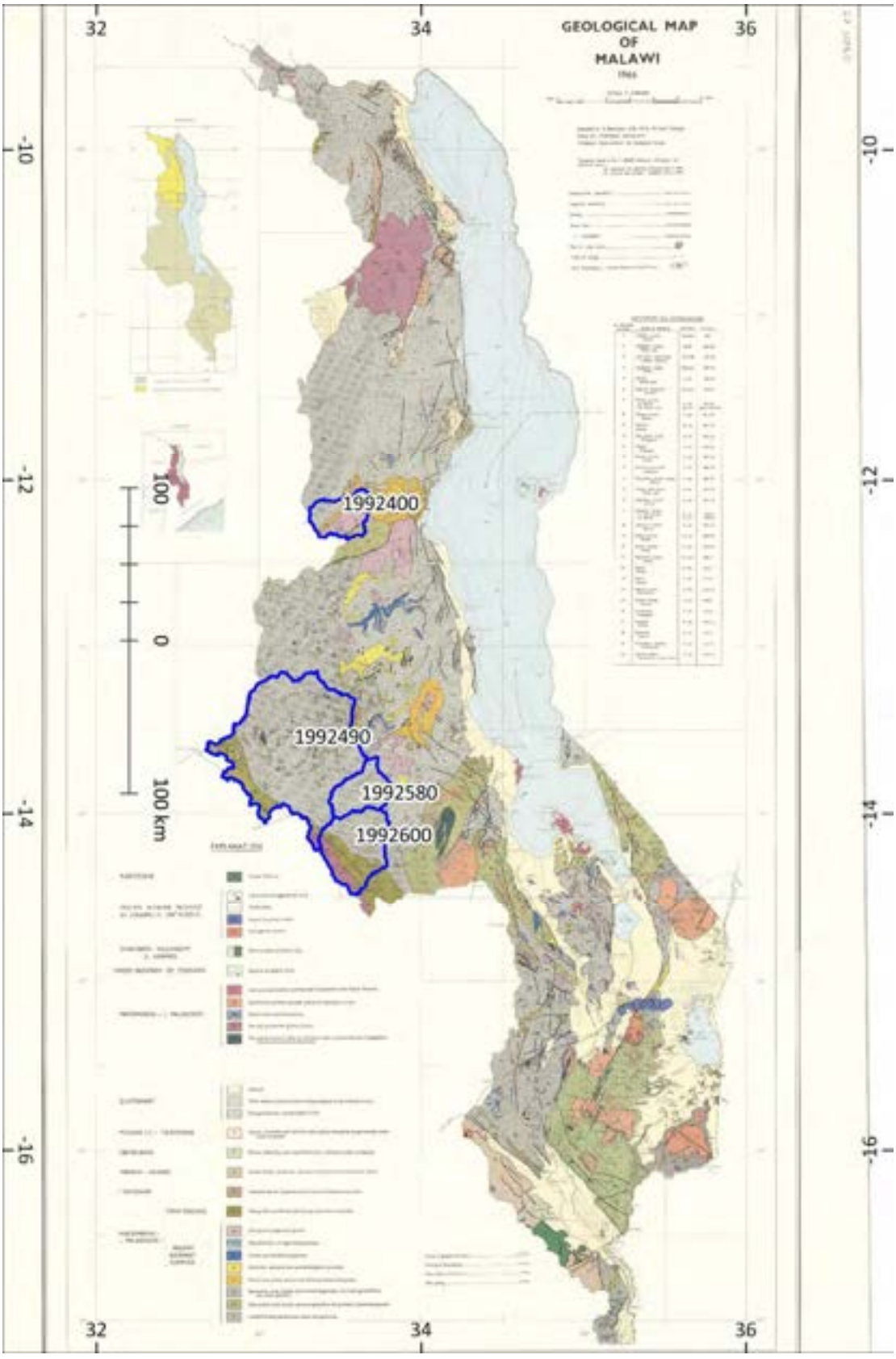

Geol. of Malawi (Bloomfield and Manson, 1966) with catchments 1992400—Q, 1992490—R, 1992580—S and 1992600—T.

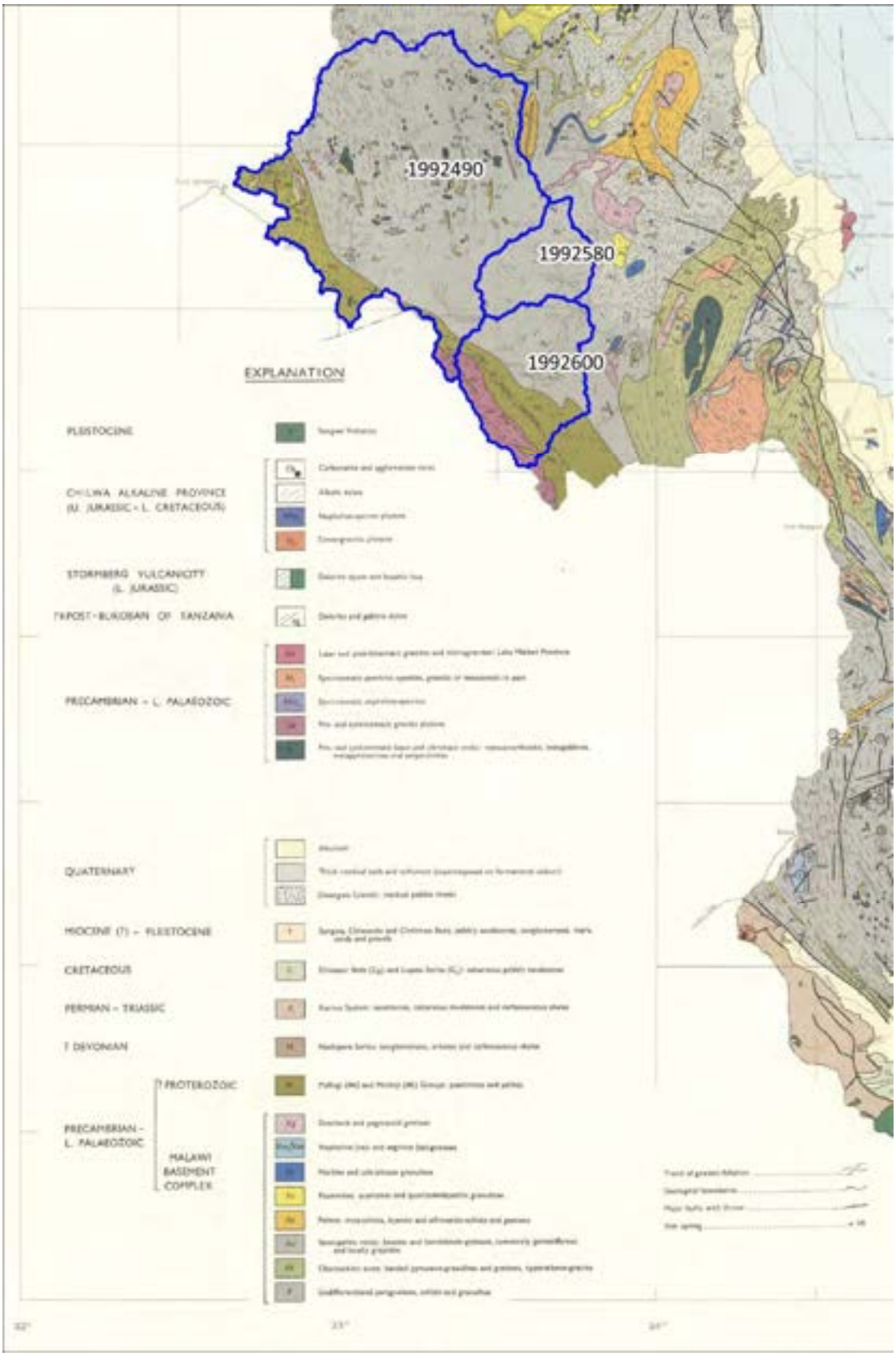

Legend to Geological map of Malawi (Bloomfield and Manson, 1966).

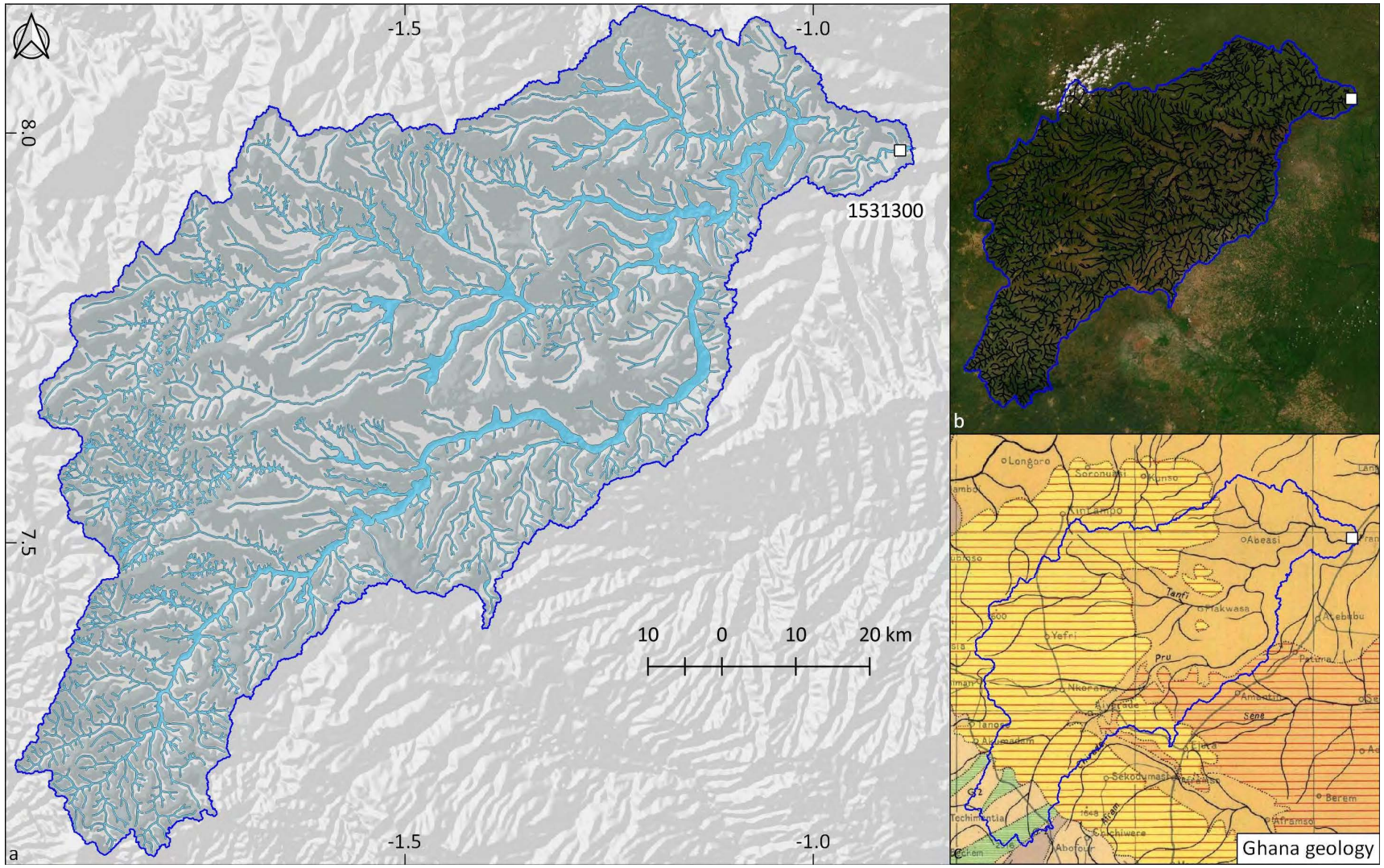

Catchment A-1531300.

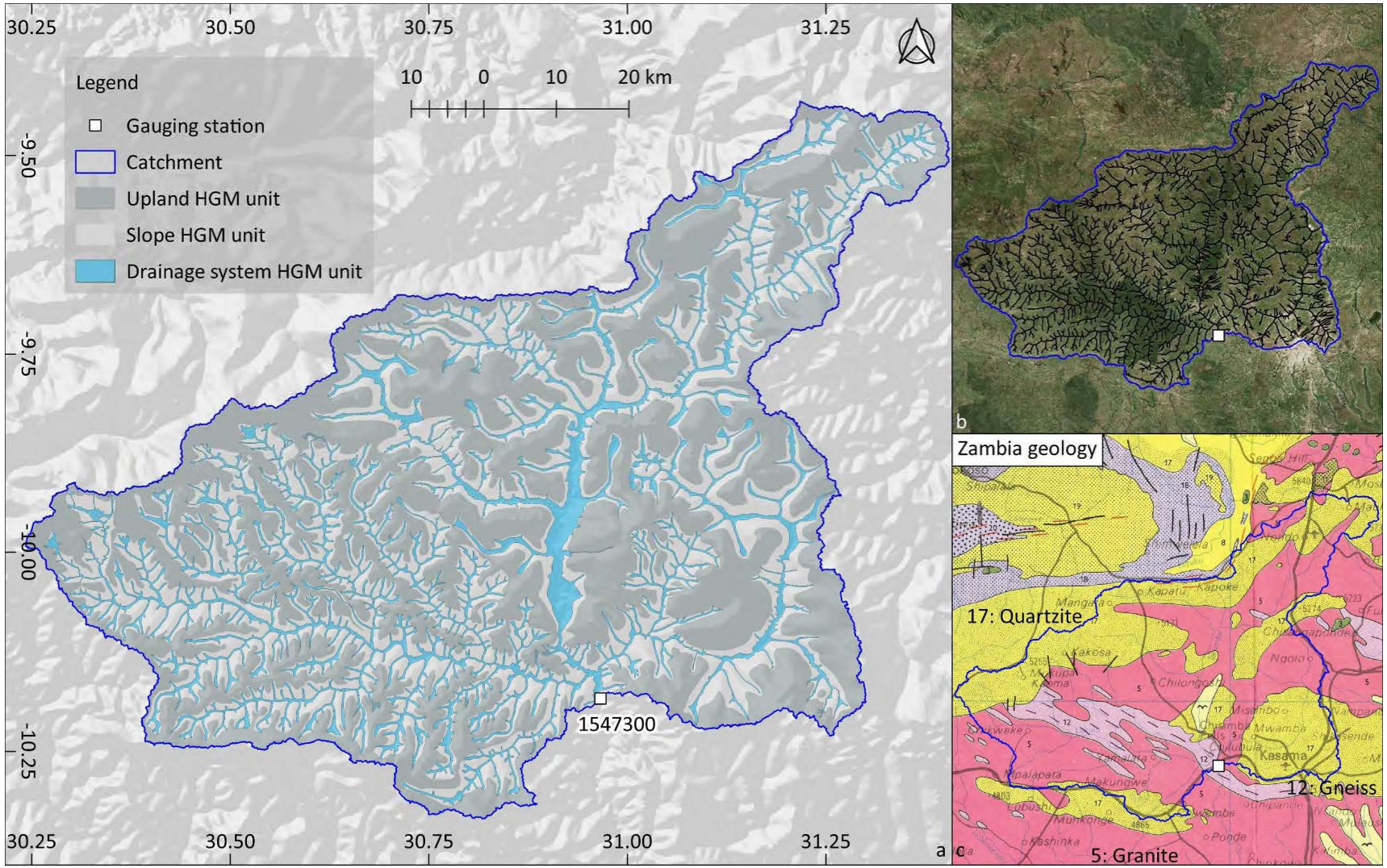

Catchment B-1547300.

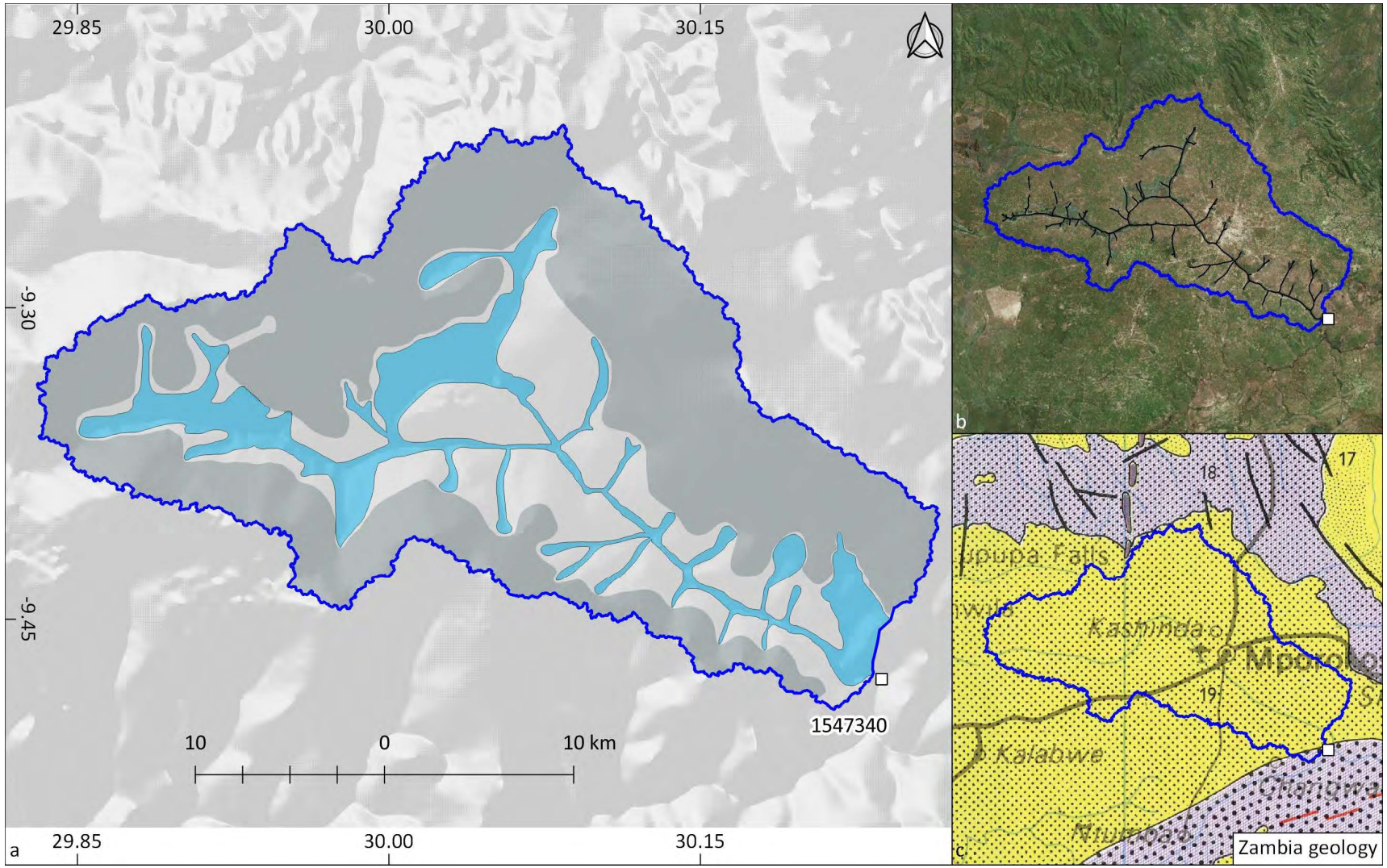

Catchment C-1547340.

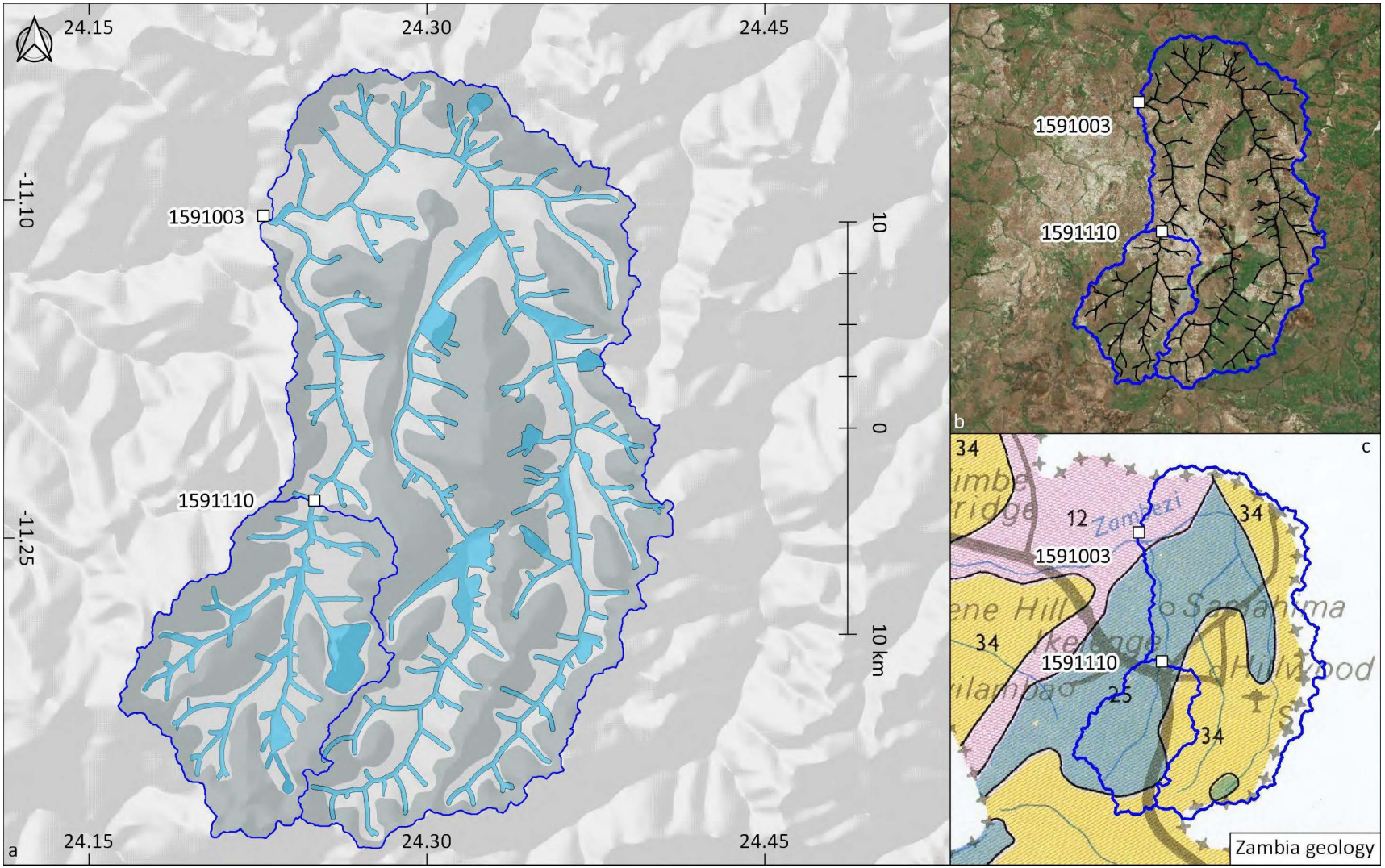

Catchment D-1591003 and F-1591110.

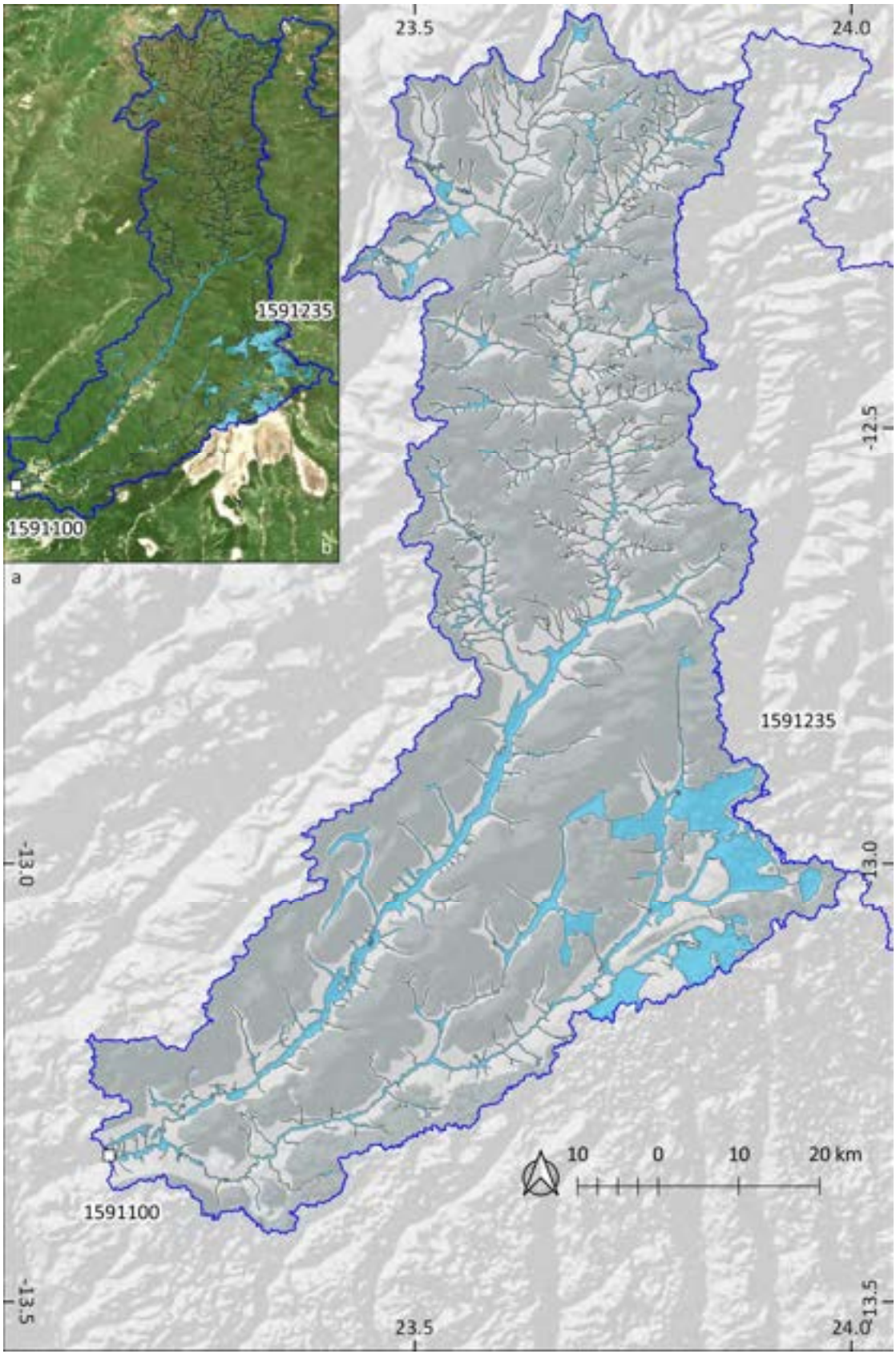

Catchment E-1591100.

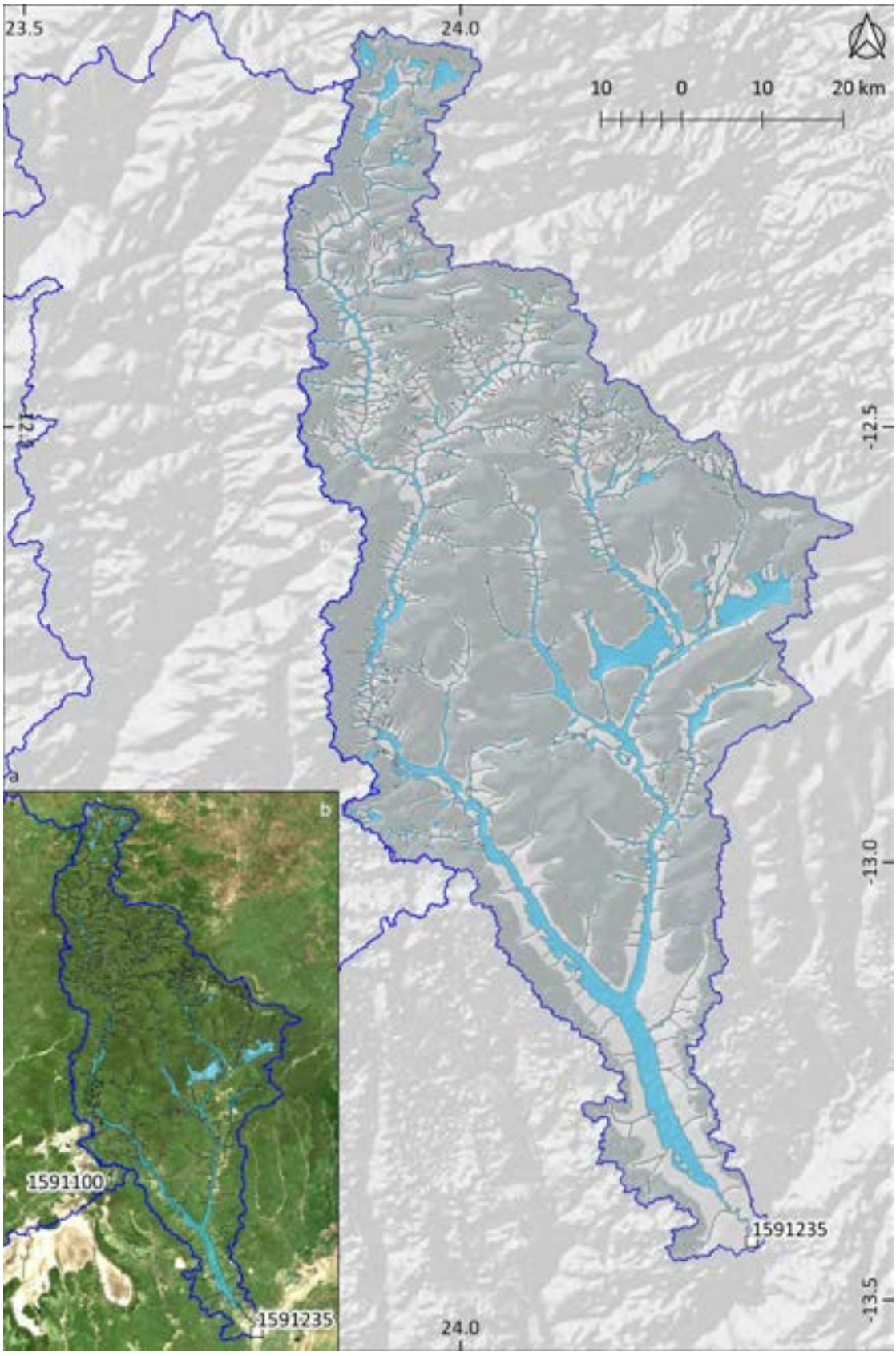

Catchment G-1591235.

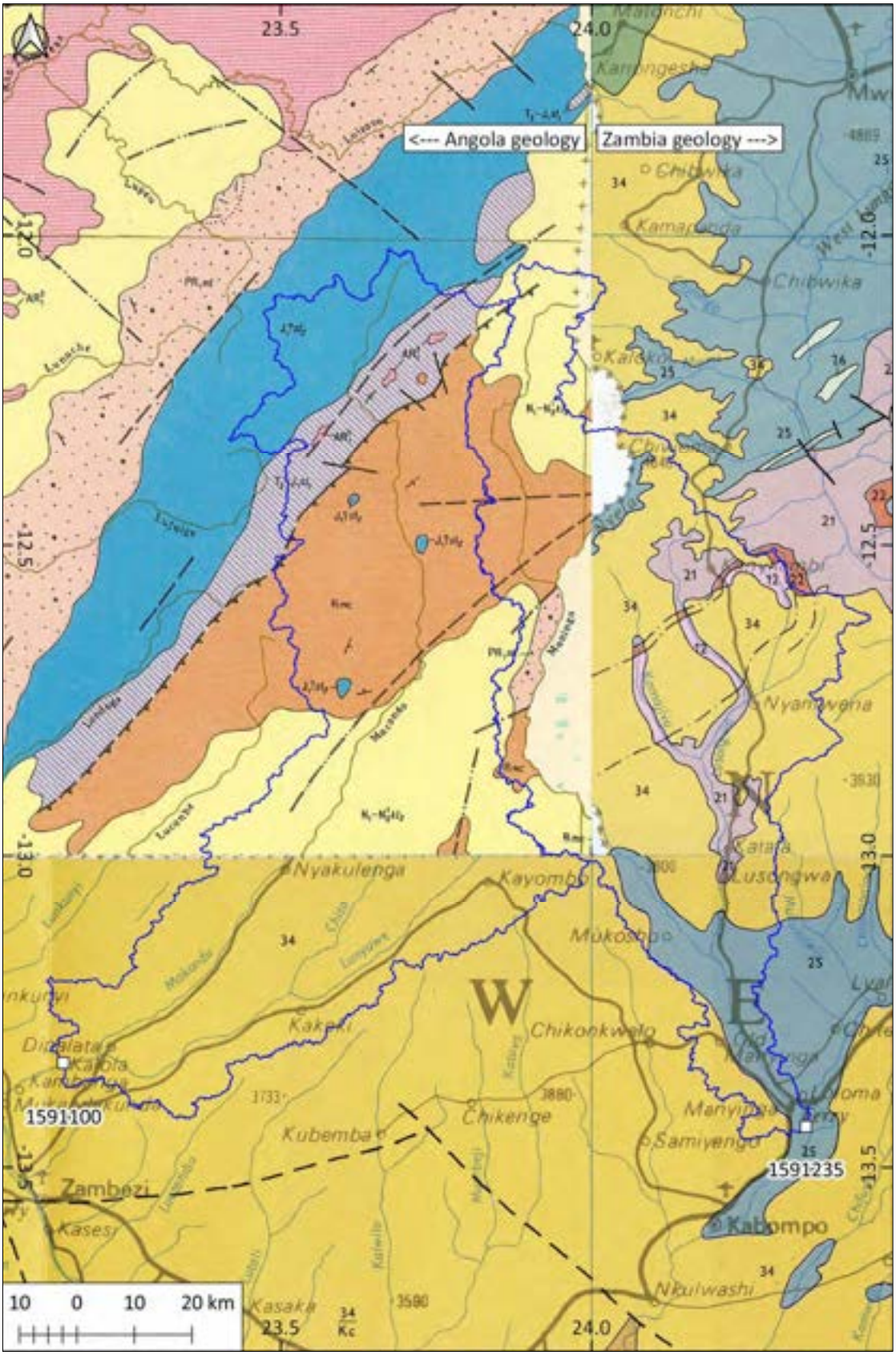

Catchment E-1591100 and G-1591235.

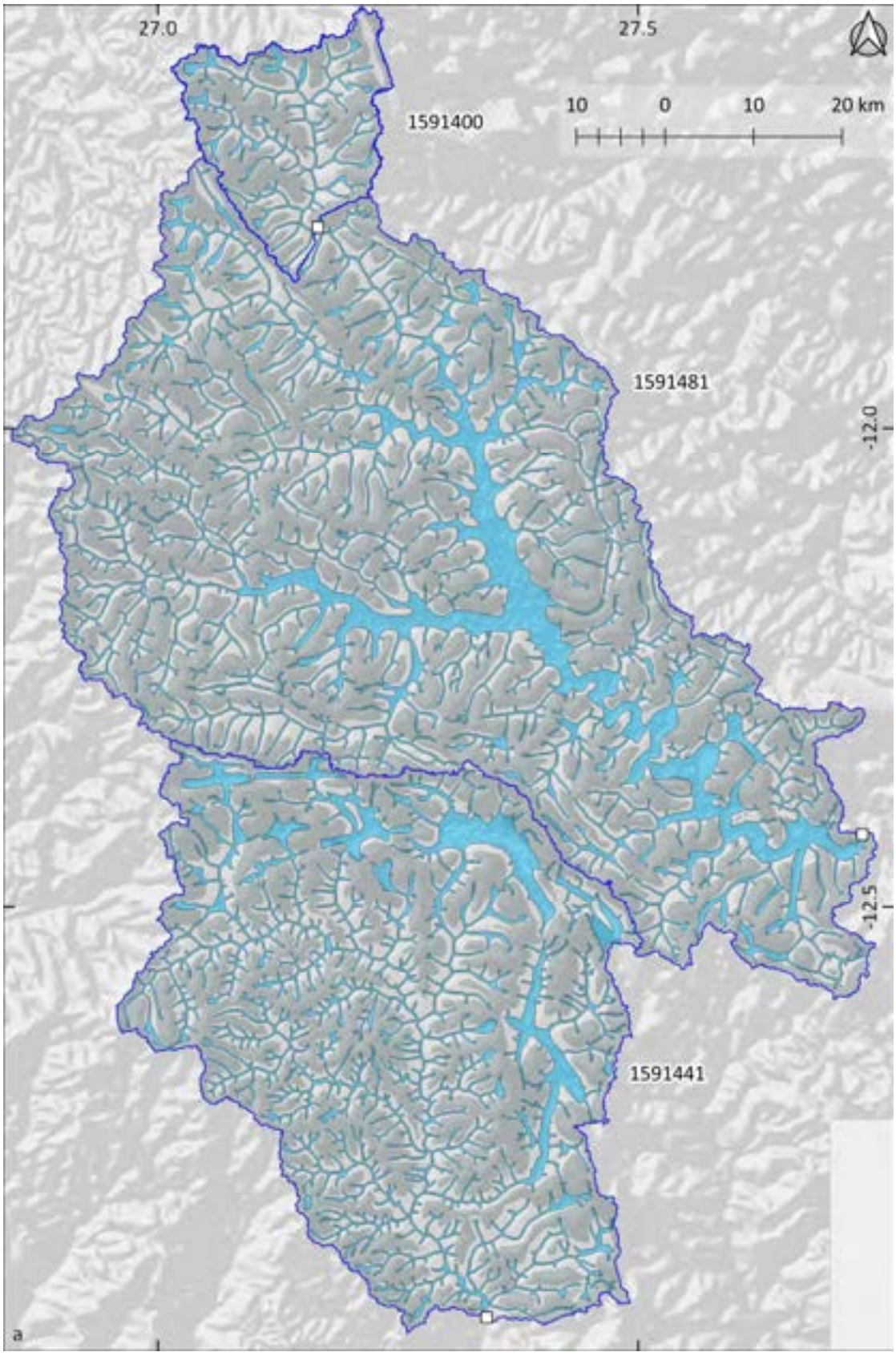

Catchment H-1591400, I-1591441 and J-1591481.

Catchment H-1591400, I-1591441 and J-1591481.

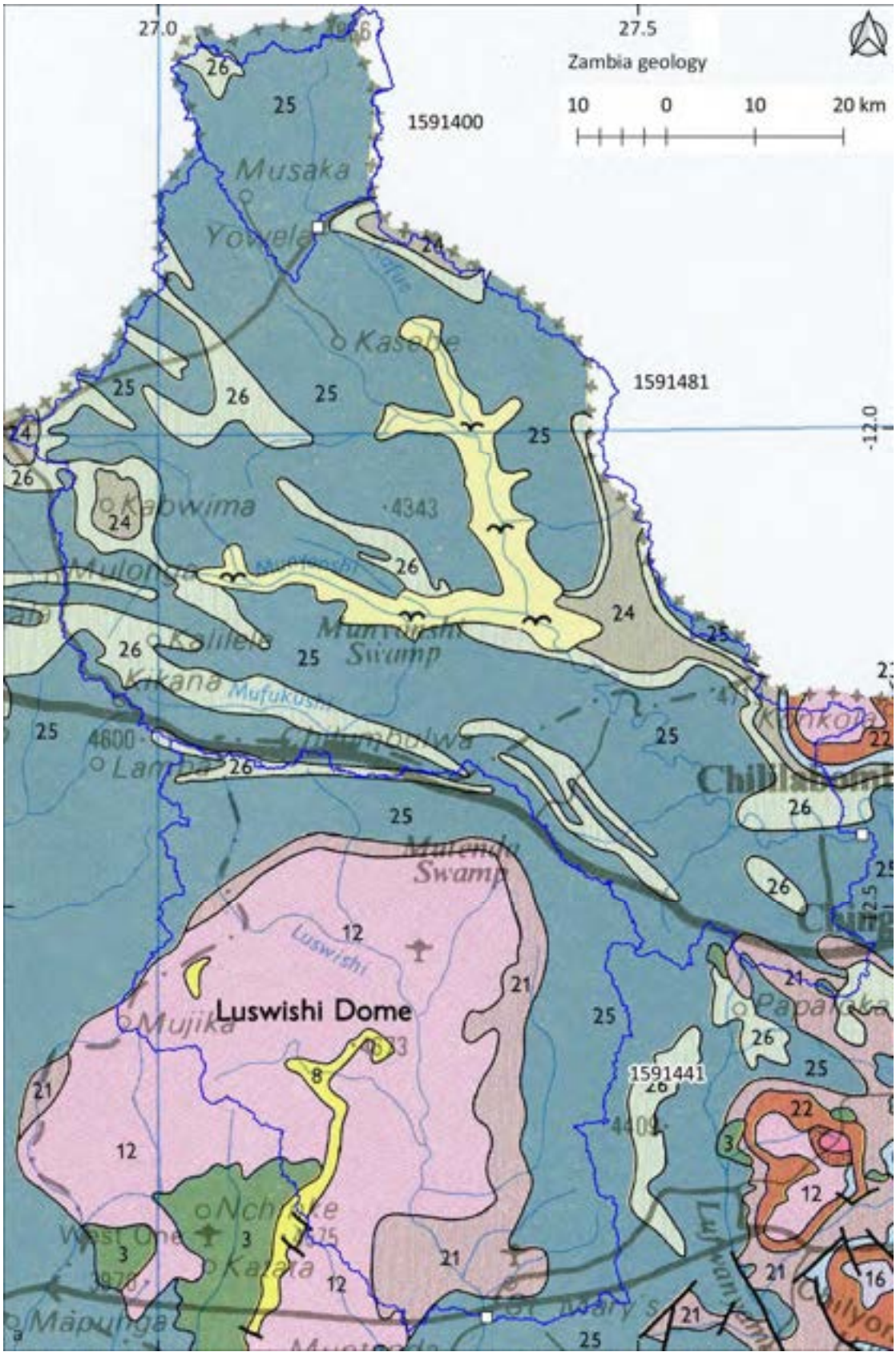

Catchment H-1591400, I-1591441 and J-1591481.

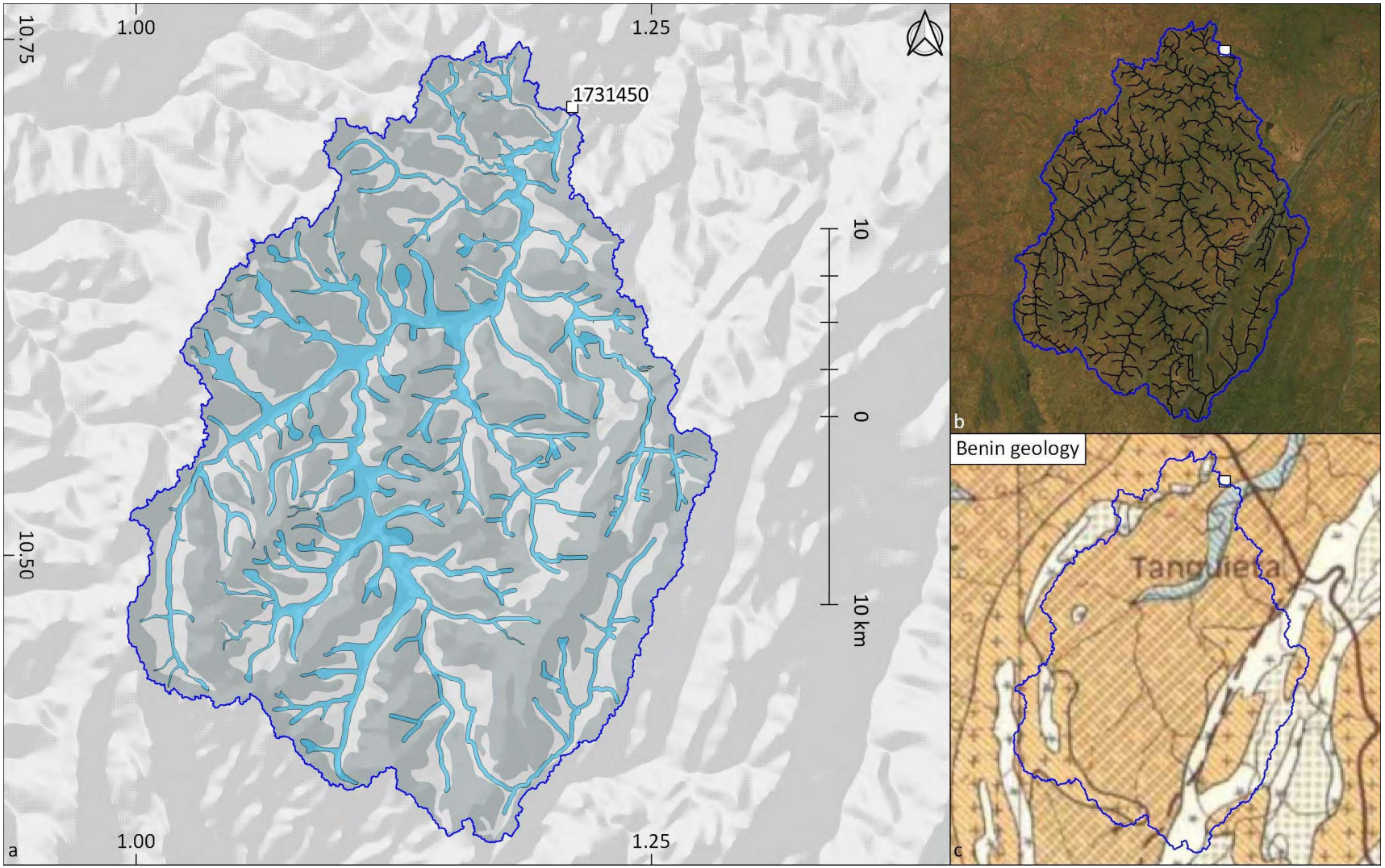

Catchment K-1731450.

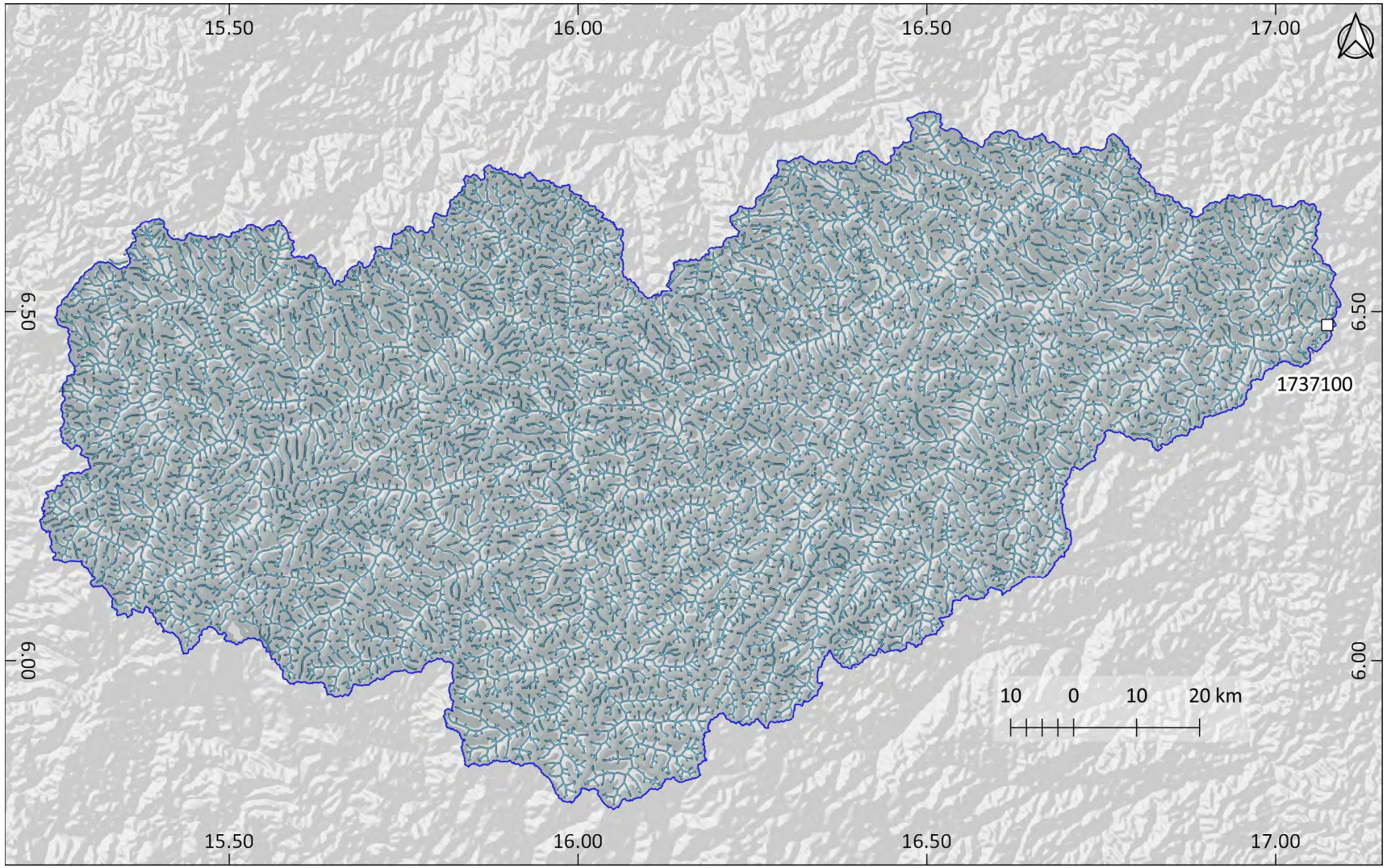

Catchment L-1737100.

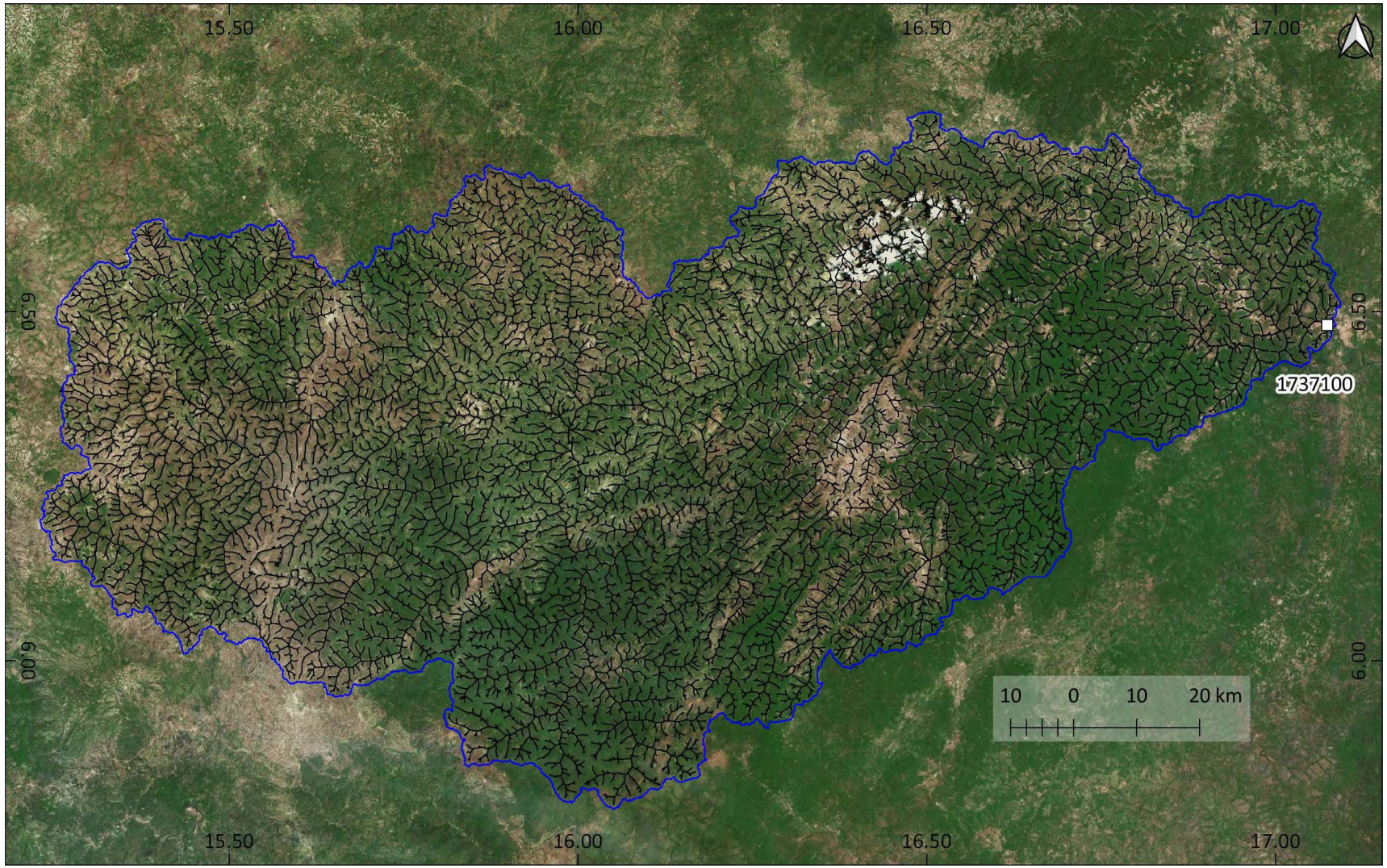

Catchment L-1737100.

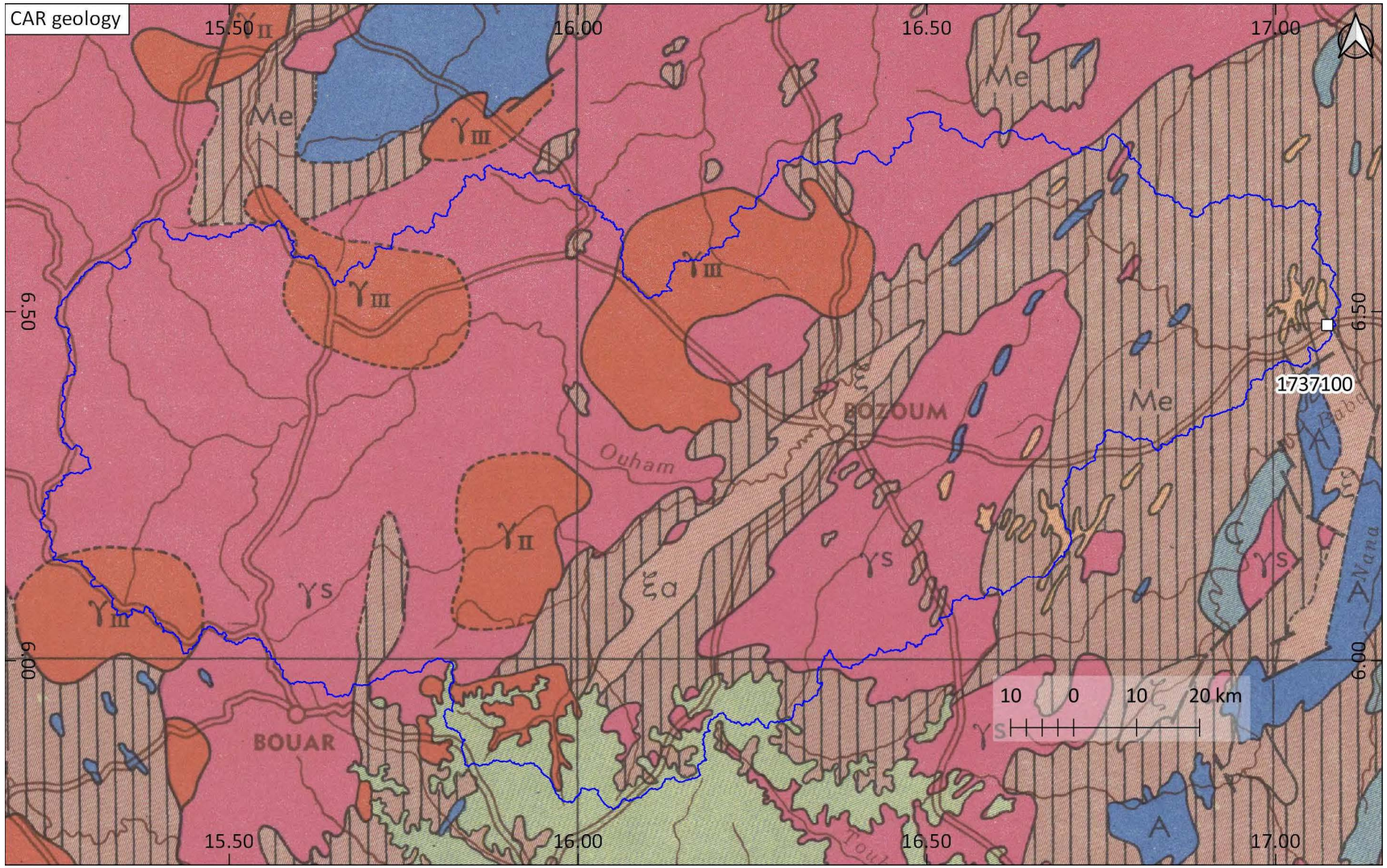

Catchment L-1737100.

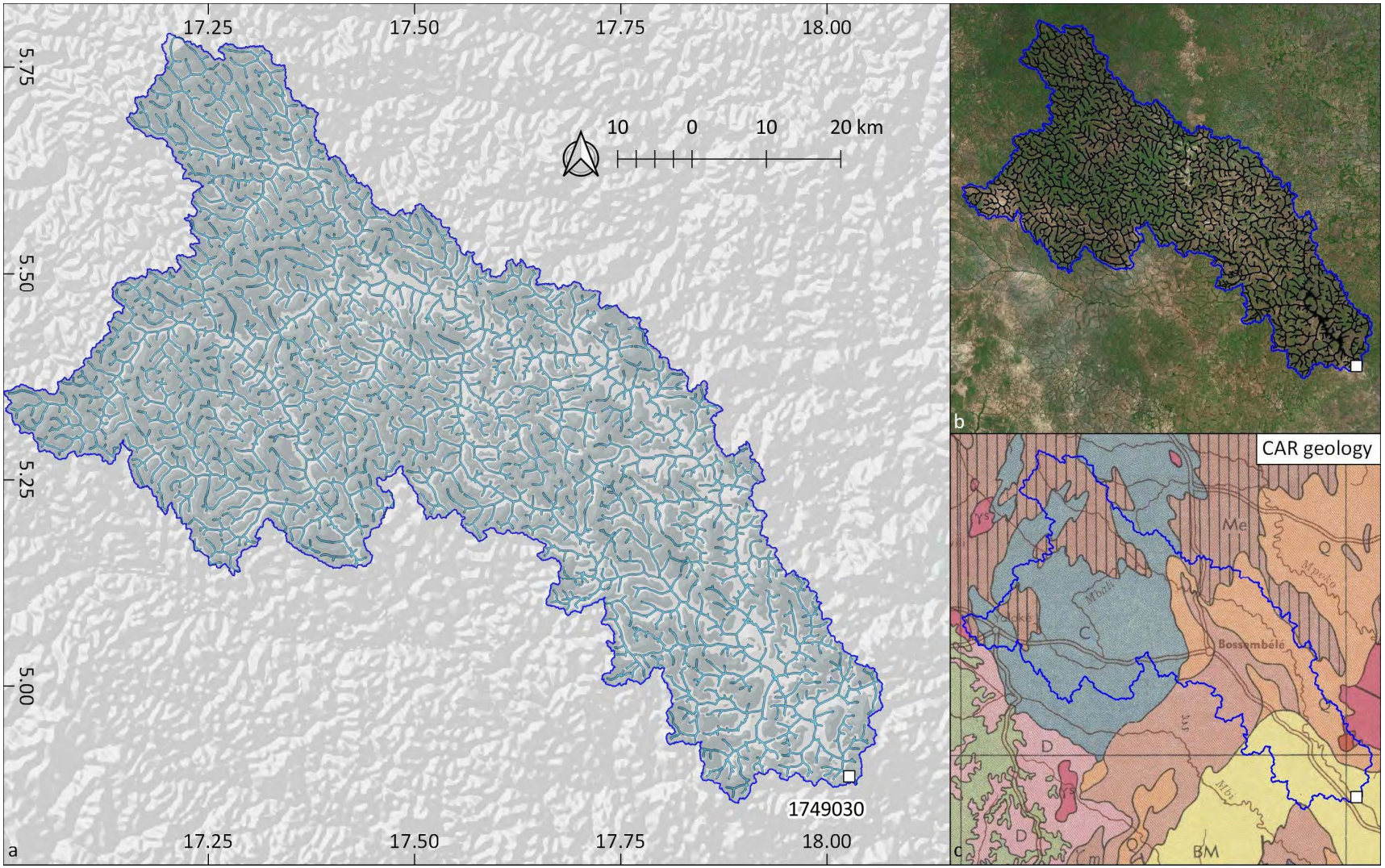

Catchment M-1749030.

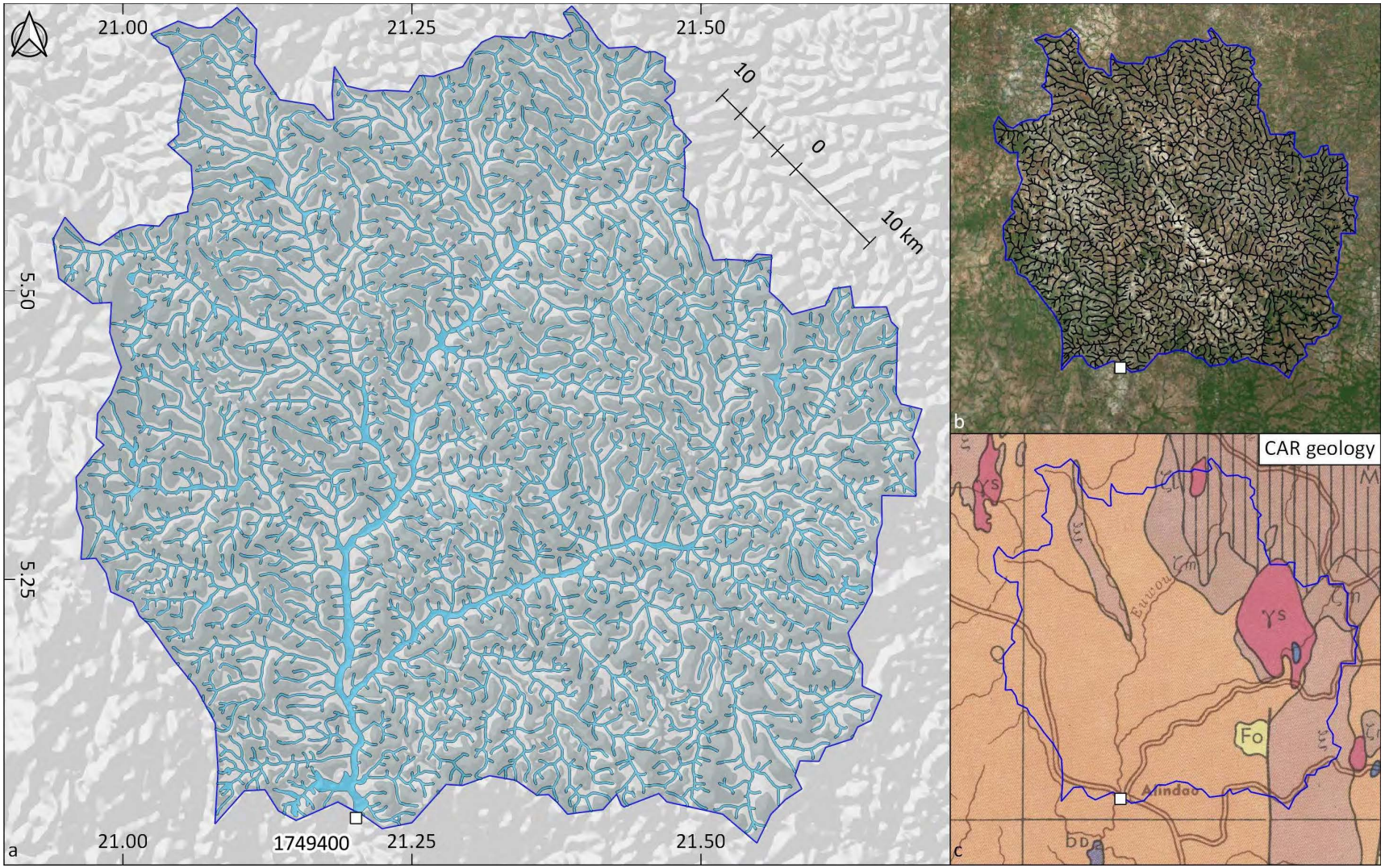

Catchment N-1749400.

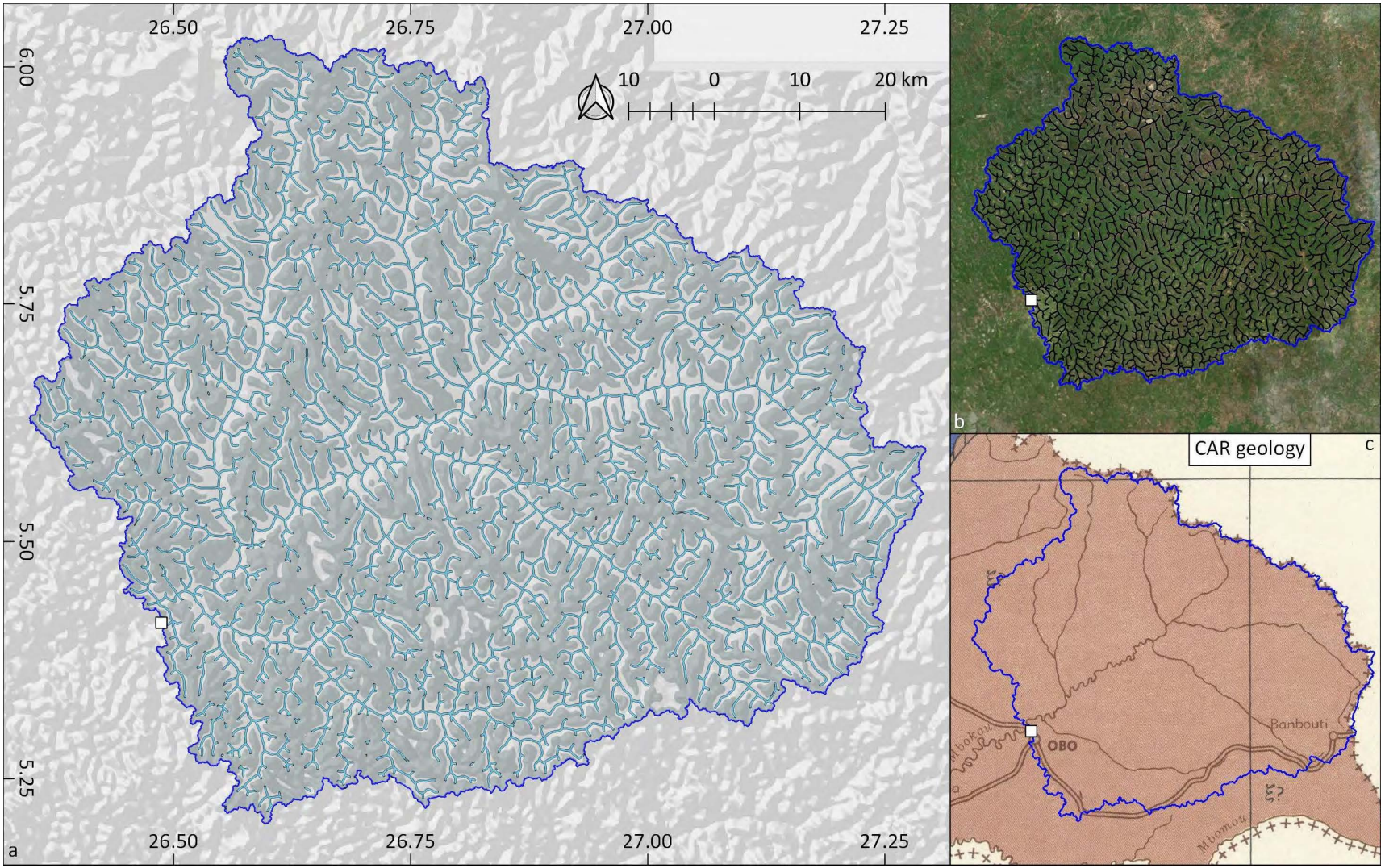

Catchment O-1749800.

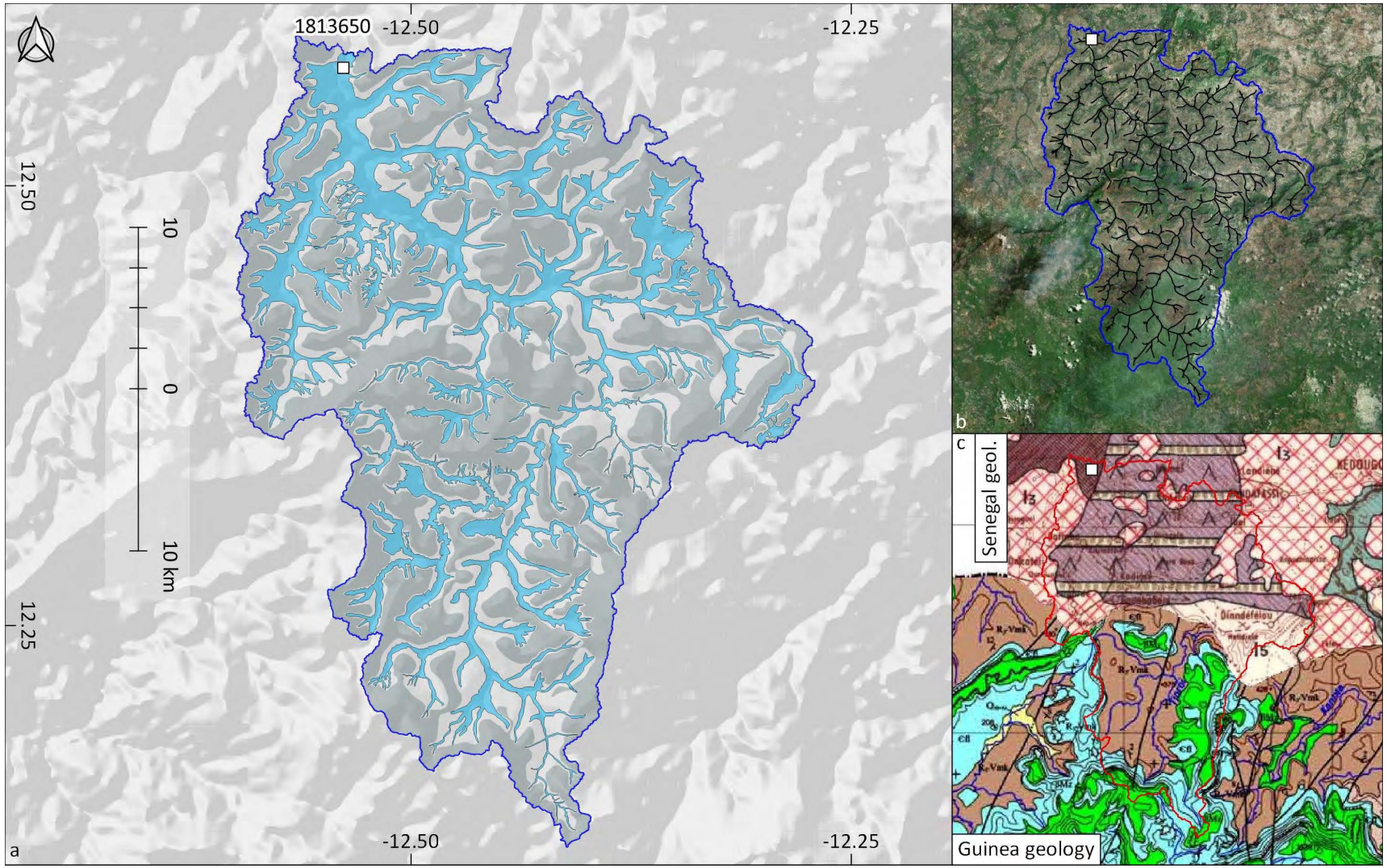

Catchment P-1813650.

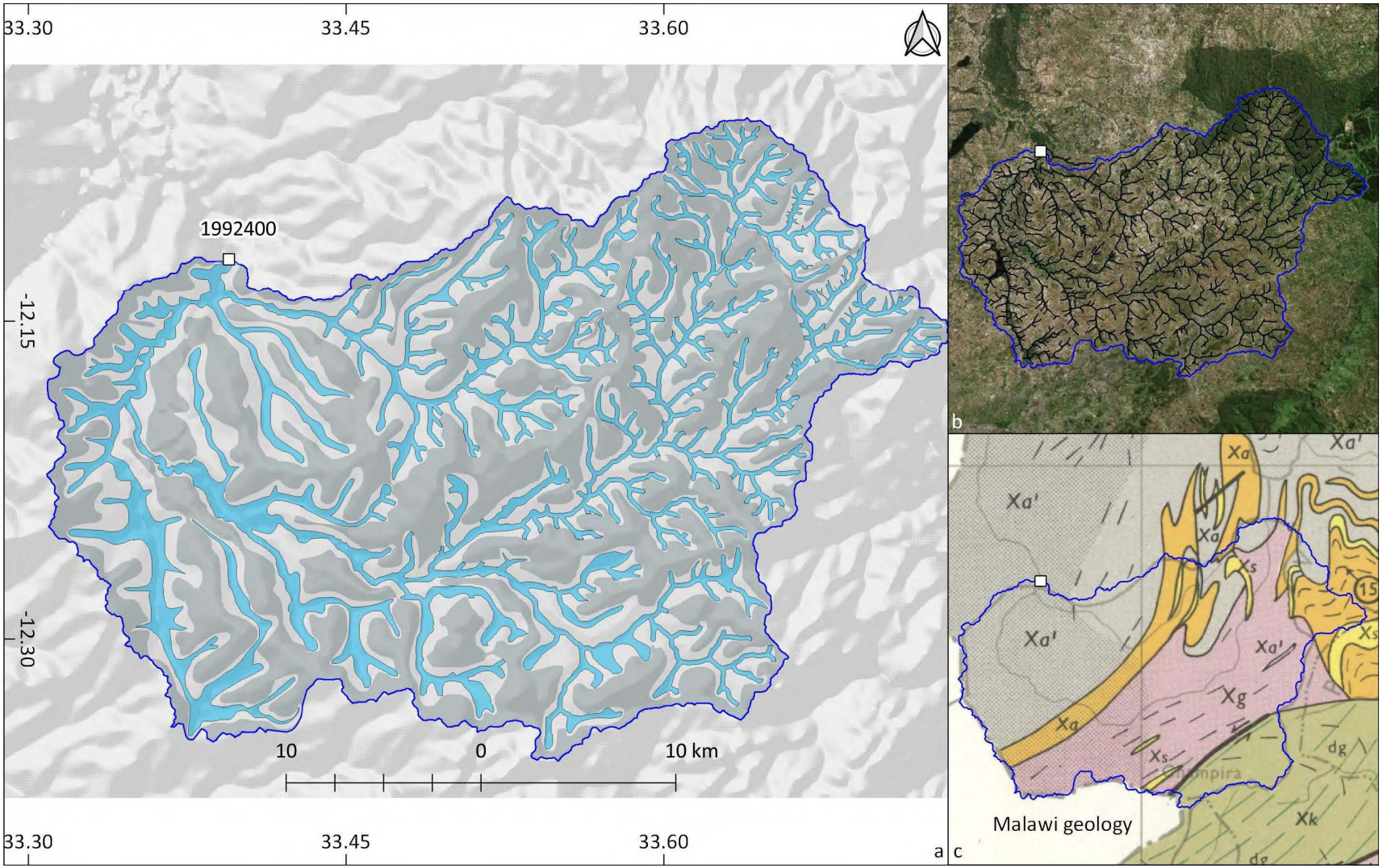

Catchment Q-1992400.

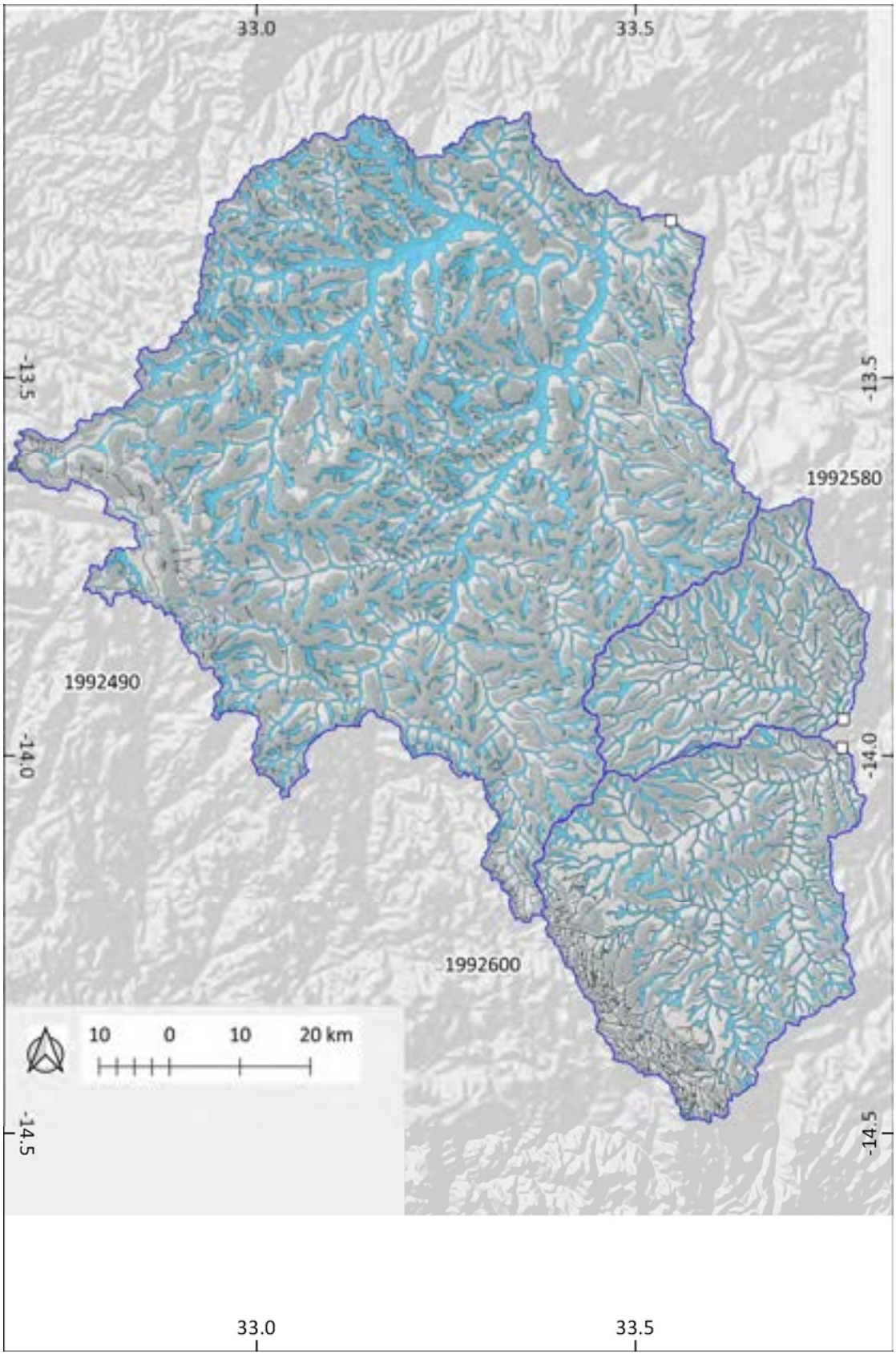

Catchment R-1992490, S-1992580 and T-1992600.

Catchment R-1992490, S-1992580 and T-1992600.

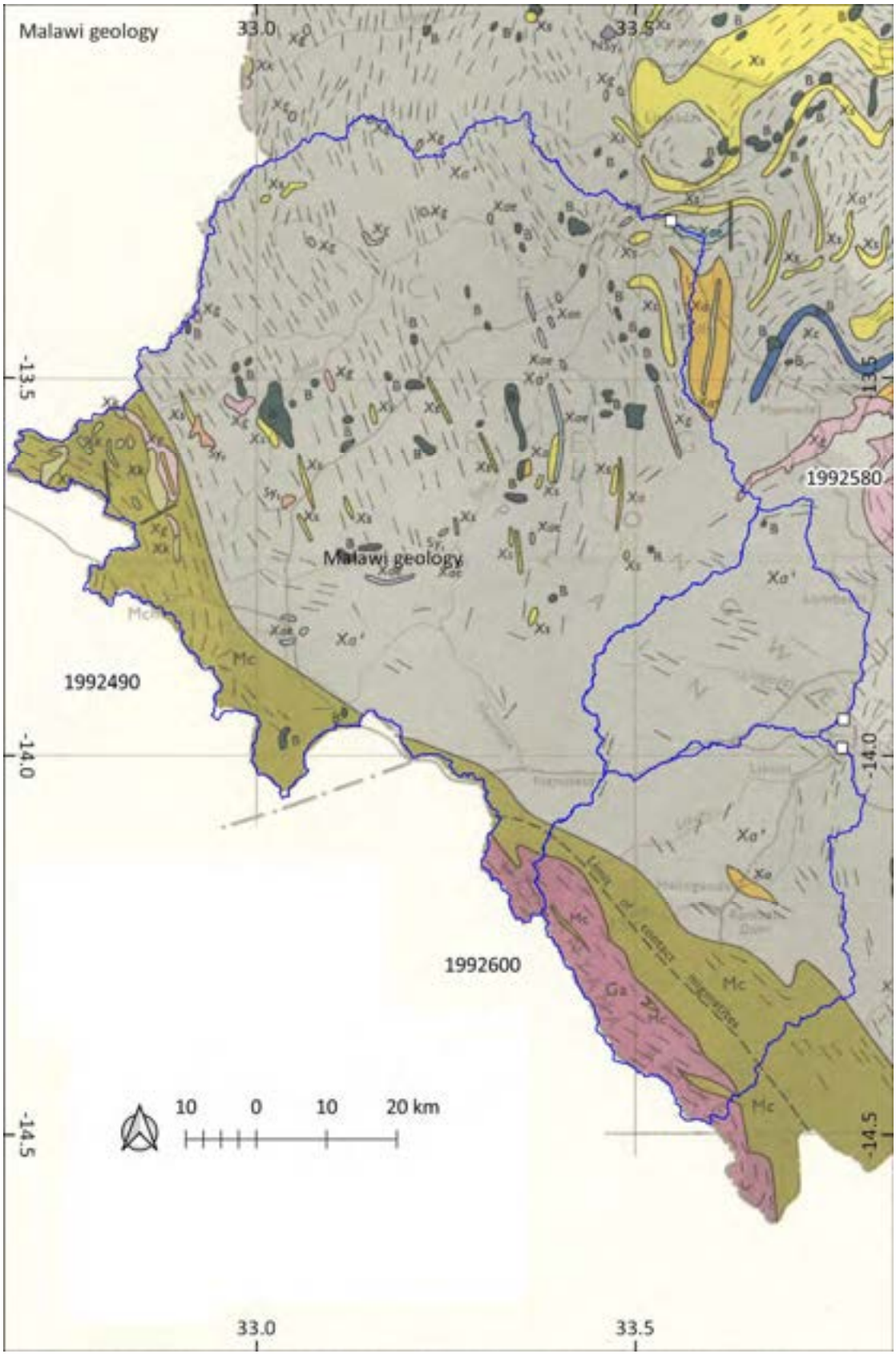

Catchment R-1992490, S-1992580 and T-1992600.

Appendix E: Precipitation and evapotranspiration of the reference catchments

1. The Google earth engine codes for generating precipitation and evapotranspiration are given in digital format.
2. The complete data set generated in Google earth engine for precipitation and evapotranspiration are given in digital format.
3. The individual precipitation and evapotranspiration of the 20 reference catchments are illustrated in the following figures. The catchments are labelled according to the GRDC id and referenced as capital letters in Table 5.1.

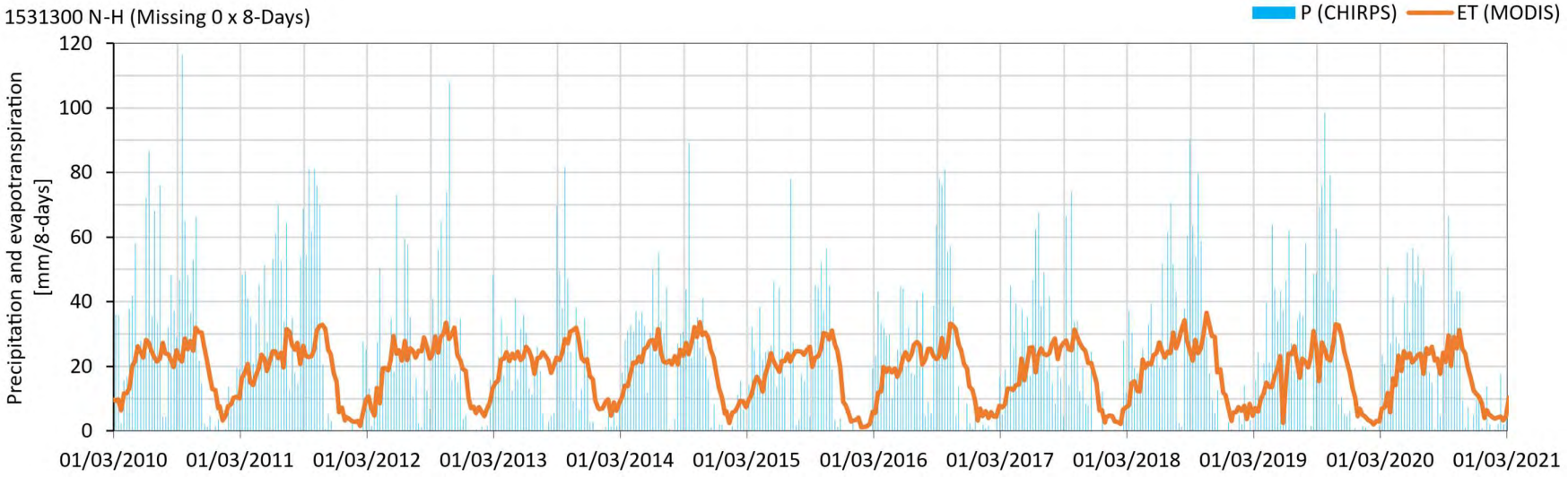
1531300 N-H (Missing 0 x 8-Days)
P (CHIRPS)
ET (MODIS)
Precipitation and evapotranspiration [mm/8-days]
120
100
80
60
40
20
0
01/03/2010
01/03/2011
01/03/2012
01/03/2013
01/03/2014
01/03/2015
01/03/2016
01/03/2017
01/03/2018
01/03/2019
01/03/2020
01/03/2021

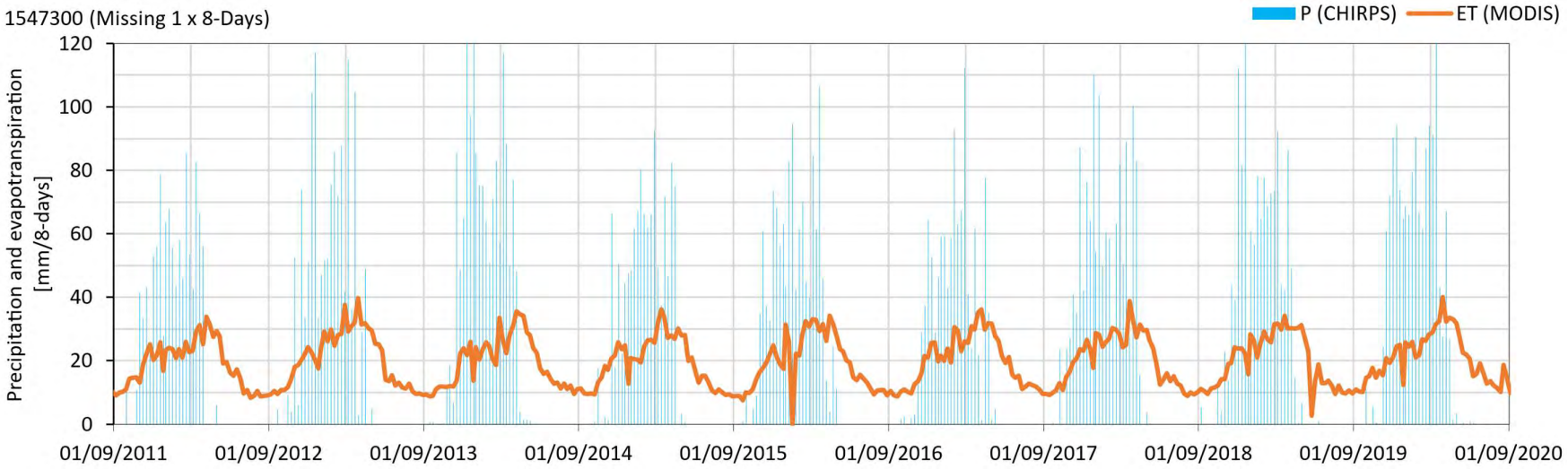
1547300 (Missing 1 x 8-Days)
P (CHIRPS)
ET (MODIS)
Precipitation and evapotranspiration [mm/8-days]
120
100
80
60
40
20
0
01/09/2011
01/09/2012
01/09/2013
01/09/2014
01/09/2015
01/09/2016
01/09/2017
01/09/2018
01/09/2019
01/09/2020

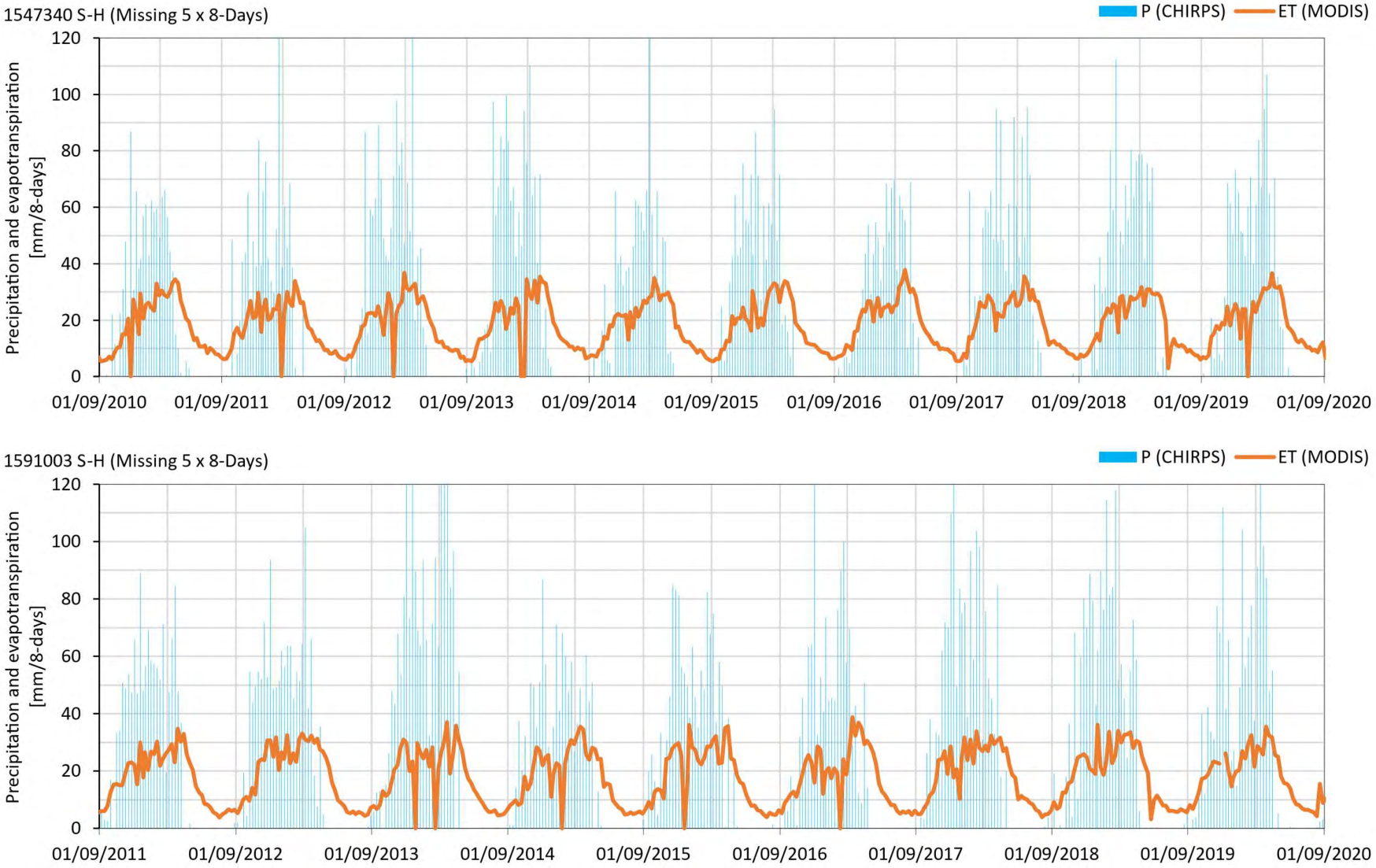
1547340 S-H (Missing 5 x 8-Days)
P (CHIRPS)
ET (MODIS)
Precipitation and evapotranspiration [mm/8-days]
120
100
80
60
40
20
0
01/09/2010
01/09/2011
01/09/2012
01/09/2013
01/09/2014
01/09/2015
01/09/2016
01/09/2017
01/09/2018
01/09/2019
01/09/2020
1591003 S-H (Missing 5 x 8-Days)
P (CHIRPS)
ET (MODIS)
Precipitation and evapotranspiration [mm/8-days]
120
100
80
60
40
20
0
01/09/2011
01/09/2012
01/09/2013
01/09/2014
01/09/2015
01/09/2016
01/09/2017
01/09/2018
01/09/2019
01/09/2020

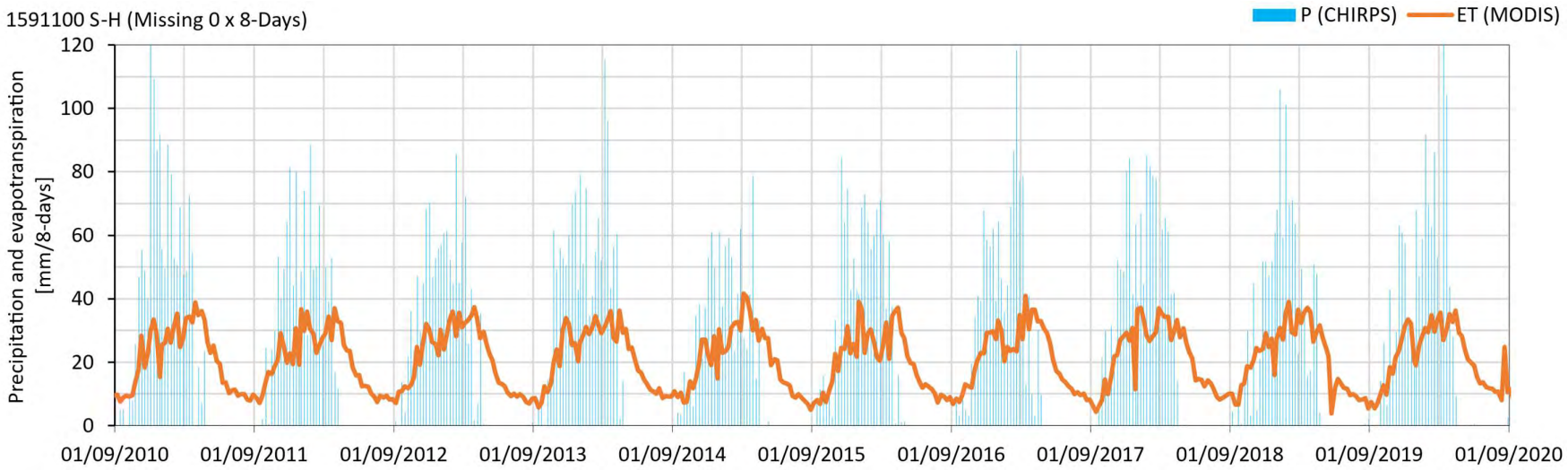
1591100 S-H (Missing 0 x 8-Days)
P (CHIRPS)
ET (MODIS)
Precipitation and evapotranspiration [mm/8-days]
120
100
80
60
40
20
0
01/09/2010
01/09/2011
01/09/2012
01/09/2013
01/09/2014
01/09/2015
01/09/2016
01/09/2017
01/09/2018
01/09/2019
01/09/2020

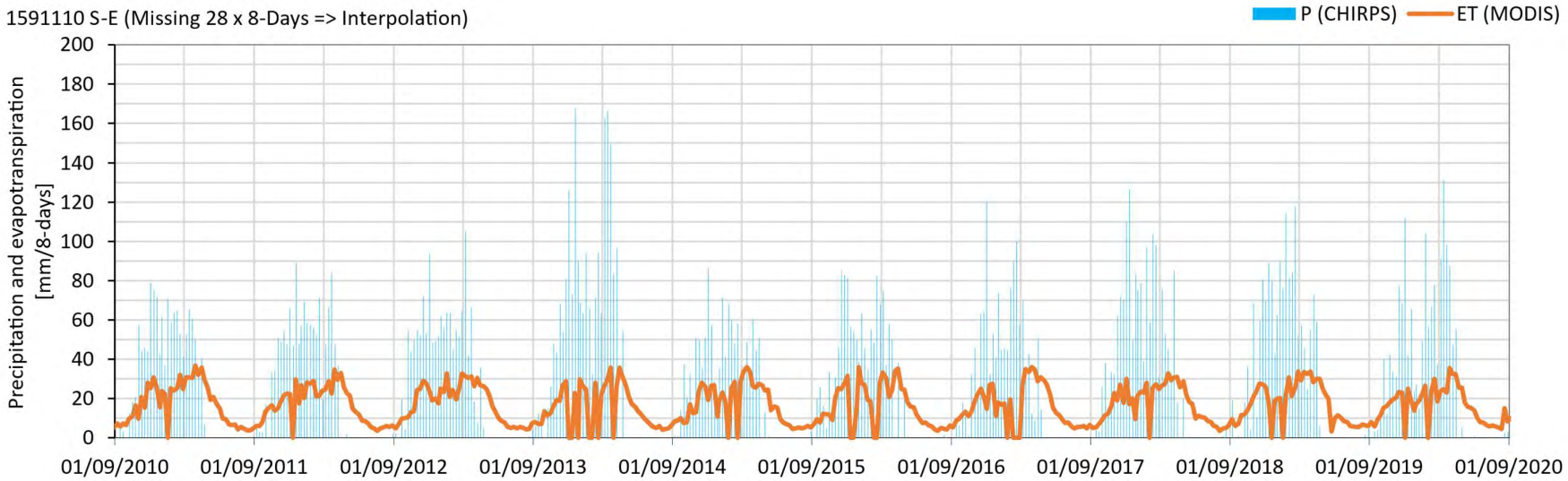
1591110 S-E (Missing 28 x 8-Days => Interpolation)
P (CHIRPS)
ET (MODIS)
Precipitation and evapotranspiration [mm/8-days]
200
180
160
140
120
100
80
60
40
20
0
01/09/2010
01/09/2011
01/09/2012
01/09/2013
01/09/2014
01/09/2015
01/09/2016
01/09/2017
01/09/2018
01/09/2019
01/09/2020

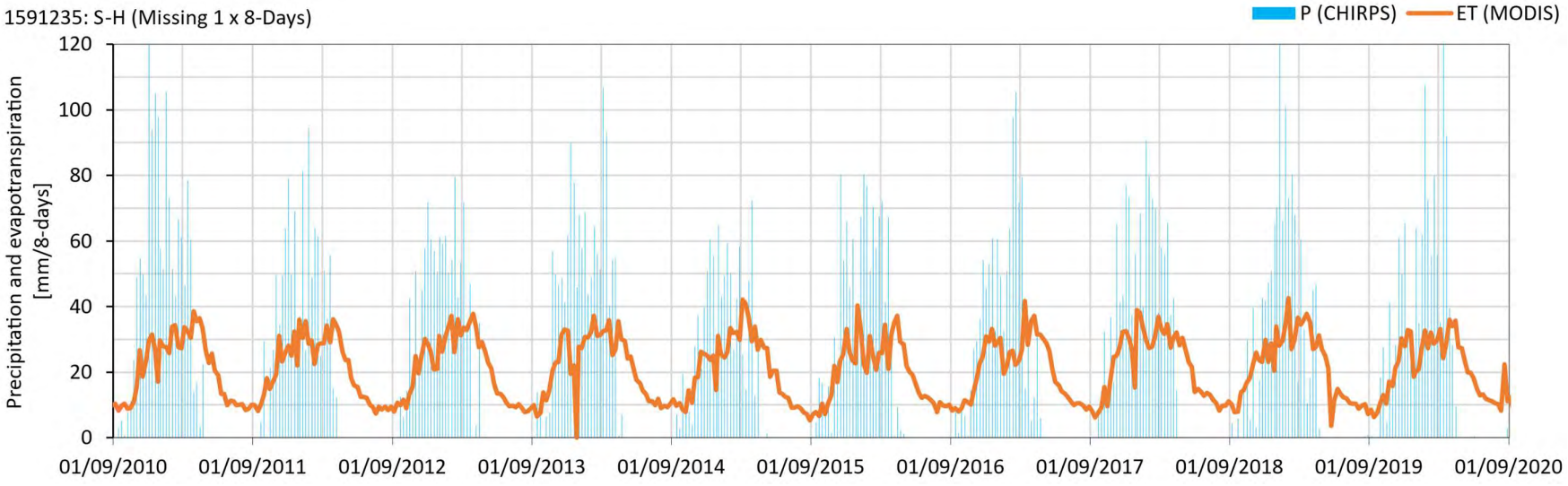
1591235: S-H (Missing 1 x 8-Days)
P (CHIRPS)
ET (MODIS)
Precipitation and evapotranspiration [mm/8-days]
120
100
80
60
40
20
0
01/09/2010
01/09/2011
01/09/2012
01/09/2013
01/09/2014
01/09/2015
01/09/2016
01/09/2017
01/09/2018
01/09/2019
01/09/2020

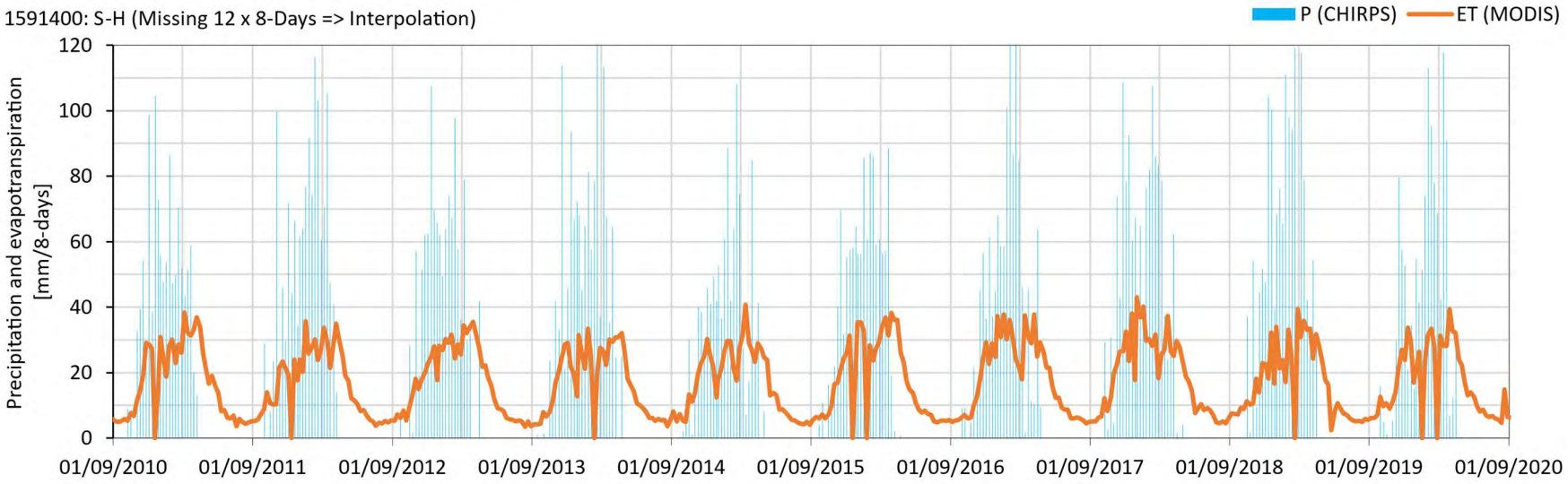
1591400: S-H (Missing 12 x 8-Days => Interpolation)
P (CHIRPS)
ET (MODIS)
Precipitation and evapotranspiration [mm/8-days]
120
100
80
60
40
20
0
01/09/2010
01/09/2011
01/09/2012
01/09/2013
01/09/2014
01/09/2015
01/09/2016
01/09/2017
01/09/2018
01/09/2019
01/09/2020

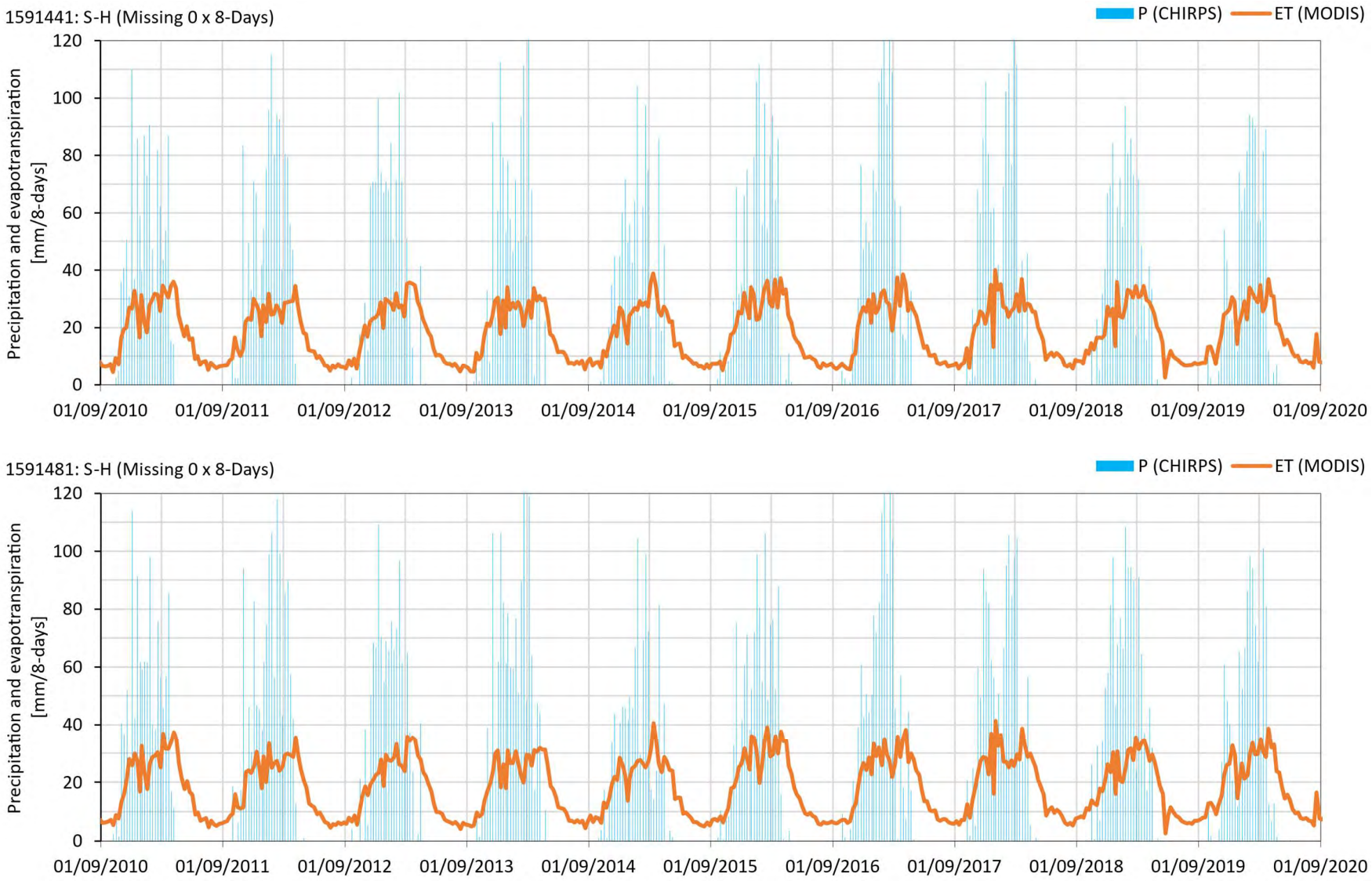
1591441: S-H (Missing 0 x 8-Days)
P (CHIRPS)
ET (MODIS)
Precipitation and evapotranspiration [mm/8-days]
120
100
80
60
40
20
0
01/09/2010
01/09/2011
01/09/2012
01/09/2013
01/09/2014
01/09/2015
01/09/2016
01/09/2017
01/09/2018
01/09/2019
01/09/2020
1591481: S-H (Missing 0 x 8-Days)
P (CHIRPS)
ET (MODIS)
Precipitation and evapotranspiration [mm/8-days]
120
100
80
60
40
20
0
01/09/2010
01/09/2011
01/09/2012
01/09/2013
01/09/2014
01/09/2015
01/09/2016
01/09/2017
01/09/2018
01/09/2019
01/09/2020

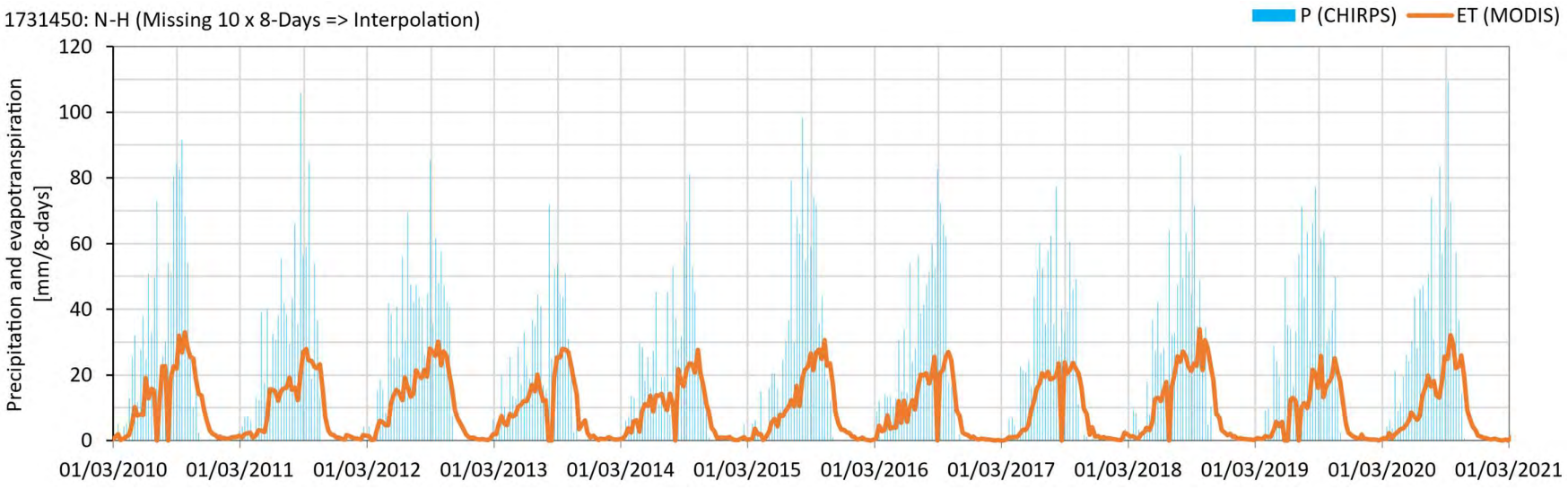
1731450: N-H (Missing 10 x 8-Days => Interpolation)
P (CHIRPS)
ET (MODIS)
Precipitation and evapotranspiration [mm/8-days]
120
100
80
60
40
20
0
01/03/2010
01/03/2011
01/03/2012
01/03/2013
01/03/2014
01/03/2015
01/03/2016
01/03/2017
01/03/2018
01/03/2019
01/03/2020
01/03/2021

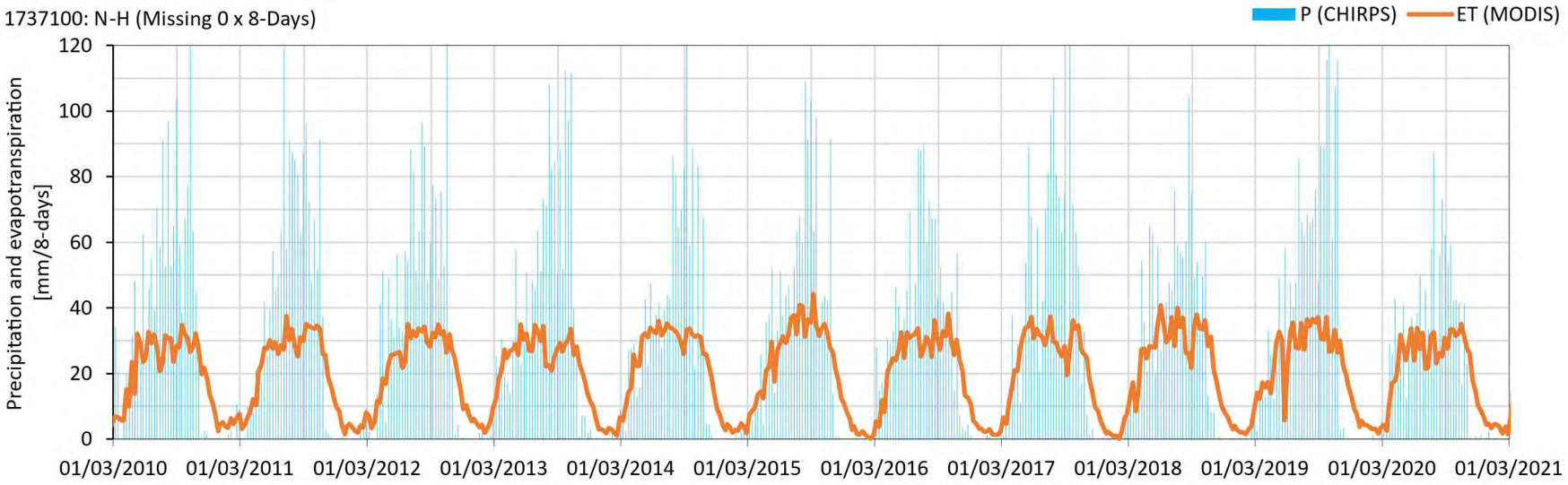
1737100: N-H (Missing 0 x 8-Days)
P (CHIRPS)
ET (MODIS)
Precipitation and evapotranspiration [mm/8-days]
120
100
80
60
40
20
0
01/03/2010
01/03/2011
01/03/2012
01/03/2013
01/03/2014
01/03/2015
01/03/2016
01/03/2017
01/03/2018
01/03/2019
01/03/2020
01/03/2021

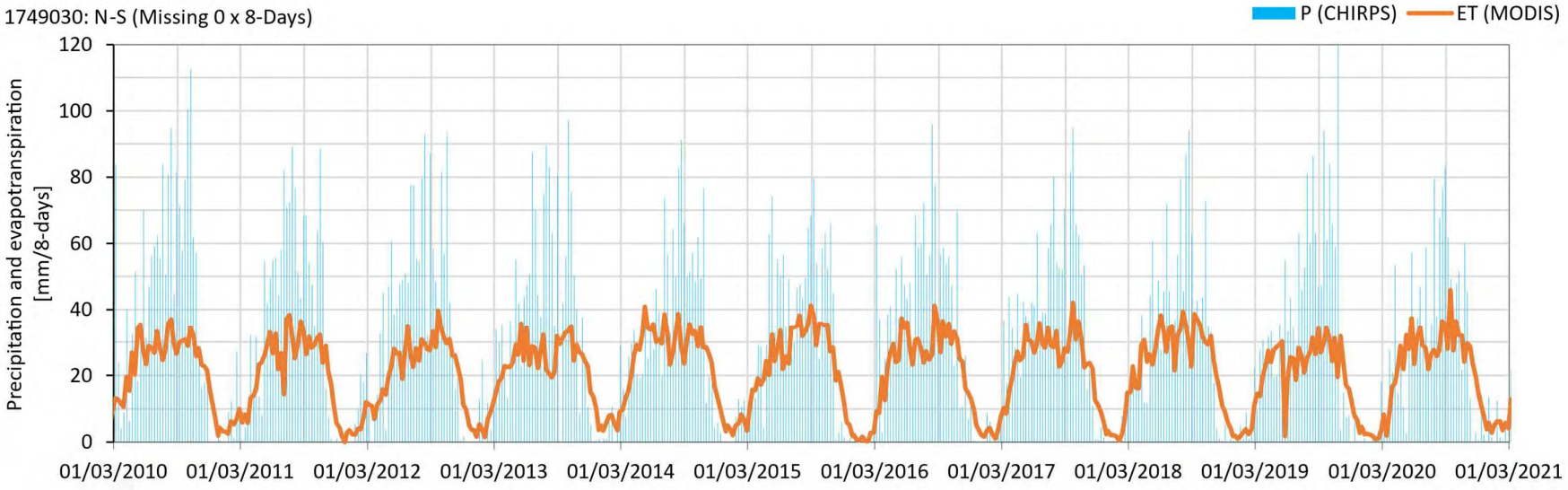
1749030: N-S (Missing 0 x 8-Days)
P (CHIRPS)
ET (MODIS)
Precipitation and evapotranspiration [mm/8-days]
120
100
80
60
40
20
0
01/03/2010
01/03/2011
01/03/2012
01/03/2013
01/03/2014
01/03/2015
01/03/2016
01/03/2017
01/03/2018
01/03/2019
01/03/2020
01/03/2021

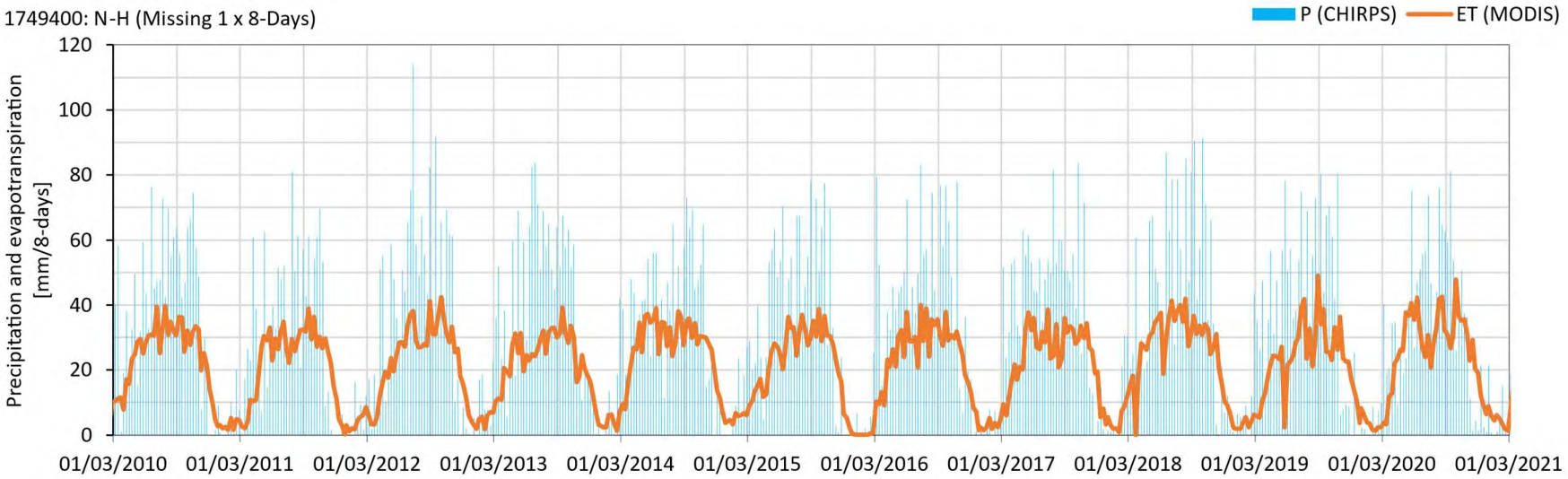
1749400: N-H (Missing 1 x 8-Days)
P (CHIRPS)
ET (MODIS)
Precipitation and evapotranspiration [mm/8-days]
120
100
80
60
40
20
0
01/03/2010
01/03/2011
01/03/2012
01/03/2013
01/03/2014
01/03/2015
01/03/2016
01/03/2017
01/03/2018
01/03/2019
01/03/2020
01/03/2021

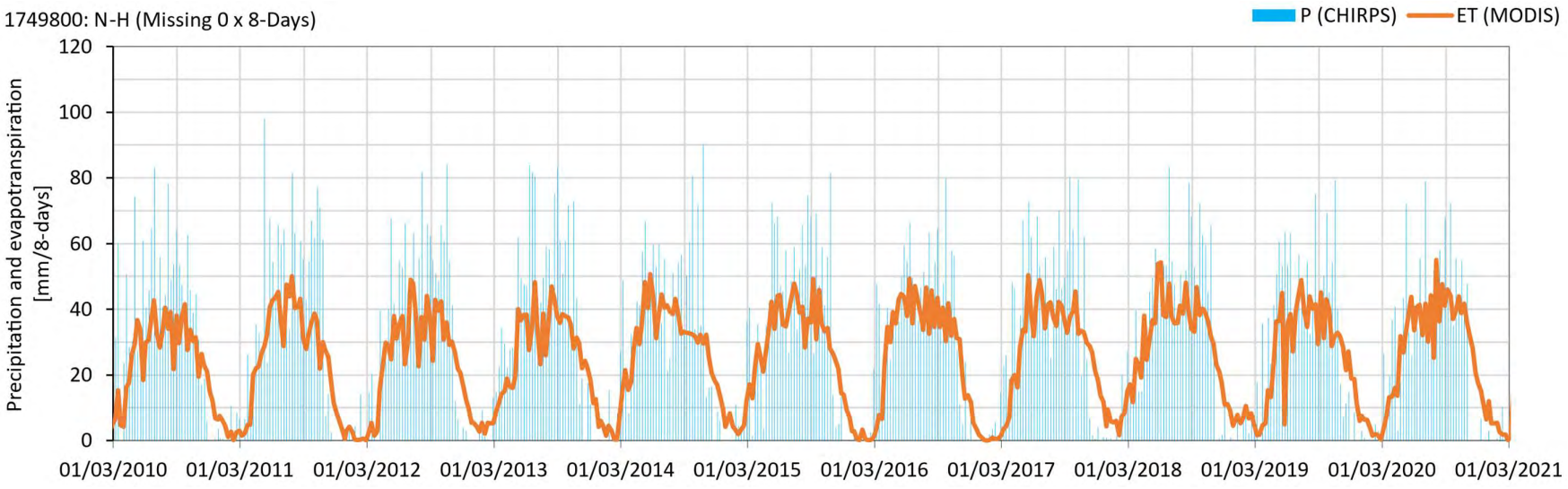
1749800: N-H (Missing 0 x 8-Days)
P (CHIRPS)
ET (MODIS)
Precipitation and evapotranspiration [mm/8-days]
120
100
80
60
40
20
0
01/03/2010
01/03/2011
01/03/2012
01/03/2013
01/03/2014
01/03/2015
01/03/2016
01/03/2017
01/03/2018
01/03/2019
01/03/2020
01/03/2021

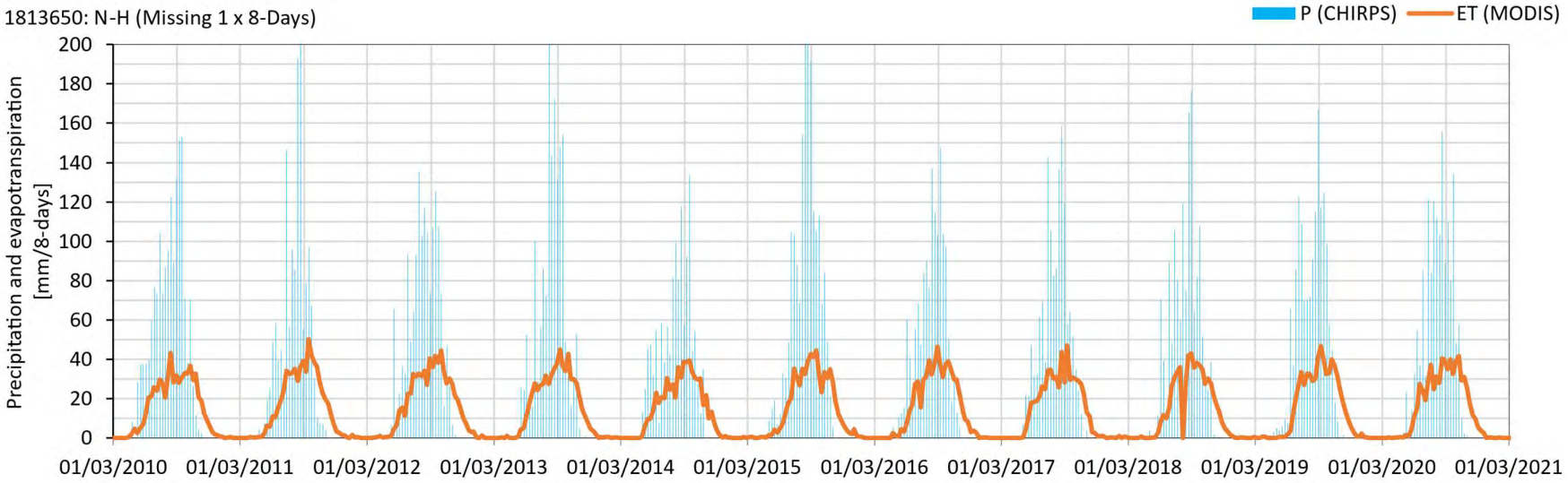
1813650: N-H (Missing 1 x 8-Days)
P (CHIRPS)
ET (MODIS)
Precipitation and evapotranspiration [mm/8-days]
200
180
160
140
120
100
80
60
40
20
0
01/03/2010
01/03/2011
01/03/2012
01/03/2013
01/03/2014
01/03/2015
01/03/2016
01/03/2017
01/03/2018
01/03/2019
01/03/2020
01/03/2021

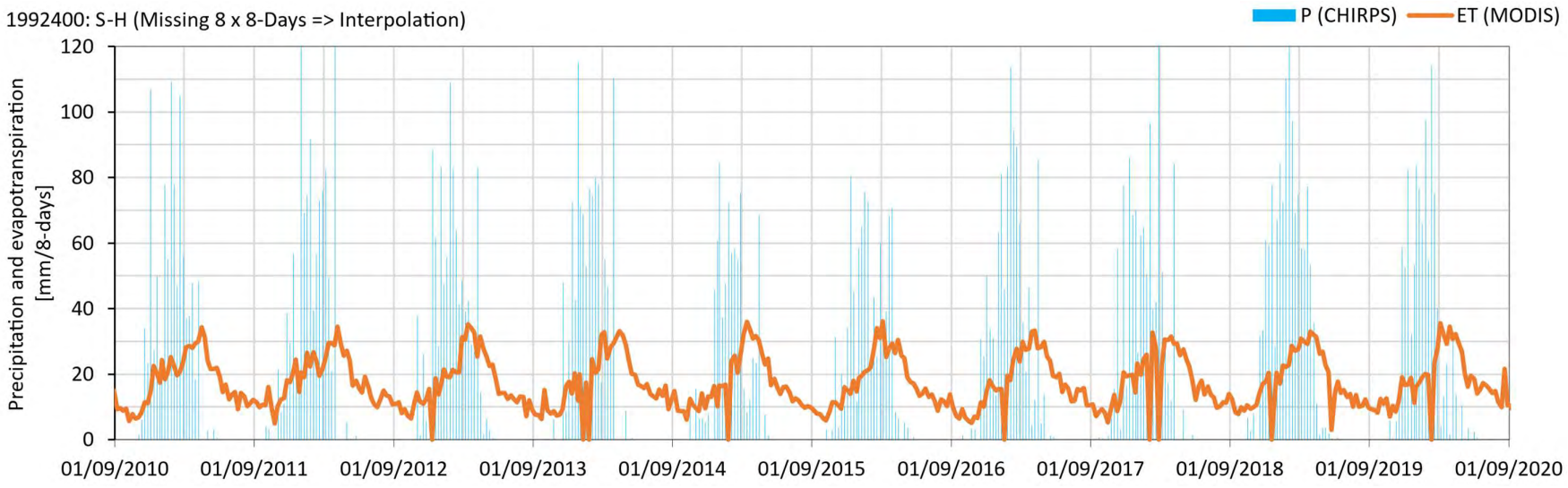
1992400: S-H (Missing 8 x 8-Days => Interpolation)
P (CHIRPS)
ET (MODIS)
Precipitation and evapotranspiration [mm/8-days]
120
100
80
60
40
20
0
01/09/2010
01/09/2011
01/09/2012
01/09/2013
01/09/2014
01/09/2015
01/09/2016
01/09/2017
01/09/2018
01/09/2019
01/09/2020

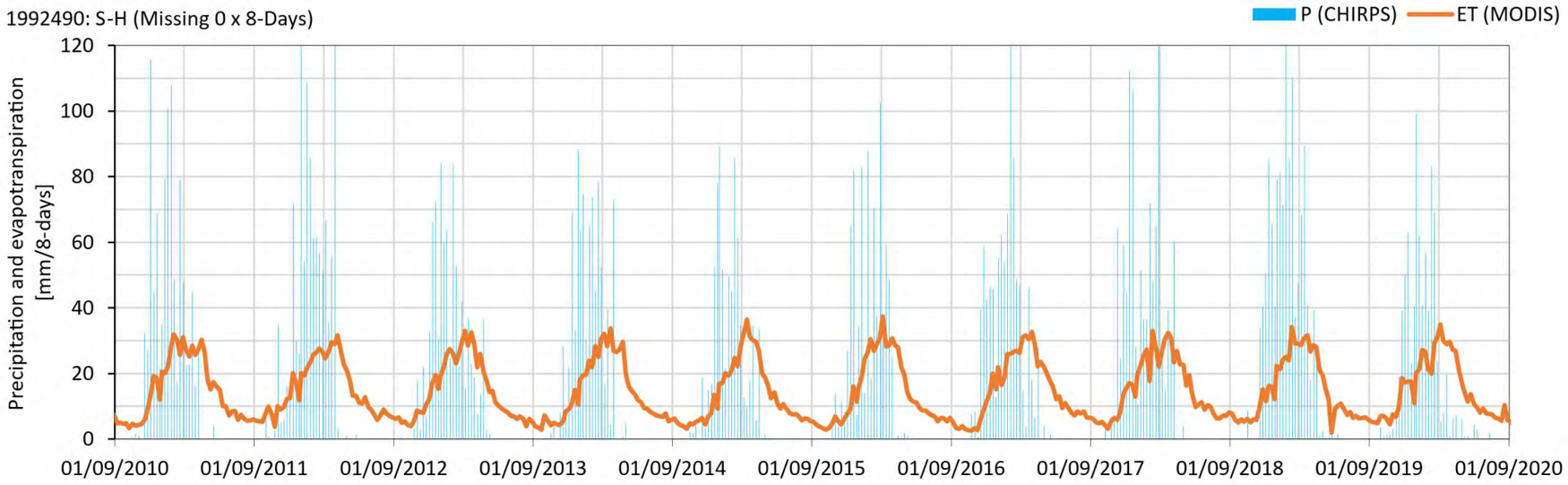
1992490: S-H (Missing 0 x 8-Days)
P (CHIRPS)
ET (MODIS)
Precipitation and evapotranspiration [mm/8-days]
120
100
80
60
40
20
0
01/09/2010
01/09/2011
01/09/2012
01/09/2013
01/09/2014
01/09/2015
01/09/2016
01/09/2017
01/09/2018
01/09/2019
01/09/2020

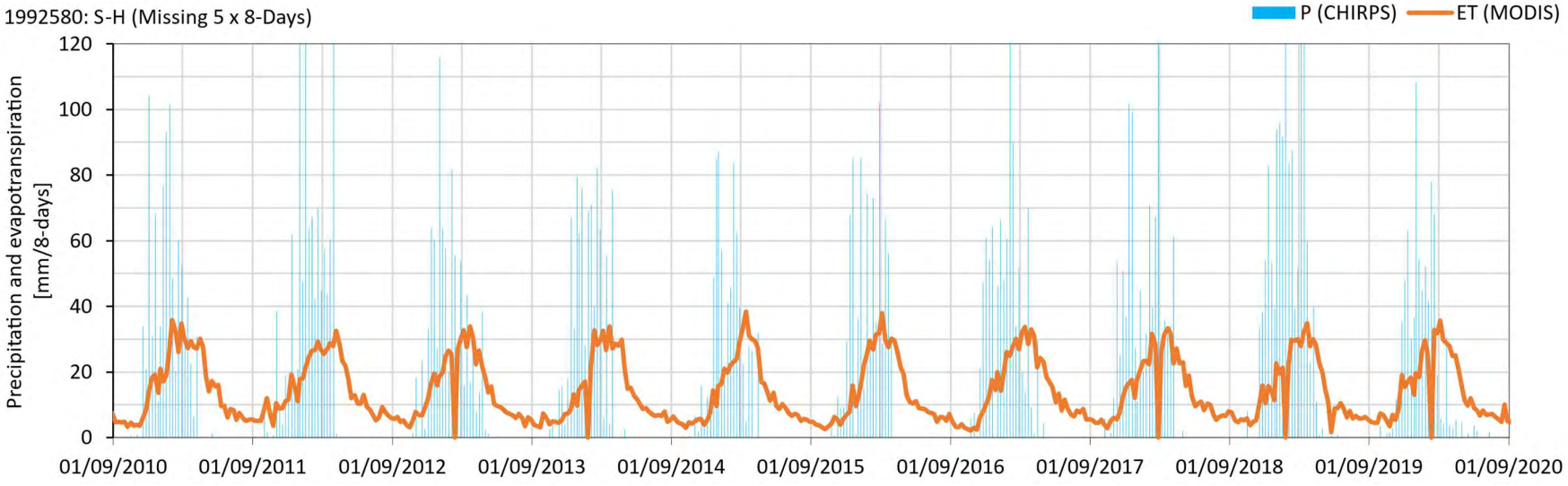
1992580: S-H (Missing 5 x 8-Days)
P (CHIRPS)
ET (MODIS)
Precipitation and evapotranspiration [mm/8-days]
120
100
80
60
40
20
0
01/09/2010
01/09/2011
01/09/2012
01/09/2013
01/09/2014
01/09/2015
01/09/2016
01/09/2017
01/09/2018
01/09/2019
01/09/2020

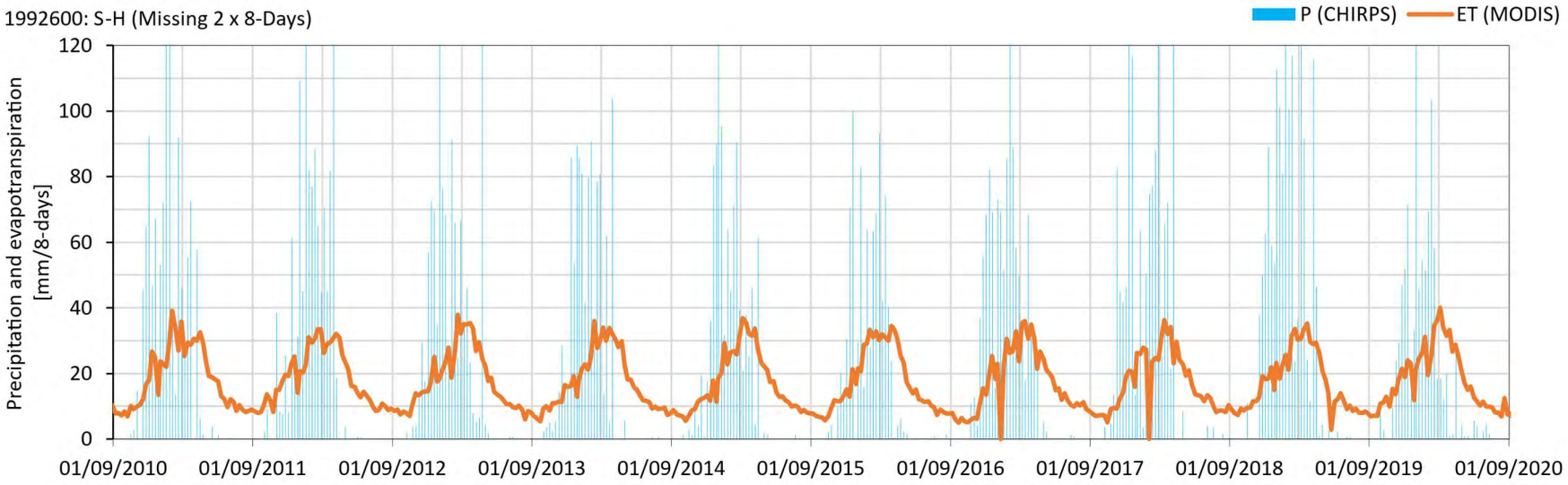
1992600: S-H (Missing 2 x 8-Days)
P (CHIRPS)
ET (MODIS)
Precipitation and evapotranspiration [mm/8-days]
120
100
80
60
40
20
0
01/09/2010
01/09/2011
01/09/2012
01/09/2013
01/09/2014
01/09/2015
01/09/2016
01/09/2017
01/09/2018
01/09/2019
01/09/2020

Appendix F: Hydrograph separation of the reference catchments

1. The program and codes for hydrograph separation are given in digital format.
2. The entire dataset for the 20 catchments is given in digital format.
3. The additional hydrograph separation data and parameter, i.e. Stream flow recession curves and recession parameter (a and b) are given in digital format.
4. The individual hydrographs of the 20 reference catchments are illustrated in the following figures. The catchments are labelled according to the GRDC id and referenced as capital letters in Table 5.1. In each figure are given:
    a. The discharge measurements obtained from GRDC.
    b. The base flow and runoff obtained from hydrograph separation.
    c. The precipitation from CHIRPS.

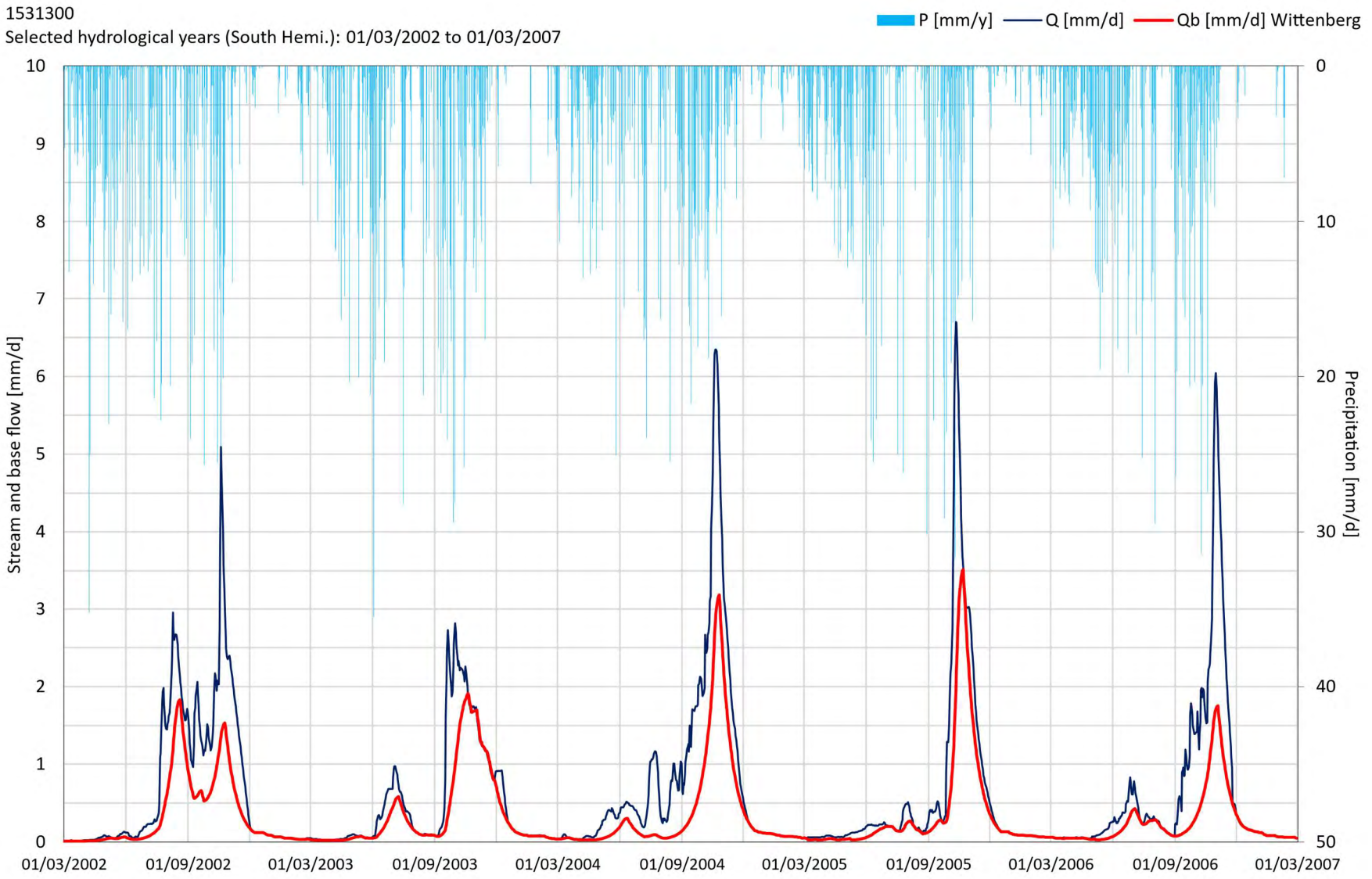
1531300
Selected hydrological years (South Hemi.): 01/03/2002 to 01/03/2007
P [mm/y]
Q [mm/d]
Qb [mm/d] Wittenberg
Stream and base flow [mm/d]
Precipitation [mm/d]
0
1
2
3
4
5
6
7
8
9
10
0
10
20
30
40
50
01/03/2002
01/09/2002
01/03/2003
01/09/2003
01/03/2004
01/09/2004
01/03/2005
01/09/2005
01/03/2006
01/09/2006
01/03/2007

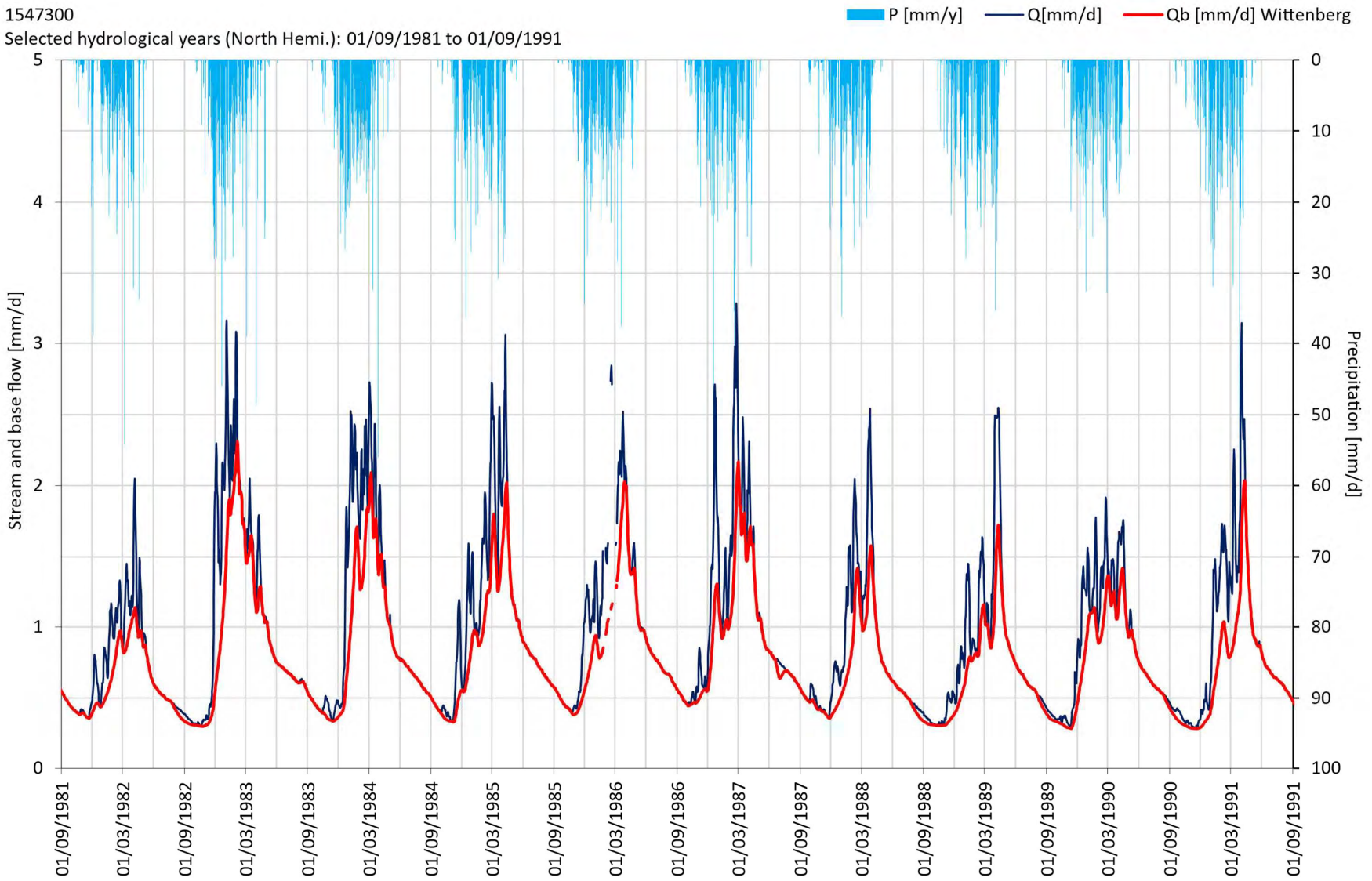
1547300
Selected hydrological years (North Hemi.): 01/09/1981 to 01/09/1991
P [mm/y]
Q[mm/d]
Qb [mm/d] Wittenberg
Stream and base flow [mm/d]
Precipitation [mm/d]
0
1
2
3
4
5
0
10
20
30
40
50
60
70
80
90
100
01/09/1981
01/03/1982
01/09/1982
01/03/1983
01/09/1983
01/03/1984
01/09/1984
01/03/1985
01/09/1985
01/03/1986
01/09/1986
01/03/1987
01/09/1987
01/03/1988
01/09/1988
01/03/1989
01/09/1989
01/03/1990
01/09/1990
01/03/1991
01/09/1991

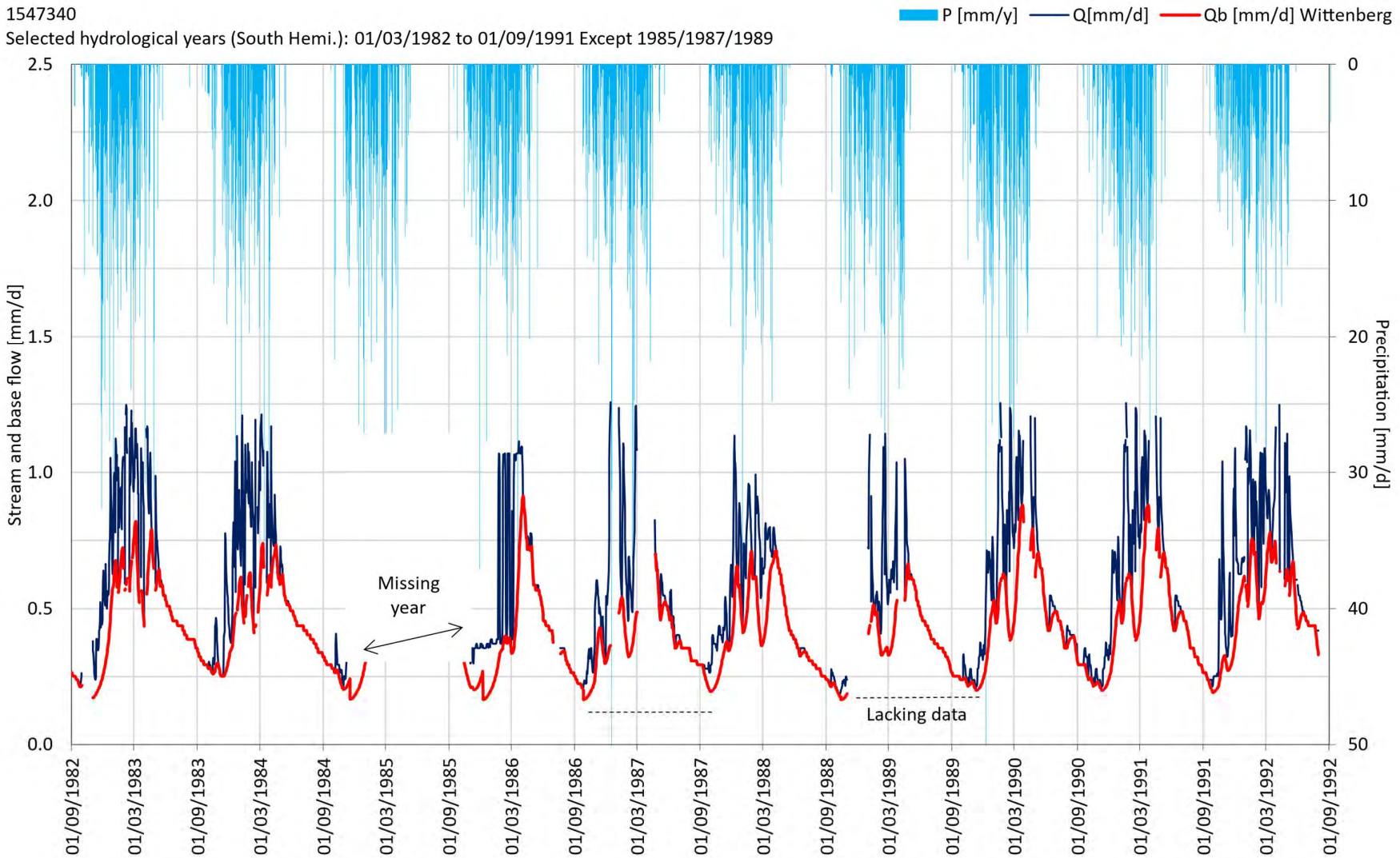
1547340
Selected hydrological years (South Hemi.): 01/03/1982 to 01/09/1991 Except 1985/1987/1989
P [mm/y]
Q[mm/d]
Qb [mm/d] Wittenberg
Stream and base flow [mm/d]
Precipitation [mm/d]
2.5
2.0
1.5
1.0
0.5
0.0
0
10
20
30
40
50
Missing year
Lacking data
01/09/1982
01/03/1983
01/09/1983
01/03/1984
01/09/1984
01/03/1985
01/09/1985
01/03/1986
01/09/1986
01/03/1987
01/09/1987
01/03/1988
01/09/1988
01/03/1989
01/09/1989
01/03/1990
01/09/1990
01/03/1991
01/09/1991
01/03/1992
01/09/1992

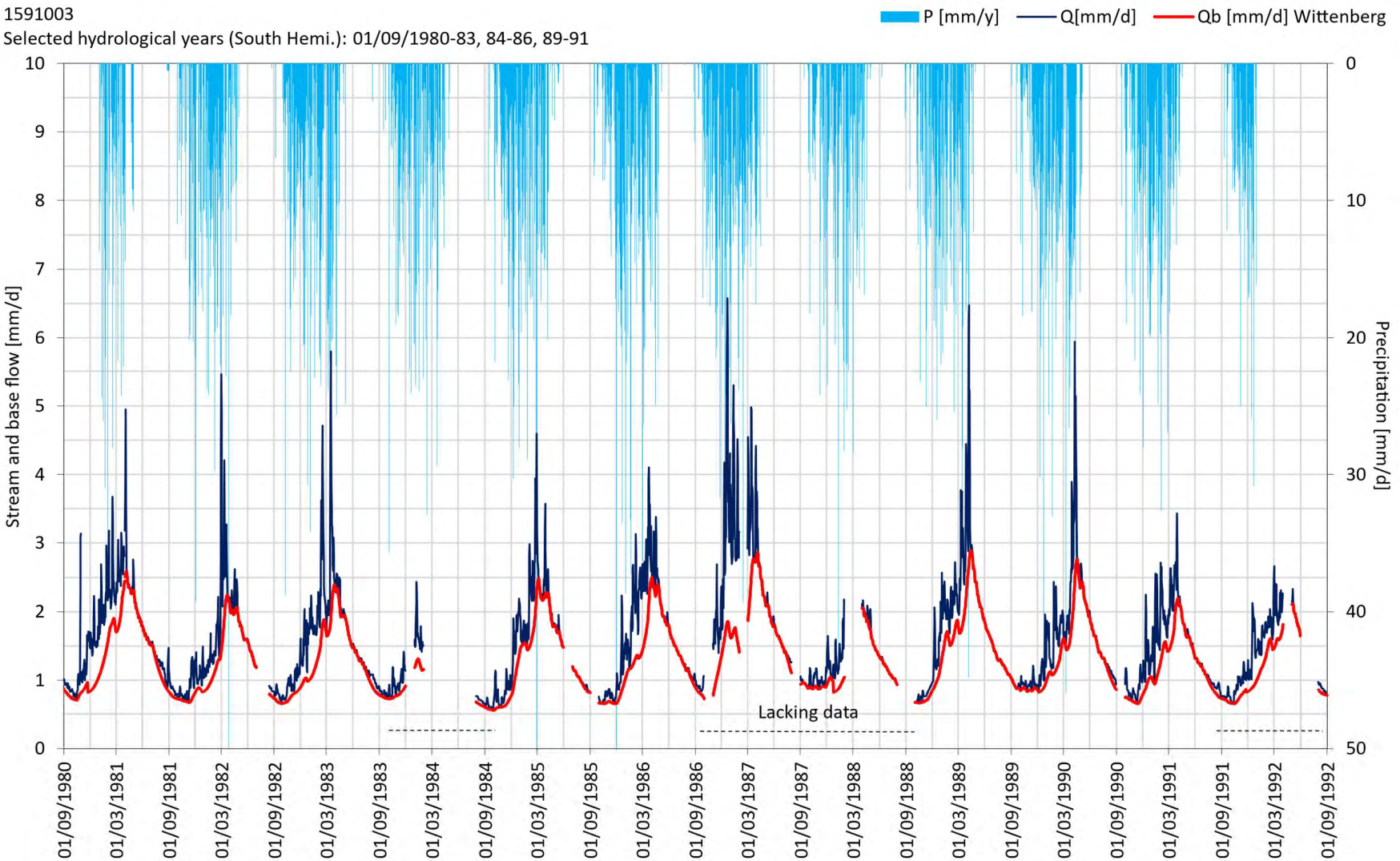
1591003
Selected hydrological years (South Hemi.): 01/09/1980-83, 84-86, 89-91
P [mm/y]
Q[mm/d]
Qb [mm/d] Wittenberg
Stream and base flow [mm/d]
Precipitation [mm/d]
Lacking data
01/09/1980
01/03/1981
01/09/1981
01/03/1982
01/09/1982
01/03/1983
01/09/1983
01/03/1984
01/09/1984
01/03/1985
01/09/1985
01/03/1986
01/09/1986
01/03/1987
01/09/1987
01/03/1988
01/09/1988
01/03/1989
01/09/1989
01/03/1990
01/09/1990
01/03/1991
01/09/1991
01/03/1992
01/09/1992

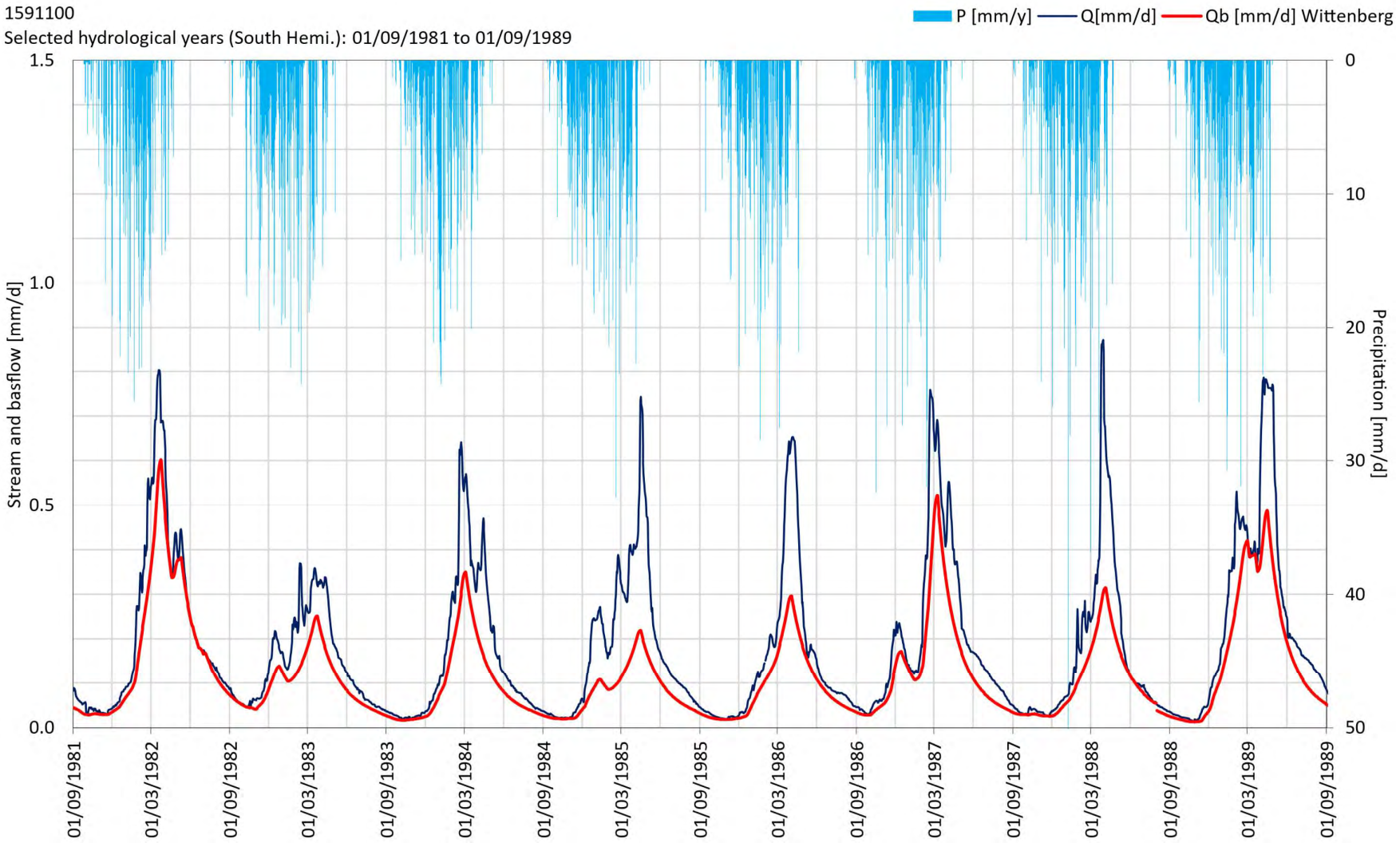
1591100
Selected hydrological years (South Hemi.): 01/09/1981 to 01/09/1989
P [mm/y]
Q[mm/d]
Qb [mm/d] Wittenberg
Stream and basflow [mm/d]
Precipitation [mm/d]
1.5
1.0
0.5
0.0
0
10
20
30
40
50
01/09/1981
01/03/1982
01/09/1982
01/03/1983
01/09/1983
01/03/1984
01/09/1984
01/03/1985
01/09/1985
01/03/1986
01/09/1986
01/03/1987
01/09/1987
01/03/1988
01/09/1988
01/03/1989
01/09/1989

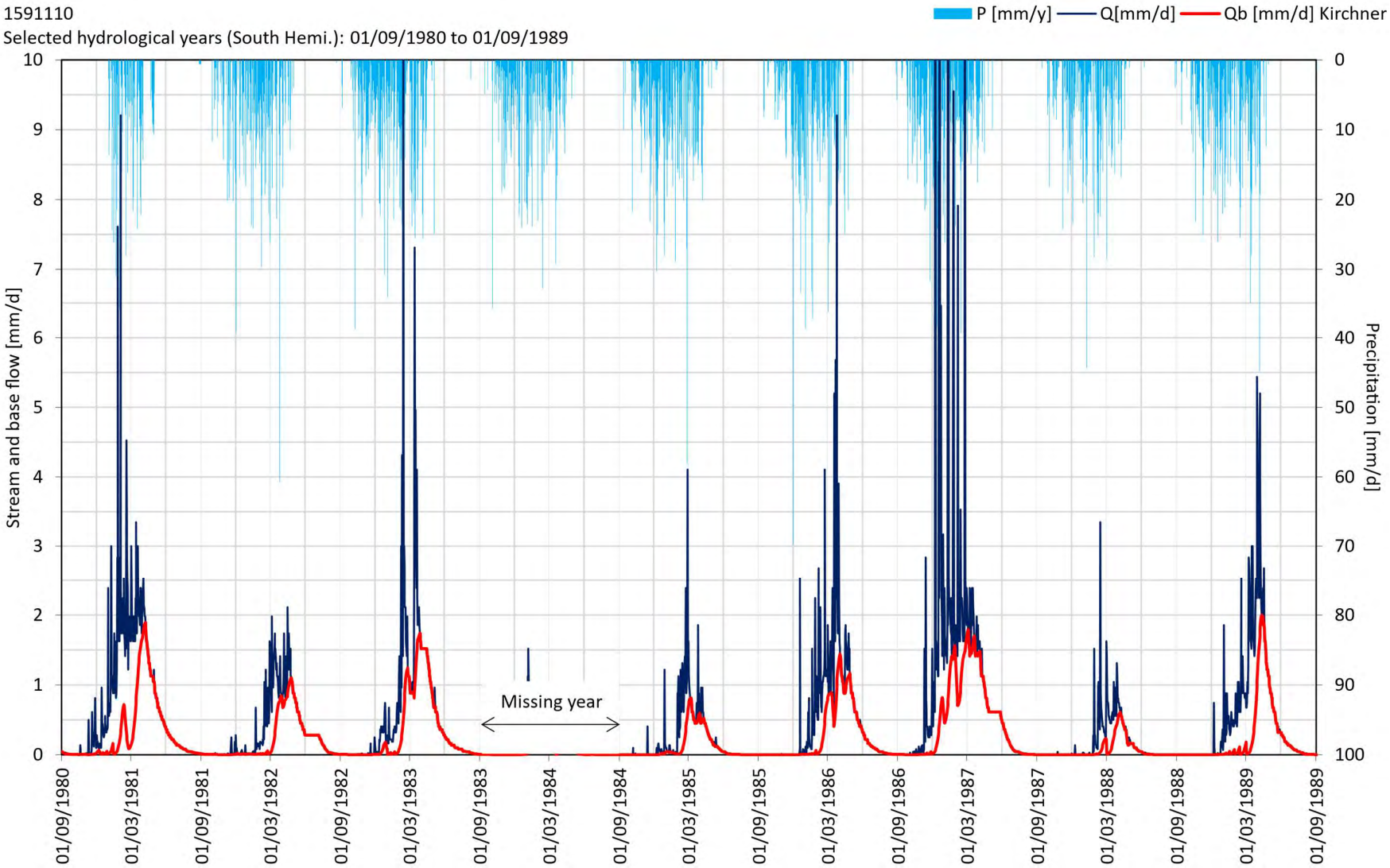
1591110
Selected hydrological years (South Hemi.): 01/09/1980 to 01/09/1989
P [mm/y]
Q[mm/d]
Qb [mm/d] Kirchner
Stream and base flow [mm/d]
Precipitation [mm/d]
Missing year
01/09/1980
01/03/1981
01/09/1981
01/03/1982
01/09/1982
01/03/1983
01/09/1983
01/03/1984
01/09/1984
01/03/1985
01/09/1985
01/03/1986
01/09/1986
01/03/1987
01/09/1987
01/03/1988
01/09/1988
01/03/1989
01/09/1989

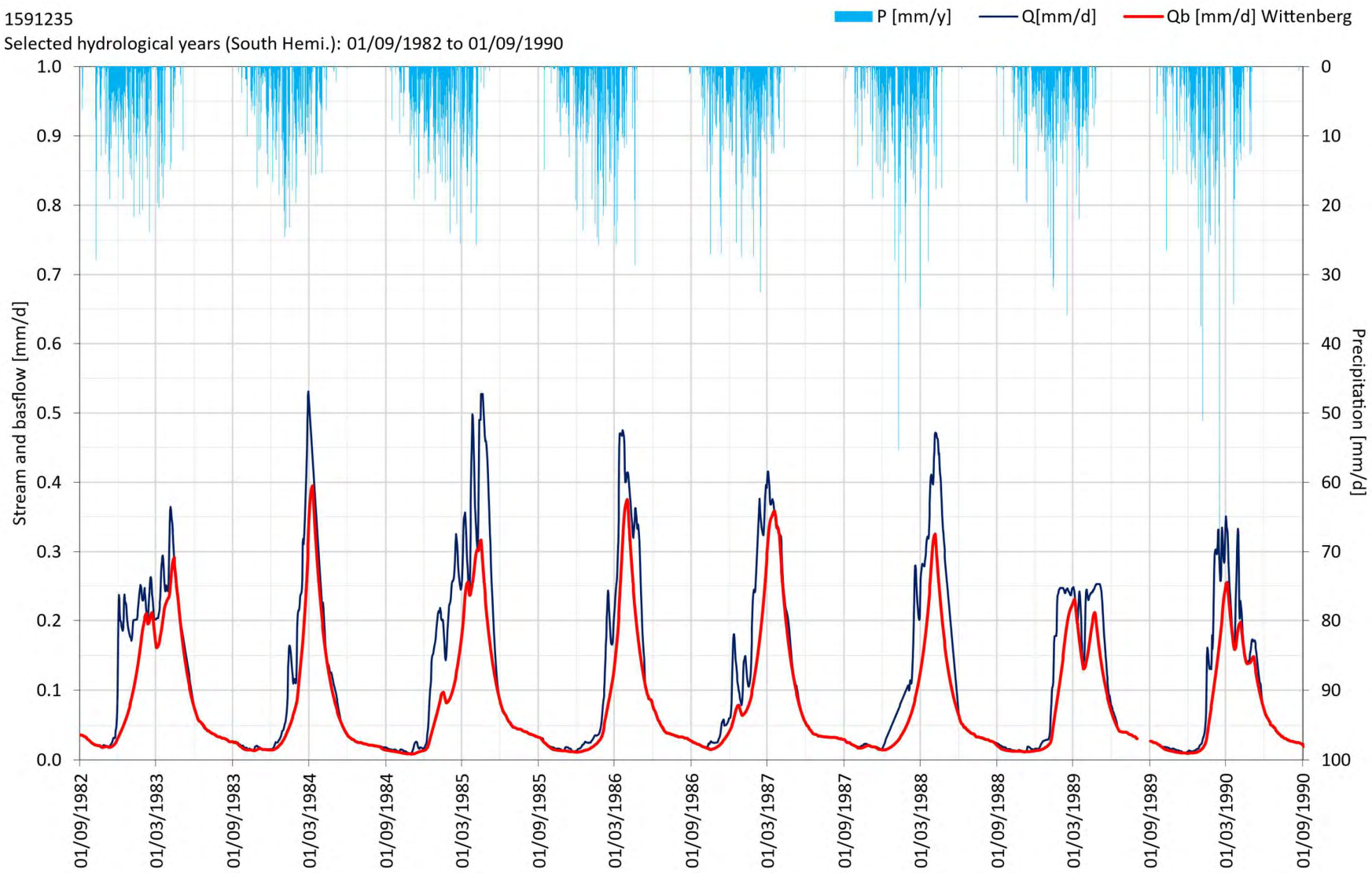
1591235
Selected hydrological years (South Hemi.): 01/09/1982 to 01/09/1990
P [mm/y]
Q[mm/d]
Qb [mm/d] Wittenberg
Stream and basflow [mm/d]
Precipitation [mm/d]
1.0
0.9
0.8
0.7
0.6
0.5
0.4
0.3
0.2
0.1
0.0
0
10
20
30
40
50
60
70
80
90
100
01/09/1982
01/03/1983
01/09/1983
01/03/1984
01/09/1984
01/03/1985
01/09/1985
01/03/1986
01/09/1986
01/03/1987
01/09/1987
01/03/1988
01/09/1988
01/03/1989
01/09/1989
01/03/1990
01/09/1990

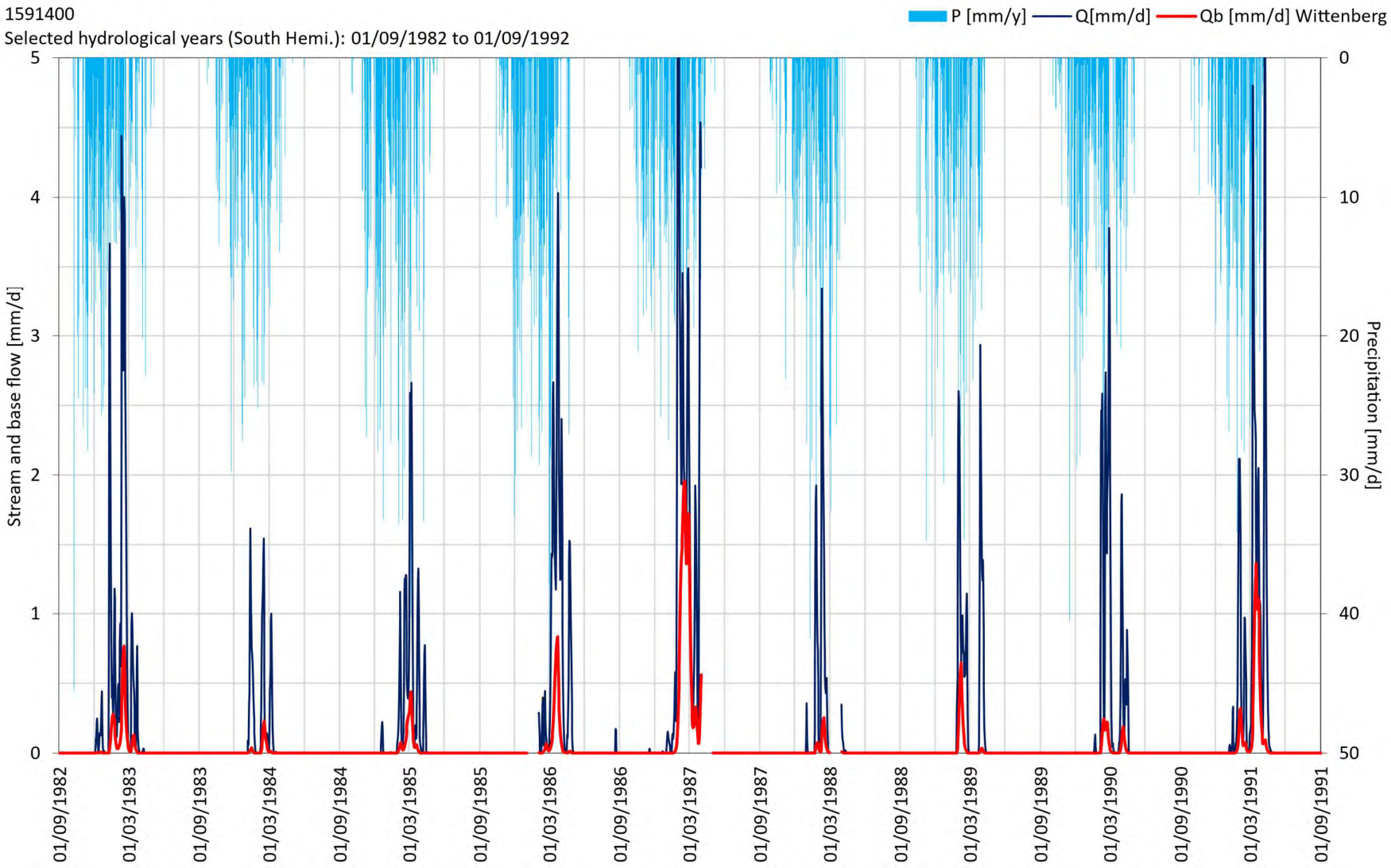
1591400
Selected hydrological years (South Hemi.): 01/09/1982 to 01/09/1992
P [mm/y]
Q[mm/d]
Qb [mm/d] Wittenberg
Stream and base flow [mm/d]
Precipitation [mm/d]
0
1
2
3
4
5
0
10
20
30
40
50
01/09/1982
01/03/1983
01/09/1983
01/03/1984
01/09/1984
01/03/1985
01/09/1985
01/03/1986
01/09/1986
01/03/1987
01/09/1987
01/03/1988
01/09/1988
01/03/1989
01/09/1989
01/03/1990
01/09/1990
01/03/1991
01/09/1991

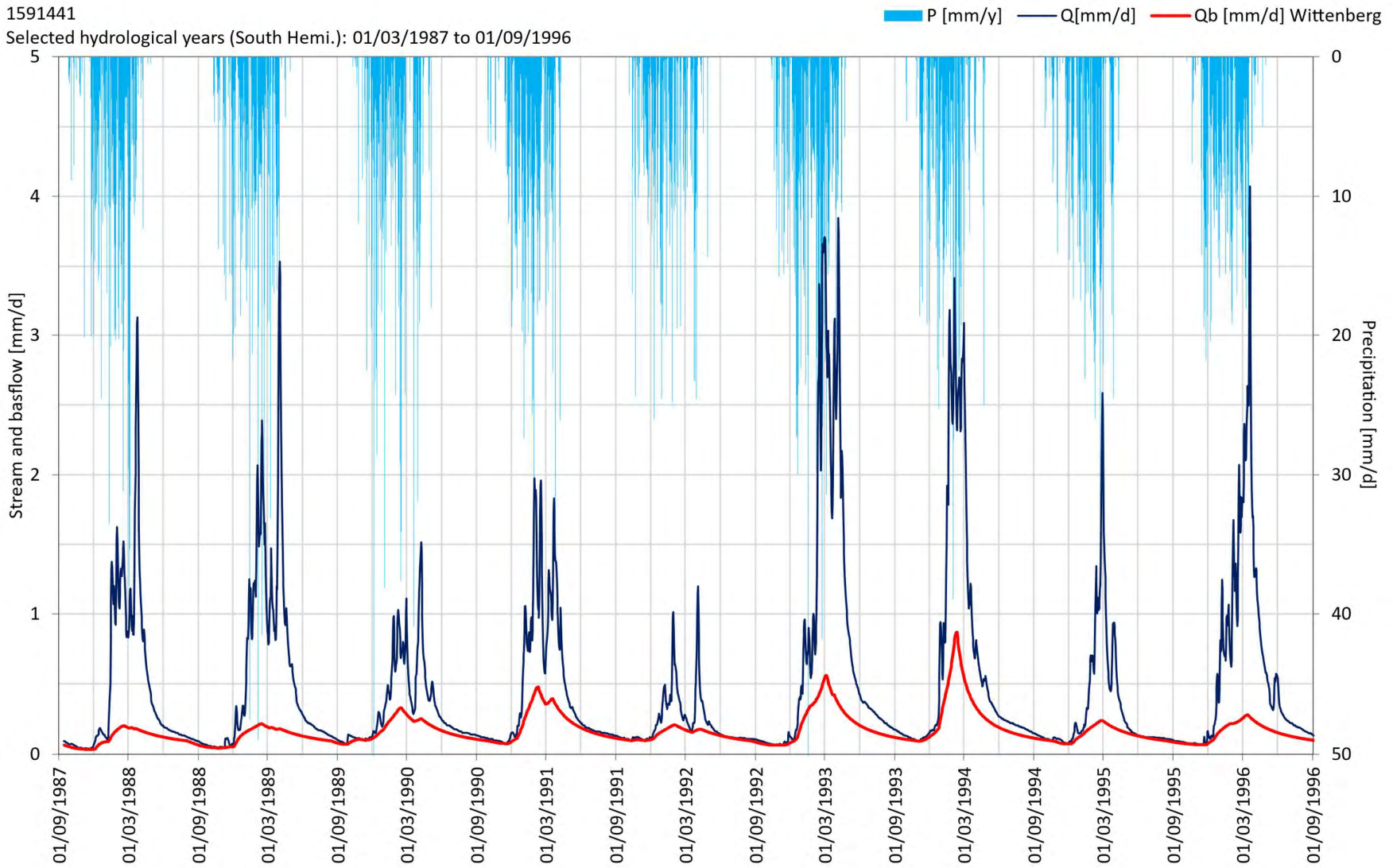
1591441
Selected hydrological years (South Hemi.): 01/03/1987 to 01/09/1996
P [mm/y]
Q[mm/d]
Qb [mm/d] Wittenberg
Stream and basflow [mm/d]
Precipitation [mm/d]
0
1
2
3
4
5
0
10
20
30
40
50
01/09/1987
01/03/1988
01/09/1988
01/03/1989
01/09/1989
01/03/1990
01/09/1990
01/03/1991
01/09/1991
01/03/1992
01/09/1992
01/03/1993
01/09/1993
01/03/1994
01/09/1994
01/03/1995
01/09/1995
01/03/1996
01/09/1996

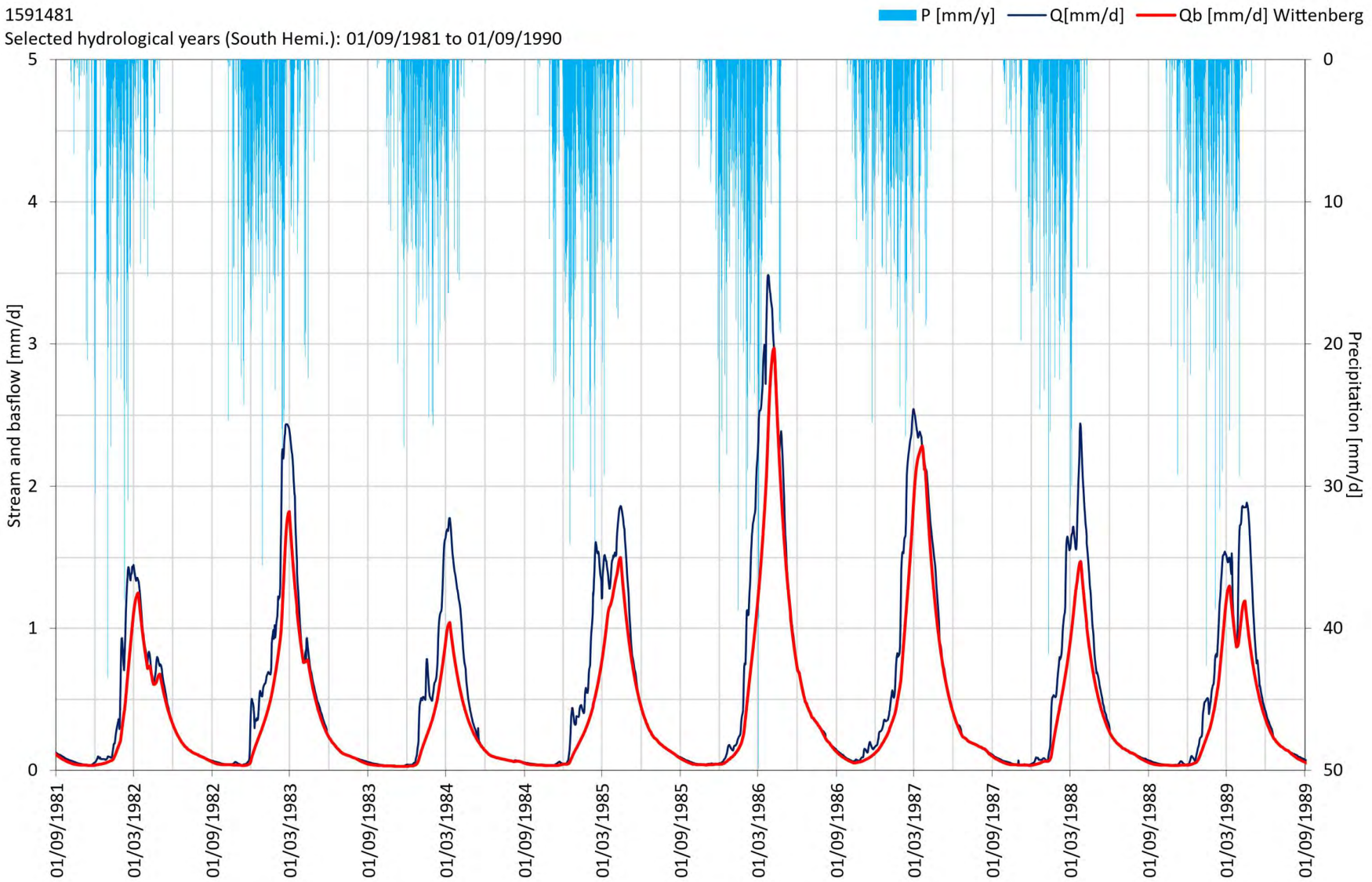
1591481
Selected hydrological years (South Hemi.): 01/09/1981 to 01/09/1990
P [mm/y]
Q[mm/d]
Qb [mm/d] Wittenberg
Stream and basflow [mm/d]
Precipitation [mm/d]
0
1
2
3
4
5
0
10
20
30
40
50
01/09/1981
01/03/1982
01/09/1982
01/03/1983
01/09/1983
01/03/1984
01/09/1984
01/03/1985
01/09/1985
01/03/1986
01/09/1986
01/03/1987
01/09/1987
01/03/1988
01/09/1988
01/03/1989
01/09/1989

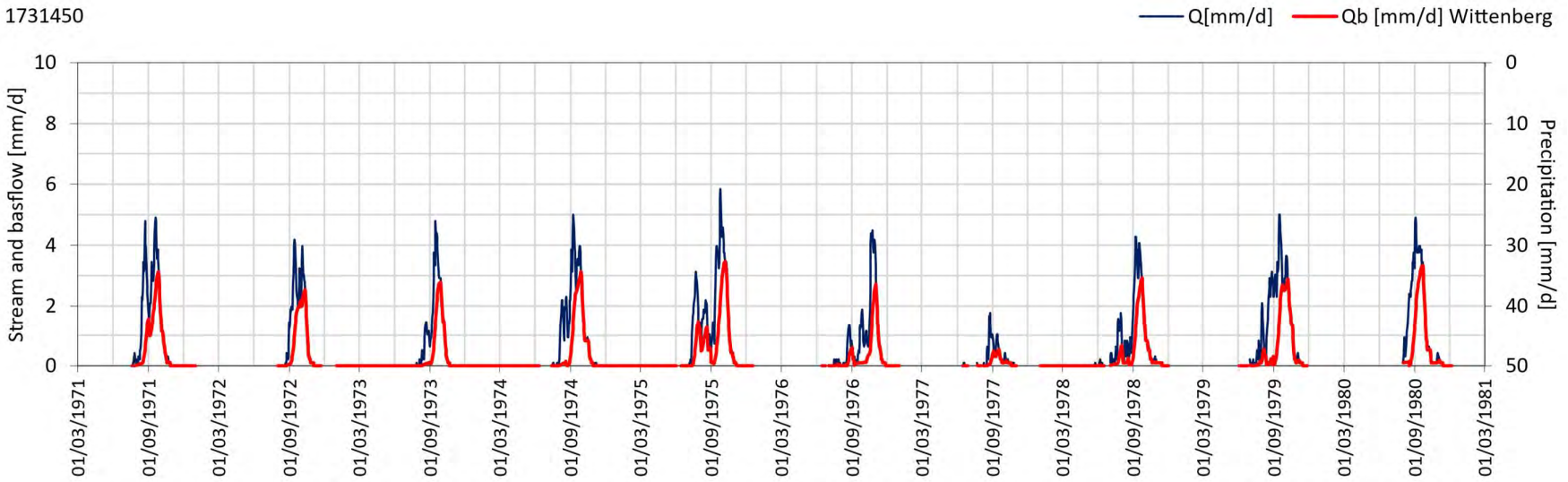
1731450
Q[mm/d]
Qb [mm/d] Wittenberg
Stream and basflow [mm/d]
Precipitation [mm/d]
0
2
4
6
8
10
10
20
30
40
50
01/03/1971
01/09/1971
01/03/1972
01/09/1972
01/03/1973
01/09/1973
01/03/1974
01/09/1974
01/03/1975
01/09/1975
01/03/1976
01/09/1976
01/03/1977
01/09/1977
01/03/1978
01/09/1978
01/03/1979
01/09/1979
01/03/1980
01/09/1980
01/03/1981

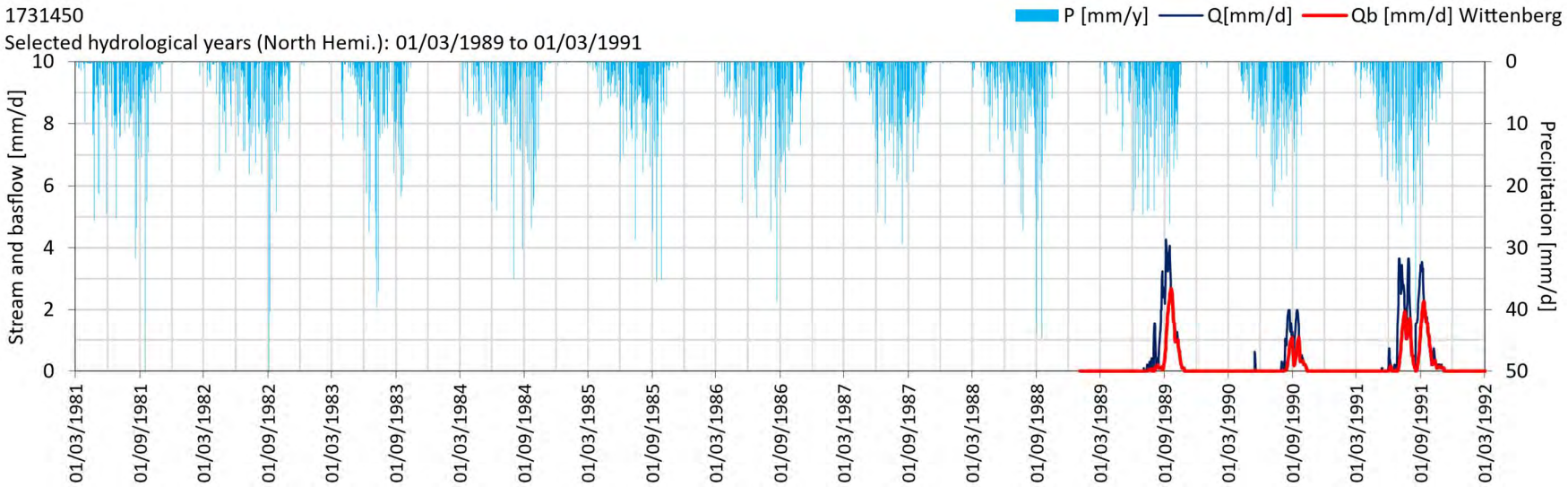
1731450
Selected hydrological years (North Hemi.): 01/03/1989 to 01/03/1991
P [mm/y]
Q[mm/d]
Qb [mm/d] Wittenberg
Stream and basflow [mm/d]
Precipitation [mm/d]
0
2
4
6
8
10
10
20
30
40
50
01/03/1981
01/09/1981
01/03/1982
01/09/1982
01/03/1983
01/09/1983
01/03/1984
01/09/1984
01/03/1985
01/09/1985
01/03/1986
01/09/1986
01/03/1987
01/09/1987
01/03/1988
01/09/1988
01/03/1989
01/09/1989
01/03/1990
01/09/1990
01/03/1991
01/09/1991
01/03/1992

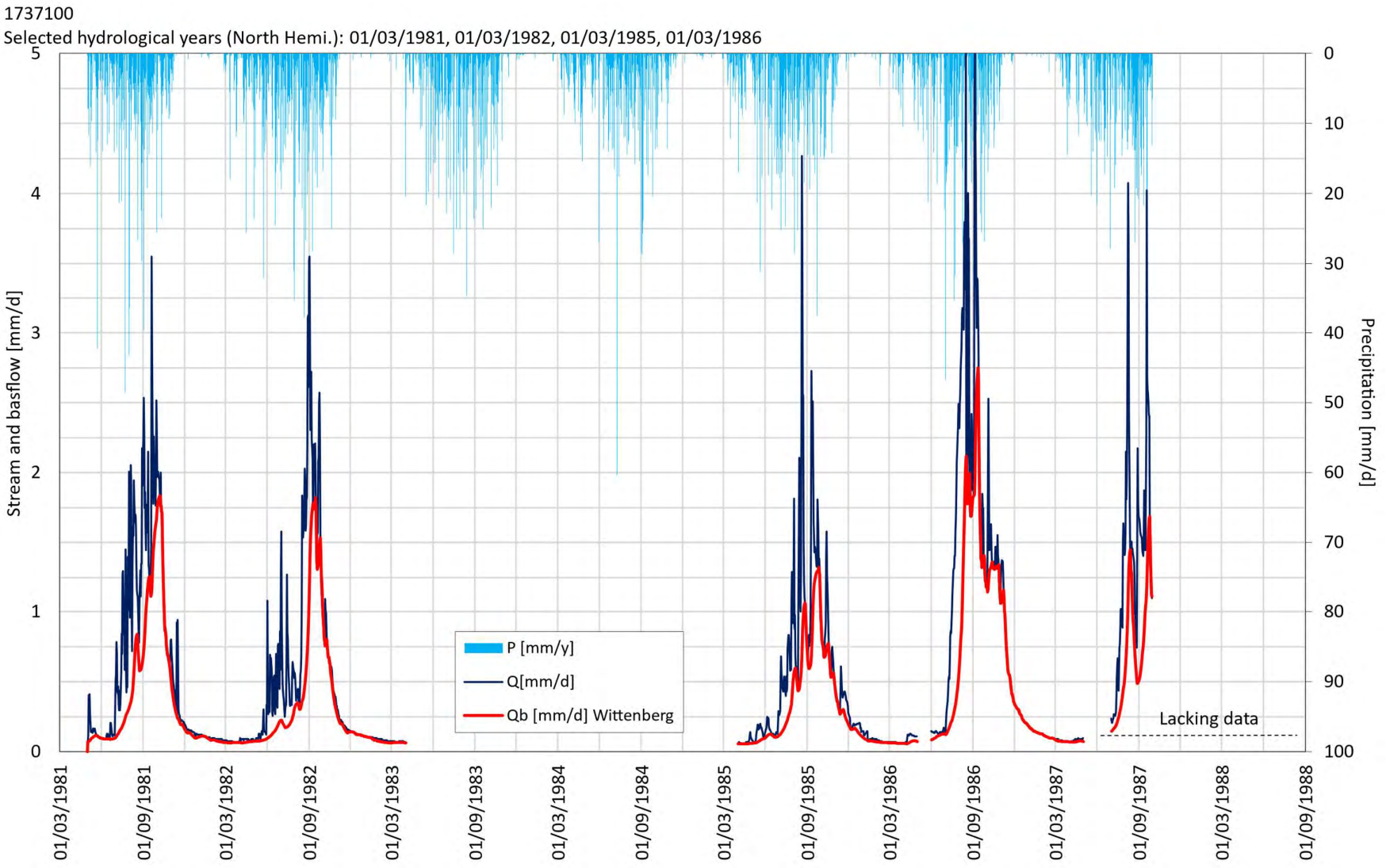
1737100
Selected hydrological years (North Hemi.): 01/03/1981, 01/03/1982, 01/03/1985, 01/03/1986
Stream and basflow [mm/d]
Precipitation [mm/d]
P [mm/y]
Q[mm/d]
Qb [mm/d] Wittenberg
Lacking data
0
1
2
3
4
5
0
10
20
30
40
50
60
70
80
90
100
01/03/1981
01/09/1981
01/03/1982
01/09/1982
01/03/1983
01/09/1983
01/03/1984
01/09/1984
01/03/1985
01/09/1985
01/03/1986
01/09/1986
01/03/1987
01/09/1987
01/03/1988
01/09/1988

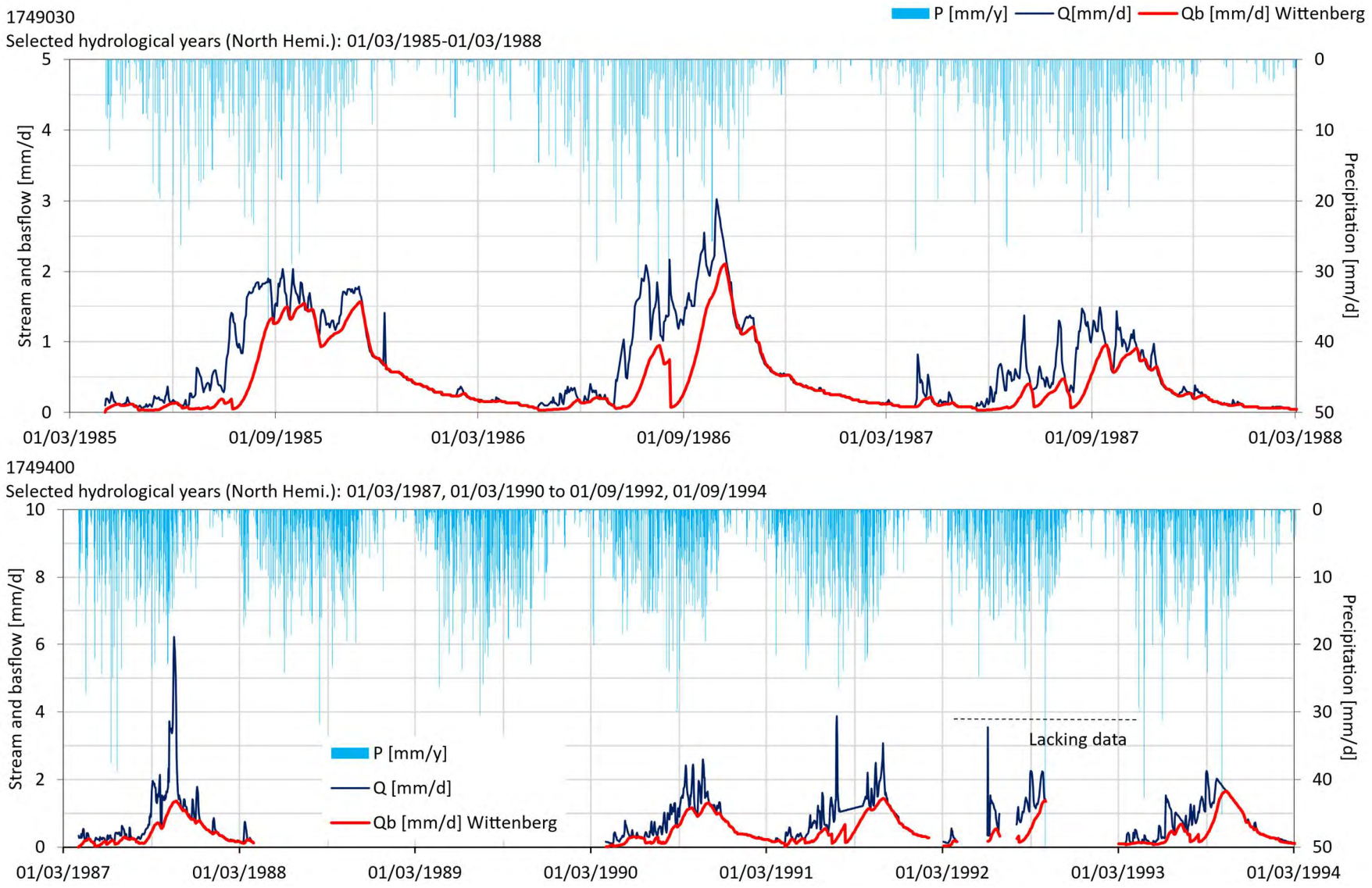
1749030
Selected hydrological years (North Hemi.): 01/03/1985-01/03/1988
P [mm/y]
Q[mm/d]
Qb [mm/d] Wittenberg
Stream and basflow [mm/d]
Precipitation [mm/d]
01/03/1985
01/09/1985
01/03/1986
01/09/1986
01/03/1987
01/09/1987
01/03/1988
1749400
Selected hydrological years (North Hemi.): 01/03/1987, 01/03/1990 to 01/09/1992, 01/09/1994
Lacking data
Q [mm/d]
01/03/1989
01/03/1990
01/03/1991
01/03/1992
01/03/1993
01/03/1994

1749800
Selected hydrological years (North Hemi.): 01/03/1986-01/03/1988 and 01/03/1990-01/03/1993

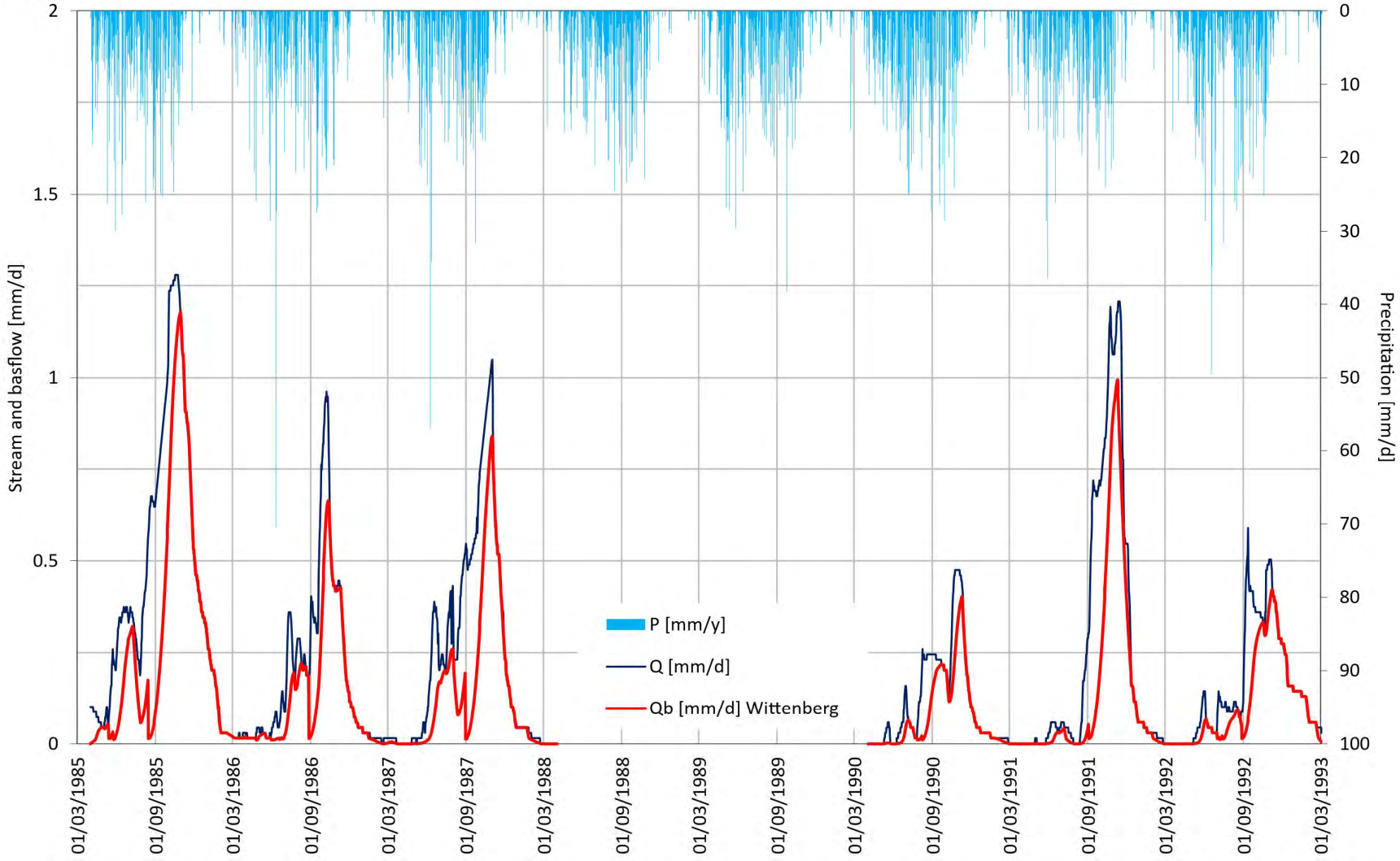

1813650
Selected hydrological years (North Hemi.): 01/03/1981 to 01/09/1983 and 01/03/1984 to 01/09/1987

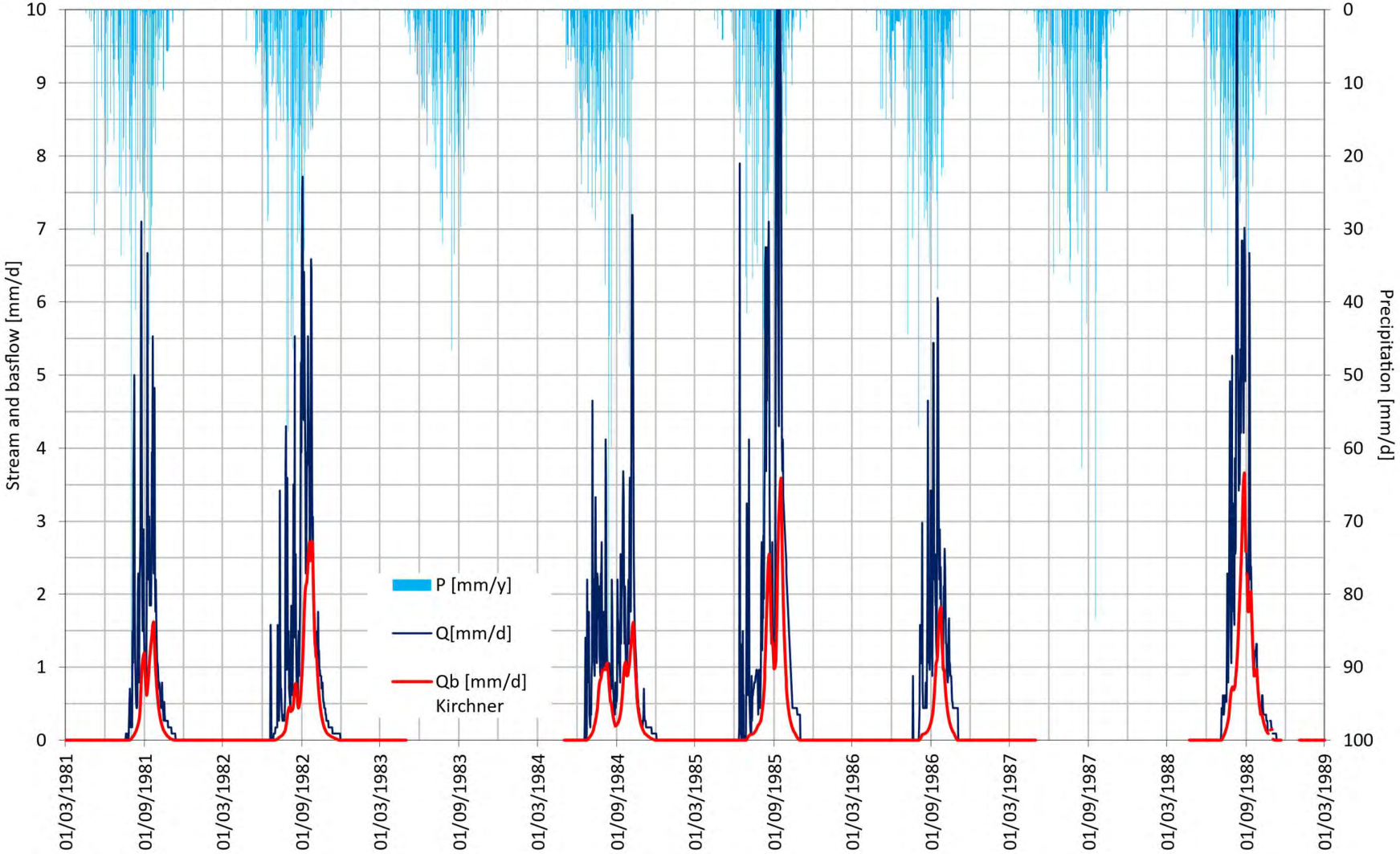

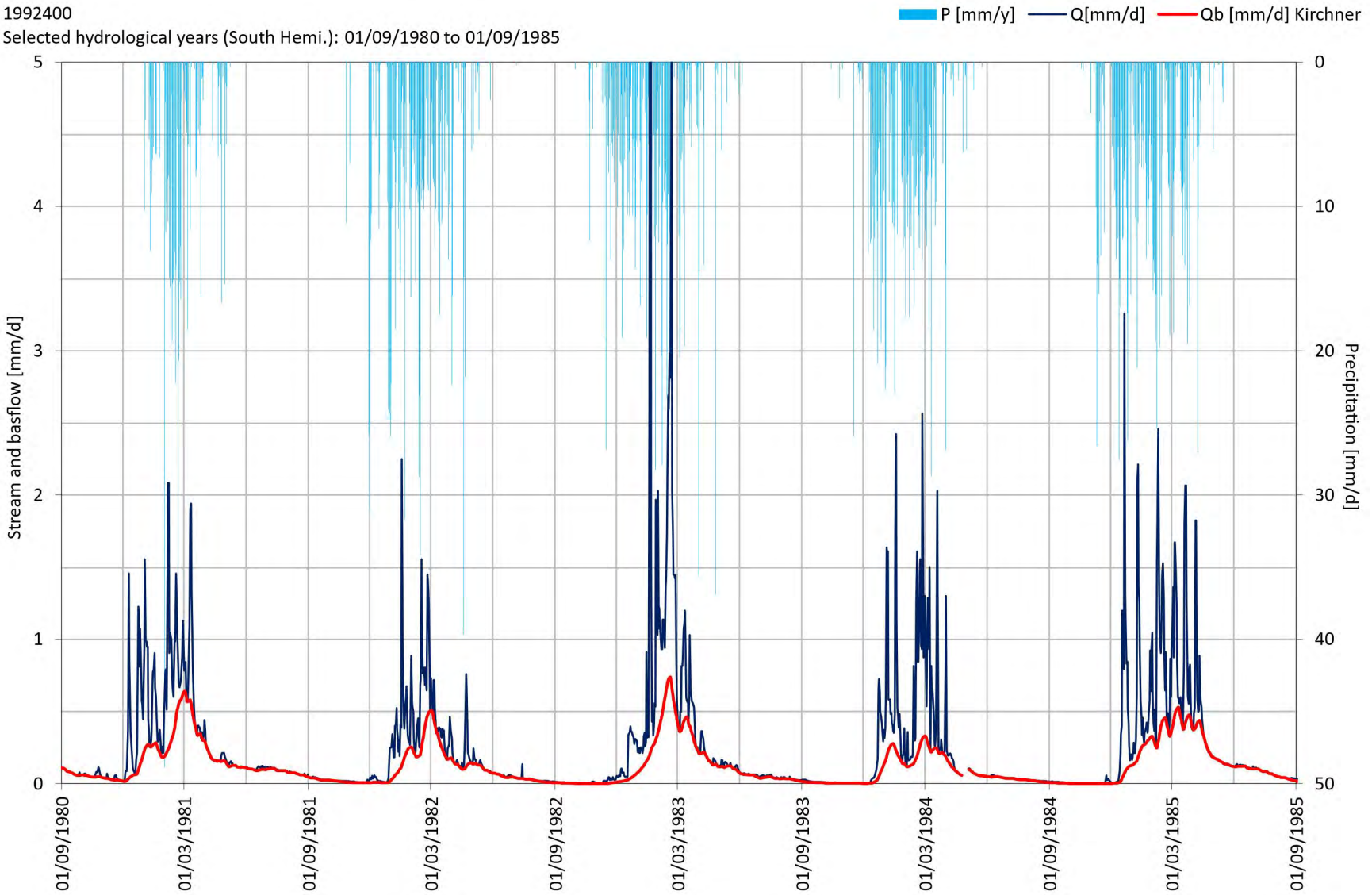
1992400
Selected hydrological years (South Hemi.): 01/09/1980 to 01/09/1985
P [mm/y]
Q[mm/d]
Qb [mm/d] Kirchner
Stream and basflow [mm/d]
Precipitation [mm/d]
0
1
2
3
4
5
0
10
20
30
40
50
01/09/1980
01/03/1981
01/09/1981
01/03/1982
01/09/1982
01/03/1983
01/09/1983
01/03/1984
01/09/1984
01/03/1985
01/09/1985

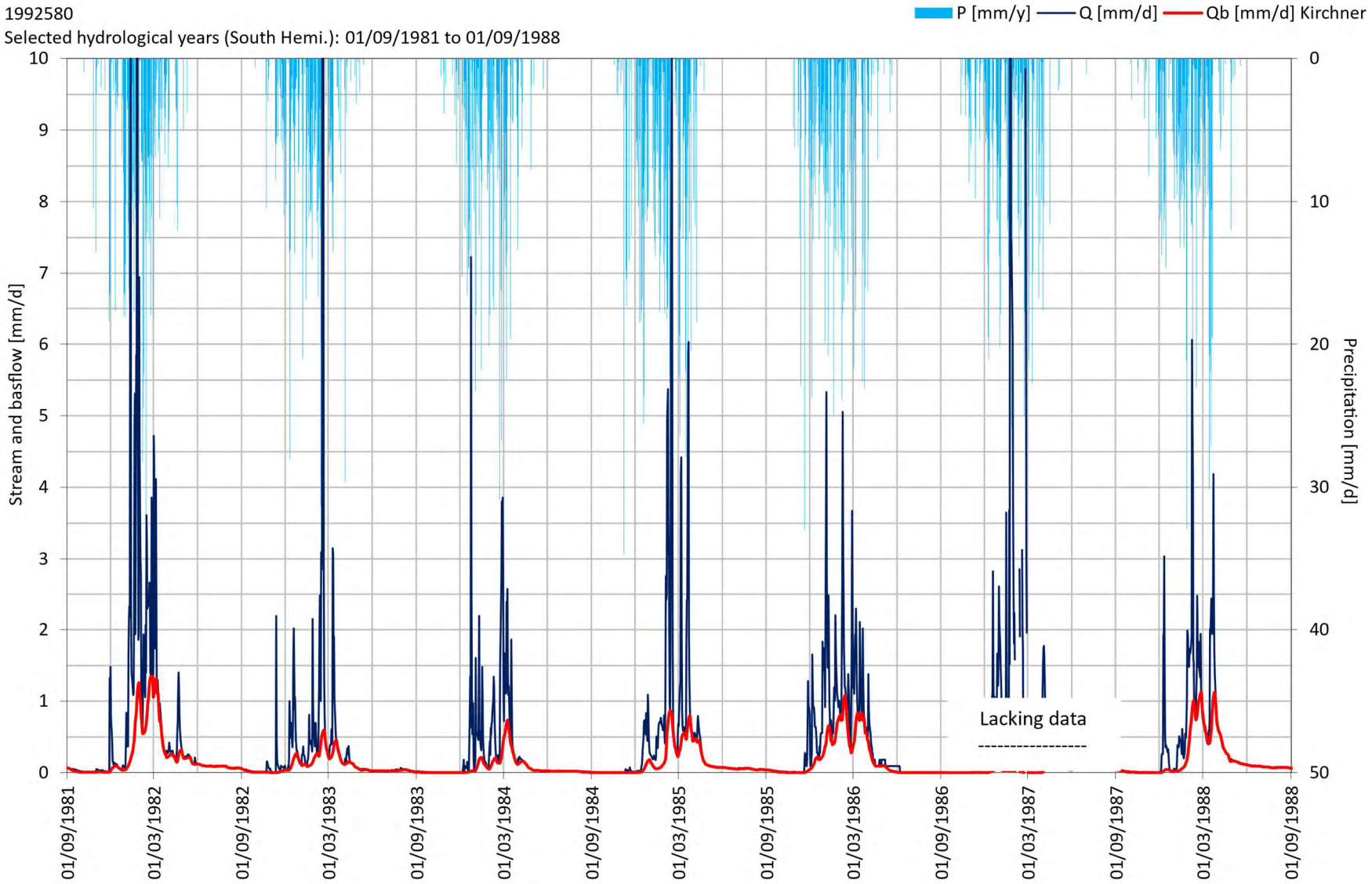
1992580
Selected hydrological years (South Hemi.): 01/09/1981 to 01/09/1988
P [mm/y]
Q [mm/d]
Qb [mm/d] Kirchner
Stream and basflow [mm/d]
Precipitation [mm/d]
Lacking data
01/09/1981
01/03/1982
01/09/1982
01/03/1983
01/09/1983
01/03/1984
01/09/1984
01/03/1985
01/09/1985
01/03/1986
01/09/1986
01/03/1987
01/09/1987
01/03/1988
01/09/1988

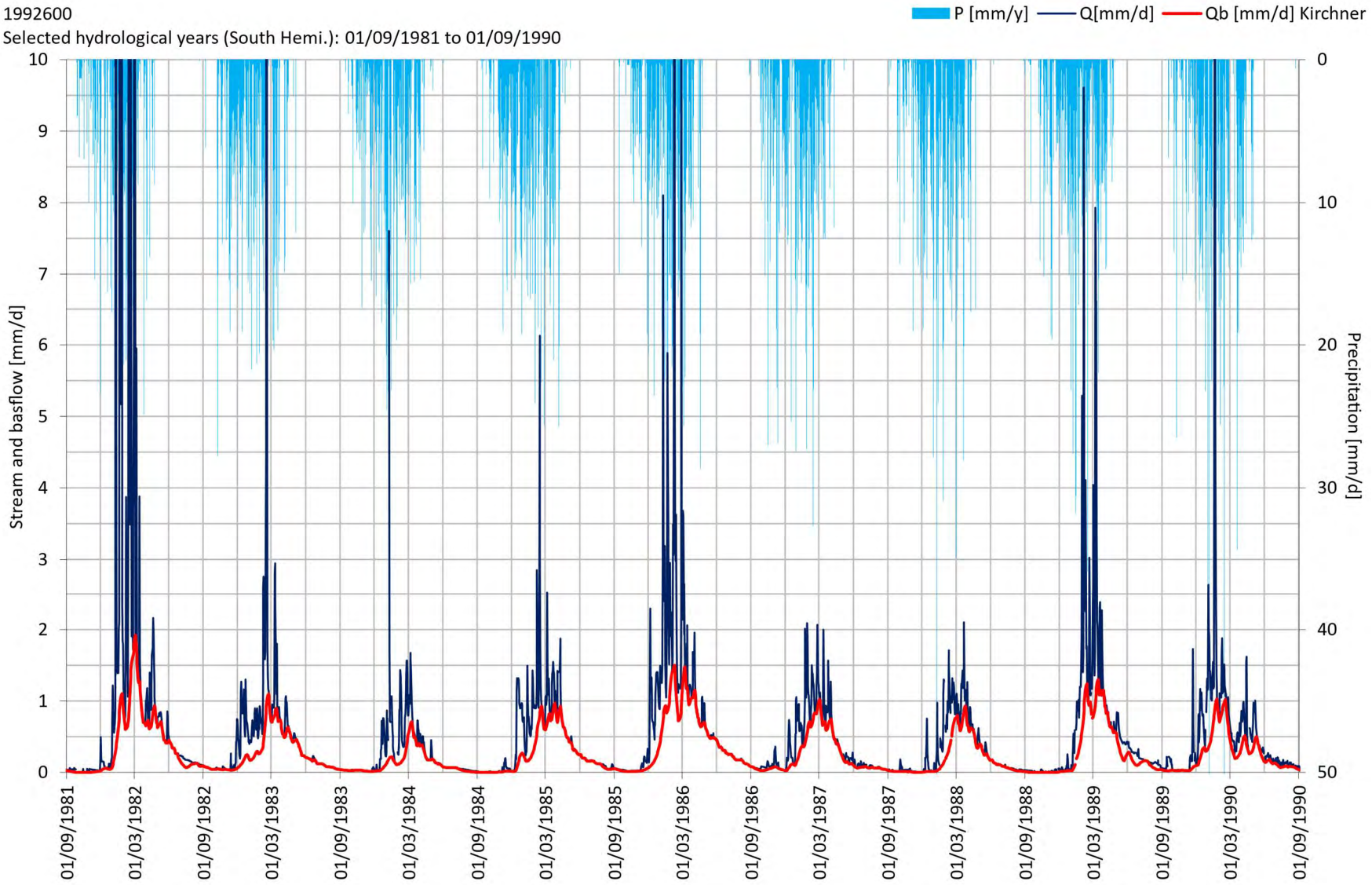
1992600
Selected hydrological years (South Hemi.): 01/09/1981 to 01/09/1990
P [mm/y]
Q[mm/d]
Qb [mm/d] Kirchner
Stream and basflow [mm/d]
Precipitation [mm/d]
0
1
2
3
4
5
6
7
8
9
10
0
10
20
30
40
50
01/09/1981
01/03/1982
01/09/1982
01/03/1983
01/09/1983
01/03/1984
01/09/1984
01/03/1985
01/09/1985
01/03/1986
01/09/1986
01/03/1987
01/09/1987
01/03/1988
01/09/1988
01/03/1989
01/09/1989
01/03/1990
01/09/1990